
# MODELLING OF SOLDER INTERCONNECTION'S PERFORMANCE IN PHOTOVOLTAIC MODULES FOR RELIABILITY PREDICTION

**MUSA TANKO ZARMAI**

**DOCTOR OF PHILOSOPHY**
**2016**

# MODELLING OF SOLDER INTERCONNECTION'S PERFORMANCE IN PHOTOVOLTAIC MODULES FOR RELIABILITY PREDICTION

**MUSA TANKO ZARMAI** B.Eng (Hons.), M.Eng

School of Engineering, Faculty of Science and Engineering

University of Wolverhampton

Wolverhampton, UK

A thesis submitted in partial fulfilment of the requirements of the University of Wolverhampton for the degree of Doctor of Philosophy

February 2016



Signature……

Date……..

## DECLARATION

This work has not been submitted in substance for any degree or award at any university or place of learning other than that of Doctor of Philosophy (Ph.D.) being studied at the University of Wolverhampton nor is being submitted concurrently in candidature for any degree or other award. I also declare that this thesis is the result of my own work, except where otherwise stated. Other sources used in this work are acknowledged by explicit references and I have not plagiarised the work of others.

…….. ……

Musa Tanko Zarmai Date

(Student)

…… ……

Professor Nduka Nnamdi Ekere Date

(Director of Studies)

# DEDICATION

This work is dedicated to God Almighty the creator of heaven and earth who gave me the understanding, knowledge and wisdom to carry out this research. To God be all the glory and praise!

# ACKNOWLEDGEMENTS

This work would not have been possible without the help of God. Therefore, I hereby acknowledge the extraordinary grace of God which was sufficiently granted to me to undertake and complete this PhD programme.

I would like to express my sincere thanks to the Petroleum Technology Development Fund (PTDF), Nigeria which provided the funds used in carrying out this research work. I am especially thankful to my Director of Studies, Prof. Ndy Ekere for his time, guidance and patience as well as for providing me with the opportunity to learn. Also, I am very grateful to my second supervisor Prof. Chike Oduoza for his constant encouragement, valuable advice, tremendous support and insightful comments. He has been an exceptional role model and excellent mentor providing me with inspiration for high quality professional work. I acknowledge and thank Dr. Emeka Amalu for his time, comments and all other contributions.

Many other people have contributed to this work in one form or another for which I very much appreciate. In particular, I thank Prof. Ian Sollitoe, Prof. Mike Thelwall, Dr. Ezekiel Chinyio, Dr. David Oloke and Mr. Maurice Ihebale for all their contributions. My special thanks go to my wife Elizabeth Zarmai for her understanding, encouragement and prayers. Likewise, I thank my children Shekwonyadu, Shekwogaza and Shekwoyemi for their patience and support. Finally, my foremost thanks go to my parents Deacon Tanko Zarmai and Mrs Kande Tanko Zarmai who sacrificed their comfort for my education.

# ABSTRACT

Standard crystalline silicon photovoltaic (PV) modules are designed to continuously convert solar energy into electricity for 25 years. However, the continual generation of electricity by the PV modules throughout their designed service life has been a concern. The key challenge has been the untimely fatigue failure of solder interconnections of solar cells in the modules due to accelerated thermo-mechanical degradation. The goal of this research is to provide adequate information for proper design of solar cell solder joint against fatigue failure through the study of cyclic thermo-mechanical stresses and strains in the joint. This is carried-out through finite element analysis (FEA) using ANSYS software to develop the solar cell assembly geometric models followed by simulations. Appropriate material constitutive model for solder alloy is employed to predict number of cycles to failure of solder joint, hence predicting its fatigue life. The results obtained from this study indicate that intermetallic compound thickness ($T_{IMC}$); solder joint thickness ($T_{SJ}$) and width ($W_{SJ}$) have significant impacts on fatigue life of solder joint. The impacts of $T_{IMC}$ and $T_{SJ}$ are such that as the thicknesses increases solder joint fatigue life decreases. Conversely, as solder joint width ($W_{SJ}$) increases, fatigue life increases. Furthermore, optimization of the joint is carried-out towards thermo-mechanical reliability improvement. Analysis of results shows the design with optimal parameter setting to be: $T_{IMC}$ -2.5μm, $T_{SJ}$ -20μm and $W_{SJ}$ -1000μm. In addition, the optimized model has 16,264 cycles to failure which is 18.82% more than the expected 13,688 cycles to failure of a PV module designed to last for 25 years.

# CONTENTS

# FIGURES

# TABLES

# NOMENCLATURE

## (a) ABBREVIATION

| | |
|---|---|
| 3D | Three-dimensional |
| Ag | Silver |
| ALT | Accelerated life testing |
| ANOVA | Analysis of variance |
| ARC | Anti-reflection coating |
| ATC | Accelerated thermal cycling |
| CdTe | Cadmium telluride |
| CIGS | Copper indium gallium selenide |
| c-Si | Crystalline silicon |
| CTE | Coefficient of thermal expansion |
| Cu | Copper |
| DOE | Design of experiments |
| FE | Finite element |
| FEA | Finite element analysis |
| FEM | Finite element modelling |
| HPC | High-performance computation |
| IEC | International electro-technical commission |
| IR | Infra-red |
| IMC | Inter-metallic compound |
| LFC | Laser fired contact |
| LHS | Left hand side |
| MTTF | Mean time to failure |
| N-type | Negative type |
| NEMI | National electronics manufacturing initiative |
| P-type | Positive type |
| Pb | Lead |
| PoF | Physics of failure |
| PV | Photovoltaic |
| R&D | Research and development |
| RHS | Right hand side |
| SEM | Scanning electron microscope |
| Si | Silicon |
| SnAgCu | Tin-Silver-Copper |

## (b) NOTATION

| | |
|---|---|
| a-Si:H | Hydrogenated amorphous silicon |
| β | Shape parameter; volumetric expansion coefficient |
| $b$ | Solder joint thickness |
| $C'$ | Inverse of creep ductility |
| $C_1$, $C_2$, $C_3$, $C_4$ | Constants in Garofalo-Arrhenius creep model |
| $\delta\theta$ | Range of temperature cycling limit |
| $\delta V_T$ | Change in total volume of solder layer |
| $\Delta W$ | Change in strain energy |
| $\Delta\omega_{acc}$ | Change in accumulated creep energy density per cycle |
| $\Delta W_{ave}$ | Averaged change in strain energy density |
| E | Young's modulus |
| $E_{IMC}$ | Effect of IMC |
| $E_j$ | Effect of factor $j$ |
| ε | Creep strain |
| $\varepsilon_{acc}$ | Accumulated creep strain per cycle |
| $\dot{\varepsilon}_{cr}$ | Creep strain rate |
| $F$ | Force |
| $F_{jmax}$, $F_{jmin}$ | Maximum and minimum value of factor $j$ |
| G | Elastic shear modulus |
| $h$ | Solder joint width |
| I | Second moment of area |
| $i$ | Model number; value number |
| $j$ | Control factor |
| $k$ | Flexural stiffness |
| $L$ | Component length |
| $L_9$ | Orthogonal array with nine designed parameter settings |
| μc-Si:H | Hydrogenated microcrystalline silicon |
| M | Model |
| m | Mean of signal-to-noise ratio |
| $N_f$ | Number of repetitions or cycles to failure |
| σ | Equivalent stress |
| $\sigma_{SR}$ | Equivalent stress in solder only region |
| $\sigma_{WJ}$ | Equivalent stress in whole joint |

| | |
|---|---|
| Q/R | Activation energy/Boltzmann's constant |
| R | Universal gas constant |
| S/N | Signal-to-noise |
| T | Absolute temperature |
| $T_{IMC}$ | IMC thickness |
| $T_{SJ}$ | Solder joint thickness |
| v | Poisson ratio |
| $V_1, V_2, V_3$ | Solder volume in region 1, 2 and 3 respectively |
| $V_1^i$ , $V_2^i$ | Volume of element at the start point and end point of one cycle respectively |
| $V_T$ | Volume of element *i* |
| $V_T$ | Total volume of three regions in whole solder layer |
| W' | Creep energy density for failure |
| $w_{acc}$ | Accumulated creep energy density per cycle |
| $W_{SJ}$ | Solder joint width |
| $W_1^i$ , $W_2^i$ | Total accumulated strain energy density in one element at the starting point and the end point of one thermal cycle respectively |
| *y* | Deflection |
| Z | Shape of soldered interconnector connecting front of one solar cell to back of another cell |

# CHAPTER 1

# INTRODUCTION

# Chapter 1

# Introduction

## 1.1 Background

The reality that the on-going climate change has a devastating effect on our planet has dawned on governments and people globally. The main cause of climate change is attributed to the ongoing profuse and unrestrained burning of fossil fuels. Renewable energy systems such as photovoltaic (PV) and wind energy systems present an alternative option to fossil fuel systems. In line with the foreseeable future trend of renewable energy utilization, some developing countries are investing more on renewable energy infrastructure and in low-carbon fossil fuel schemes thereby avoiding high-carbon fossil fuel systems being decommissioned in the developed world. Among the renewable energy systems, PV systems have gained wider acceptance worldwide and currently, there is an accelerated production and installation of PV systems for electric power generation as an alternative to fossil fuel systems. Unlike fossil fuel systems which release harmful substances to the environment during operations, PV systems use solar energy which is sustainable and environmentally friendly for electric power generation. Interestingly, the PV industry has been booming with high growth rate for more a decade (Aberle, 2009) producing a variety of PV systems. The PV systems are now used to supply power to several critical and non-critical devices and systems in various sectors such as: Telecommunication – to power satellites, radio/television relay stations, and remote stations for data

acquisition and transmission; Agriculture – to power water pumps and greenhouses; Health – to power refrigerators and also for lighting especially in remote locations; Public services - on-grid and off-grid electric utility, street lighting, and traffic lights; Residential – to power household devices and systems and Transportation – for power augmentation in some tricycles, cars and trucks. Figure 1.1 shows some typical PV installations in field operations. The failure of the PV systems to deliver power, especially to critical devices and systems in operations can cause accident with catastrophic and life-threatening consequences. It is therefore imperative to obtain proper understanding on how and when PV systems fail in order to avoid their premature and catastrophic failures.

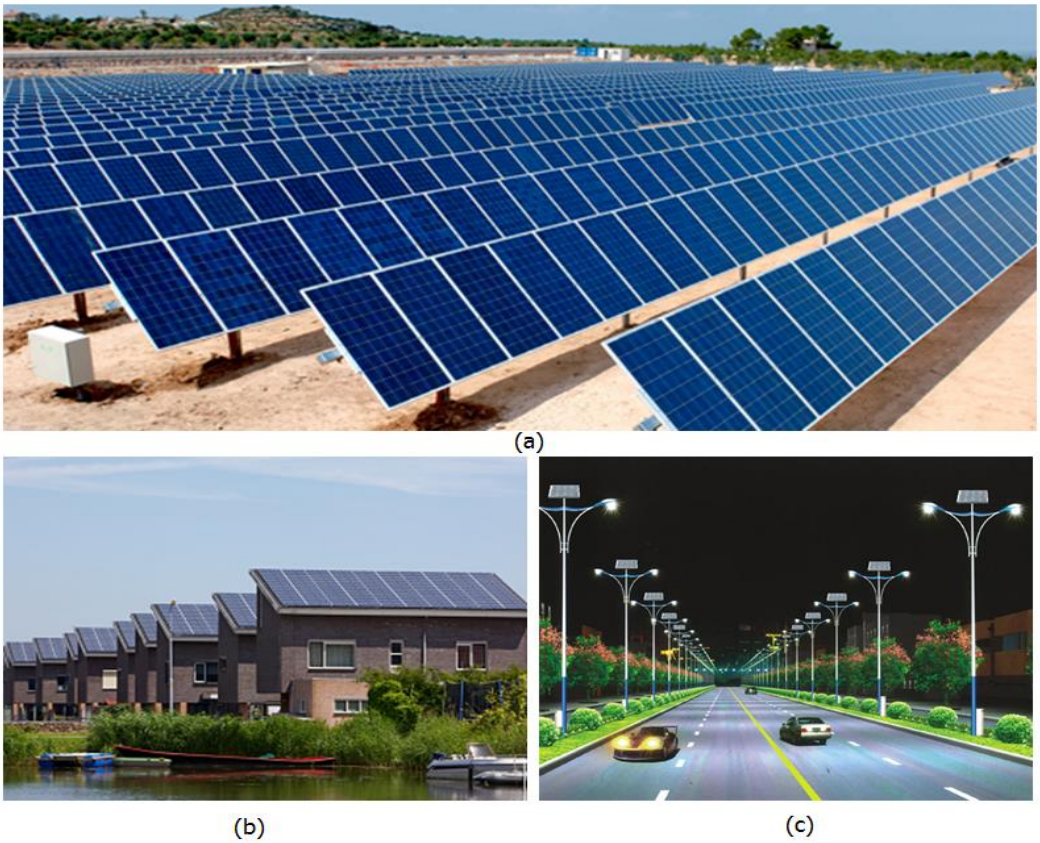


**Figure 1.1 Typical PV module installations showing:**
**(a) electric power utility plant (b) residential systems**
**(c) street lighting systems**

A typical PV system consists mainly of interconnected and encapsulated solar cells which form a module. Most PV modules are made with wafer-based crystalline silicon (c-Si) solar cells while the rest are made with thin-film solar cells. Wafer-based cells are made of either monocrystalline or multicrystalline silicon. On the other hand, thin-film solar cells are mostly made of either hydrogenated amorphous silicon (a-Si:H), hydrogenated microcrystalline silicon (μc-Si:H), cadmium telluride (CdTe), or copper indium gallium selenide (CIGS). Furthermore, crystalline silicon solar cells have higher energy conversion efficiency when compared with thin-film solar cells. Also, larger quantities of crystalline silicon solar cells are produced globally compared with other types. For instance, in 2014, the global PV module production using crystalline silicon solar cells was 90.737% of the total production (Burger, *et al.,* 2015). This clearly shows that crystalline silicon solar cells dominate the global market and this trend is expected to continue for years as durability of new module types made of thin-films are yet to be fully tested in the field. Therefore crystalline silicon PV modules have been chosen for this study due to their massive applications worldwide and higher efficiency.

## 1.2 Research problem

According to IEC standard 61215, typical crystalline silicon photovoltaic (PV) modules should be able to continuously convert solar energy into electricity for 25 years (Arndt and Puto, 2011). However, the premature field failures of

these modules have been a concern. Analysis of failed modules indicate that failure of interconnects is a key type of field failure observed. Crystalline silicon PV modules contain interconnects such as silicon semiconductor wafer, silver (Ag) electrodes and long ribbon strips, usually made of copper (Cu) and coated with solder material. The Ag electrode is used as bus-bar and deposited on the silicon wafer. The Ag bus-bar is interconnected to the Cu ribbon strip by soldering them together thereby forming a solder joint between the Ag bus-bar and the Cu ribbon strip. This arrangement enables electrical, thermal and mechanical connection to the module interconnects. Therefore, when the silicon wafer generates electricity, it is transmitted via the Ag electrode and the solder joint to the Cu ribbon strip which finally delivers it to the desired point. Likewise, the solder joint provides a thermal conduit for heat generated during operations to be dissipated away from the silicon wafer. Still, the solder joint acts as a mechanical support to hold the interconnect components together. The ribbon strip interconnects each solar cell to the adjacent one while carrying the generated electric current. However, untimely failure of solder joints has been identified as a key thermo-mechanical reliability issue in crystalline silicon PV modules (McCluskey, 2010; Cuddalorepatta *et al.*, 2010). Therefore, the research problem is improvement of thermo-mechanical reliability of solder interconnection in crystalline silicon PV modules so that they can perform up to the desired lifespan of 25 years.

As has been mentioned, materials interconnected together consist of silicon wafer, Ag electrode, solder joint and Cu ribbon. Each of these interconnection materials has a different coefficient of thermal expansion (CTE). When the PV module is in use during the daily field service, the solder joints experience cyclic thermo-mechanical loads due to expansion and contraction of interconnect materials as a result of CTE mismatch of the materials. The cyclic thermo-mechanical loads cause weakening of the solder material, that is, the solder material undergoes fatigue. Thermal cycling is the main cause of fatigue in solder joint and with every thermal cycle, there is a progressive and localized structural damage of the solder material. Thermo-mechanical fatigue loads have significant effect on the solder joint in PV module and cause accelerated thermo-mechanical degradation. Over time, the damage accumulates eventually resulting in failure of the solder joint. The accelerated thermo-mechanical degradation of the solder joint material has been identified as the critical reliability issue of the PV module assembly (McCluskey, 2010). A reliable solder joint is the ability of the solder interconnection to maintain functionality in the PV module where in use. The functionality of the solder joint is affected by daily thermal cycling as well as the effect of passing clouds. The daily thermal cycling and effect of passing clouds experienced by the PV module during service life is the cause of the thermo-mechanical degradation of the solder joint in the module. Furthermore, when 95.5Sn3.8Ag0.7Cu solder is used, $Ag_3Sn$ and $Cu_6Sn_5$ intermetallic compounds (IMC) are formed at the interface joint between solder and Ag electrode as well as between solder and Cu ribbon respectively

during soldering for interconnection. These IMCs continue to grow and increase in thickness as the PV module operates eventually reaching a threshold when solder joint cracks and finally fails. The effect of IMC on the thermo-mechanical reliability of solder joint needs to be evaluated in-depth for more understanding and reliability improvement. Parameters of solder joint such as solder joint thickness and width on the thermo-mechanical reliability also need to be evaluated for improved solder joint parameter setting.

Proper understanding of the effect of IMC and solder joint parameters on the thermo-mechanical reliability of solder joints will enable optimization of solder joint parameter setting for improved thermo-mechanical reliability in the PV modules. Optimizing the solder joint parameter setting enables the provision of adequate solder material to withstand thermo-mechanical loading thereby avoiding premature failure. Therefore, in-depth understanding of the thermo-mechanical degradation of the solder joints is necessary to enable accurate reliability prediction of PV modules. It is necessary to identify the critical mean-time-to-failure (MTTF) of solder joints in PV modules. When the MTTF is known, adequate plans can be made for schedule maintenance either for system repairs, component replacement or for a combination of system repairs and component replacement.

## 1.3 Statement of the hypothesis and research questions

The statement of the hypothesis and research questions is in the following sub-sections.

### 1.3.1 Statement of the hypothesis

Optimizing the parameters of lead-free solder interconnection in crystalline silicon PV module can improve the thermo-mechanical reliability of the assembly.

### 1.3.2 Research questions

Solder joint in crystalline silicon solar cell assembly interconnects Cu ribbon and Ag bus-bar as mentioned earlier. Presented in Fig. 1.2 is a schematic cross-section of typical crystalline Si solar cell assembly showing IMC thickness, solder joint thickness and width.

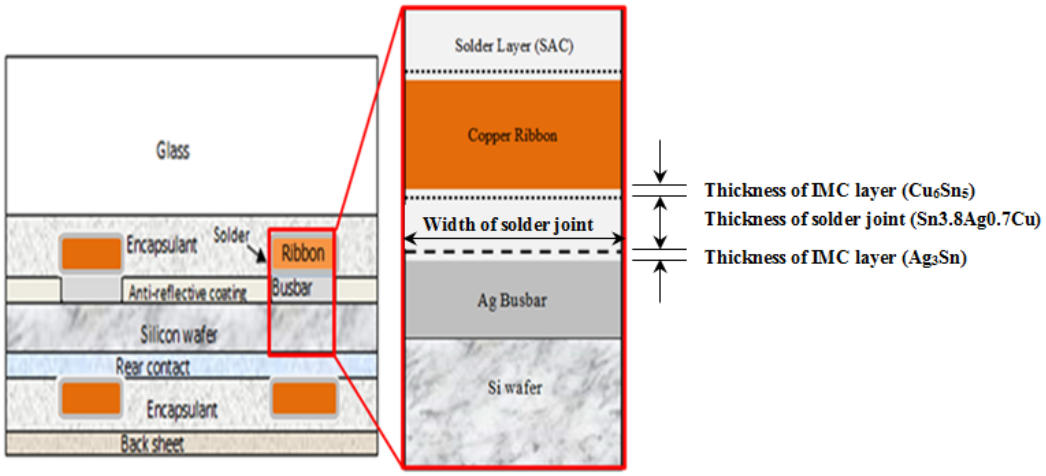


**Figure 1.2 Schematic of cross-section of typical crystalline Si solar cell assembly showing IMC thickness, solder joint thickness and width**

Based on the statement of hypothesis and with reference to Fig. 1.2, the research questions for this study are as follows:

- Does the formation and presence of intermetallic compound (IMC) in solder joints of PV module impacts its reliability significantly?
- What is the effect of IMC thickness on fatigue failure of solder interconnection in PV module?
- What is the effect of solder joint thickness on thermo-mechanical reliability of the solder joint in PV module?
- What is the effect of solder joint width on thermo-mechanical reliability of the solder joint in PV module?
- What is the optimal parameter setting of solder joint in PV module for thermo-mechanical reliability improvement?

## 1.4 Motivation for research

The photovoltaic market is growing fast. Global cumulative installed PV capacity was nearly 40 $GW_p$ ($W_p$, is peak power produced under standard test conditions) in 2010 (Ardani and Margolis, 2011). This was an increase of 16.6 $GW_p$ or 131% when compared with the installed capacity in 2009. Furthermore, it was nearly seven times the 2.4$GW_p$ installed capacity of 2007. The fast market growth is expected to continue in years to come. It is expected that around year 2020, the world annual production of PV cells will be around 100 $GW_p$ (Saga, 2010). To meet this demand, silicon solar cells stand out as the most viable option suitable to meet the target volume

production (Saga, 2010). However, crystalline silicon PV systems experience degradation during field operations just like many other systems, most often culminating in system failure. It has been reported that the continual generation of electricity by crystalline silicon PV modules in the field for a minimum life span of 20 years has been a concern (Saga, 2010; Jeong, *at al.*, 2010; Gress, *et al.*, 2010; Klengel, *et al.*, 2011). One of the key challenges is untimely failure of crystalline silicon solar cells interconnection in the modules (Sakamato, *et al.,* 2012). Solder joints are the critical part of c-Si PV interconnections and they fail and crack as a result of thermo-mechanical cyclic loads. The crack results in discontinuity and loss of connection between adjacent solder materials in the interconnection. Consequently electricity generated in the affected solar cell cannot be transmitted via the solder interconnection to a neighbouring solar cell in a PV module. This is a concern because failure of the solder interconnections implies that the PV module cannot deliver generated electricity to critical devices and systems. PV module failure is so critical that even very low failure rates of less than 1 in 10,000 are noticeable and unacceptable (Wohlgemuth, *et al.*, 2008). The main failure mechanism responsible for the failure of solder interconnection in PV modules is thermal fatigue and the resulting failure mode is loss of connection. McCluskey (2010), reported that in a BP study, of all the types of failure observed, 40.7% were due to cell or interconnect breakage. The findings reported by McCluskey, in addition to other similar findings by Han *et al.* (2012) and Kato (2012), have identified

the reliability of PV interconnections as the main challenge in PV modules performance in the field.

Furthermore, intermetallic compounds (IMCs) are formed at the solder-ribbon interface during the soldering process for interconnection of solar cells. These IMCs play a crucial role in solder joint deformation where inhomogeneous and local strains develop at the interface. As mentioned in Section 1.1, during the field service life of the PV modules, the IMCs continue to form and increase in thickness. When the IMC thickness reaches a particular threshold, failure of the solder joint occurs. This author did not come across modelling and simulation information in literature on the effect of IMC thickness on solder joint reliability in crystalline silicon PV modules. There were, however, information on IMC growth obtained from experiments. Therefore, the effect of IMC thickness on mechanical strength of solder joint reliability needs to be investigated using finite element analysis (FEA). In addition, the effects of solder width and thickness on solder joint reliability need to be investigated. This will enable the determination of optimum parameter setting for solder joint geometry which can ensure thermo-mechanical reliability of solder interconnections in crystalline silicon PV modules.

The goal of this study is to contribute to knowledge and understanding of solder interconnection in solar cell assembly of crystalline silicon PV modules

through: determination of the contribution of the formation, presence and critical thickness of IMC to the thermo-mechanical reliability of solder joints in crystalline PV modules; evaluation of the effect of solder joint thickness and width on solder joint thermo-mechanical reliability; prediction of cycles to failure of the solar cell solder joint in the PV module and setting optimum parameters for solder joints in PV modules.

## 1.5 Aim and objectives of the research

The research aim and objectives are presented in the following two parts.

### 1.5.1 Research aim

The aim of this research is to study the thermo-mechanical reliability of lead-free solder interconnections in crystalline silicon PV modules.

### 1.5.2 Research objectives

The objectives of this research are to:

(a) Study the failure mode and identify the failure mechanisms of the solder joints in crystalline silicon solar cells of PV modules

(b) Establish the contribution of thickness of IMC on the interconnection failure

(c) Evaluate the effect of solder joint thickness and width on the interconnection failure

(d) Predict the mean time to failure of the solar cell solder joint in the PV module

(e) Optimise parameter settings of solar cell solder joint in crystalline silicon PV modules

## 1.6 Research Programme

The research programme is presented in Fig. 1.3. It gives an overview of the plan used for this study.

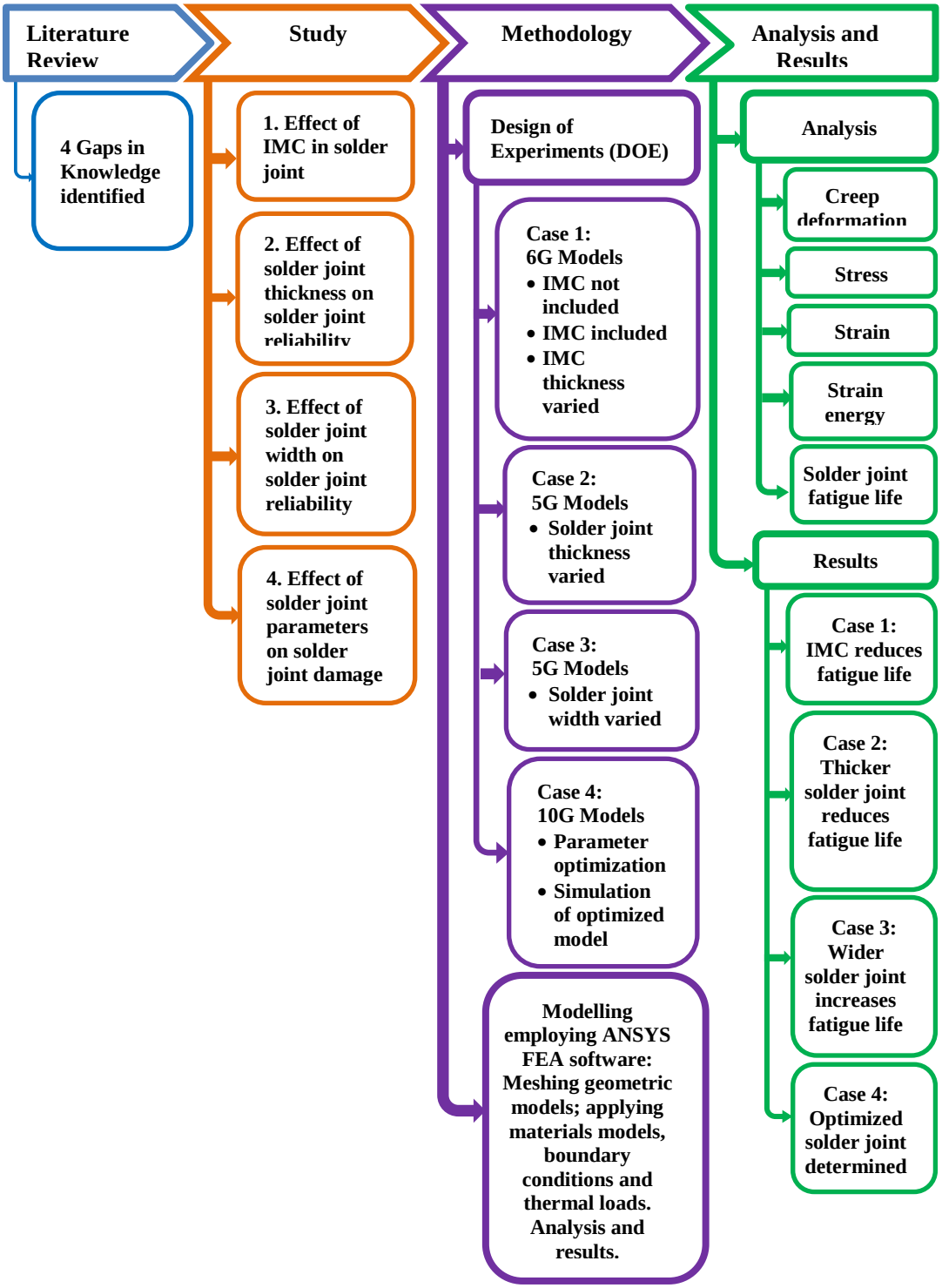


**Figure 1.3 Programme of PhD research work**

## 1.7 Significant findings

This study has considered several factors that impact the thermo-mechanical reliability of solder joints in solar cell assembly. In doing that, various parameters of solder joints were analysed and some findings obtained. Listed in the following are findings deemed as significant in this study:

(i) The study establishes that the presence of IMC in solder joints of solar cell assembly significantly affects solder joint fatigue life. Comparative analysis of models of solar cell assembly shows that solder joint containing IMC has a predicted fatigue life of 15317cycles to failure while that of solder joint without IMC is 32493 cycles to failure. This shows a 52.85% change of predicted fatigue life from solder joint without IMC. Therefore, the inclusion of IMC layer in solder joint models for the study of thermo-mechanical reliability of the joints is crucial to ensure accurate modelling and simulation results.

(ii) Still on IMC, the study reveals that as IMC thickness increases in the solder joint of solar cell assembly, predicted fatigue life of the joint decreases. Simulation results obtained indicate that when IMC thickness is 1μm, predicted fatigue life is 15317 cycles to failure, while when the thickness increases to 4μm, the predicted fatigue life decreases to 13023 cycles to failure. Subsequently, it is essential that solder joints should be designed to have adequate capacity to withstand IMC thickness throughout the duration of the PV module lifetime.

(iii) Also, the study establishes that solder joint thickness impacts solder joint fatigue life such that the thicker the joint, the shorter the fatigue life. From the study results, when solder joint thickness is 20μm, predicted fatigue life is 14174 cycles to failure, while when the thickness increases to 30μm, the predicted fatigue life decreases to 10794 cycles to failure. For that reason, appropriate solder joint thickness should be used in solar cell assembly in order to reduce thermo-mechanical stresses in the joint and extend fatigue life of the joint.

(iv) In a related finding, the study shows that the wider the solar cell solder joint, the longer the fatigue life. The study results demonstrate that when solder joint width is 1000μm, predicted fatigue life is 14174 cycles to failure, while when the width increases to 1400μm, the predicted fatigue life increases to 15729 cycles to failure. On the other hand, wider solder joints increase shadowing losses of the solar cell thereby reducing the cell efficiency. Consequently, compromise is required between increase in solder joint width and shadowing losses as well as desired fatigue life.

(v) Moreover, the findings outlined above demonstrate that geometric parameters of solder joint in solar cell assembly have significant impacts on thermo-mechanical reliability of the joints. Therefore, optimization of solder joint parameter setting is crucial to obtain a joint which accumulates minimal creep strain energy density and potential for longer fatigue life.

(vi) Optimization conducted reveals that solder joint thickness has the most significant effect on the thermo-mechanical reliability of solder joints. Analysis of results selected towards thermo-mechanical reliability improvement shows the design with optimal parameter setting to be: solder joint thickness - 20μm, solder joint width - 1000μm, and IMC thickness – 2.5μm. Furthermore, the optimized model has the least damage in the solder joint and shows a reduction of 47.96% in accumulated creep strain energy density per cycle compared to the worst case original model. Moreover, the optimized model has 16264 cycles to failure compared with the expected 13688 cycles to failure of a PV module designed to last for 25 years. Thus, the fatigue life of the optimized model is 18.82% longer than that of the design expectation.

## 1.8 Thesis overview

This thesis consists of nine chapters. Chapter 1 presents the introduction to the thesis. It outlines the research background, motivation for the research as well as aim and objectives of this study. Furthermore, the research programme, significant findings, thesis overview as well as publications from the study are also presented in this chapter. The review of relevant literature covering PV modules, crystalline silicon PV module assembly including brief overview of crystalline silicon solar cells, solder joint reliability, interconnection technology as well as interconnection material are contained

in Chapter 2. Also in this chapter is a discussion on failure of solder joints in PV modules and fatigue life prediction of solder joints. Methodology for this research is presented in Chapter 3 and it includes a brief description of modelling and simulation with ANSYS Academic Research software and a concise overview of Taguchi's approach to design of experiments. Chapter 4 deals with evaluation of thermo-mechanical reliability of solder joints in solar cell assembly. The chapter explains the modelling and simulation of solder joints in solar cell assembly with and without IMC. It further discusses simulation results of creep strain and strain energy as well the effect of IMC on solder joint fatigue life. In Chapter 5, study of the effect of intermetallic compound thickness on thermo-mechanical fatigue life of solder joints in solar cell assembly is presented. The modelling and simulation of solder joints in solar cell assembly with various IMC thicknesses are presented in this chapter. Moreover, the chapter discusses creep strain and stress on the various IMC thicknesses of solder joints. The discussion in this chapter progresses to explain the evaluation of hysteresis loop of the solder joints. Likewise in this chapter is the study on strain energy and evaluation of accumulation of strain energy density. Lastly, the chapter presents a study on solder joint fatigue life to determine the effect of IMC thickness on the thermo-mechanical reliability of solder joints. Evaluation of the effect of solder joint thickness on thermo-mechanical fatigue life of solder joints in solar cell assembly is presented in Chapter 6. This chapter considers modelling and simulation of solder joints in solar cell assembly with various solder joint thicknesses. Results and discussion on the study of stress, creep

strain and creep energy density in solder joint are also presented. In addition, the chapter presents a study on the effect of solder joint thickness on solder joint fatigue life. An evaluation of the effect of solder joint width on thermo-mechanical fatigue life of solder joints in solar cell assembly is contained in Chapter 7. Modelling and simulation of solder joints in solar cell assembly with various solder joint widths are discussed in this chapter. This chapter also contains results and discussion on the study of stress, creep strain and creep energy density in solder joint. Analysis of the effect of solder joint width on solder joint fatigue life is presented as well in this chapter. Chapter 8 focusses on evaluating the critical design parameters of solder joints that impact thermo-mechanical reliability of the joints in crystalline silicon solar cell assembly in order to optimize their designs. Design of experiments using the Taguchi approach and signal-to-noise ratio are presented in this chapter. Also, finite element modelling and simulation carried out and results obtained are also presented. Besides, discussion of results is presented too and consists of characterization and quantification of damage on various solder joint parameter settings, evaluation of main effect and interaction and also comparison of the optimal design with the worst design. The conclusions drawn from this study and recommendations for further work are presented in Chapter 9. The recommendations are presented in two categories and consist of general recommendations as well as specific recommendations.

## 1.9 Publications from the study

The output from this study was used to write seven (7) Journal and Conference papers. The lists of papers in journal and conference publications are presented in the following sub-sections.

### 1.9.1 Journal publications:

1. M.T. **Zarmai**, N.N. Ekere, C. F. Oduoza, E.H. Amalu. Optimization of thermo-mechanical reliability of solder joints in crystalline silicon solar cell assembly. Microelectronics Reliability (Elsevier) – 59 (2016), 117-125.

2. M.T. **Zarmai**, N.N. Ekere, C. F. Oduoza, E.H. Amalu. A review of interconnection technologies for improved crystalline silicon solar cell photovoltaic module assembly. Applied Energy (Elsevier), 154 (2015), 173-182.

3. M.T. **Zarmai**, N.N. Ekere, C. F. Oduoza, E.H. Amalu. Effect of intermetallic compounds on thermo-mechanical reliability of lead-free solder joints in solar cell assembly. International Journal of Mechanical Engineering (IJME), Vol. 4. Issue 6, (2015), 29-38.

4. Musa T. **Zarma**i, N.N. Ekere, C.F. Oduoza, Emeka H. Amalu. Evaluation of thermo-mechanical damage and fatigue life of solar cell solder interconnections. Robotics and Computer-Integrated Manufacturing (Elsevier), article under review.

### 1.9.2 Conference publications:

1. M.T. **Zarmai**, N.N. Ekere, C. F. Oduoza, E.H. Amalu. Effect of IMC thickness on thermo-mechanical reliability of lead-free solder joints in solar cell assembly. Proceedings of TechConnect Conference, Washington DC, USA, 2015, Vol. 4, pp. 286-289.

2. M.T. **Zarmai**, N.N. Ekere, C. F. Oduoza, E.H. Amalu. Thermo-mechanical reliability of lead-free solder joints in solar cell assembly. Proceedings of the 25$^{th}$ International Conference on Flexible Automation and Intelligent Manufacturing (FAIM), Wolverhampton, UK, 2015, Vol. 1, pp. 640-647.

3. M.T. **Zarmai**, N.N. Ekere, C. F. Oduoza, E.H. Amalu. Effect of intermetallic compounds on thermo-mechanical reliability of lead-free solder joints in solar cell assembly. Proceedings of Asia-Pacific Conference on Engineering & Applied Sciences (APCEAS), Osaka, Japan, 2015, Part 1, pp. 328-336.

# CHAPTER 2

# LITERATURE REVIEW

# Chapter 2

# Literature Review

## 2.1 Introduction

Presented in this chapter is the review of relevant works previously carried out on PV modules. The review proceeds to focus on crystalline silicon PV module assembly and its solder joint reliability challenges as well as fatigue life prediction of the joint. The review of PV modules is focussed on their classification in terms of constituent material. In addition, available information on global module production and installation are provided.

The conventional assembly procedure of crystalline silicon (c-Si) PV module is briefly described. Interconnection technology used for solar cells to form the c-Si PV module is reviewed and the interconnection challenges mentioned. Interconnection material as well as solder joint reliability are reviewed to identify key factors impacting on the solder joint reliabilty.

Fatigue life prediction of solder joints for c-Si PV modules is briefly discussed including constitutive model for lead-free 95.5Sn3.8Ag0.7Cu (SnAgCu) solder alloy. This is necessary for identifying a comprehensive description of solder behaviour from creep models as well as life prediction models for solder joint. The aim is to obtain a robust life prediction model that will produce more accurate results for solder joints in c-Si PV modules.

## 2.2 PV modules

A PV module is a packaged assembly of interconnected solar cells mounted on a supporting structure. The PV module can be used as a single unit in a PV system or as a combination of several modules to form a larger PV system to generate and supply electricity in several applications. PV modules are known by the type of solar cells used in forming them. Solar cells are classified according to the constituent material used in fabricating them. The major types of solar cells manufactured commercially are wafer-based cells made of monocrystalline silicon (mono c-Si) and multicrystalline silicon (multi c-Si) as well as thin-film cells made of hydrogenated amorphous silicon (a-Si:H), hydrogenated microcrystalline silicon (μc-Si:H), cadmium telluride (CdTe) and copper indium gallium selenide (CIGS). Presented in Fig. 2.1 are the classification of major commercial solar cells and their range of solar energy conversion efficiencies. It can be observed from Fig. 2.1 that wafer-based crystalline silicon solar cells, consisting of mono c-Si (Saga, 2010) and multi c-Si (Saga, 2010), have higher energy conversion efficiency when compared with thin-film solar cells consisting of a-Si:H (Sunshot Initiative, 2013a), μc-Si:H (Shah, *et al.*, 2004), CdTe (Sunshot Initiative, 2013b) and CIGS (Sunshot Initiative, 2013c). Usually, solar cell efficiency is higher than its PV module efficiency due to losses arising from interconnection of the cells to form the module.

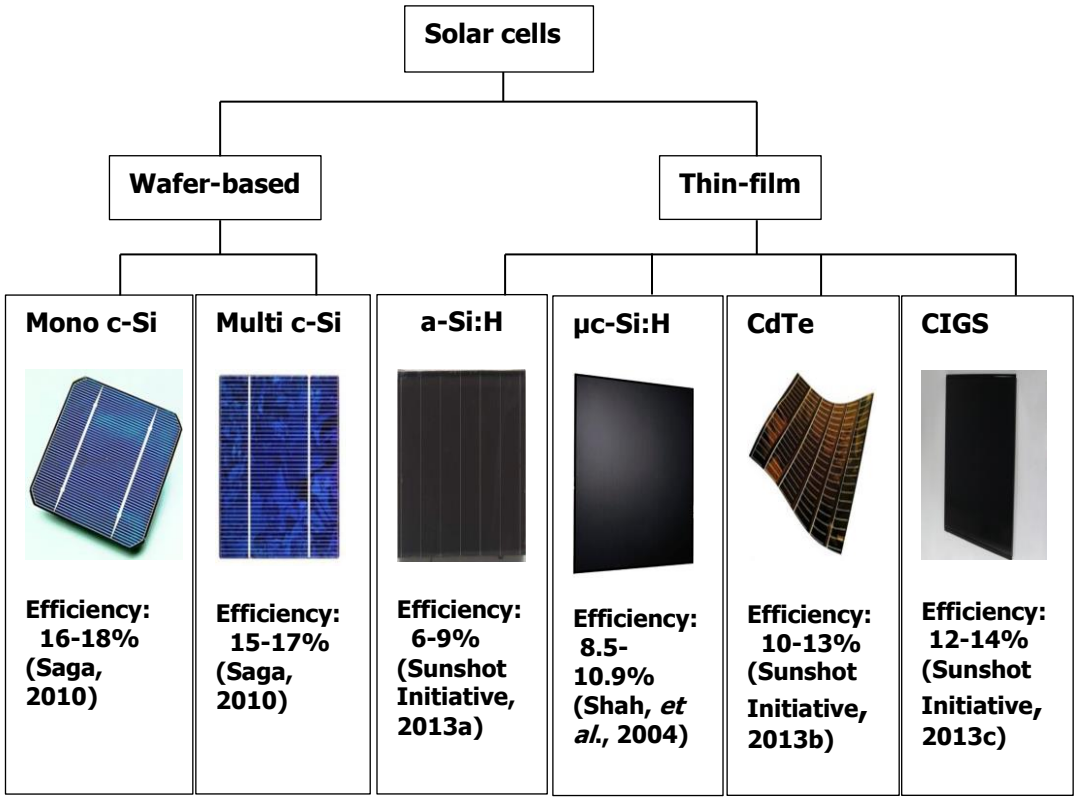


**Figure 2.1 Classification of solar cells and range of conversion efficiency**

Depicted in Fig. 2.2 is the distribution of global PV modules production in terms of technology by major solar cell manufacturing companies in 2014. The figure shows that crystalline silicon solar modules make up the major production by the manufacturing companies accounting for about 43.1$GW_p$ of total production or 90.737%. The market dominance of crystalline silicon PV modules is expected to continue for years as durability of new module types are yet to be fully tested in the field. Therefore, since crystalline silicon PV modules are the dominant modules produced globally with massive applications worldwide as well as higher efficiency compared to other module types, they have been chosen for this study.

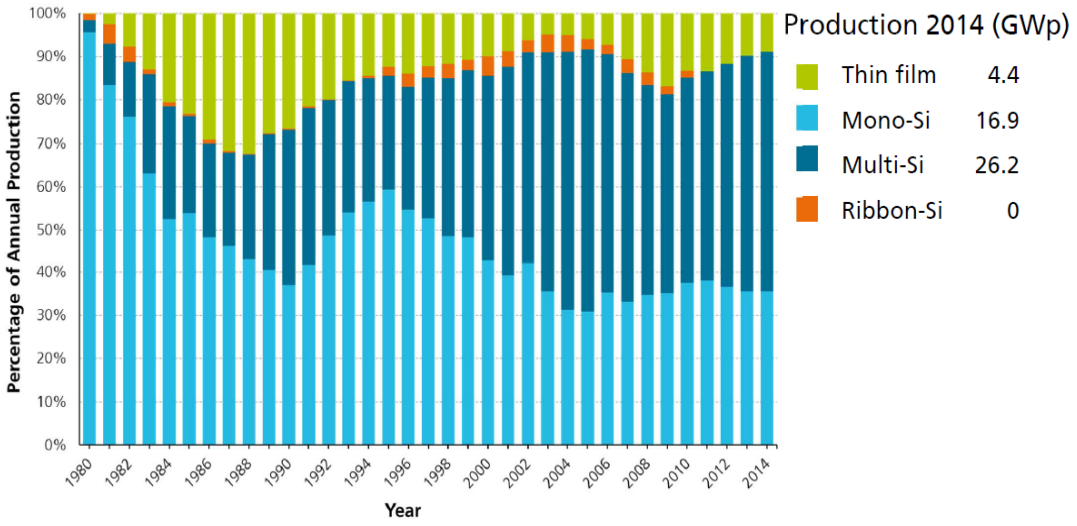


**Figure 2.2 Distribution of global PV modules production in terms of technology by major solar cell manufacturing companies (Burger, *et al.*, 2015).**

It was stated earlier in section 1.2 that global cumulative installed PV capacity was nearly 40 $GW_p$ in 2010. In that same year 2010, global solar cell and module revenue increased by 85% from $16.8 billion in 2009 to $31.1 billion (Ardani and Margolis, 2011). The huge amount of money invested in the PV industry is a testimony to the viability of the industry and the seriousness accorded it by investors.

## 2.3 Crystalline silicon solar cell assembly

This sub-section presents a discussion on crystalline silicon solar cell assembly in four parts. These four parts are: crystalline silicon solar cells, solder joint reliability, interconnection technology and interconnection material.

### 2.3.1 Crystalline silicon solar cells

Wafer-based crystalline silicon solar cells are the most common and widely used solar cells with a production history of over 60 years. The solar cells have a high global capacity for production and also deliver the highest efficiencies of energy conversion. Silicon is the primary feedstock used in the fabrication of crystalline silicon wafers for use in making solar cells. The manufacturing process of solar cells begins with the use of silicon wafer as a base. A layer of emitter material is deposited on this base on which a layer of an anti-reflection coating (ARC) is in turn deposited on. Two layers of silver in grid form are then printed on the cell's semiconductor material such that the metallization penetrates the ARC layer and makes contact with silicon wafer to form the front metal contact and collect electric current generated. The printed contacts are fired. Typically, aluminium contacts are also printed at the back surfaces of the cell material. The typical structure of a c-Si solar cell is shown in Fig. 2.3 and consists basically of seven layers. As can be seen from the figure, a back contact material supports a positive type (P-type) semiconductor layer which also has a negative type (N-type) semiconductor layer on it. The ARC is overlaid on the latter and ensures passage of all light to the silicon crystalline layers while minimizing reflection. A transparent adhesive is deposited on the overlaid coating. This layer is secured by a protective glass cover (Dirjish, 2012).

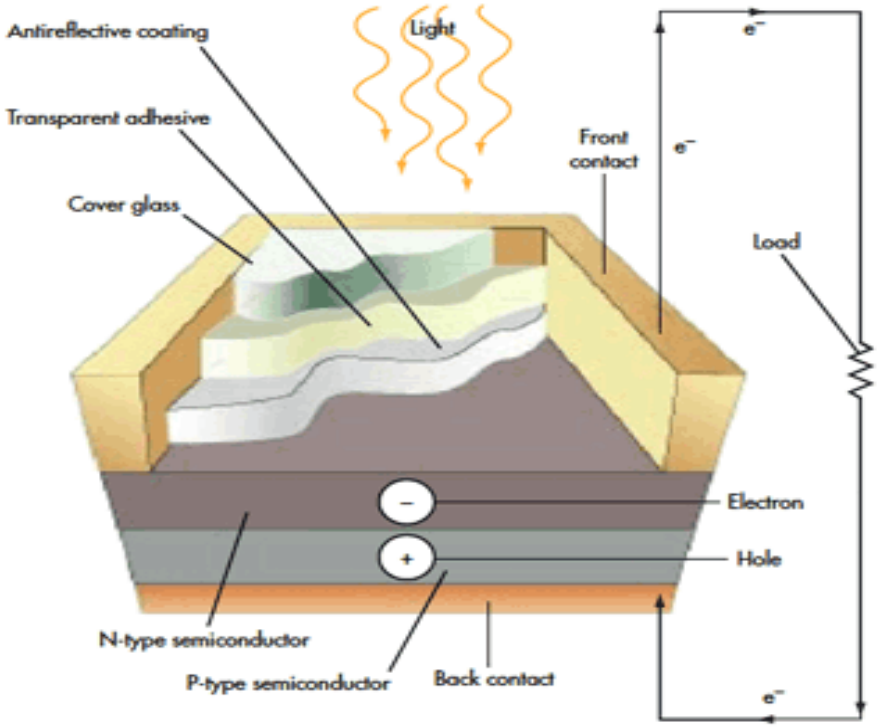


**Figure 2.3 Schematic of a crystalline silicon solar cell (Dirjish, 2012).**

When the cells have been fabricated, they are then interconnected with other cells in series and parallel to form a PV module of the required voltage and current. Presented in Fig. 2.4 is the primary processing steps of wafer-based monocrystalline silicon PV module (Goodrich, *et al.*, 2013) while Fig. 2.5 depicts a typical Packaging of Crystalline Silicon PV Module (Webb and Hamilton, 2011).

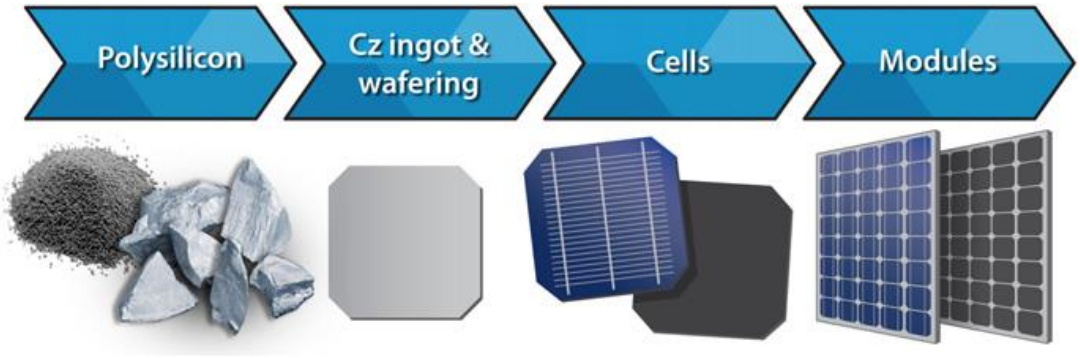


**Figure 2.4 Primary processing steps of wafer-based monocrystalline silicon PV module (Goodrich, *et al.*, 2013).**

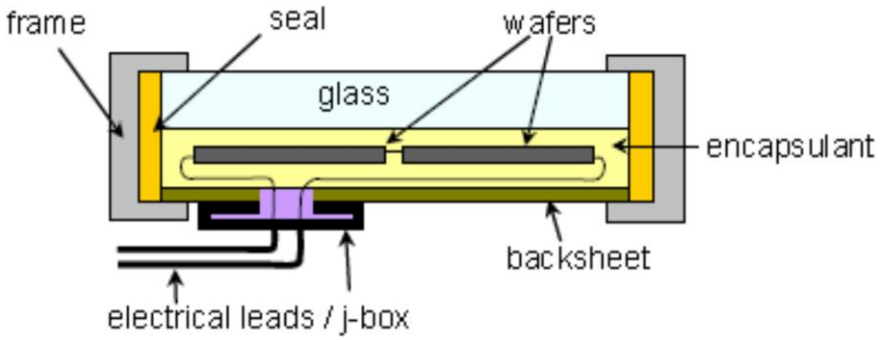


**Figure 2.5 Typical packaging of crystalline silicon PV module (Webb and Hamilton, 2011).**

### 2.3.2 Solder joint reliability

The manufacturing of the PV module should ensure the solder joint maintains integrity and reliability through subsequent manufacturing processes as well as during service conditions. The enhancement of reliability, availability and durability of PV module components is now more critical especially for mission critical systems. The generation of electricity from PV modules depend on local weather which also affects their lifetime. For instance, a module in desert weather is expected to have a shorter

lifetime compared to the one in either a tropical or temperate weather as reported by Han *et al*. (2012). Thus, the higher temperatures in the desert which cause faster degradation of PV modules suggest that temperature has effect on PV module components. Furthermore, studies by various researchers such as Jeong *et al*. (2011), Sakamoto *et al*. (2012), Jeong *et al.* (2012), Skoczek *et al*. (2009) and Granata *et al*. (2009) indicate that diurnal temperature cycle impacts on the PV modules during field operations causing degradation which eventually result in failure of the PV module. Irrespective of weather condition, PV modules undergo degradation whenever they are exposed to daily sunlight due to thermal loading. In addition, Betts (2004) reported that in the majority of situations, passing clouds often cause more than 20$^{o}$C temperature variation multiple times during the day, while the diurnal temperature cycle causes in the range of 12$^{o}$C variation once over a 24 hour period. The effect of these variations is cyclic thermo-mechanical fatigue loading on solar cell solder interconnection resulting in the formation and growth of IMC in the solder joint. Such loading degrades the solar cell assembly and eventually PV module failure occurs.

Photovoltaic modules failure and reliability can be analysed with regards to field service operations. When PV modules are deployed for service operations, their behaviour can be described using reliability "bathtub" curve (Pregelj, *et al*., 2001; Kumar and Sarkar, 2013). Figure 2.6 shows a bathtub curve for a well-designed PV module. It can be observed from the figure that

during service operations, the module undergoes three stages of behaviour. At stage 1 commonly known as 'infant mortality,' the failure rate is high but decreases over time. The next stage is stage 2 known as 'useful life' where the failure rate is constant over a relatively long period of time. The final stage is stage 3 known as the 'wear-out period' where the failure rate sharply increases as the module comes to the end of its designed lifetime. Furthermore, the use of mean time to failures (MTTF) as a random variable is a common approach in reliability engineering which is also applied in the case of PV modules (Pregelj, *et al.*, 2001). It can be assumed that the MTTF can be modelled as Weibull distributed variable and used to predict the failure rate of the PV modules during their field operations. The Weibull distribution is widely used in reliability analysis mainly due to its flexibility and ability to represent the three different periods discussed.

The Weibull distribution is a continuous probability distribution. The probability density function of a Weibull random variable, for instance *X*, is (Klutke, *et al.*, 2003; Teimouri and Gupta, 2013):

$$fX\,(x) = \frac{\beta}{\alpha}\left(\frac{x-\mu}{\alpha}\right)^{\beta-1} e^{-\left(\frac{x-\mu}{\alpha}\right)^{\beta}} \qquad (2.1)$$

for $x > \mu,\ \beta > 0,$ and $\alpha > 0.$ The parameters $\beta, \alpha$ and $\mu$ are known as the shape, scale and location parameters respectively. If the quantity *X* is a "time-to-failure", the Weibull distribution gives a distribution for which the failure rate is proportional to a power of time. In using the Weibull

distribution, the shape parameter β, is assigned to provide more information about the nature of failure mode. As shown in Fig. 2.6 if β<1, the PV module is at stage 1, the burn-in/infant mortality stage with high initial failures. Nonetheless, if β=1, the module is at stage 2, the useful life stage with failures occurring randomly and independent of time. However, if β>1, the module is at stage 3, the wear-out stage with high frequent failures till the end of the projected lifetime of the module.

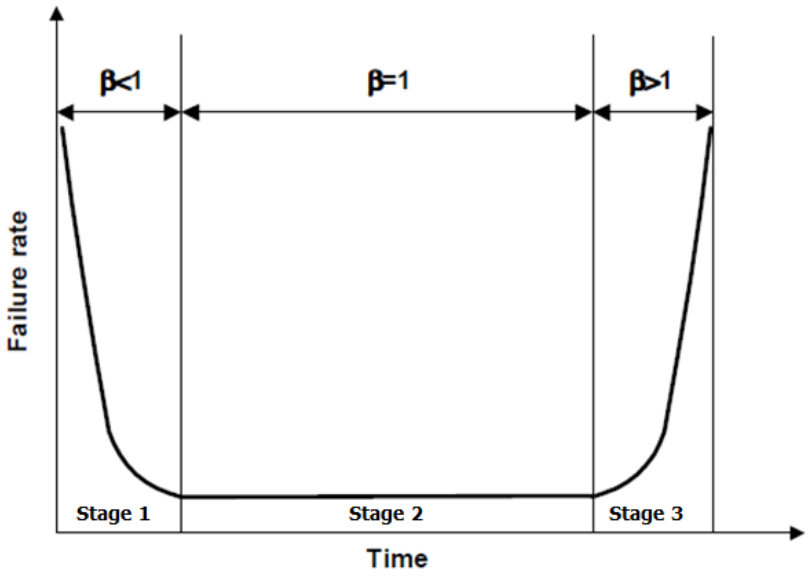


**Figure 2.6 Bathtub curve for a well-designed PV module (Pregelj, *et al.*, 2001)**

Among the components of crystalline silicon PV modules, solder joint is the most critical. The thermo-mechanical reliability of solder joints in crystalline silicon PV modules is of paramount importance as the failure of solder joints implies non-delivery of generated electricity. It is for this reason that there is more concern on the reliability of solder joint compared to the other components in the PV module. The reliability of solder joints can be affected

by a variety of application conditions such as vibration, mechanical shock, thermo-mechanical fatigue, thermal aging and humidity (Lechovič, *et al.*, 2009). However, the focus on thermo-mechanical reliability of solder joints is due to the detrimental effects of thermo-mechanical loading on the joints during service operations. For instance, factors such as passing clouds and diurnal temperature cycle cause temperature fluctuations severely impacting the solder joints although the joints are designed to have the capacity to function effectively within a temperature range of -40$^{o}$C to 85$^{o}$C (Grunow, 2010). Therefore, it is crucial that solder joints are properly designed to provide adequate interconnection throughout the functional lifetime of crystalline silicon PV modules.

### 2.3.3 Interconnection technology

Solder joints are used to interconnect Cu tabbing ribbon with Ag bus-bar in crystalline silicon solar cell assembly as shown in Fig. 2.7. Moreover, crystalline silicon solar cells are interconnected with each other using the conventional 'Z' interconnection technology as presented in Fig. 2.8. In order to carry out the interconnection of the solar cells, printed contacts at the front and back surfaces of the cells are soldered to highly conductive ribbon strips for current transfer from the front of one cell to the back of a neighbouring cell in a series connection (Jeong, *et al.*, 2011). By soldering the solar cells in this form the solder joints function as electrical connection, mechanical support and thermal conduit which make the reliability of the joint multi-faceted. Consequently, the reliability of solder joints can be

affected by a variety of application conditions such as vibration, mechanical shock, thermo-mechanical fatigue, thermal aging and humidity (Lechovic, *et al.*, 2013).

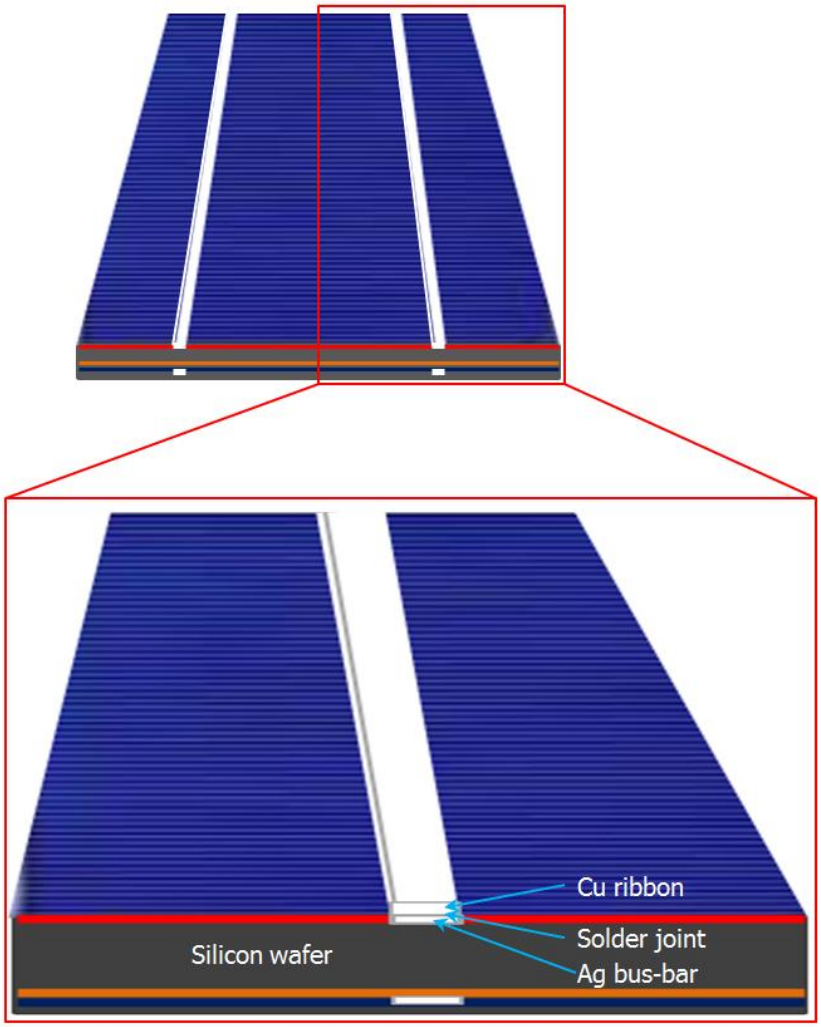


**Figure 2.7 Typical solder joint in crystalline silicon solar cell assembly sandwiched between copper ribbon and silver bus-bar**

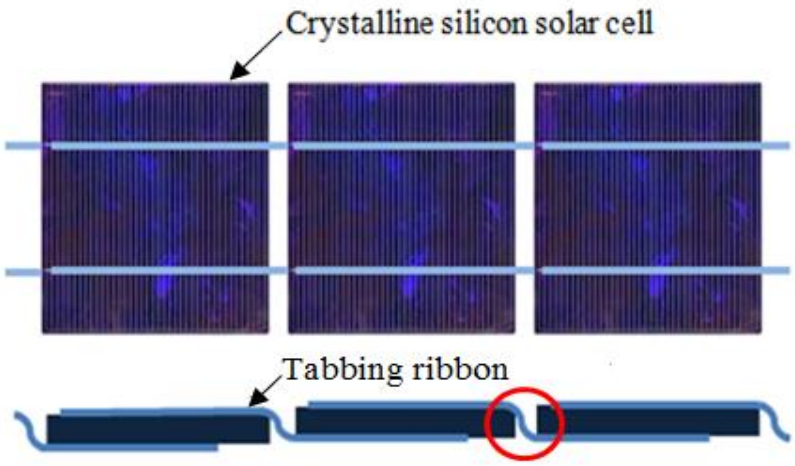


**Figure 2.8 Crystalline silicon solar cells interconnected in series with tabbing ribbon**

This interconnection technology has been used for decades with lead-based solder as the interconnection material. The current situation is that there is a transition from the use of lead-based solder to lead-free solder. This became necessary in order to avoid hazardous lead-based solder which is harmful. Consequently, more understanding of lead-free solder joints in PV modules is crucial to ensure reliable solder interconnection in the modules.

### 2.3.4 Challenges of interconnection technology

McCluskey (2010) and Cuddalorepatta *et al*. (2010) reported that the soldered interconnect joint is the most susceptible part of the assembly. Moreover, in a BP Solar study of PV module field failures, Wohlgemuth (2008) reported that cell/interconnect break accounted for 40.7% of all types of field failures observed. Presented in Fig. 2.9 are all types of field failures observed in that study. The substantial failure of interconnects

demonstrate their crucial role and the need to provide urgent solution to this critical challenge.

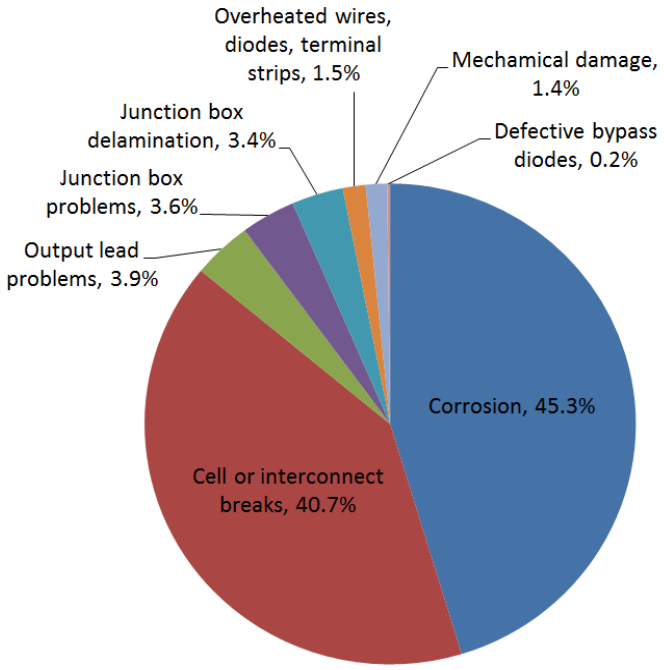


**Figure 2.9 Types of PV module field failures observed (Cuddalorepatta, *et al.*, 2010).**

In addition, the current trend of crystalline silicon solar cells production involves the use of thinner and wider silicon wafers. When cells are made wider, thicker interconnection ribbon is required to conduct larger currents. The thickness of ribbon wire is limited by built-up stresses in the soldered joint. Furthermore, there is a transition from lead-based solders to lead-free solders. Lead-free solders have higher melting points which imply higher thermal stresses on the solder interconnection of solar cells during soldering. These are some of the challenges to the existing soldering technology used

for the interconnection of solar cells; hence in-depth study of PV module solder joint is required to improve reliability.

The assembly of crystalline silicon solar cells results in other associated challenges which limit the quantity of energy generated as well as imparts the thermo-mechanical reliability of PV modules. These challenges include series resistance, shadowing losses and induced thermo-mechanical stress in the solar cells.

Series resistance losses are one of the major challenges associated with the interconnection of solar cells to form PV modules. These losses are created due to metallization for contact formation and the subsequent tabbing for current collection. In order to reduce these losses, new concepts are being developed with additional objectives of providing contacts for thinner wafers. This objective is aimed at: reducing material cost, ensuring low-stress interconnection between cells and enabling the ease of modules manufacture (Löffler, *et al.*, 2010). However, many of the new concepts are not yet viable or commercially acceptable.

Another key challenge of interconnection technology is shadowing losses. When cells are made wider, thicker interconnection ribbon is required to conduct larger currents. It is reported in (Kerschaver and Beaucarne, 2010) that increase in the width of interconnection ribbon cross-section increases the shadowing losses proportionally. The thickness of ribbon strip is limited

by built-up stresses in the soldered joint. The differences in coefficient of thermal expansion between ribbon interconnection materials and silicon account for this stress accumulation (Kerschaver and Beaucarne, 2010; Bultman, *et al*., 2000). Furthermore, stress occurrence at the edge of the wafers due to bending of the interconnection ribbon strip which connects the front side with the rear of the neighbouring wafer (Bultman, *et al*., 2000) impacts the reliability of the assembly. This situation entails that the interconnection technology makes a compromise between width and thickness of ribbon strip. Apart from shadowing losses, there are also recombination losses which are not influenced by interconnection technologies. However, reduction of these losses is desirable to enhance solar cell efficiency. This reduction can be achieved through the use of Laser-Fired Contact (LFC) process, particularly for the rear surface, to fabricate solar cells with a high quality rear surface (Mette, 2007; Zeman, 2009).

Induced thermo-mechanical stress in the solar cells is another challenge associated with the manufacture of solar cells in the current form. The manufacturing process of interconnecting wafer-based silicon solar cells involves the use of infra-red (IR) reflow soldering. The soldering process consists of two phases. These are stringing or tabbing as well as bussing. The former involves the interconnection of solar cells with each other to form strings while the later deals with the assembly of the strings of solar cells to form PV module (Chen, 2012; Grunow, 2010). However, this interconnection procedure is difficult and the IR soldering induces high mechanical stress in

the solder joint which accelerates fatigue related damage. Eventually, module failure occurs during field operations thereby halting energy generation.

### 2.3.5 Interconnection material

Solders, which are used as interconnection material in PV modules, are reviewed to understand their behaviour when undergoing daily thermal cycling. Since IMC has a significant effect on the integrity of solder joint during the daily thermal cycling, it is reviewed in order to obtain adequate information for a more reliable solder joint.

#### 2.3.5.1 Solders

Solders are used extensively as electrical interconnects in PV modules for interconnecting solar cells. Similarly, solders are also used in microelectronics packaging for attaching electronic components to circuit boards. Eutectic or near eutectic tin-lead solders have been the most widely used solder materials because of their low melting temperature, high ductility and good wetting to other metals. On the other hand, the presence of lead in lead-based solders makes the solders toxic with consequences of health and environmental impacts. This concern caused the European Union and Japan to adopt legislation aimed at phasing out lead usage in the electronics industry. In compliance with the recommendation of the National Electronics Manufacturing Initiative (NEMI) (Che, *et al.*, 2005), lead-free solder alloys are now mainly used in the industry as electrical interconnects. Though there are various types of lead-free solders, the most studied and widely used solder materials are SnAg and SnAgCu alloy (Pei and Qu, 2005). When solder

alloy is subjected to thermo-mechanical loading, the alloy undergoes elastic and inelastic deformation. The solder alloy is known to display nonlinear visco-plastic behaviour. Solder deformation primarily comprises elastic, plastic and creep strains (Cuddalorepatta, 2010). The constitutive behaviour of the solder can be represented by constitutive models made from combination of elastic, plastic, viscoelastic and visco-plastic/creep models (Sitaraman and Kacker, 2005). Some researchers have used 96.5Sn3.5Ag solder alloy for soldered assemblies employing shear and tensile loading such as in PV modules (Sitaraman and Kacker, 2005). However, Cuddalorepatta (2010) reported that while modelling a PV module solder interconnection, the relevant partitioned constitutive and durability constants for Sn3.5Ag were not available in literature. Hence constants for near eutectic Sn3.8Ag0.7Cu (SnAgCu) were used because of the similarity of the SnAgCu to Sn3.5Ag. It is vital to use a model that accurately describes the lead-free solder together with appropriate model constants. This is imperative because the thermo-mechanical reliability of PV modules depends mainly on the fatigue and creep behaviour of solder joints.

#### 2.3.5.2 Intermetallic compounds

Solder joints in crystalline silicon PV modules are sandwiched between silicon solar cell wafer and interconnection ribbon commonly made of copper. In this study, Pb-free 95.5Sn-3.8Ag-0.7Cu solder alloy is used. When this solder is used in the soldering process for solar cells interconnection, intermetallic compounds (IMCs) are formed at the solder-copper ribbon interface as well

as at the solder-silver interface through diffusion processes and continue to grow in size through the service lifetime of the module as it operates in the field (Schmitt, *et al.*, 2012; Yang *et al.*, 2014). Predominant IMCs formed in Sn3.8Ag0.7Cu solder joints are $Cu_3Sn$ and $Cu_6Sn_5$ at the solder/Cu interface and $Ag_3Sn$ at the solder/Ag interface (Schmitt, *et al.*, 2012; Che and Pang, 2012a). Factors that the IMC mostly depends on are the composition of solder, temperature and time (Schmitt, *et al.*, 2012). The growth of IMC in the joint has detrimental effects on the quality of the joint and its reliability (Schmitt, *et al.*, 2012). In an experimental study, Schmitt *et al.* 2012) reported that IMCs decrease the performance and reliability of solder joints in PV modules. As the IMC grows, it increases in thickness and creates a diminishing solder volume, hence less reliability of the solder joint. These IMCs play a crucial role in solder joint deformation where inhomogeneous and local strains develop at the interface. When the IMC thickness reaches a particular threshold, failure of the solder joint occurs. This indicates that the development and growth of IMC at the interface of solder and bond region affects the structural integrity of solder joints (Che and Pang, 2012a). Therefore, IMCs are critical in terms of solder joint reliability and need to be considered in reliability analysis. Further study of the effect of IMC thickness on thermo-mechanical fatigue life of solder joint is crucial because the global production of PV modules is predominantly made with wafer-based crystalline silicon solar cells. For instance, in 2013, wafer-based crystalline silicon PV modules accounted for about 90.956% of global module production (Burger, *et al.*, 2014). There is the vital need to improve the

reliability of wafer-based crystalline silicon PV modules which account for greater percentage of PV module production. Figure 2.10 shows a schematic of cross-section of typical crystalline Si solar cell assembly. Specifically, Fig. 2.10(a) shows a typical encapsulated crystalline silicon solar cell assembly with the different components made of various materials. On the other side, Fig. 2.10(b) shows soldered interconnects including IMC layers for the solder-copper and the solder-silver interfaces.

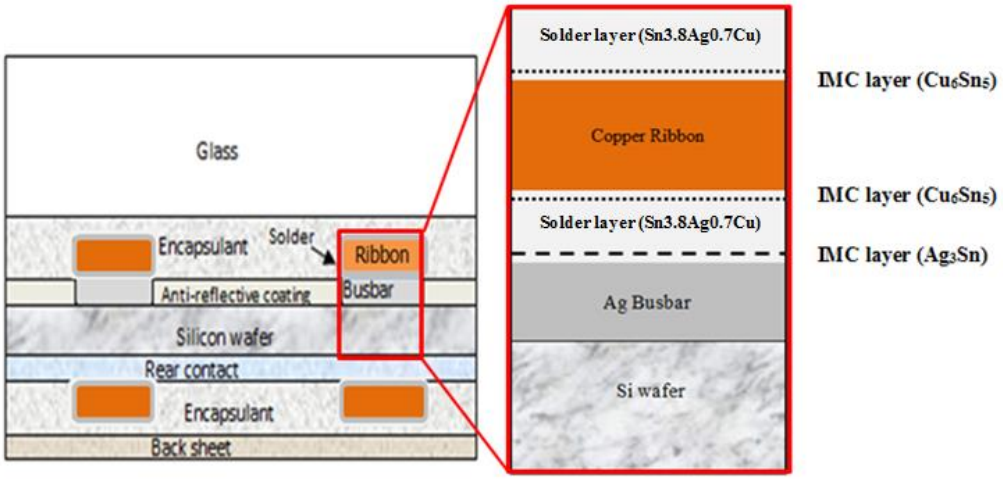


(a) (b)

**Figure 2.10 Schematic of cross-section of typical crystalline Si solar cell assembly showing:**
**(a) Encapsulated solar cell assembly**
**(b) Soldered interconnects including IMC layers**

A number of researchers have conducted previous studies on the effect of formation and growth of IMC on reliability of solder joints in crystalline silicon solar cells. These researchers include references (Schmitt *et al*, 2012), (Jung and Kontges, 2013) and (Yang, *et al*., 2014). The investigations involved the use of experimental methods and also the study of the effect of IMC on the

mechanical strength of solder joints as well as adhesion and durability of the joints. Previous experimental studies by other researchers such as Schmitt *et al*. (2012) and Yang *et al*. (2014) on the formation and growth of IMC layers in crystalline silicon solar cells, results indicated that IMC layer thickness can grow from 0 to 12μm depending on type of solder (lead-based solder or lead-free solder), thermal cycling and other factors. However, this gradual IMC growth cannot be modelled dynamically through finite element modelling. In order to overcome this issue, the usual approach is to build individual geometric models each with a different IMC layer thickness from the other and then simulate each model separately as was done by Che and Pang (2012a). This approach approximates the gradual growth of IMC in the solder joint over time; hence it is adopted and used in this study. The determination of IMC layer thickness to be used in this study was in accordance with values obtained experimentally by other researchers. Literature on research employing finite element modelling to study reliability of interconnection in PV modules which incorporates IMC is scarce - notwithstanding that FEM method is a valuable tool for product design and development (Chiou, *et al*., 2011) and far less costly. Also, in the experimental investigation conducted by Schmitt *et al*. (2012) on lead-free SnAg3.5 solder, it was found that IMC layer thickness grew up to 4μm. Hence, in this study, IMC layer thicknesses ranging from 1μm to 4μm are used to build geometric models as these values are within the experimental range. The FEM method is used in this study to simulate the non-linear creep deformation of solder joints in crystalline silicon solar cell assembly because

many researchers have employed similar method in their investigations on solder joints in other electronic devices. In particular, modelling and simulation study with IMCs included in the geometric models is needed for the determination of damage caused by thermo-mechanical loading on solder joint during thermal cycling and field operations. Such a study where effect of IMC on fatigue damage is determined will enable solder joint fatigue life prediction. Therefore, the unavailability of such a study indicates that there is a gap in knowledge with respect to the effect of IMC on thermo-mechanical reliability of solder joints in crystalline silicon solar cell assembly.

### 2.3.6 Failure of solder joints in PV modules

In Fig. 2.10, it can be observed that solders are used as interconnect material between ribbon and silicon wafer via busbar. For many years of crystalline silicon solar cell production, lead-based solders were used for the interconnection. However, lead (Pb) based solder is hazardous to health, hence the need for a transition from Pb-based solder to Pb-free solder as interconnection material as mentioned earlier. Some typical lead-free solders used in industry for PV module production are listed in Table 2.1. Likewise, Table 2.1 shows other component materials used in encapsulated crystalline silicon modules, material type, thickness and coefficient of thermal expansion (CTE). As the table shows, the CTE of ribbon, solder, bus-bar and Si cell are different. The range of CTEs for module component is from $2.6\times10^{-6}$/K for monocrystalline silicon cell to $30\times10^{-6}$/K for Tedlar backsheet. This indicates

a range of CTEs of magnitude more than 10 times from component with least value of CTE to the one with highest value of CTE. The variation causes large mismatch in the thermal expansion and contraction that occur during module operations and which induce mechanical stresses in the module (Saga, 2010).

Manufacturers of crystalline silicon solar cells produce cells of various surface area dimensions. Interestingly, the manufacturers have been increasing the standard surface area of the cells. In earlier times, the standard surface area of crystalline silicon solar cells was 100 × 100 $mm^2$ (Xakalashe and Tangstad, 2011). Eventually, the surface area of the cells was increased to 125 × 125 $mm^2$. Currently, majority of the cells predominantly multi-crystalline, are manufactured with a surface area of 156 x 156 $mm^2$. Still, it is expected that in the near future, the surface area of the cells will increase further to 210 x 210 $mm^2$ (Jong, 2006; Erath, 2010). When solar cells are made wider, thicker interconnection ribbons are required to conduct larger currents. For instance, solar cells with dimensions of 125 × 125 $mm^2$, 156 x 156 $mm^2$ and 210 x 210 $mm^2$ generate 4-5A, 7-8A and 13-14A of current respectively (Jong, 2006). However the thickness of ribbon strip is limited by built-up stresses in the soldered joint which occur during solder reflow process as well as thermo-mechanical stresses caused by CTE mismatches during thermal cycling. The built-up stresses are commonly known as residual stresses and have been known to affect the flexural strength of

solder joints. Depending on the solder joint thickness, warpage of the solar cell assembly can occur (Lai, *et al.*, 2013). Preferably, solder joint thickness should have adequate capacity to transfer generated current with minimal residual stresses in the joint. In addition, the solder joint should have enough thickness to properly function as a mechanical support as well as a thermal conduit. Furthermore, it can be observed from Table 2.1 that solder joint thickness varies from 0.5μm to 50μm which indicates a wide range in thickness. Considering that the same size of solar cell surface area is used by the manufacturers of either monocrystalline or multi-crystalline silicon solar cells, the wide variation in solder joint thickness shown in Table 2.1 indicates the existence of a gap in knowledge. Predominant solder joint thicknesses used by different manufacturers are usually between the range of 10μm and 40μm (Rogelj, *et al.*, 2012). Based on this range of values, this study used solder joint thickness in the range of 20μm and 30μm in the models.

Another key solder joint parameter is its width. Determining the appropriate solder joint width is critical as there are some associated challenges. One of the challenges associated with solder joint width is its effect on solar cell efficiency. Current solar cells energy conversion efficiencies are remarkable when compared with what was obtainable some years back. For instance, the efficiency of crystalline silicon solar cell was 4% in 1954 (Cutter, 2012, p.31) but increased considerably to lab cell efficiency of 25.6% and 20.8% in 2014 for monocrystalline and multi-crystalline solar cells respectively (Burger, *et al.*, 2015). In order to maximize the solar cell efficiency, the

surface area of the solar cell must have minimal obstruction of the sun rays which is required to generate electricity. However, the conventional interconnection technology of crystalline silicon solar cells requires two or three Cu ribbon strips of a particular width to be soldered unto the surface of the solar cell. The consequence is that the soldered Cu ribbon strips take up valuable surface area of the solar cells thereby casting shadows and reducing the surface area of the cells. The implication of this situation is that the capacity of the solar cells to generate energy from the covered surface is lost. Thus one of the key challenges of conventional interconnection technology is shadowing losses. Kerschaver and Beaucarne (2010) reported that increase in the width of interconnection ribbon cross-section increases the shadowing losses proportionally. The differences in coefficient of thermal expansion between ribbon interconnection materials and silicon account for this stress accumulation (Kerschaver and Beaucarne, 2010; Bultman, *et al*. 2012) Furthermore, stress occurrence at the edge of the wafers due to bending of the interconnection ribbon strip which connects the front side with the rear of the neighbouring wafer (Bultman, *et al*. 2012) impacts the reliability of the assembly. This situation entails that conventional interconnection technology makes a compromise between width and thickness of ribbon strip. However, the ribbon strip is coated with solder which is reflowed during soldering to form a joint with Ag bus-bar as mentioned several times. Consequently, the width of the ribbon strip determines the minimum width of the solder joint. It is desirable that solder joint width is minimized to reduce shadowing losses because the wider the

solder joint, the wider the shadow on the solar cell and the lesser the amount of current generated by the solar cell. An appropriate solder joint width is therefore required to minimize shadowing losses and increase solar cell efficiency. Manufacturers and researchers used various solder joints in crystalline silicon solar cell assembly. The solder joint width used ranges from 1000μm to 3000μm (Cuddalorepatta, 2010; Klengel, *et al.*, 2011; Gierth, *et al.*, 2012). The solder joint width selected for the models in this study are from 1000μm to 1400μm. These solder joints widths were selected so as to minimize shadowing losses which will otherwise occur if wider ones are selected.

Hence, from the foregoing, two gaps of knowledge have been identified thus: the effect of solder joint thickness as well the effect of solder joint width on solder joint thermo-mechanical reliability needs to be investigated in order to obtain more knowledge and understanding towards reliability improvement.

**Table 2.1. Typical component materials used in encapsulated crystalline silicon PV modules**

| Component | Typical Material | Thickness (μm) | CTE ($10^{-6}$/K) |
|---|---|---|---|
| Solar cell (Saga, 2010; Jong, 2006) | Monocrystalline Si | 160-240 | 2.6 |
| | Multicrystalline Si | 200-300 | 3.5 |
| Cover plate (Illuminated side) (Willeke and Weber, 2013, p.144; Webb and Hamilton, 2011) | Glass | 3000-4000 | 10 |
| Encapsulant (Cuddalorepatta, *et al.*, 2010) | EVA | 460-500 | 15 |
| Anti-reflective coating (ARC) (Sopori, et al., 2004; Diebold, 2003; Nagel, et al.,1999; Chuang, et al., 2004) | Titanium Oxide ($TiO_2$) | 0.05-0.1 | 8-10 |
| | Silicon Nitride ($SiN_x$) | 0.07-0.1 | 1.67-2.3 |
| Solder (Wirth, 2010; Rogelj, et al., 2012; Moyer, et al. 2010) | 96.5Sn/3.5Ag | 10-40 | 20.2-21.7 |
| | 95.5Sn/3.8Ag/0.7Cu | 10-40 | 17.6-23.2 |
| Tabbing ribbon (Wiese, et al., 2010) | Copper (Cu) | 75-200 | 16.5-17 |
| Bus-bar (Front contact) (Zemen, et al., 2012; Moyer, et al. 2010, Wiese, et al., 2010) | Silver (Ag) | 8-28 | 9.8-18 |
| Rear contact (Chen, et al., 2008; Wiese, et al., 2010) | Aluminium/Silver (Al/Ag) | 15-40 | 11.9 |
| Back sheet (Armstrong and Hurley, 2010; Arangu, et al., 2014) | Tedlar | 100-325 | 30 |

Solder joints are inhomogeneous and consist of different materials. While in field operations, PV modules are exposed to daily thermal cycling which affect the solder material. The repeated thermal cycling results in the accumulation of strain energy in the joint. Solder material is made up of grain structure which is inherently unstable (Engelmaier, 1997). Under thermal loading, the grain structure reduces the accumulated internal energy of a fine-grained structure by growing in size. Elevated temperatures and induced strain energy enhances the grain growth process. As the grains grow, contaminants concentrate increasingly at the grain boundaries thereby

weakening these boundaries. Figure 2.11 shows the effects of accumulating fatigue damage in solder joint structure. It can be observed from the figure that at the initial stage, the solder material is made up of fine-grained structure. After about 25% of the fatigue life has been consumed, micro voids can be found at the grain boundary intersections. Over time, these micro-voids grow into micro-cracks after about 40% of the fatigue life. Eventually, these micro-cracks grow and coalesce into macro-cracks leading to total fracture.

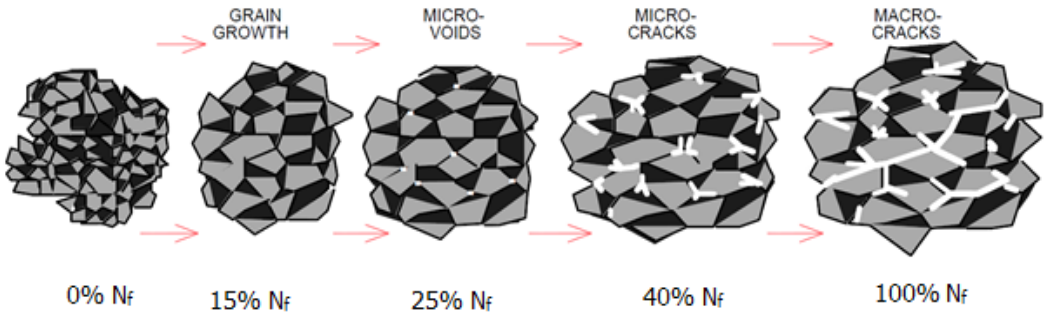


**Figure 2.11 Effects of accumulating fatigue damage in solder joint structure (Engelmaier, 1997)**

This failure mechanism is caused by thermo-mechanical fatigue loading of the joint and it is time-dependent. Figure 2.12 shows a SEM image of fatigue damage in solder interconnection which has been subjected to long-term field operations. Fatigue degradation in solder interconnects is caused by repeated operational and environmental elevated temperature excursions (Saga, 2010). These excursions induce cycles of stress in the joint. The induced stress is occasioned by the differences in CTE of the bonded

materials which includes ribbon, busbar and solder materials. Thus, the parameter of solder joint should be designed with consideration of the differences in CTE such that minimal stress is induced in the solder joint during expansion and contraction of the joint. It is important to avoid high flexural stiffness which inhibits adequate expansion and contraction of the joint during thermal cycling. The flexural stiffness depends on the thickness of solder joint such that the thicker the joint, the stiffer it is. Therefore, proper solder joint thickness should be used to prevent inducing high cycles of stress arising from the cyclic loading. There are many observable phenomena associated with this type of loading. The interconnection could experience metal segregation, grain boundary coarsening/cracking, increased series resistance and heating. These observations cause loss of connection (Klengel, *et al.*, 2011; Schmitt, *et al.*, 2012) which has been classified as a type of failure mode. This situation is worse when the solder bond is poor. Thus, proper solder bond need be formed especially with lead-free solders which have about 40$^{o}$C higher melting point than lead-based solders (Schmitt, *et al.*, 2012).

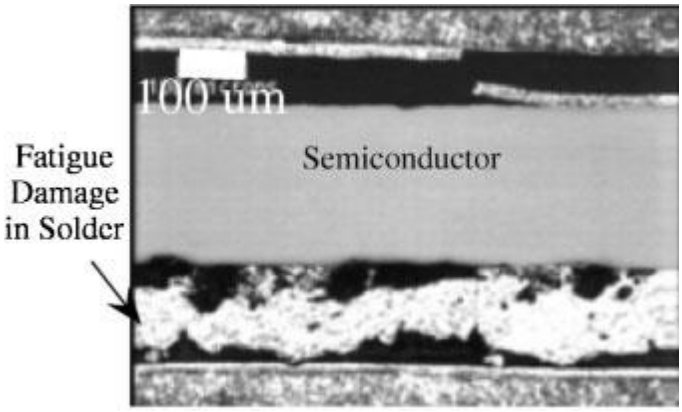


**Figure 2.12 SEM image of solder in solar cell assembly subjected to long-term field exposure showing significant solder fatigue damage (Saga, 2010).**

Solder joint fatigue damage is critical to the thermo-mechanical reliability of the joint. Therefore, the determination of accurate fatigue damage is essential for improving the number of cycles to failure of solder joints in order to ensure reliable PV module performance. Wohlgemuth *et al*. (2010) recommended the use of multiple solder bonds on each tabbing ribbon as well as the use of softer ribbon and provision for stress relief as ways for alleviating solder bond failures. However, by knowing and quantifying the fatigue damage in solder joints, the joints can be designed and built to withstand the damage and avoid premature failures. The design of the solder joint involves using appropriate parameters especially solder joint thickness and width in addition to consideration for IMC thickness. Furthermore, it is necessary to analyse the effect of solder joint thickness on flexural stiffness in order to avoid constraining the joint from suitable expansion and contraction during thermal cycling. In addition, the effect of the combined parameters on solder joint damage needs to be investigated. Therefore, there is a gap in knowledge on the effect of solder joint

parameters on solder joint fatigue damage. The acquisition of this knowledge will be useful in the prediction of solder joint fatigue damage and in the design of robust solder joints in PV modules thereby ensuring thermo-mechanical reliability and quality assurance.

As discussed earlier, crystalline silicon PV modules have remain dominant due to their advantages such as decades of proven technology, higher efficiency than most of their thin-film competitors, decreasing cost of production as well as increasing demand. Since this trend is expected to continue for a long time, certain aspects of the manufacturing technology of crystalline silicon PV modules such as solder joint interconnection still need to be improved especially with the module expected to last up to 25 years. Hence, this situation warrant optimization of solder joint design parameters particularly solder joint thickness and solder joint width as well consideration of IMC thickness at the solder interfaces. It is desirable that solder joint width is minimized to reduce shadowing losses because the wider the solder joint, the wider the shadow on the solar cell and the lesser the amount of current generated by the solar cell. Conversely, the solder joint thickness should have adequate capacity to transfer generated current to the desired point with minimal stress. Moreover, it is desirable that optimal solder joint thickness and width are such that minimal accumulation of creep strain energy density occurs in the solder joint in order to enable longer fatigue life.

It is known that accelerated thermal cycling (ATC) tests are usually used to experimentally determine the thermo-mechanical reliability of a package (Huan, 2010). However, the process consumes time and is costly. A better option is numerical analysis of thermo-mechanical reliability of devices as performed by several researchers such as Ladani (2010) and also Yang and Tan (2010). Such numerical evaluation enables faster, low-cost and efficient determination of thermo-mechanical reliability of solder joints before the device or product is manufactured. Therefore, in this study, numerical evaluation is carried out to optimize solder joint design parameters with focus on solder joint thickness and solder joint width as well IMC thickness which forms and grows at the solder interfaces. This will enable the design of an optimal solder joint in solar cell assembly with the required thermo-mechanical reliability.

### 2.3.7 Theoretical analysis of effect of solder joint thickness on flexural stiffness

As mentioned earlier, during the thermal cycling of solder joints in solar cell assembly, the joints undergo expansion and contraction. In effect, the solder joints experience bending moments and deflection under loading. The deflection of the solder joint under loading is dependent on its flexural stiffness. The flexural stiffness of solder joint is a measure of its resistance to bending. Basically, flexural stiffness of solder joint is the product of the material stiffness (*E*, which is Young's modulus of elasticity) and the second

moment of area ($I$, which describes the stiffness generated by the cross-sectional geometry of the solder joint); rephrased from reference (Etnier, 2001). The flexural stiffness of the solder joint depends on its material properties and geometry. The geometry of solder joint in solar cell assembly is assumed to be rectangular consisting of solder joint thickness, width and length. However, the critical dimensions of solder joint are the thickness and width which form the cross-sectional area where load is applied. Depending on the flexural stiffness of solder joints, deflection of the joints maybe severe especially if the solar cell assembly is subjected to large thermo-mechanical load. Therefore, the relationship between flexural stiffness and solder joint thickness and its effect on the thermo-mechanical reliability of solder joint is investigated using the varied solder joint thicknesses. This theoretical analysis is aimed at putting into perspective the effect of solder joint thickness on flexural stiffness and relating it to the subsequent simulation results.

Figure 2.13 shows a schematic cross-section of solar cell assembly. Figure 2.13(a) portrays the assembly in a horizontal position while Fig. 2.13(b) shows the assembly as a cantilever carrying concentrated load. Furthermore, Fig. 2.13(b) indicates the path of deflection when the concentrated load is applied.

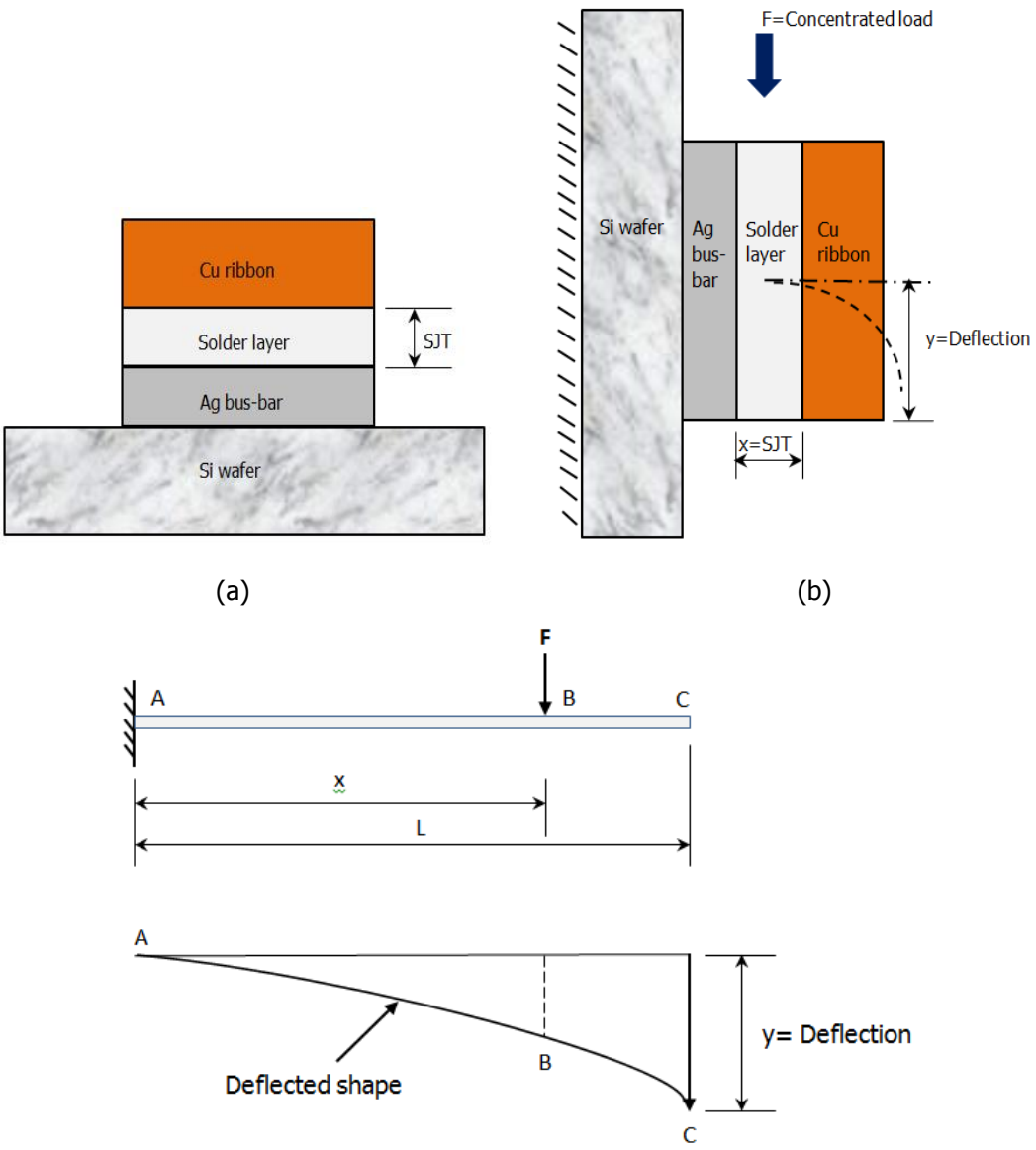


**Figure 2.13 Schematic of solder joint in Si solar cell assembly showing:**
**(a) Assembly in a horizontal position**
**(b) Assembly as a cantilever carrying a concentrated load**
**(c) Simple cantilever of the solar cell assembly**

Considering the configuration of solder joint shown in Fig. 2.13 as a cantilever carrying a concentrated load *F*, the deflection is given as (Benham, *et al.*, 1996, p.190):

$$y = \frac{F}{2EI}\left(Lx - \frac{L^3}{3}\right) \tag{2.2}$$

where $E$ is Young's modulus and $I$ is second moment of area of solder joint. But at the point of load application, $x$ is component length, $L$. Therefore, replacing $x$ with $L$ in Eq. 2.2 gives:

$$y = \frac{F}{2EI}\left(L^3 - \frac{L^3}{3}\right)$$

Thus

$$y = \frac{FL^3}{3EI} \tag{2.3}$$

From Fig. 2.13, the component length, $L$ corresponds to the solder joint thickness which is designated as $T_{SJ}$. Replacing $L$ with $T_{SJ}$ and substituting into Eq. 2.3 the following equation is obtained for solder joint deflection:

$$y = \frac{F\left(T_{SJ}\right)^3}{3EI} \tag{2.4}$$

It is vital to determine the flexural stiffness of solder joint in order to assess its effect on thermo-mechanical reliability of the joint. As stated earlier, flexural stiffness of solder joint is the product of the Young's modulus of elasticity $E$, and the second moment of area $I$. Thus, the flexural stiffness can be expressed as follows:

$$Flexural\ stiffness, K = E \times I \tag{2.5}$$

But $I$ is the second moment of area about the centroid and is given by:

$$I = \frac{bh^3}{12} \tag{2.6}$$

where in Fig. 2.13 $b$ is solder joint thickness, $T_{SJ}$ and $h$ is solder joint width which is designated as $W_{SJ}$. Substituting $I$ in Eq. 2.5 with Eq. 2.6 gives:

$$K = E \times \frac{(T_{SJ})(W_{SJ})^3}{12}$$

Let $C = \frac{E}{12}$ then flexural stiffness in solder joint of solar cell assembly is:

$$K = C(T_{SJ})(W_{SJ})^3 \tag{2.7}$$

## 2.4 Fatigue life prediction of solder joint

Thermo-mechanical reliability of solder joints in PV modules is crucial in ensuring continuous power supply by the module. During service operations, PV module components including solder joints are subjected to daily temperature fluctuations caused by solar energy and heat dissipation in the module package. This develops thermally-induced stresses in the module components causing thermal expansion mismatch between the different materials of the assembly thereby impacting the solder joint. Due to the daily diurnal temperature variation arising from the rotation of the sun as well as passing clouds, the thermal loading on the solder joint is cyclic resulting in stress reversals with the potential of inelastic strain accumulation in the solder joint. This inelastic strain accumulates with repeated cycling causing weakness and structural damage in the solder joint, resulting in creep deformation and fatigue. The mechanism of creep depends on temperature and stress. For low cycle fatigue loadings with low temperature ramp

velocities solder creep is the most important contributor to deformation. In this study, the stress and strain values will be obtained from simulation results. A typical deformation characteristic of solder joint is usually presented in graph form. Figure 2.14 shows a typical creep curve of solder joint under constant stress condition. It can be observed from Fig. 2.14 that under constant stress, the solder joint undergoes deformation in four stages. The first stage consists of the initial elastic and plastic strain in the solder joint due to the initial application of load. As time goes on, the joint experiences a gradual increase in strain at the second stage also known as the primary creep stage. At that stage the strain rate is relatively high, but slows with increasing time. This is due to work hardening in the joint. The third stage is the secondary creep stage where the creep rate eventually reaches a minimum and becomes almost constant. This stage is also known as steady-state creep. Ultimately, the fourth stage is reached which is the tertiary stage where the creep rate accelerates exponentially with stress due to necking phenomena. This leads to final fracture of the solder joint.

The solder materials in solar cell assemblies are subjected to thermo-mechanical loads during accelerated thermal cycling tests as well as in service operation. The resultant effect of the loads is deformation of the solder material. This is due to mismatch of coefficient of thermal expansion (CTE) of silicon wafer, silver bus-bar, solder, copper ribbon strip and other components. The mismatch leads to thermo-mechanical induced non-linear

deformation in the solder joint of solar cell assembly. The induced deformations in the solar cell assembly cause the solder materials to develop cyclic inelastic plastic and creep strains which cause cumulative fatigue damage resulting in failure of the solder joints (Pang, 2012; Hund and Burchett, 1991). This occurs when the cyclic strain increases to a particular high value and the ensuing damage in the solder material cause fatigue cracking in the solder joints thereby resulting in premature failure of the PV module's functional life (Hund and Burchett, 1991). Creep of a solder material is often characterized by its steady state creep strain rate (Pang, 2012). According to Che and Pang (2004), the steady state creep model of solder is of major concern due to its contribution to total creep deformation.

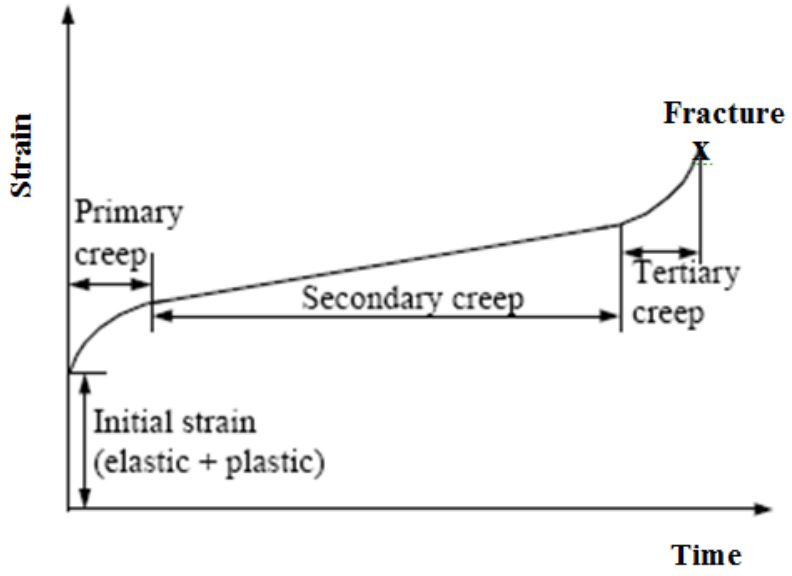


**Figure 2.14 Typical creep curve of solder joint under constant stress condition (Dwayne, 2009)**

Solders have fatigue lifetime such that as the thermal loading continues, the ultimate resultant effect is solder joint cracking and interconnect failure. Fatigue life prediction has become necessary with the migration from lead-

based solders to lead-free solders in the electronics industry. In the PV industry, the use of SnAgCu solder alloy has become widespread for interconnecting solar cells, hence the need for proper prediction of fatigue failure of SnAgCu solder joints. Additionally, the use of fatigue life prediction lessens design cycle time thereby reducing the use of experimental testing to evaluate reliability of solder joints. However, in order to carry out prediction, life prediction models are needed to evaluate reliability at the solder joint design stage. Consequently, appropriate fatigue models are used in predicting the service lifetime of solder joints in PV modules. In this situation, four key factors that should govern fatigue life prediction are: material behaviour, simulation techniques, fatigue life prediction methodology and test data. The material constitutive model for lead-free SnAgCu solder alloy is vital in the development of thermo-mechanical model for fatigue prediction. The constitutive model for lead-free SnAgCu solder alloy usually consists of creep and visco-plastic models for describing solder behaviour (Sitaraman and Kacker, 2005). Appropriate constitutive models are used to predict number of cycles to failure of solder joint, hence predicting fatigue life of the joint.

### 2.4.1 Constitutive model for SnAgCu Solder

This sub-section presents a discussion on the constitutive material model for SnAgCu solder used in this research to study solder joints in crystalline silicon solar cell assembly.

### 2.4.1.1 Creep models

Solder joints in solar cell assemblies undergo thermo-mechanical loading during accelerated thermal cycling tests as well as in field service. Creep deformation occurs in a solder joint when thermo-mechanical loading is imposed on the solder joint and it deforms over time to reduce the load. Several researchers have developed constitutive models to describe the elastic and inelastic deformation behaviour of solder alloys. In particular, a number of researchers have proposed constitutive models for SnAgCu solder alloys. Some of these proposed constitutive relations for SnAgCu solder alloys were compiled by Syed (2004) and are presented in Table 2.2.

**Table 2.2 Constitutive relations for SnAgCu solder (Syed, 2004)**

| Proponent | Constitutive model | Parameter and value |
|---|---|---|
| **Wiese *et al.* (2003)** | $\dot{\varepsilon}_{cr} = A_1 exp\left(\frac{H_1}{kT}\right)\left(\frac{\sigma}{\sigma_n}\right)^{n_1} + A_2 exp\left(\frac{H_2}{kT}\right)\left(\frac{\sigma}{\sigma_n}\right)^{n_2}$ | **$A_1$=4E-7$s^{-1}$, $H_1/k$=3223(K), $n_1$=3.0, $A_2$=1E-12$s^{-1}$, $H_2/k$=7348(K), $n_2$=12, $\sigma_n$= 1Mpa, E(MPa)=59533-66.667T(K)** |
| **Schubert *et al.* (2003)** | $\dot{\varepsilon}_{cr} = A_1[sinh(\alpha\sigma)]^n exp\left(\frac{-H_1}{kT}\right)$ | **$A_1$=277984$s^{-1}$, α=0.02447$MPa^{-1}$, n=6.41, $H_1/k$=6500(K), E(MPa)=61251-58.5T(K), CTE=20.0ppm/K, Poisson's ratio=0.36** |
| **Zhang *et al.* (2003)** | $\dot{\varepsilon}_{cr} = A_1[sinh(\alpha\sigma)]^n exp\left(\frac{-H_1}{kT}\right)$ | **$A_1$=143.4$s^{-1}$, α=0.108$MPa^{-1}$, n=3.7884, $H_1/k$=7567(K), E(MPa)=24224-0.0206T(K)** |
| **Morris *et al.* (2003)** | $\dot{\varepsilon}_{cr} = A_1 exp\left(\frac{H_1}{kT}\right)\left(\frac{\sigma}{\sigma_n}\right)^{n_1} + A_2 exp\left(\frac{H_2}{kT}\right)\left(\frac{\sigma}{\sigma_n}\right)^{n_2}$ | **$H_1/k$=11425(K), $n_1$=6.6, $H_2/k$=9020(K), $n_2$=10.7, G(MPa)=27360-40.5T(K)** |

According to Syed (2004), the constitutive relation proposed by Wiese *et al.* (2003) shown in Table 2.2 consists of two identified mechanisms for steady

state creep deformation for bulk Sn4.0Ag0.5Cu solder. The mechanisms were attributed to climb controlled or low stress and combined glide/climb or high stress behaviour which represents steady state creep behaviour using double power law model.

Also in Table 2.2 is the constitutive model proposed by Schubert *et al.* (2003) after testing several SnAgCu solder compositions as follows: Sn3.8Ag0.7Cu, Sn3.5Ag0.75Cu, Sn3.5Ag0.5Cu and Castin$^{TM}$. Syed (2004) explains that two regions for stress-strain rate behaviour were identified by Schubert *et al.* (2003) where they postulated the high stress region as power law break-down region, and chose hyperbolic sine function to simulate creep behaviour.

Similarly, the constitutive model proposed by Zhang *et al*. (2003) in Table 2.2 is a hyperbolic sine function and data was generated from single lap shear specimen of Sn3.9Ag0.6Cu solder alloy as stated by Syed (2004). Furthermore, Zhang *et al*. (2003) also postulated power law break-down at high values of stress using hyperbolic sine function to model the steady state creep behaviour of the solder. The fourth constitutive model in Table 2.2 was proposed by Morris et al and it is also a double power law model like the first model. As explained by Syed (2004), it was developed using single lap shear specimens of Sn3.0Ag0.5Cu solder joints. In this case, for the low and high stress regions, the stress exponents of 6.6 and 10.7 respectively were suggested. One of the solder constitutive models commonly used in finite

element analysis (FEA) is the Garofalo-Arrhenius creep model. The Garofalo-Arrhenius creep model is basically the Schubert *et al.* (2003) model shown in Table 2.2 and is also known as hyperbolic sine creep equation. Creep of a solder material is often characterized by its steady-state creep strain rate (Pang, 2012). The solder is assumed to exhibit elastic, bilinear kinematic hardening after yield.

A number of researchers such as Cuddalorepatta *et al*. (2010) and Kraemer *et al*. (2013) in their study on durability of solder interconnect in PV cells and mechanical integrity of different types of PV modules respectively used the hyperbolic sine creep equation for modelling and simulation. Thus in this study, the hyperbolic sine creep equation is used to simulate the creep behaviour of Sn3.8Ag0.7Cu solder joints. The steady state creep strain rate is given by (Syed, 2004):

$$\dot{\varepsilon}_{cr} = A_1[sinh(\alpha\sigma)]^n exp\left(\frac{-H_1}{kT}\right) \tag{2.8}$$

This equation is then re-written into equation (2.9) in the required format of input for implicit Garofalo-Arrhenius creep model:

$$\dot{\varepsilon}_{cr} = C_1[sinh(C_2\sigma)]^{C_3} exp^{-C_4/T} \tag{2.9}$$

The constants $C_1$, $C_2$, $C_3$ and $C_4$ are parameters for Sn-3.8Ag-0.7Cu solder and are presented in the Table 2.3:

**Table 2.3 Garofalo creep parameters for Sn3.8Ag0.7Cu solder (Syed, 2004)**

| Parameter | $C_1$ (1/s) | $C_2$ $(MPa)^{-1}$ | $C_3$ | $C_4$ (K) |
|---|---|---|---|---|
| Value | 2.7798E+05 | 2.447E-02 | 6.41 | 6500 |

### 2.4.2 Life prediction models

The fatigue life of solder subjected to thermal cycling is usually predicted using fatigue life prediction models. One of the commonly used fatigue life prediction models is the hyperbolic sine constitutive equation. The hyperbolic sine constitutive equation is a damage mechanism-based life prediction model. The primary damage mechanism for SnAgCu solder during thermal cycling is creep and it is used to simulate the material behaviour. Therefore, the life prediction model has to be theoretically based on creep deformation (Syed, 2004). The creep deformation is stored internally throughout the volume of the solder joint as creep strain energy. Creep strain energy per unit volume of material is referred to as creep strain energy density. Creep damage accumulates in the solder joint in the form of creep strain and creep strain energy density. Life prediction models containing creep strain and creep strain energy density have been developed to predict fatigue life of solder joints subjected to thermal cycling loading. There are two common life prediction models used to predict fatigue life of solder joints. One of the models contains accumulated creep strain while the other contains accumulated creep strain energy density. Fatigue life of solder joints are determined using number of repetitions or cycles to failure. The fatigue life is

also referred to as mean-time-to-failure (MTTF). Table 2.4 outlines creep fatigue life models for SnAgCu solders.

Syed (2004) reports that both accumulated creep strain and energy density models were obtained through experimental studies and can be used for life prediction with acceptable results. Therefore these two models are hereby further described. The number of repetitions or cycles to failure using accumulated creep strain is given by (Syed, 2004):

$$N_f = (C' \varepsilon_{acc})^{-1} \quad (2.10)$$

Similarly, number of repetitions or cycles to failure using accumulated creep energy density per cycle is given by (Syed, 2004):

$$N_f = (W' w_{acc})^{-1} \quad (2.11)$$

Where, $N_f$ = Number of repetitions or cycles to failure

$\varepsilon_{acc}$ = Accumulated creep strain per cycle

$\varepsilon f$ = Creep ductility or the strain at the onset of failure

$C' = {}^{1}/_{\varepsilon f}$ inverse of creep ductility

$W'$ = Creep energy density for failure

$w_{acc}$ = Accumulated creep energy density per cycle

**Table 2.4 Predictive creep fatigue life models for SnAgCu solder (Syed, 2004)**

| S/No | Name of creep fatigue life model | Model |
|---|---|---|
| 1 | Partitioned accumulated strain (Double power) | $N_f = (0.106\mathcal{E}_{acc}^{I} + 0.045\mathcal{E}_{acc}^{II})$ |
| 2 | Total accumulated strain | $N_f = (0.0468\mathcal{E}_{acc})^{-1}$ |
| 3 | Creep energy density | $N_f = (0.0015w_{acc})^{-1}$ |
| 4 | Accumulated creep strain (Hyperbolic) | $N_f = (0.0513\mathcal{E}_{acc})^{-1}$ |
| 5 | Creep energy density (Sine) | $N_f = (0.0019w_{acc})^{-1}$ |

The value of the accumulated creep strain induced or accumulated creep energy density per cycle in a solder joint is calculated and used to determine the number of cycles to failure. The constants $C'$ and $W'$ have been experimentally determined to be 0.0513 and 0.0019 respectively (Syed, 2004). Though both Eq. 2.10 and Eq. 2.11 predict number of cycles to failure of solder joint, Eq. 2.11 is preferable as it gives more accurate results compared with Eq. 2.10 (Syed, 2004). This is because creep strain energy density used in Eq. 2.11 is a robust damage indicator of solder joint as it is based on the deformation internally stored throughout the volume of the joint during thermal loading hence creep strain energy density captures the entire deformation in the joint. On the other hand, creep strain accumulates in the solder joint over three different stages of creep and the accumulated creep strain value obtained is less adequate as a damage indicator when compared with creep strain energy density. Therefore, in this study, Eq. 2.11 is used for prediction of solder joint fatigue life. In practice, the averaged value of change in accumulated creep energy density per cycle ($\Delta\omega_{acc}$) is commonly used for calculating cycles to failure. To obtain the averaged accumulated creep energy density per cycle ($\Delta\omega_{acc}$), the average change in

strain energy density, $\Delta W_{ave}$, is calculated from simulation results and must be normalized by the volume of the solder elements used for fatigue analysis. The volume-averaged method has been widely used by other researchers such as Syed (2004), Pang and Che (2006) and Che and Pang (2012b) for the calculation of the accumulated creep energy density per cycle in solder joints. The use of volume averaging technique minimizes the effect of mesh sensitivity as well as stress concentration on solder joint fatigue life prediction. The averaged change in strain energy density obtained through the volume-averaged method is given as (Pang and Che, 2006; Che and Pang, 2012b):

$$\Delta W_{ave} = \frac{\sum_{i}^{n} W_2^i . V_2^i}{\sum_{i}^{n} V_2^i} - \frac{\sum_{i}^{n} W_1^i . V_1^i}{\sum_{i}^{n} V_1^i} \tag{2.12}$$

Where $W_2^i$, $W_1^i$ is the total accumulated strain energy density in one element at the end point and the starting point of one thermal cycle respectively, $V_2^i$, $V_1^i$ is the volume of element at the end point and start point of one cycle respectively, and n is the number of selected elements to calculate averaged strain energy density. Furthermore, it is known that the averaged strain energy density is sensitive to the elements selected for fatigue analysis. This is because the peripheral area of the solder joint interface has higher stress concentration under thermal cycling loading compared to the centre area of the interface. It is due to this situation that solder joint crack initiation commences from the peripheral area and propagates to the centre of the

joint eventually resulting in complete failure of the joint. Hence, the outermost elements are selected for averaging volume of solder joint for fatigue life prediction. Generally, the damage in solder joint is averaged over 10% of volume consisting of the elements in the critical site (Ladani, 2008). Such approach provides adequate values in the prediction of solder joint fatigue life.

## 2.5 Summary

In this chapter, a review of relevant literature on PV modules including the various types of solar cell was presented. The review focussed particularly on crystalline silicon solar cell assembly and its solder joint interconnection. It revealed that there are associated challenges with the predominant interconnection technology used in the manufacture of crystalline silicon solar cell assembly which involves soldering of copper ribbon on the surface of the cells. This interconnection technique is not ideal because the soldering process induces thermo-mechanical stresses in the cells as well as in the solder joints. In addition, interconnecting copper ribbon on the front-to-back surface of solar cells results in significant series resistance and shadowing losses. During the field operations of crystalline silicon PV modules, the solder joints experience thermo-mechanical loading, IMCs are formed and continue to grow; solder joints degrade and shadowing losses caused by solder joint width reduce solar cell efficiency. As the thermo-mechanical loading continues, solder joints may eventually fail sometimes prematurely.

In order to avoid premature failure of solder joints, the geometry of the joints must be properly designed and optimized taking into consideration the issue of IMC growth as well as solder joint thickness and width. Moreover, exact solder joint damage determination is vital for accurate fatigue life prediction.

Based on the review results, four gaps in knowledge were identified highlighting the effects of:

- Intermetallic compound (IMC) on thermomechanical reliability of solar cell solder joint.
- Solder joint thickness on the thermo-mechanical reliability of the joint.
- Solder joint width on the thermomechanical reliability of the joint.
- Solder joint parameters on solder joint damage.

Subsequent study of the four cases will provide more knowledge and understanding on the damage of solder joints which is needed for fatigue life prediction of the joints. In view of this, a review of fatigue life prediction of solder joints was carried out in order to identify the proper solder constitutive and life prediction models to be utilized in this study. Accurate prediction of solder joint fatigue life is crucial for the fabrication of solder joints with adequate thermo-mechanical reliability throughout the useful life of the PV module. In order to study the effect of thermal load on thermo-mechanical reliability of solder joints, a systematic approach was developed and is presented as research methodology in the next chapter.

# CHAPTER 3

# RESEARCH METHODOLOGY

# Chapter 3

# Research Methodology

## 3.1 Introduction

In the preceding chapter, it was pointed out that thermo-mechanical reliability of solar cell interconnection in PV module is dependent primarily on the solder joint capacity to withstand degradation throughout the useful lifetime of the PV module. In order to carry out a thorough study of thermo-mechanical reliability of solder joints in crystalline silicon solar cell assembly, a research methodology was developed and is hereby presented in this chapter. The chapter outlines a brief overview of the modelling and simulation approach used in this study as well as the FEA software code. The FEA software code used in this study is ANSYS Academic Research Release 14 and it is used to build the geometric models and to simulate the thermal cycling on solder joints in solar cell assembly. The properties of materials required for ANSYS modelling and simulation are also presented in this chapter. Furthermore in this chapter is a discussion on experimental design required to obtain in-depth understanding of the effects of varying solder joint parameters. This is achieved by properly designing experiments which can capture various phenomena detrimental to solder joint thermo-mechanical reliability. Thus, a concise outline of Taguchi method of design of experiments used in this study is presented. The discussion on Taguchi method used to design experiments which were carried out virtually through

modelling and simulation includes the concept of signal-to-noise ratio and how it is used to achieve experimental objectives.

## 3.2 Modelling and simulation

This sub-section consists of a brief introduction as well as a discussion on finite element modelling (FEM) with ANSYS.

### 3.2.1 Context

An appropriate modelling and simulation approach is required to obtain accurate results. In this study, the modelling approach for reliability prediction is based on the Physics of Failure approach (PoF). The PoF approach uses knowledge of root-cause failure processes to prevent failure by incorporating reliability into the design process (Cartwright, *et al.*, 1999). The approach involves: identifying potential failure mechanisms of the PV module, failure site in the module interconnection and failure modes of the solder joint; fatigue modelling; determining the changeability effect for each design parameter; calculating the effective reliability function; and accepting the design if the estimated mean time to failure meets or exceeds the requirement. Solder joint is a critical item of the PV module assembly and its failure, mainly as a result of fatigue, limits the lifetime of the entire assembly. Therefore solder joint must be properly designed against fatigue failure. The methodology for fatigue modelling consists of four process steps (Lee, et al., 2000). The process steps, viz: definition of a constitutive equation which forms the basis for modelling; translation of the constitutive

equation into a Finite Element Analysis (FEA) software programme, model creation and simulation; the use of FEA results for the creation of a model to predict the number of cycles to failure; and the testing as well as verification of the model using thermal cycling data. Analysis of the solder joint is carried out using finite element models. A brief outline of the finite element method and the modelling and simulation process using ANSYS is outlined in sub-section 3.2.2.

### 3.2.2 Finite Element Modelling with ANSYS

Many engineering problems have complex material properties, boundary conditions and structures. Interconnected solar cells which are encapsulated to form a PV module present such a case. In such cases, analytical solutions are difficult to obtain hence not suitable. The finite element method was developed to provide a solution to this type of problem. At the centre of the finite element method is the accurate representation of complex geometry using an assemblage of subdomains called finite elements. As a numerical technique, the finite element method connects many simple element equations over many small finite elements, to approximate a more complex equation over a larger domain to find approximate solutions. The finite element modelling software developed by ANSYS has been successfully used by several researchers to carry out modelling and simulation of solar cell solder joint thermo-mechanical reliability. The simulation carried out by these researchers is aimed at static structural analysis of solder joint in solar cell assembly. Some of the researchers that have successfully used ANSYS

software code to study solar cells in PV modules include Wiese *et al*. (2010), Thakur *et al*. (2012), Lai *et al.* (2013), Kraemer *et al*. (2013) and Park *et al*. (2014). Based on the positive results obtained by these researchers, this software has been adopted in this study and used to carry out modelling and simulation of solder joints in solar cell assembly. The ANSYS software is being used in this study to calculate stresses, strains and creep strain energy values for solar cell solder joints in PV modules under simulated conditions. In order to achieve this, geometric models of crystalline silicon solar cell assembly are built and assigned the exact dimensions of a physical assembly. Furthermore, material properties of the assembly components are assigned appropriately to the models. Virtual experiments are then carried out using the ANSYS Workstation to simulate the physical conditions and for analysis of the solar cell assembly. In particular, ANSYS DesignModeler is used to build the geometric models and ANSYS Static Structural code is used for analysis.

The general modelling and simulation process used in ANSYS is presented in Fig. 3.1. The process commences with the creation of a proper geometric model of the solar cell assembly which can be modified to meet desired requirements. Other process steps include definition of element type, material properties, mesh and refining as well as boundary conditions and loads. When the process steps are deemed satisfactory, the running of the simulation can be initiated. Finally, the results obtained are processed and checked to ensure the values are generally as expected.

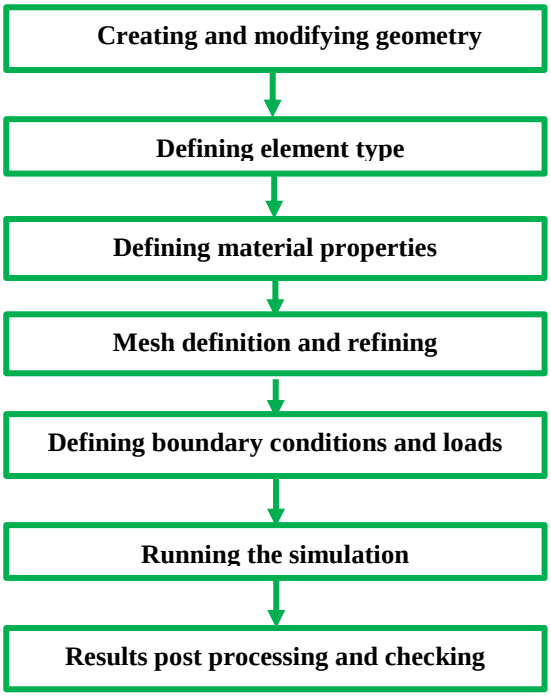


**Figure 3.1 Modelling and simulation process used in ANSYS**

As mentioned earlier, the modelling software used in this study is ANSYS Academic Research Release 14. Due to the huge computation involved in simulating the solar cell assembly, a work station computer was used to carry out High Performance Computation (HPC). The work station computer used in this study to carry out the HPC was Bespoke Desktop ANSYS Workstation with a RAM of 65,452MB located in the School of Engineering, University of Wolverhampton, UK. In particular, the ANSYS software used throughout this research is ANSYS Release 14.0 simply known as ANSYS 14. This study utilized three-dimensional (3D) models so as to capture the complete solid model of solder joint interconnection. The use of 3D models enabled a more precise solder joint damage simulation.

### 3.2.2.1 Background and Methodology

In this study, a full model of crystalline silicon solar cell assembly was built using ANSYS DesignModeler. The model represents a part of a crystalline PV module and consists of a single solar cell with all the basic components of the module such as cover glass, interconnection ribbon, solder layer, bus-bar, silicon wafer, rear contact, back-sheet and others as shown in Fig. 3.2. Presented in Fig. 3.3 is the full geometric model of the solar cell assembly built for this study which is based on the schematic configuration shown in Fig. 3.2. The dimension of the geometric model is 156 x 156mm$^2$ which is the same with the dimensions of a real multicrystalline silicon solar cell assembly which is the main type of solar cell in production globally (Jong, 2006; Chen, *et al.*, 2008; Grunow, 2010; Erath, 2010). Figure 3.3(a) shows the meshed solar cell assembly while Fig. 3.3(b) shows two interconnecting ribbons soldered to the surface of the solar cell wafer just as it is in the real solar cell assembly. Work station computer was used to carryout High Performance Computation (HPC) involved in simulating the assemblies. Quarter symmetry of the geometric model was simulated to lessen modelling time and disc space.

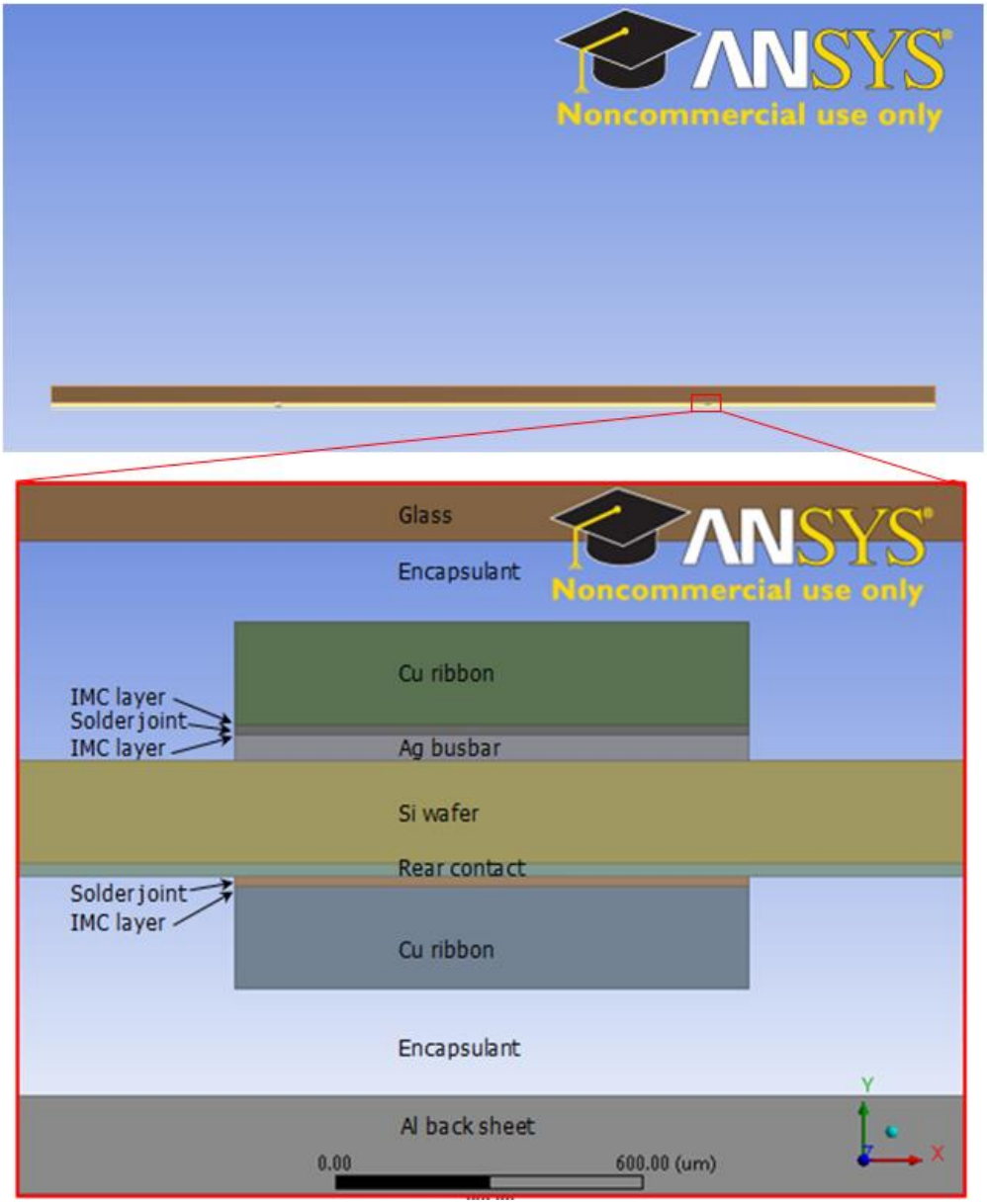


**Figure 3.2 Cross-section of encapsulated crystalline Si solar cell assembly model**

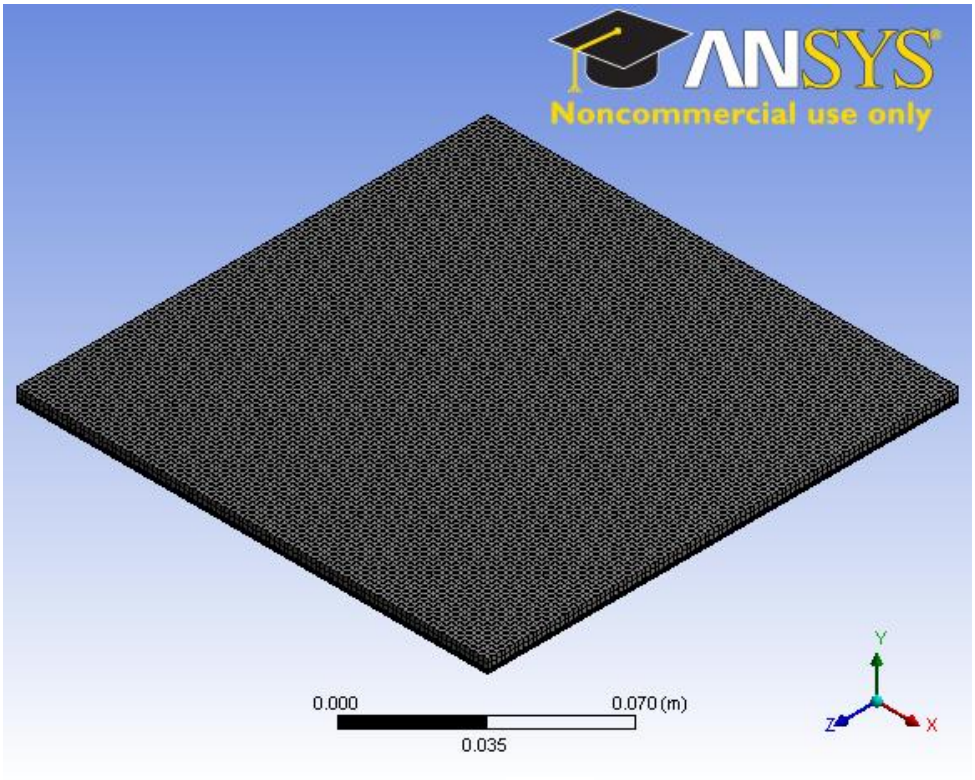


(a)

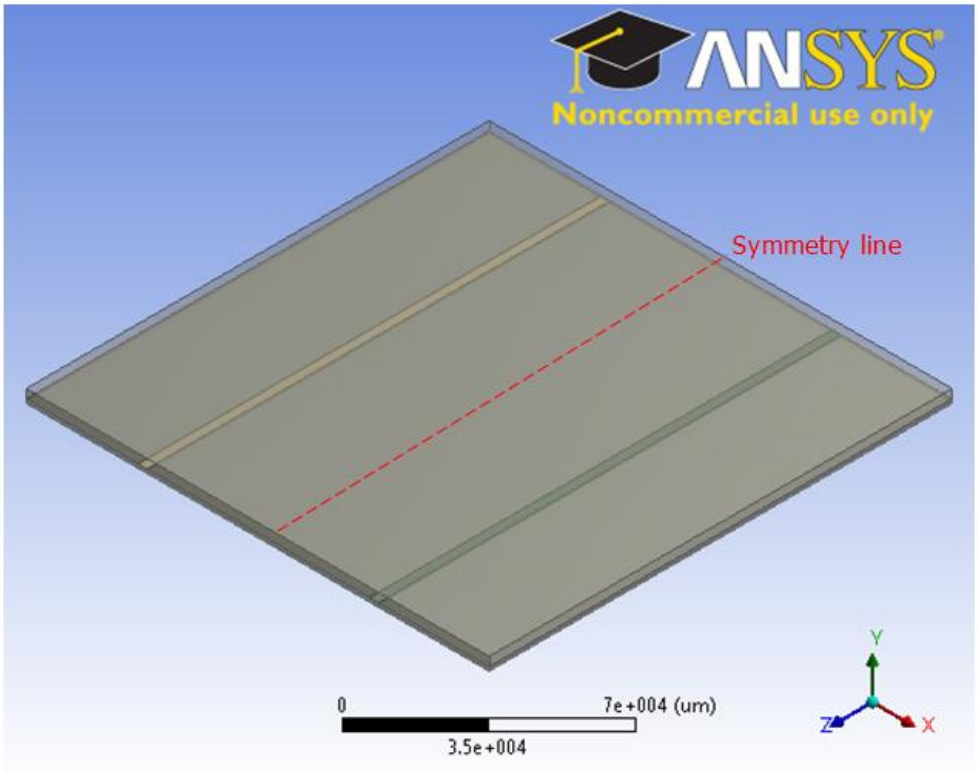


(b)

**Figure 3.3 Full geometric model of crystalline Si solar cell assembly showing: (a) Meshed solar cell assembly (b) Two interconnecting ribbons**

### 3.2.2.2 Materials and their properties

The cross-section of solar cell assembly presented in Fig. 3.2 and more details presented in Fig. 2.10 shows that the solar cell assembly consists of various materials with dissimilar properties. The main interconnection materials are Sn3.8Ag0.7Cu solder, Cu ribbon, Ag bus-bar, IMCs and Si wafer. These materials and their corresponding properties are assigned to the geometric models built for this study. The mechanical properties of these materials such as Young's modulus, CTE, Poisson ratio and shear modulus are presented in Table 3.1.

**Table 3.1 Mechanical properties of materials in crystalline Si solar cell assembly**

| Component | Young's modulus E (GPa) | CTE α ($10^{-6}$/ °C) | Poisson ratio v | Shear modulus G (GPa) |
|---|---|---|---|---|
| Glass (Webb and Hamilton, 2011) | 73.3 | 8.5 | 0.21 | 30.289 |
| Eva encapsulant (Eitner, *et al.*, 2011) | 0.011 | 270 | 0.4999 | 0.00367 |
| Cu ribbon (Amalu and Ekere, 2012) | 129 | 17 | 0.34 | 48.134 |
| IMC (Amalu and Ekere, 2012) | 110 | 23 | 0.3 | 42.308 |
| Solder-Sn3.8Ag0.7Cu (Amalu and Ekere, 2012) | 43 | 23.2 | 0.3 | 16.538 |
| Ag busbar (Engineering Toolbox, 2015) | 72.4 | 10.4 | 0.37 | 26.423 |
| Si wafer (Hopcroft, *et al.*, 2010) | 130 | 3.5 | 0.22 | 53.279 |
| Al rear contact (Engineering Toolbox, 2015) | 69 | 11.9 | 0.33 | 25.94 |
| Tedlar backsheet (Wiese, *et al.*, 2012) | 1.4 | 30 | 0.4 | 0.5 |

#### 3.2.2.2.1 Constitutive solder model

The Sn3.8Ag0.7Cu Solder alloy is modelled as visco-plastic material in solar cell assemblies experiencing both rate-dependent and rate-independent inelastic deformation as it undergoes thermo-mechanical loading during accelerated thermal cycling tests (ATC), accelerated life testing (ALT) as well as in field service. The solder is assumed to exhibit elastic, bilinear kinematic hardening after yield. It was earlier mentioned in Section 2.4.1.1 that the elastic and inelastic deformation behaviour of the solder alloy is described by constitutive models and that the Garofalo-Arrhenius hyperbolic sine creep equation has been successfully utilized by numerous researchers for simulation. Thus in this study, the Garofalo-Arrhenius hyperbolic sine creep equation is employed in the finite element analysis (FEA) to simulate the creep behaviour of the Sn3.8Ag0.7Cu solder joints.

#### 3.2.2.2.2 Loads and boundary conditions

In order to simulate the behaviour of PV modules in field operations, geometric models of crystalline silicon solar cell assembly are subjected to accelerated thermal cycling utilizing International Electro-technical Commission (IEC) 61215 standard for photovoltaic panels (Arndt and Puto, 2011) to simulate thermal stresses on the materials of the models. The models are subjected to six accelerated thermal cycling (ATC) in 25 load steps between -40$^{o}$C to 85$^{o}$C. The temperature loading starts from 25$^{o}$C, ramped up at a rate of 3$^{o}$C/min to 85$^{o}$C, where it has hot dwell for 20 min. It

is then ramped down to -40$^{o}$C at a rate of 6$^{o}$C/min, where it has cold dwell for 20 min. The thermal cycling profile is presented in Fig. 3.4 and it is utilized to simulate actual cycling profile used during thermal load test.

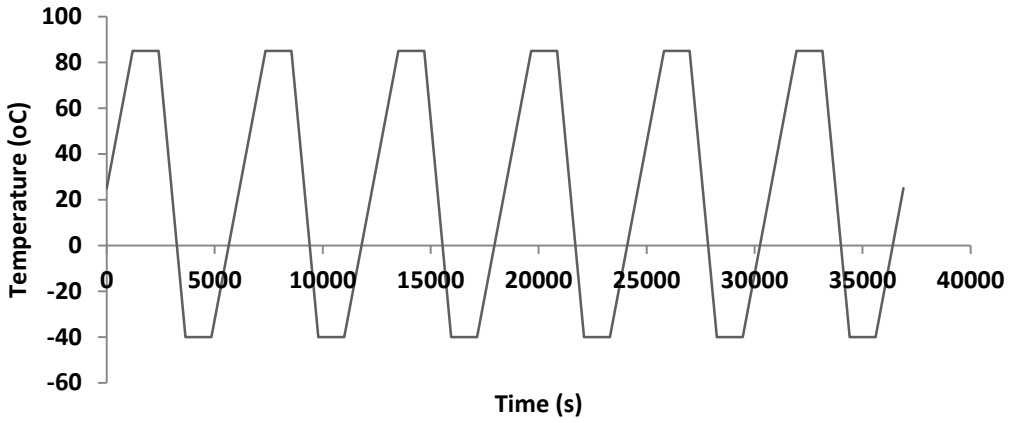


**Figure 3.4 Plot of temperature profile of thermal load test condition used in the crystalline Si solar cell assembly (Amdt and Puto, 2011)**

Several outputs may be obtained from the simulation of solder joints in solar cell assembly and in this study, the key desirable outputs are equivalent stress, equivalent strain and strain energy density.

### 3.2.3 Model Validation

In order to confirm the accuracy and effectiveness of the developed finite element models, validation of the models are done by comparing simulation results with experimental results or in the alternative with experimental or simulation results obtained by other researchers. This second option has become the only option in this case due to limited availability of test facilities. Thus, the preferable option of design, fabrication and assembly of interconnected solar cell assembly test vehicle and subjecting the test vehicle

to limited accelerated thermal cycling experiments is not possible in this study. Hence, to validate simulation results from this study, comparison is made with results obtained by other researchers.

## 3.3 Taguchi's approach to design of experiments

This sub-section discusses the concept of design of experiments with a particular focus on Taguchi approach. The sub-section contains two parts: Introduction to Taguchi method and signal-to-noise (S/N) ratio.

### 3.3.1 Introduction to Taguchi method of DOE

Design of experiments (DOE) is a tool used by engineers and scientists to design and develop products as well as to develop and improve processes (Montgomery, 2013, pp.8-11). The DOE is a systematic method used to determine the relationship between factors affecting a product or process and the output of that product or process. It can be said that DOE is used to find cause-and-effect relationships. The information on the relationship is required to manage product or process inputs in order to optimize the output. In an ordinary experiment, one or more product/process variables (or factors) are changed in order to observe the effect the changes have on one or more response variables. The DOE is an efficient procedure for planning experiments so that the data obtained can be used for analysis to produce valid and objective conclusions. The DOE commences with the

determination of the objectives of an experiment. This is followed by selection of product or process factors to be used in the study. Thus in an experimental design, detailed experimental plans are laid out in advance before doing the experiment. Moreover, a well-planned design of experiment enables maximum amount of information to be obtained for a certain amount of experimental effort.

There are several types of DOEs in use. The main types of DOEs are full factorials, response surface analysis, mixture experiments, evolutionary operations, fractional factorials and screening experiments (Montgomery, 2013, pp.5-7; JMP® 8, 2009). Full factorial experiments completely consider all factors included in the experimentation and can require many experimental runs if many factors at many levels are investigated. Response surface analysis is used on series of full factorial experiments to map response and generate mathematical equations that describe how factors affect the response. Mixture experiments are to study how changes in a formulation affect the final properties of a material. Evolutionary operations are optimization techniques which usually use two factors to study small, step changes in factor levels to incrementally explore the operating bounds of the process. Fractional factorial designs are derived from full factorial matrices but they consider more factors with fewer runs. Screening experiments are crucial fractional factorial experiments. These experiments

screen the factors or variables in the process and determine which of the critical variables affect the process output.

Although there are numerous DOE tools in use, yet, Taguchi method is popularly used in diverse fields because it is aimed at improving quality as well as allowing the effects of several factors to be determined simultaneously and efficiently (Taguchi, 1995). Taguchi DOE was developed by a Japanese engineer and statistician whose full name was Dr Genichi Taguchi. His approach to DOE is based on screening experiments. The Taguchi DOE is a designed experiment which allows the choice of a product or process that is robust such that it performs more consistently in the environment in which it is used. Also, it can be reiterated that Taguchi method for DOE is based on quality philosophy aimed at the development of products and processes that are robust to environmental factors and other sources of variability (Montgomery, 2013, pp.8-21; Davies, *et al*., 2015). Robustness in this context is a measure of the ability of the product or process to perform consistently with minimal effect from the uncontrollable noise factors due to operation or manufacturing. In Taguchi DOEs it is known that while some factors that cause variability can be controlled, there are other factors that are uncontrollable. The uncontrollable factors are called noise factors. The identification of controllable factors (control factors) that minimize the effect of noise factors is paramount in Taguchi DOEs. In the course of experimentation, noise factors are controlled to force variability to occur. Thereafter, optimal control factor settings that make the process or product robust or resistant to variation from the noise factors are

determined. A product designed using this approach will be robust and deliver more consistent performance regardless of the operating environment. Furthermore, the use of Taguchi method for DOE substantially reduces product and process development lead time and cost. The benefit of this method is that products and processes are developed which perform better in the field and have higher reliability than those developed using other methods. Taguchi DOEs use orthogonal arrays to structure the experiments. Orthogonal arrays are matrices of numbers made up of columns and rows. In every matrix of the array, each column represents a factor which affects the outcome of the process under study while the row represents a level of the factor. The orthogonal arrays are used to estimate the effects of factors on the response mean and variation with focus primarily on main effects. Furthermore, orthogonal arrays are balanced in respect to the settings of the factor levels which are weighted equally such that every factor level occur an equal number of times in each column regardless of the size of the array. Due to this, each factor can be assessed independently of all the other factors. Therefore, the effect of one factor does not affect the estimation of a different factor. This can reduce the time and cost associated with the experiment when fractional factorial designs are used. In order to make a product robust, the Taguchi approach generally uses 8-process steps to optimize the parameters of the product (Chomsamutr and Jongprasithporn, 2012). The following are the eight steps.

- Identification of the performance characteristics (responses) to optimize and product parameters to control (test).
- Determination of the number of levels for each of the tested parameters.
- Selection of an appropriate orthogonal array and assigning each tested parameter into the array.
- Conducting an experiment based on the arrangement of the orthogonal array
- Calculation of the S/N ratio for each combination of the tested parameters.
- Analysis of the experiment result using the S/N ratio and ANOVA test.
- Finding the optimal level for each of the process parameters.
- Conducting the confirmation experiment to verify the optimal product parameters.

The Taguchi method of DOE has been successfully used by several researchers to design experiments for solder joint thermo-mechanical reliability. Some of the researchers that have successfully applied Taguchi method for DOE include Zhang *et al.* (2015), Shu *et al.* (2012), Yan and Tan (2011), Kim *et al*. (2010) and Ye *et al*. (2010). Based on the desired and satisfactory results obtained by such researchers, the Taguchi method of DOE has been adopted and used in this study. Application of Taguchi method for DOE in this research enables the selection of the best matching combination of geometric parameters for improving the thermo-mechanical reliability of solder joints in solar cell assembly under thermal cycling.

### 3.3.2 Concept of signal-to-noise ratio

The Taguchi method utilizes the concept of signal-to-noise ratio for analysis. The concept of signal-to-noise (S/N) ratio is used to measure how the performance response varies relative to the desired value under different noise conditions. Thus, the S/N ratio provides a measure of the impact of noise factors on performance. The larger the S/N ratio, the more robust the product is against noise. Taguchi DOE applies S/N ratio to quantify the factor effect to a desired performance response. Accordingly, calculation of the S/N ratio depends on the experimental objective. There are three standard S/N ratios in use and each is suitable for a particular objective. Table 3.2 presents these ratios employed in Taguchi DOE. The terms *y*, *n* and *s* are response, number of data points and standard deviation respectively.

**Table 3.2 Signal-to-noise ratio for Taguchi DOE (Davies, *et al.*, 2015)**

| Performance Response | Signal-to-noise ratio |
|---|---|
| **Smaller the Better (Minimization): Used for making the system response as small as possible** | $S/N_S = -10 \log \left( \frac{\sum_{i=1}^{n} y_i^2}{n} \right)$ |
| **Nominal is Best (Nominalization): Used for reducing the variation around a target** | $S/N_T = 10 \log \left( \frac{\bar{y}^2}{s^2} \right)$ |
| **Larger is Better (Maximization): Used for making the system response as large as possible** | $S/N_L = -10 \log \left( \frac{1}{n} \sum_{i=1}^{n} \frac{1}{y_i^2} \right)$ |

As shown in Table 3.2, whenever the desired performance response is required to be as small as possible, then minimization is carried out and the smaller-the-better expression of the signal-to-noise ratio is used. Likewise nominalization is carried out to reduce variation around a target and the nominal-is-best expression of signal-to-noise ratio is utilized. Similarly, the larger-is-better expression of signal-to-noise ratio is utilized whenever maximization is desired in order to make the system response as large as possible. The case in this study concerns thermo-mechanical reliability of solder joint under thermal loading where creep damage in the joint is prevalent. Consequently, minimization of creep damage in the solder joint of solar cell assembly is essential to ensure longer fatigue life. A robust indicator of creep damage of solder joint is creep strain energy density which is based on the deformation internally stored throughout the volume of the joint during thermal loading. Therefore, in order to minimize creep damage, the performance response slated for this study is minimization of creep strain energy density in the solder joint. Hence, the smaller-the-better expression of the signal-to-noise ratio is utilized for computation. The computed values of signal-to-noise ratio are subsequently employed to determine the optimal parameter setting of solder joints in solar cell assembly.

## 3.4 Summary

The research methodology developed for the study of thermo-mechanical reliability of solder joints in crystalline silicon solar cell assembly was

presented in this chapter. The methodology involves the use of FEA software code for modelling and simulation as well as the use of Taguchi method of DOE for experimental design and optimization. Following a concise overview of Finite Element Modelling, the process of modelling and simulation with ANSYS FEA software code used in this study was discussed. Furthermore, ANSYS DesignModeler is used to build virtual geometric models of solar cell assembly for subsequent simulation. The geometric models of solar cell assembly consist of various components; hence the material properties to be assigned to each component of the assembly were presented. In addition, the constitutive solder model used as well as the loads and boundary conditions to be imposed on the models to simulate the thermal cycling on solder joints were also presented. Several outputs may be obtained from the simulation of solder joints in solar cell assembly such as equivalent stress, equivalent strain and strain energy density. Besides, Taguchi method of DOE was introduced highlighting the process steps used in its application. The concept of signal-noise-ratio was also discussed including mathematical expressions for desired performance response such as minimization, nominalization and maximization. In this study, the objective is to minimize the fatigue damage in solder joint, thus the desired performance response is minimization; hence the corresponding mathematical expression is utilized accordingly. In the following chapter, an evaluation of thermo-mechanical reliability of solder joint in solar cell assembly is presented. The evaluation utilizes ANSYS software code to model and simulate solder joint behaviour when subjected to thermal loading.

# CHAPTER 4

# EVALUATION OF THERMO-MECHANICAL RELIABILITY OF SOLDER JOINTS IN SOLAR CELL ASSEMBLY

# Chapter 4

# Evaluation of Thermo-mechanical Reliability of Solder Joints in Solar Cell Assembly

## 4.1 Introduction

This chapter presents the evaluation of solar cell solder joint thermo-mechanical reliability. This is necessary because the mismatch of coefficient of thermal expansion (CTE) of Si wafer, Ag bus-bar, solder, Cu ribbon strip and other components, leads to thermo-mechanical induced non-linear deformation in the solar cell assembly. Therefore, an investigation of steady state creep for non-linear deformation of SnAgCu solder joints in crystalline silicon solar cell assembly is needed to obtain more understanding of the degradation of solder material with particular focus on the effect of IMC formation at the interfaces. The IMC layer formed at the interfaces is as shown earlier in Fig. 2.10(b). In particular, the effect of IMC in solder joint is analysed to determine the extent of degradation caused by it in the joint.

The study in this chapter employs finite element modelling (FEM) to simulate the non-linear deformation of SnAgCu solder joints in two models of crystalline silicon solar cell assembly. One of the models contains IMC in the interface joints between solder and copper ribbon while the other, which is the control, does not contain IMC in the joints. The Garofalo-Arrhenius steady state creep constitutive model for SnAgCu solder will be used in this study to simulate the degradation of solder material. Therefore, presented in

this chapter is the methodology used for the study of the effect of IMC on the thermo-mechanical reliability of solder joints as well as results obtained from modelling and simulation followed by discussion. The methodology describes the solder joint parameters used, including IMC thickness.

The methodology used for this study comprises theoretical analysis of effect of IMC layer in solder joint as well as modelling and simulation. In the case of modelling and simulation, the study utilizes FEM discussed in section 3.2.2.1 for this investigation. Also, Garofalo-Arrhenius creep model discussed in section 3.2.2.2 was used in this study. Furthermore, this study utilizes 156 x 156 $mm^2$ multi-crystalline silicon solar cell assembly. The study of induced strain in solar cell assembly is carried out using commercial ANSYS Academic Research Finite Element package. Due to the magnitude of computations involved, the High Performance Computation (HPC) was executed using a Bespoke Work Station computer in the School of Engineering. In order to lessen modelling time and disc space, quarter symmetry of the geometric models were simulated.

As discussed in section 3.2.2, meshing is one of the key process steps in finite element modelling and simulation. Mesh density has effect on the accuracy of simulation results. It is for this reason that other researchers such as Che and Pang (2012b) carried out mesh sensitivity study in order to determine appropriate mesh density of solder joint in the package under

study. Therefore, mesh sensitivity study is carried out in this study to investigate the effect of element size on simulation results. In order to carry out the investigation, three models of 156 x 156 $mm^2$ multi-crystalline silicon solar cell assembly were built using ANSYS DesignModeler. Though various solder joint thickness ranging from 10μm to 40μm are in use, typical solder joint thickness used is 20μm (Rogelj, *et al.*, 2012; Wiese, *et al.*, 2009). Thus each of the models has whole solder joint thickness of 20μm with 1μm IMC thickness at the two interfaces. The models were meshed with element size of 850μm, 1200μm and 1700μm and named Fine, Medium and Coarse respectively. The three models were subjected to six accelerated thermal cycling in 25 load steps between -40$^{o}$C to 85$^{o}$C. The temperature loading started from 25$^{o}$C, ramped up at a rate of 3$^{o}$C/min to 85$^{o}$C, where it had hot dwell for 20 min. It was then ramped down to -40$^{o}$C at a rate of 6$^{o}$C/min, where it had cold dwell for 20 min. The thermal cycling profile presented in section 3.2.2.2.2 was used to simulate actual cycling profile used during thermal load test. The simulation results obtained are used to determine appropriate mesh element size that should be used to mesh subsequent models. The use of appropriate mesh element size enables the production of accurate simulation results for other models being studied.

Subsequent study in this chapter involves determination of the effect of IMC on the thermo-mechanical reliability of solder joint. Design of experiments was carried out based on the aim and objectives. In order to determine the

effect of IMC on solder joint, a model without IMC but with the same dimensions and parameters as the models in the preceding paragraph was built and simulated. Results of simulation are compared with that of the model with IMC and the effect of IMC analysed.

## 4.2 Theoretical analysis of effect of IMC layer in solder joint

The effect of IMC layer on thermo-mechanical reliability of solder joint can be determined through numerical analysis. Figure 4.1 depicts schematic cross-section of crystalline Si solar cell assembly showing regions of solder and IMC layers. Region 1 shows IMC layer between solder layer and copper ribbon; Region 2 shows solder layer; Region 3 shows IMC layer between solder layer and silver bus-bar.

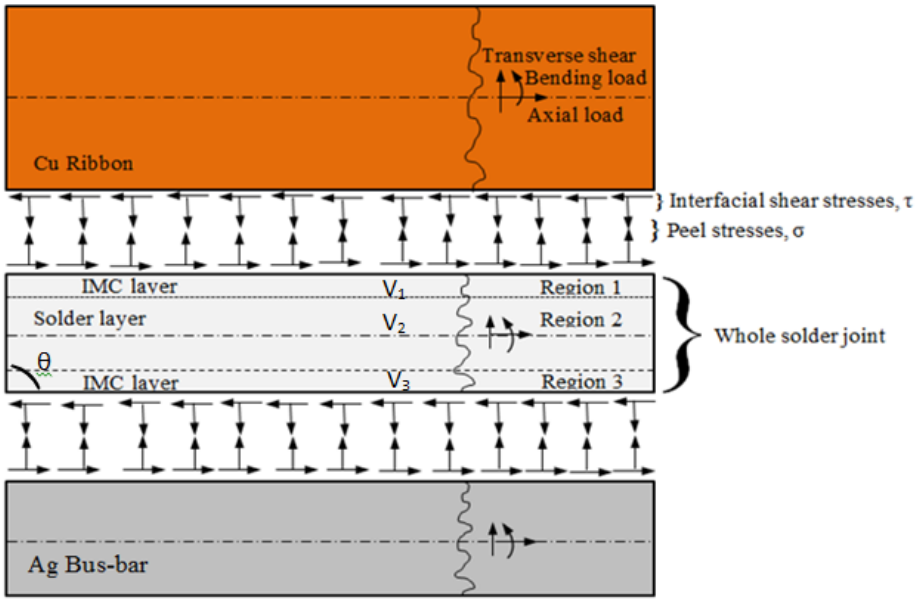


**Figure 4.1 Schematic cross-section of solar cell assembly showing regions of solder and IMC layers**

The underlying physics of thermo-mechanics involved in the creep strain deformation is governed by the equation (Amalu and Ekere, 2012):

$$\frac{dV_T}{d\theta}=\beta T \tag{4.1}$$

where $dV_T$ is the change in total volume of solder layer as a result of thermal cycling and $V_T$ is the total volume of the three regions in whole solder layer. Also, $\beta$, $\theta$ and $d\theta$ represent volumetric expansion coefficient, angle of solder joint in Fig. 4.1 and range of temperature cycling limit respectively.

Considering the whole solder joint geometry and configuration shown in Fig. 4.1,

$$V_T=V_1+V_2+V_3 \tag{4.2}$$

where 1, 2 and 3 designate the three regions of the whole solder layer respectively consisting of region 2 which is solder only region while regions 1 and 3 are IMC layers.

For solder only composition:

$$V_{T,(solder\ only)}=V_{region\ 1}+V_{region\ 2}+V_{region\ 3} \tag{4.3}$$

For solder + IMC composition:

$$V_{T,(solder+IMC)}=V_{Cu\ IMC}+V_{region\ 2}+V_{Ag\ IMC} \tag{4.4}$$

Therefore, change in volume is:

$$dV_{T,(solder\ only)}=\beta d\theta(V_{region\ 1}+V_{region\ 2}+V_{region\ 3}) \tag{4.5}$$

$$dV_{T,(solder+IMC)}=\beta d\theta(V_{Cu\,IMC}+V_{region\,2}+V_{Ag\,IMC}) \quad (4.6)$$

Rearranging Eq. 4.5:

$$\frac{dV_{T,(solder\ only)}}{V_{region\,1}+V_{region\,2}+V_{region\,3}}=\beta d\theta \quad (4.7)$$

Similarly, rearranging Eq. 4.6 gives:

$$\frac{dV_{T,(solder+IMC)}}{V_{Cu\,IMC}+V_{region\,2}+V_{Ag\,IMC}}=\beta d\theta \quad (4.8)$$

But there is negligible deformation in the IMC, thus all changes are from region 2. Therefore, Eq. 4.8 reduces to:

$$\frac{dV_{region\,2}}{V_{Cu\,IMC}+V_{region\,2}+V_{Ag\,IMC}}=\beta d\theta \quad (4.9)$$

Equation 4.7 may be rewritten as:

$$\frac{dV_{region\,1}+dV_{region\,2}+dV_{region\,3}}{V_{region\,1}+V_{region\,2}+V_{region\,3}}=\beta d\theta \quad (4.10)$$

Applying volume constancy condition, equations 4.3 and 4.4 combine to give:

$$V_T=V_{region\,1}+V_{region\,2}+V_{region\,3}=V_{Cu\,IMC}+V_{region\,2}+V_{Ag\,IMC} \quad (4.11)$$

Combination of equations 4.9, 4.10 and 4.11 yields:

$$\frac{dV_{(region\,2)}}{V_T}\Big|_{solder+IMC} \neq \frac{dV_{(region\,2)}}{V_T}+\frac{dV_{(region\,1)}+dV_{(region\,3)}}{V_T}\Big|_{solder\ only} \quad (4.12)$$

The term $\frac{dV_{(region\,2)}}{V_T}$ in Eq. 4.12 is the effect of IMC. Furthermore, it can be deduced from Eq. 4.12 that the smaller the IMC thickness in solder joint, the

closer the volume in region 2 to total solder volume in the joint. In other words, if the thickness of IMC tends to zero, in solder + IMC model, $dV_{(region\ 2)} \approx dV_T$ and thus the difference between the LHS and RHS will be minimized. Consequently, the smaller the IMC thickness in the solder joint the marginal its effect on the joint.

### 4.3 Results and discussion

In order to further study the effect of IMC on solder joint, modelling and simulation is carried out. This section discusses the results obtained from modelling and simulation in five parts. These parts are: mesh sensitivity study, creep strain study on solder joints with and without IMC, effect of IMC on creep strain behaviour of solder joints, study on strain energy and strain energy density of solder joints and effect of IMC on solder joint fatigue life.

#### 4.3.1 Mesh sensitivity study

The accuracy of simulation results depends on mesh density as earlier mentioned in chapter 3. In other words the suitability of a mesh for simulation is very vital as it can have an effect on the simulation solution. The simulation solution can be either mesh-independent or mesh dependent. The mesh-independent solution is obtained when the number of mesh elements has no effect on the simulation solution (Alawadhi, 2010, pp.381). On the other hand, the mesh dependent solution is obtained when different

numbers of mesh elements produce different simulation solution (Sigmund and Petersson, 1998). This necessitated mesh sensitivity study to investigate the effect of mesh element size on simulation results of three geometric models. Presented in Table 4.1 are parameters of the three geometric models with mesh element size of 850μm, 1200μm and 1700μm and named Fine, Medium and Coarse respectively.

**Table 4.1 Parameters of models for mesh sensitivity study**

| Model name | IMC thickness (μm) | Solder joint thickness (μm) | Solder joint Width (μm) | Solder joint volume ($mm^3$) | Mesh element size (μm) |
|---|---|---|---|---|---|
| **Fine** | **1** | **20** | **1000** | **1.56** | **850** |
| **Medium** | **1** | **20** | **1000** | **1.56** | **1200** |
| **Coarse** | **1** | **20** | **1000** | **1.56** | **1700** |

The number of mesh elements in Fine model is higher than in Medium model and the number in Medium model is higher than in Coarse model. The meshed models are shown in Fig. 4.2. From the figure as well as from Table 4.2, it can be observed that Fine model has smallest mesh element size while Coarse model has the largest mesh element size.

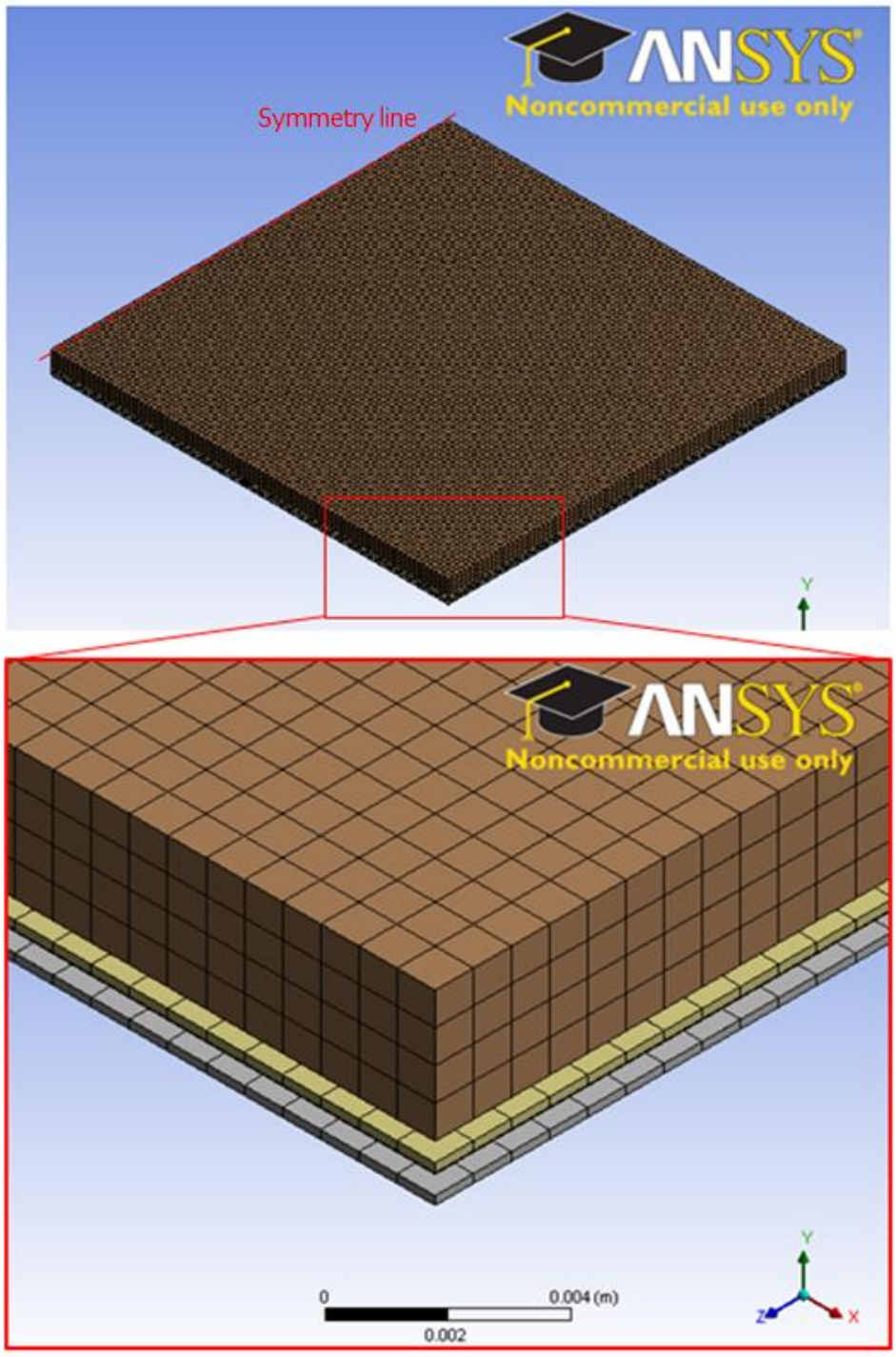


**(a) Fine model with mesh element size of 850µm**

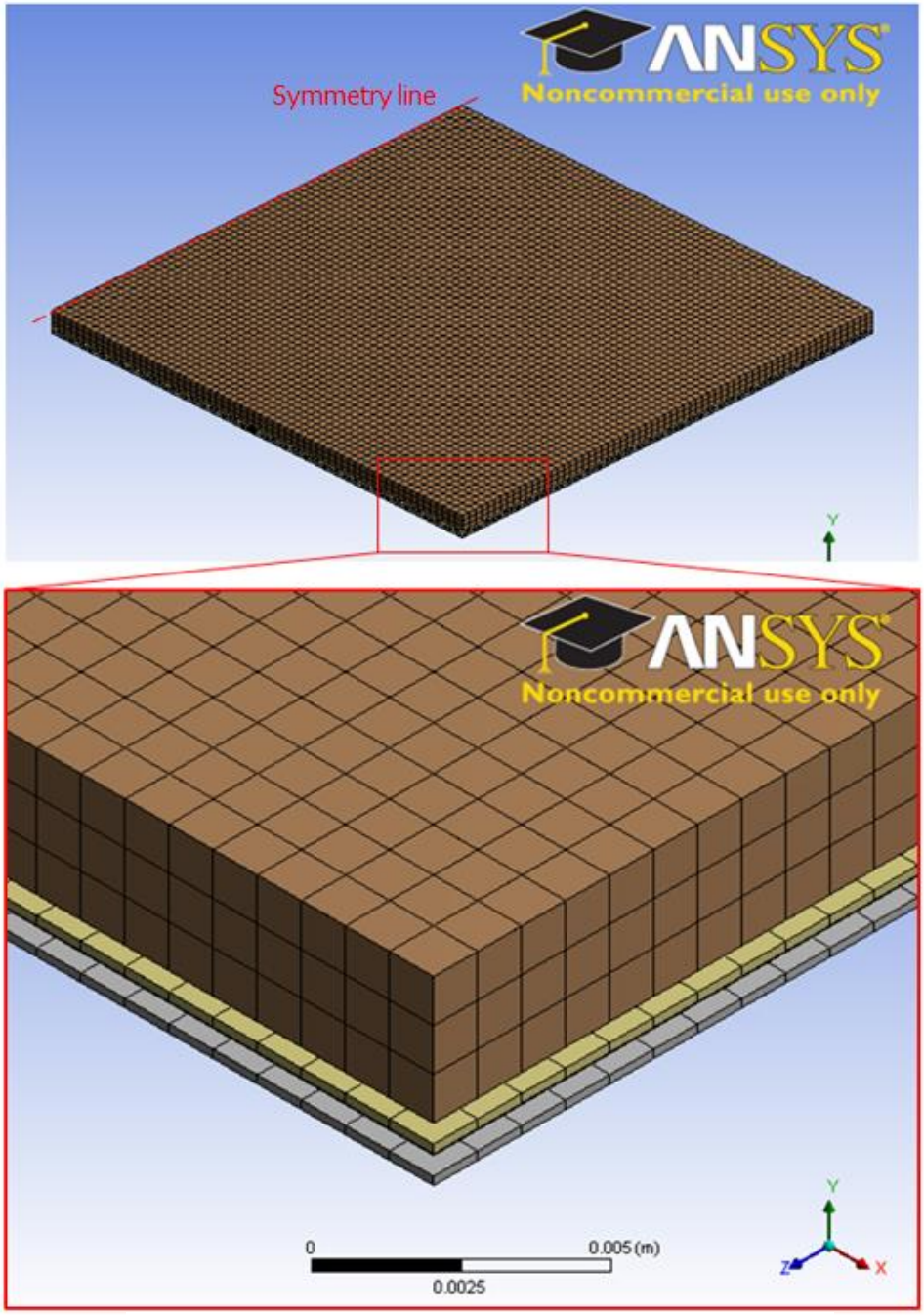


**(b) Medium model with mesh element size of 1200µm**

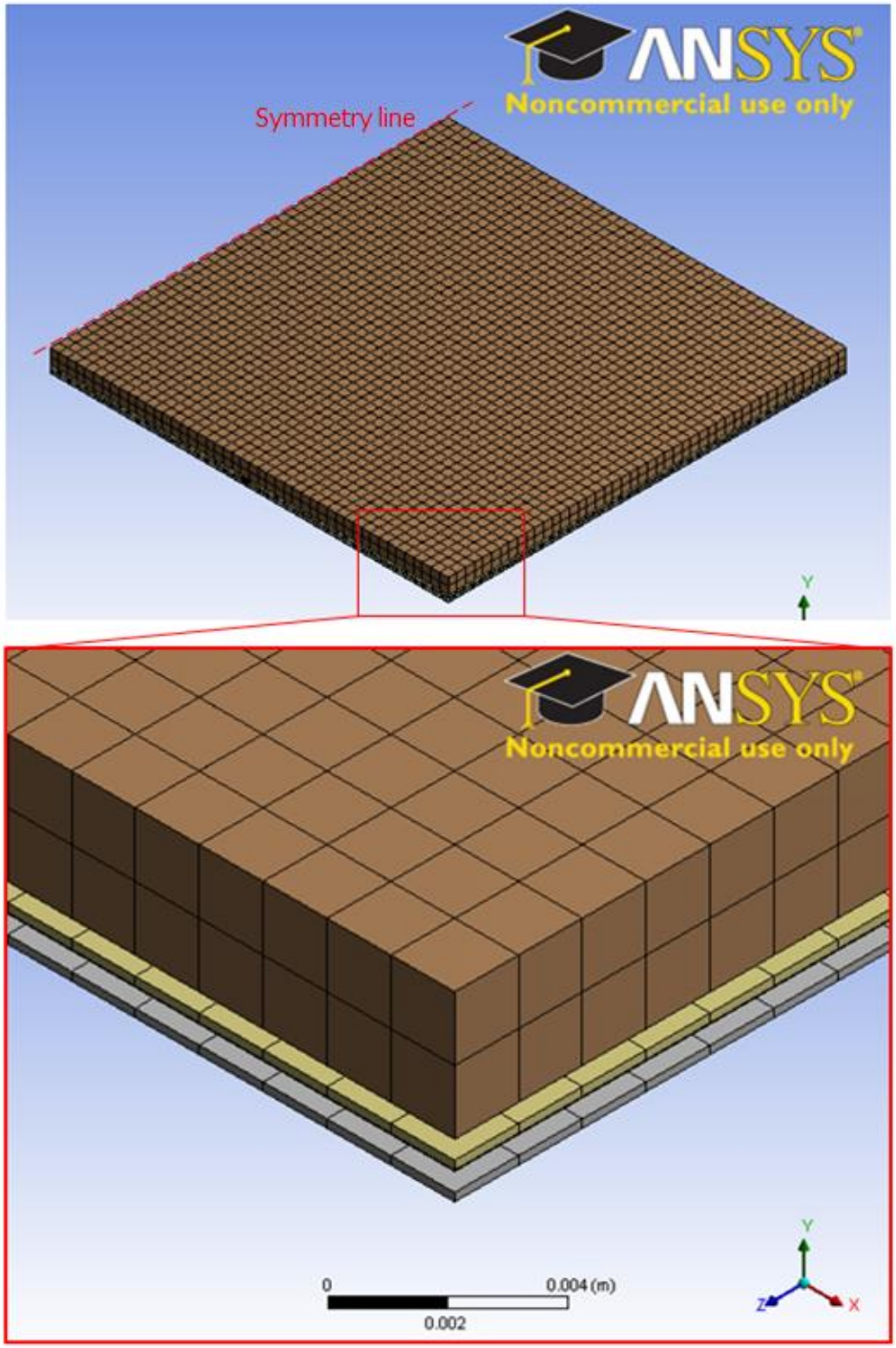


**(c) Coarse model with mesh element size of 1700µm**

**Figure 4.2 Meshed models of crystalline Si solar cell assemblies showing: (a) Fine model (b) Medium model (c) Coarse model**

The effect of mesh density on the solder joints in the models are determined by simulating the three models and obtaining their creep strain energy. The volume-averaged method discussed in section 2.4.2 is used to compute the creep strain energy densities. Results of creep strain energy density ($\omega_{acc}$) for the models are presented in Table 4.2. An observation of Table 4.2 shows that Fine model has the least accumulated strain energy density while Coarse model has the highest accumulated strain energy density. The results of solder joint average accumulated change in creep strain energy density per cycle ($\Delta\omega_{acc}$) are used to compute fatigue life of the solder joint in terms of cycles to failure. Equation 2.11 is used for the computation of cycles to failure which gives the predicted fatigue life of the three models. The predicted fatigue lives of the three models are also presented in Table 4.2. The results indicate that predicted fatigue life for Fine, Medium and Coarse models are 33587, 15317 and 8597 cycles to failure respectively. In addition, Fine model consumed the largest amount of computing time of 101719 seconds while Coarse model consumed the least time of 22068s.

**Table 4.2 Creep strain energy density and predicted life for meshed models**

| Model name | Mesh element size (μm) | $\Delta\omega_{acc}$ (mJ/mm$^3$) | Predicted fatigue life (cycles) | Computing time (s) |
|---|---|---|---|---|
| **Fine** | **850** | **0.01567** | **33587** | **101719.000** |
| **Medium** | **1200** | **0.03436** | **15317** | **39287.000** |
| **Coarse** | **1700** | **0.06122** | **8597** | **22068.000** |

Figure 4.3 shows effect of mesh element size on strain energy density of the three models. It can be observed from the figure that the Fine model, which has the least accumulated strain energy density, has the highest predicted fatigue life. Conversely, the Coarse Model which has the highest accumulated strain energy density has the least predicted fatigue life.

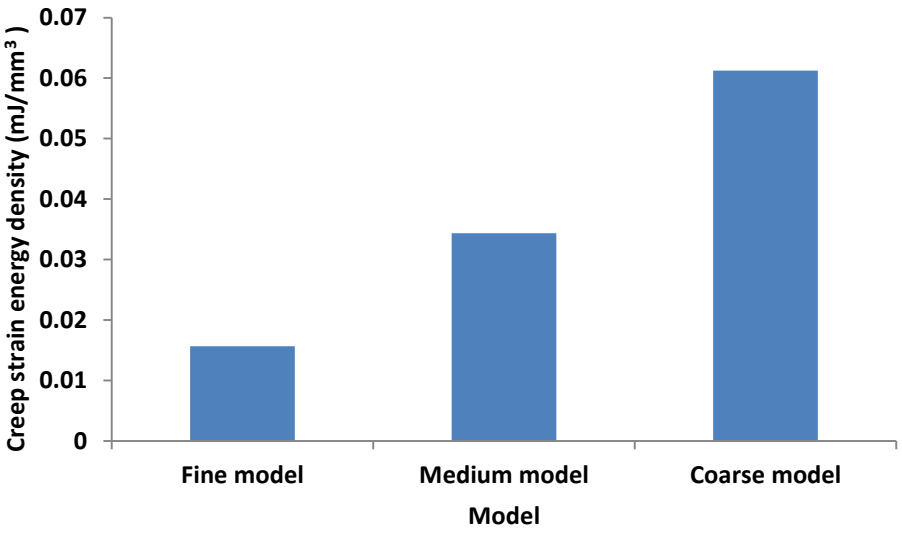


**Figure 4.3 Effect of mesh element size on strain energy density**

The analysis of simulation solution for each of the models indicates that the solution is mesh dependent as there is no unique solution common to at least two of the three models. Sigmund and Petersson (1998) stated that mesh dependent problem is one of the key numerical problems encountered in topology optimization discretized by finite elements. Presented in Table 4.3 is description of mesh dependent problems including numerical experience and prevention techniques sourced from Sigmund and Petersson (1998). It can be observed from the table that the second type of mesh dependent problem is the same type of problem in this sensitivity study.

However, as shown in the table, there is no prevention technique for this type of mesh dependent problem. This implies that in a situation like this, a critical look at mesh quality is required in order to ensure the use of appropriate number of mesh elements to give desired simulation solution.

**Table 4.3 Description of mesh dependent problems (Sigmund and Petersson, 1998)**

| Numerical Experience | Mathematical problem | Physical explanation | Prevention techniques |
|---|---|---|---|
| a. Necessarily finer and finer structure | Non existence | Convergence to microstructure | Relaxation, Perimeter, Global/local gradient constraint, mesh independent filtering |
| b. Possibly finer and finer structure | Non uniqueness | Ex.: uniaxial stress | Nothing (maybe manufacturing preference) |

Mesh quality problems have been a challenge for a while and it has not been possible to solve all the problems. It was for this reason that United States Department of Defence (DoD) High Performance Computing Modernization Program (HPCMP) hosted a workshop on Mesh Quality as reported by Thornburg (2012) in Chawner (2012). The workshop summarised the current state of affairs to include: "A mesh as an intermediate product has no inherent requirements and only needs to be sufficient to facilitate the prediction of the desired result." Furthermore, "The mesh must capture the system/problem of interest in a discrete manner with sufficient detail to enable the desired simulation to be performed." Consequently, a good mesh is the mesh that enables the achievement of project objectives. Besides, modelling and simulation are meant to emulate physical phenomena.

Therefore mesh quality in the long run depends on the solution to the physical problem and excessive fine mesh may lead to larger computational errors and unphysical solutions (Knupp, 2007; Shengwei, 2011). In view of this condition, it is necessary to analyse the physical performance of PV modules during their field operations.

The physical performance of crystalline silicon PV modules during field operations is expected to be up to 25 years. Guyenot *et al.* (2011) estimated that for 1.5 thermal cycles per day with a temperature change of about 50 $^{o}$C, expected life of solder joints in the modules for 25 years is 13688 cycles to failure. However, Kohl *et al*. (2009) in SunPower (2013) reported that in a German four-year project, a group of PV modules from 7 different manufacturers were subjected to damp heat ageing test. The results showed significant performance degradation such that projected lifetime was less than 20 years (10950 cycles to failure). Similarly, Kumar and Sarkar (2013) conducted a single constant stress accelerated life test on 20 PV modules for stress failure and obtained the least survival life to be 21 years (11497 cycles to failure). Figure 4.4 presents a plot of predicted solder joint fatigue life of Fine, Medium and Coarse models compared with the test lives obtained by Kohl *et al*. (2009) and Kumar and Sarkar (2013) as well as expected life determined by Guyenot *et al.* (2011).

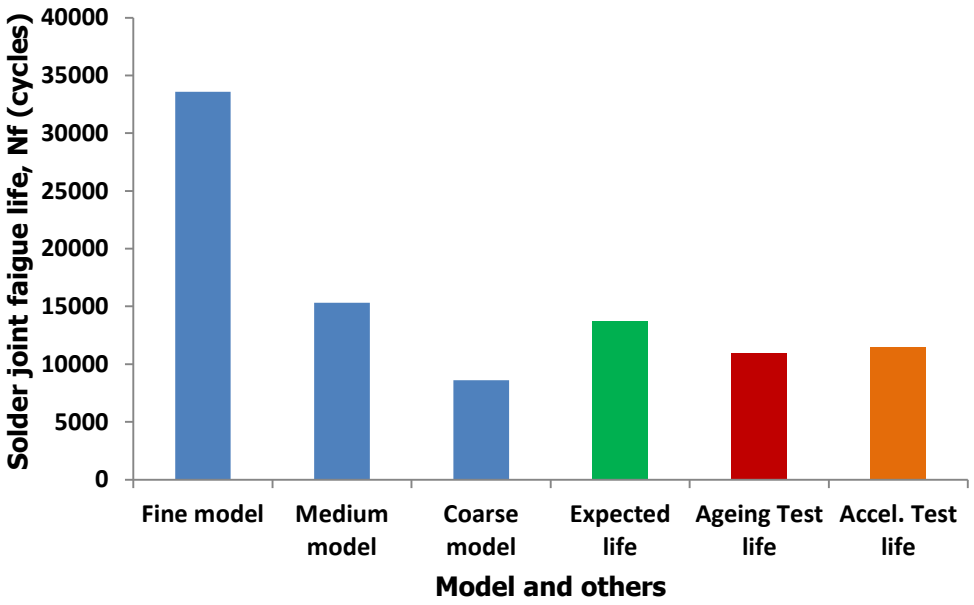


**Figure 4.4 Predicted solder joint fatigue life of models and others versus mesh type**

The results in Fig. 4.4 indicate that the predicted fatigue life of Fine model (33587 cycles to failure) is exaggerated while that of Coarse model (8597 cycle to failure) is underestimated. However, predicted fatigue life of Medium model is 15317 cycles to failure which is close to expected life of 13688 cycles to failure as projected by Guyenot *et al*. (2011) and experimental test lives of 10950 and 11497 cycles to failure as obtained by Kohl *et al*. (2009) and Kumar and Sarkar (2013) respectively. Therefore, the mesh element size of Medium model (1200μm) has provided accurate simulation result. The result obtained for the Medium model is due to the mesh element size defined for it. This indicates that appropriate definition and refining of mesh is essential to obtain accurate simulation results. In addition, the Medium model consumed lower computing resources compared with the Fine model. Hence, the mesh element size of Medium model is chosen for meshing subsequent models.

### 4.3.2 Creep strain study on solder joints with and without IMC

In the preceding section 4.3.1, three models containing IMC were simulated and results obtained for creep strain energy. Other results obtained are equivalent stress and creep strain induced in solder joints. A comparison of model containing IMC with a model that does not contain IMC is desirable to get an understanding of the effect of IMC on the solder joint. Hence, a model without IMC was built and meshed with similar mesh element size as the Medium model with IMC shown in Fig. 4.2. Presented in Fig. 4.5 are the models of crystalline Si solar cell assemblies with interconnected components. The model in Fig. 4.5(a) contains only solder without IMC while the model in Fig. 4.5(b) contains both solder and IMC. The IMC layer thickness is 1 μm at the solder/cu ribbon interface as well as at the solder/Ag bus-bar interface. The model containing only solder was simulated under the same thermal conditions as the model containing IMC. Simulation results of creep strain energy, equivalent stress and creep strain were obtained. Creep strain, equivalent stress and creep strain energy are all induced in solder joints as a result of subjecting the solar cell assembly to accelerated thermal cycling. The damage distribution of creep strain on the solder joints is one of the simulation outputs and is used to identify areas with the greatest damage in the solder joint.

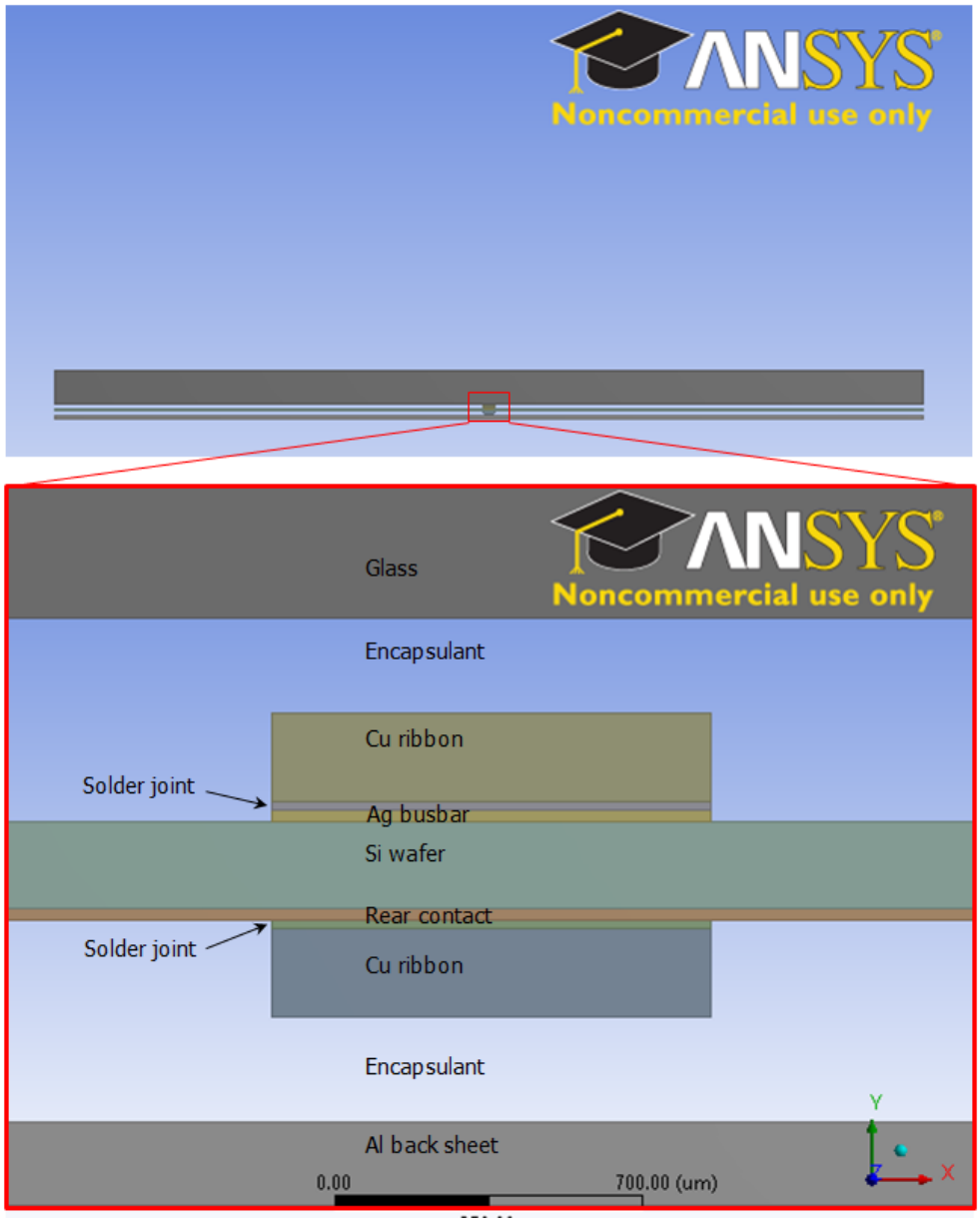


**(a) Model with interconnected components without IMC (solder only)**

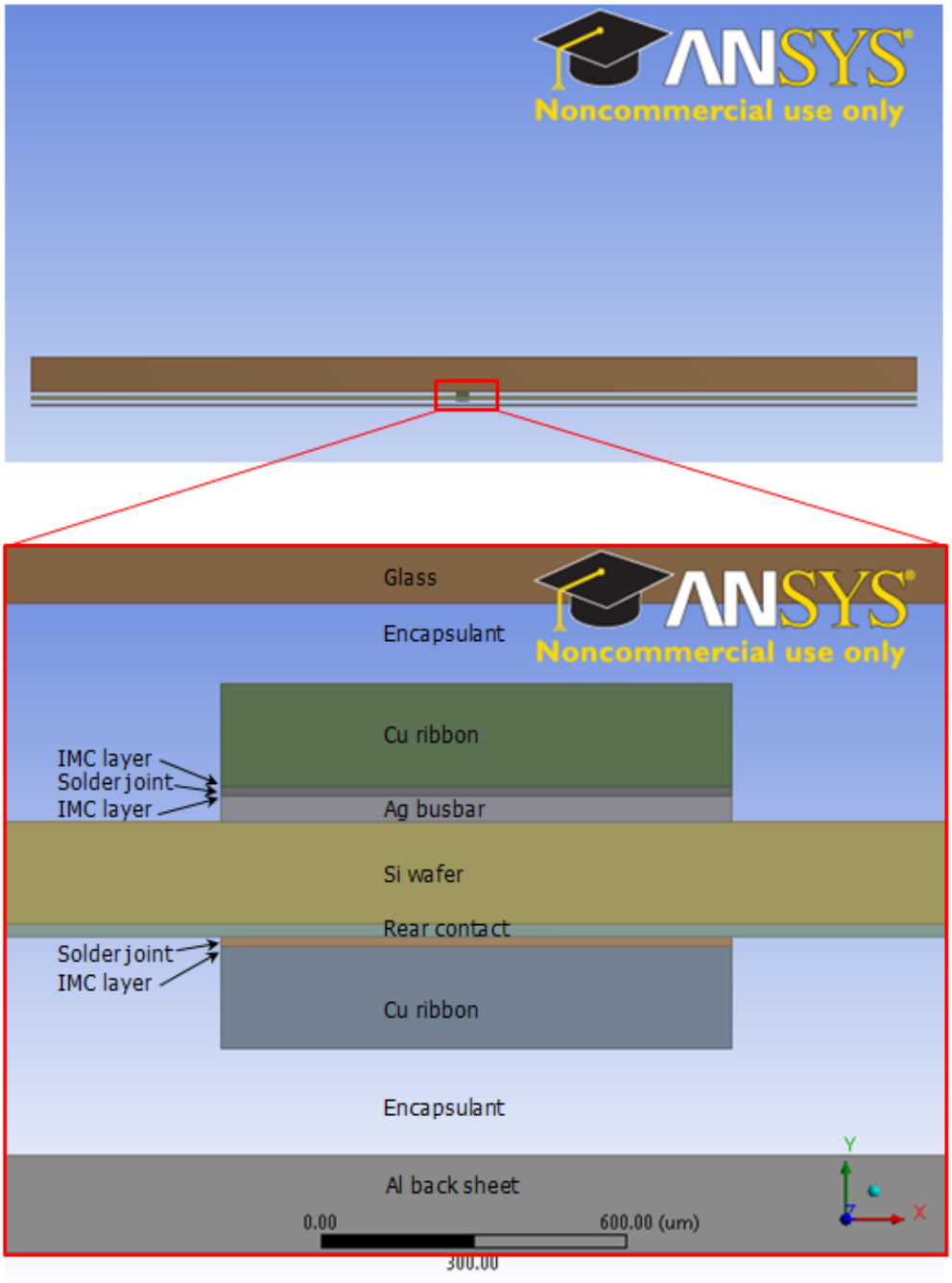


**(a) Model with interconnected components of solder + IMC**

**Figure 4.5 Cross-section of crystalline Si solar cell assemblies showing:**
**(a) Model with interconnected components without IMC (solder only)**
**(b) Model with interconnected components of solder + IMC**

The results of simulation are presented in Fig. 4.6 which shows damage distribution of creep strain on the solder joints for both the model without IMC, Fig 4.6(a), and the model with IMC, Fig. 4.6(b). In Fig. 4.6(a) showing solder joint composed of solder only, it can be observed that the worst damage is at the two ends of the solder joint while in Fig. 4.6(b) showing solder joint composed of solder + IMC, the damage is along the longitudinal section of the solder joint in addition to the damage at the ends of the joint.

Presented in Fig. 4.7 is a plot of equivalent creep strain on solder joint against load step. The plot shows that the solder joint in the model with solder only and that of the model containing IMC both experience creep strain deformation in varying degrees. The model containing IMC has larger magnitude of deformation compared to the solder only model. Likewise, there is a substantial difference in creep strain response in the two solder joint compositions. The solder joint containing solder only experienced a sharp increase in creep strain at the first temperature ramp up followed by a decrease downwards as the temperature was ramped downwards. This trend of creep strain response continued in the pattern of thermal cycling profile. In addition, it can be observed that the creep strain gradually increased from a minimum value at the beginning of the first thermal cycling to a maximum at the end of the sixth thermal cycling.

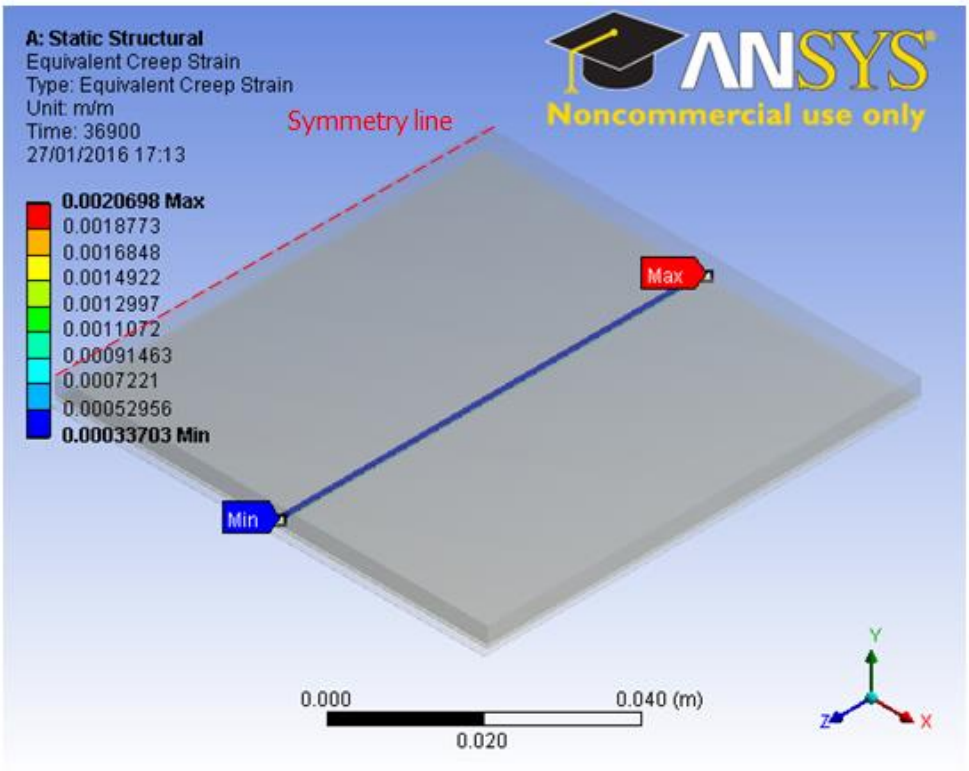


(a)

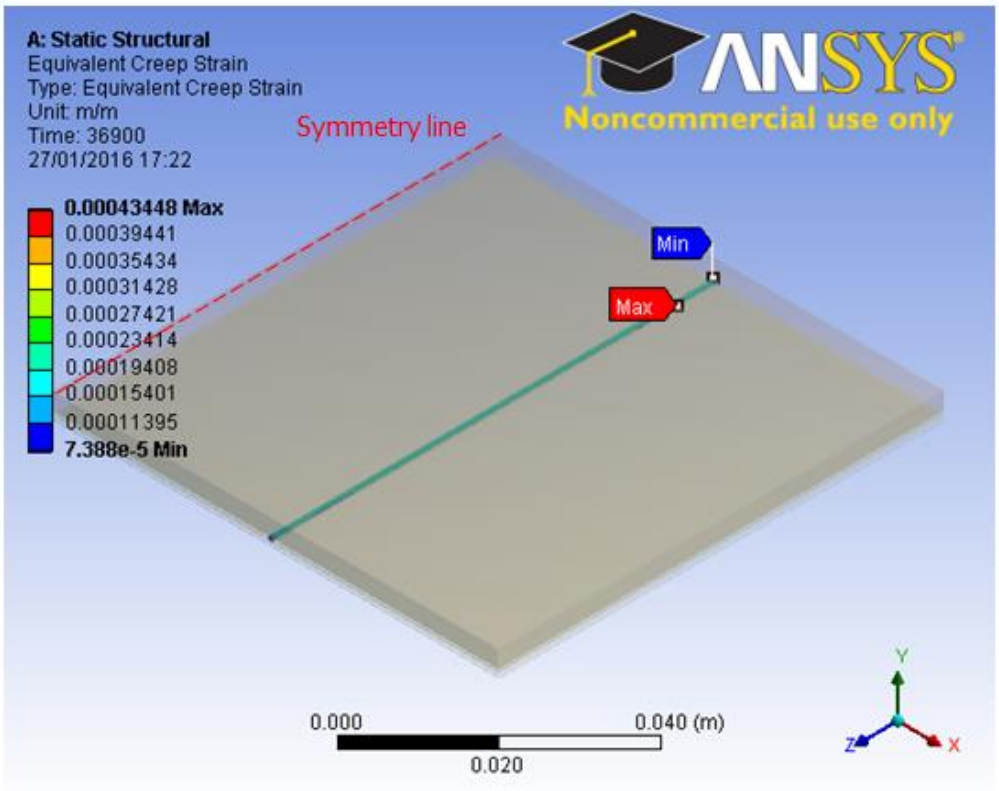


(b)

**Figure 4.6: Creep strain damage distribution showing:**
**(a) Creep strain on solder only (b) Creep strain on solder + IMC**

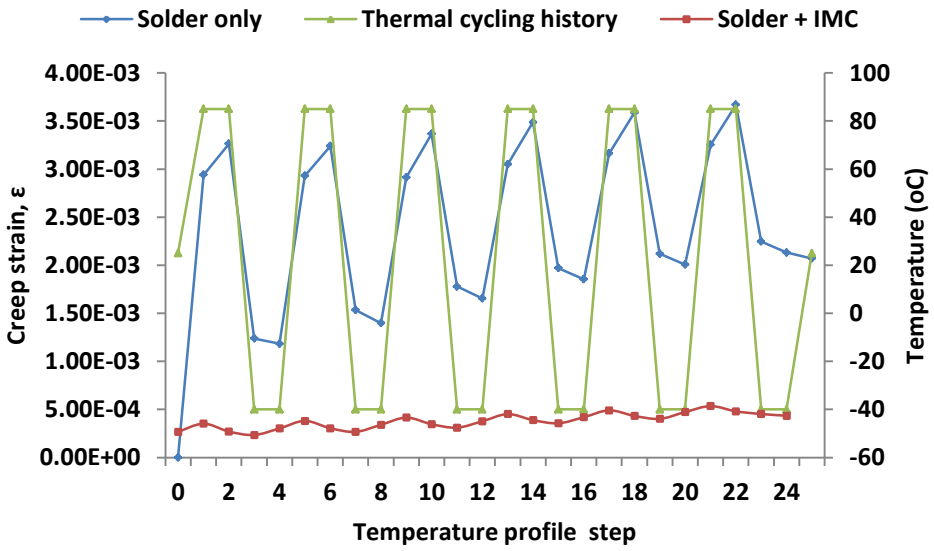


**Figure 4.7 Plot of equivalent creep strain on solder joint against temperature profile step**

### 4.3.3 Effect of IMC layer on creep strain behaviour of solder joints

The creep strain behaviour of solder joint is affected by the presence of IMC in the solder joint as can be observed in Fig. 4.7. Contrary to the behaviour of solder joint without IMC, the solder joint containing IMC appears to have strain hardened from the onset of thermal loading and stabilised through stress relaxation with fairly constant homogenous amplitude of deformation throughout the thermal cycles. The comparison of creep strain profiles of the two models indicates that the deformation amplitude in the solder joint containing IMC is higher than that in the solder only joint. This indicates that the presence of IMC in the model with IMC enables predominance of fatigue failure mechanism than in the model without IMC.

### 4.3.4 Analysis of strain energy and strain energy density in solder joints

The thermal loading on the solar cell solder joint induces creep deformation in the joint. The deformation is stored internally throughout the volume of the joint as creep energy. Creep strain energy per unit volume of material is referred to as creep strain energy density. In this study, the creep strain energy was obtained from simulation results and converted to accumulated strain energy density for each of the two models The plots of strain energy density against load step for both the model with solder only and that with solder +IMC are presented in Fig. 4.8. It can be observed from the plot that the solder joint containing solder + IMC has a peak strain energy density of about O.01mJ/mm$^3$ while that of solder only joint is about 0.008mJ/mm$^3$. This indicates that solder joint containing solder + IMC has about 25% higher strain energy density compared to solder only joint. This infers that the presence of IMC in the solder joint significantly impacts the joint. Thus, the solder joint containing IMC is more susceptible to fatigue failure than the joint without IMC.

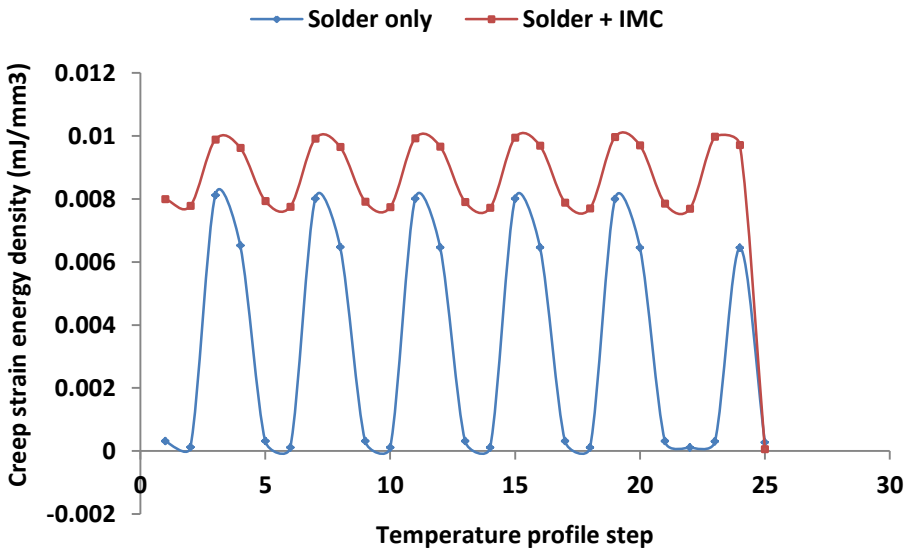


**Figure 4.8 Plot of strain energy density against temperature profile step**

### 4.3.5 Effect of IMC layer on solder joint fatigue life

The service life of solar cell solder joints can be predicted using fatigue life models as discussed in section 2.4.2. In this study, accumulated strain energy density model for life prediction is used. This is because Syed (2004) reported that the accumulated strain energy density model captures high stress effects better than the creep strain model. To compute the fatigue life of solder joint, the values of average accumulated change in creep strain energy density per cycle ($\Delta\omega_{acc}$) obtained from simulation of the models are inputted into Eq. 2.11. The computed value obtained for cycles to failure indicates the predicted fatigue life of the solder joint.

The computed cycles to failure are quantified in Table 4.2 which shows the effect of IMC on solar cell solder joint thermal fatigue life. Furthermore, in

field operations, crystalline silicon PV modules are expected to last up to 25 years. As mentioned earlier, Guyenot *et al.* (2011) estimated that for 1.5 thermal cycles per day with a temperature change of about 50 $^{o}$C, expected life of solder joints for 25 years is 13688 cycles to failure. This value of expected life is also presented in Table 4.4. The table shows that accumulated creep strain energy density for solder joint containing solder + IMC is higher than that of the joint containing solder only. Moreover, the predicted thermal fatigue life or cycles to failure of solder joint with solder + IMC is 15317 which is shorter than that of 32488 for the joint with solder only. This indicates that there is a percentage change of predicted life from solder only joint of 52.85%. Furthermore, when the value of expected life is compared with the values of the two models, it can be seen that solder only model has a value of more than double the expected lifespan while the predicted life of solder + IMC model has a value close to expected life.

**Table 4.4 Effect of IMC on solar cell solder joint fatigue life**

| Model | $W^{'}$ | $\Delta\omega_{acc}$ (mJ/mm$^3$) | Predicted life (cycles) | Expected life (cycles) | % change of predicted life from solder only joint |
|---|---|---|---|---|---|
| **Solder only** | **0.0019** | **0.01620** | **32493** | **13688** | **0** |
| **Solder + IMC** | **0.0019** | **0.03436** | **15317** | **13688** | **52.85** |

The results presented indicates that the predicted thermal fatigue life or cycles to failure of solder joint with IMC is much shorter than that of the joint with solder only. Besides, the model containing IMC predicts life more accurately compared to the model without IMC in solder joint. The

implication is that when solder joint contains IMC at the joint interface, the likelihood of fatigue failure is much higher compared to the joint without IMC. Consequently, the thermo-mechanical reliability of the solder joint is significantly impacted by the presence of IMC in the joint.

## 4.4 Conclusions

The study presented in this chapter is on the effect of intermetallic compound on thermo-mechanical reliability of lead-free solder joints in multi-crystalline silicon solar cells using finite element analysis. The results of the study shows that creep deformation gradient in the model of solder joint with IMC accumulates along the longitudinal section of the joint while for the solder only joint; the deformation gradient is at the two ends of the joint. This demonstrates that the solder joint containing solder + IMC experiences greater induced non-linear deformation than the solder only joint. The deformation amplitude in the solder joint containing IMC is higher than that in the solder only joint. This indicates that the presence of IMC in the model enables predominance of fatigue failure mechanism than in the model without IMC. Furthermore, the solder joint containing solder + IMC have considerable higher strain energy density compared to the joint with solder only. Moreover, the predicted thermal fatigue life or cycles to failure of solder joint with IMC is much shorter than that of the joint with solder only. This implies that fatigue failure is dependent on solder joint composition such that the presence of IMC in the solder joint significantly impacts the

thermo-mechanical reliability of the solder joint. Based on the results of the study, the author proposes that IMCs should be included in the geometric models employed to investigate the thermo-mechanical reliability of solder joints which consist of Sn-based solder and interconnection copper ribbon. The inclusion of IMCs will improve the accuracy of results from such study. Furthermore, IMC in solder joint increases in thickness during thermal loading with damaging effect on the solder joint. Therefore, a study on the effect of IMC thickness on thermo-mechanical fatigue life of solder joint is presented in the next chapter to gain more understanding.

# CHAPTER 5

# STUDY OF THE EFFECT OF INTER-METALLIC COMPOUND THICKNESS ON THERMO-MECHANICAL FATIGUE LIFE OF SOLDER JOINTS IN SOLAR CELL ASSEMBLY

# Chapter 5

# Study of the Effect of Inter-metallic Compound Thickness on Thermo-mechanical Fatigue Life of Solder Joints in Solar Cell Assembly

## 5.1 Introduction

The study on detrimental effect of IMC on solder joint thermo-mechanical reliability was presented in the preceding chapter. Further study of IMC effect is carried out in this chapter with particular focus on the effect of IMC thickness on thermo-mechanical fatigue life of solder joint in solar cell assembly. This study utilizes five geometric models of solar cell assemblies with different IMC thickness layers in the range of 1 to 4μm. The models were subjected to accelerated thermal cycling from -40 $^{o}$C to 85 $^{o}$C utilising IEC 61215 standard for photovoltaic panels (Amdt and Puto, 2011). The study evaluates the quantitative damage of the solder joints using the concept of hysteresis loop. Furthermore, the study evaluates the thermally induced creep deformation stored in solder joint as strain energy and its effects in the whole joint with IMC layer as well as in the solder region. The values of creep strain energy density were determined and used to predict the service lifetimes of the models. Hence, this chapter presents the methodology adopted for this study followed by modelling and simulation results obtained and discussion. The presentation of results and discussion is made up of the following six sub-sections: study on equivalent stress, study on equivalent creep strain, evaluation of hysteresis loop of solder joints in

solar cell assembly, evaluation of accumulation of strain energy density and effect of IMC on solder joint fatigue life.

The methodology adopted in this chapter is similar to the one used in chapter 4 where FEM discussed in section 3.2.2.1 is utilized to investigate the effect of IMC layers on the thermo-mechanical reliability of solder joints in multi-crystalline silicon solar cell assembly. Likewise, Garofalo-Arrhenius creep model discussed in section 3.2.2.2 was used for this study. The study of induced strain in 156 × 156mm$^2$ multi crystalline silicon solar cell assembly was carried out using commercial ANSYS Academic Research Finite Element package. Just as in chapter 4, the solar cell assembly has two printed Ag bus bars on its front surface and on the bus-bars, copper ribbon strips are soldered. Work station computers were used to carryout High Performance Computation (HPC) involved in simulating the assemblies. Quarter symmetry of the geometric model was simulated to lessen modelling time and disc space. The static structural response of the geometric models subjected to accelerated thermal cycling utilising IEC 61215 standards for photovoltaic panels were simulated. Presented in Fig. 5.1 is a cross-section of solar cell model showing IMC thickness.

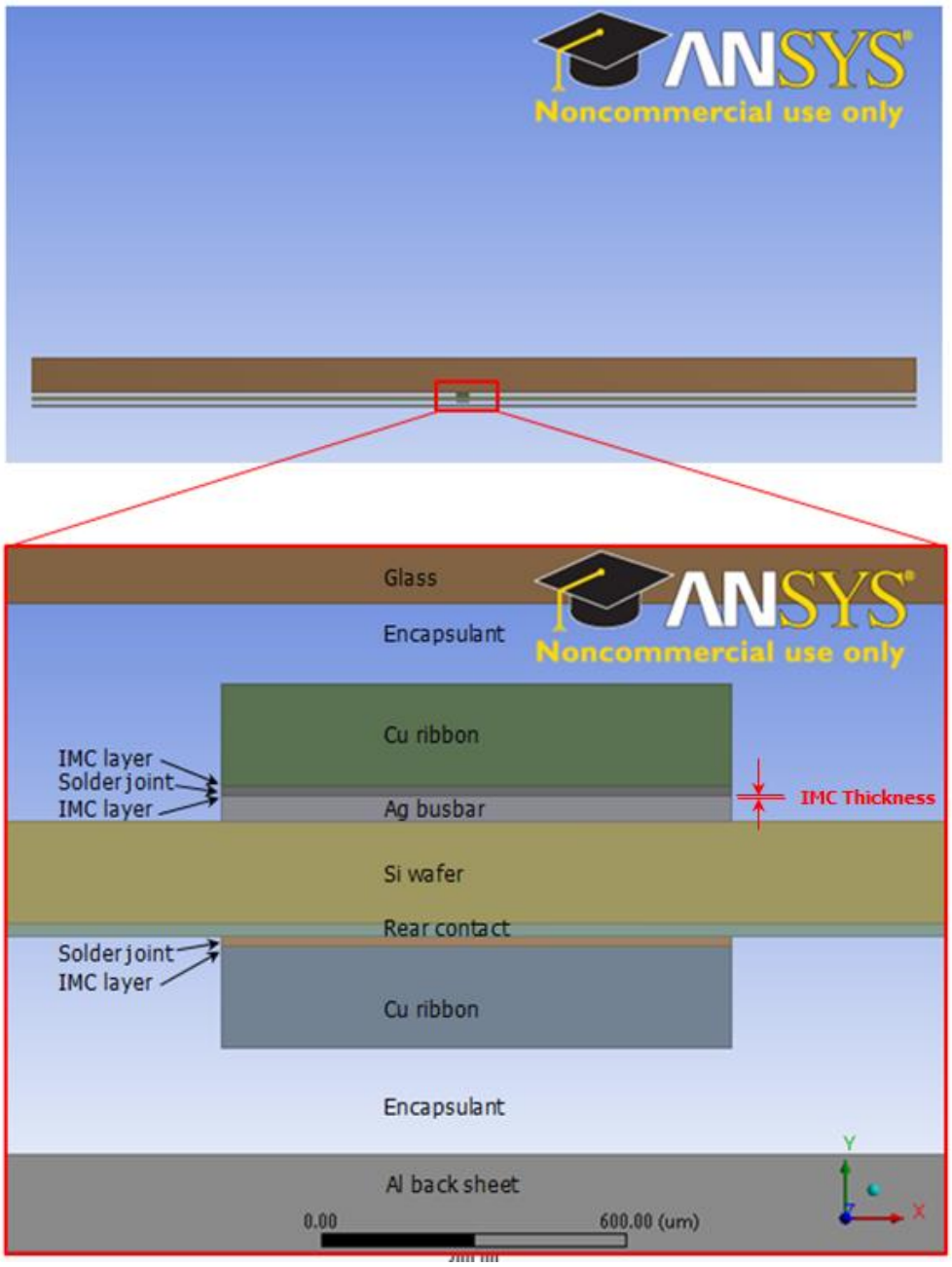


**Figure 5.1 Cross-section of solar cell model showing IMC Thickness**

The geometric models used in this study are similar to the one shown in Fig. 4.5 which had IMC layers at the two solder joint interfaces. The thickness of the IMC layers at the two sides of solder layer is assumed to be the same. Based on the experimental findings discussed in chapter 2, this study utilized five finite element geometric models of solar cell assembly with IMC layer

thickness of 1μm, 2μm, 2.5μm, 3μm and 4μm as presented in Table 5.1. These IMC layer thicknesses used in the models are within the range of thicknesses obtained experimentally by Schmitt *et al.* (2012) and Yang *et al*. (2014). The models were assigned numbers 1, 2, 3, 4 and 5 respectively and simulated separately. All the five models have the same solder joint thickness of 20μm as well as same solder joint width of 1000μm. Thus the total volume in the whole solder joint for all the models is the same 1.56 $mm^3$. In all the geometric models, the whole solder joint comprises of three regions: IMC layer at the interface joint between solder and Cu ribbon; solder region; and IMC at the interface joint between solder and Ag bus-bar. The parameters of all the five models are presented in Table 5.1. An observation of the table shows that each model has a different IMC thickness from the other such that as the IMC thickness increases, volume in solder region reduces.

**Table 5.1 Parameters of solder joints containing varied IMC thickness**

| Model number | IMC thickness (μm) | Solder joint thickness (μm) | Solder joint width (μm) | Whole joint Vol. ($mm^3$) | Solder region Vol. ($mm^3$) |
|---|---|---|---|---|---|
| **1** | **1.0** | **20** | **1000** | **1.56** | **1.404** |
| **2** | **2.0** | **20** | **1000** | **1.56** | **1.248** |
| **3** | **2.5** | **20** | **1000** | **1.56** | **1.170** |
| **4** | **3.0** | **20** | **1000** | **1.56** | **1.092** |
| **5** | **4.0** | **20** | **1000** | **1.56** | **0.936** |

The data in Table 5.1 is used to plot solder region volume against IMC thickness and is presented in Fig. 5.2. It can be observed in Fig. 5.2 that as

thickness of IMC layer increases from the low value in Model 1 to the high value in Model 5, the solder region volume decreases accordingly. Thus, for the thin IMC thickness in Model 1, solder volume is large whereas for the thick IMC thickness in Model 5, solder volume is small. Moreover, it can be noted that the plot of IMC thickness and solder region volume intersect just about Model 4. The point of intersection implies a crucial transition where further increase in IMC thickness could result in critical solder region volume and potential solder joint failure. After the intersection, the IMC thickness continues to increase while the solder region volume decreases further.

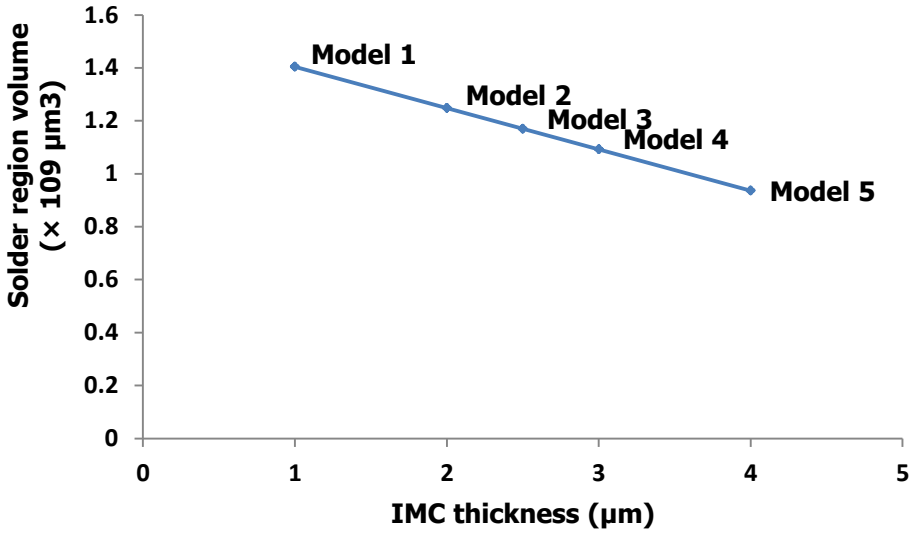


**Figure 5.2 Plot of solder region volume against IMC thickness**

The five models were subjected to six accelerated thermal cycling in 25 load steps between -40°C to 85°C. The temperature loading started from 25°C, ramped up at a rate of 3°C/min to 85°C, where it had hot dwell for 20 min. It was then ramped down to -40°C at a rate of 6°C/min, where it had cold

dwell for 20 min. The thermal cycling profile presented in section 3.2.2.2.2 was used to simulate actual cycling profile used during thermal load test.

In the analysis of simulation results, model based on whole joint is termed *model i whole solder joint* while model based on solder region is termed *model i solder region*. The "i" designates models 1-5 used in this study. The creep strain, stress and strain energy of whole joint models as well as solder region models are evaluated and comparatively analysed. Furthermore, accumulated creep strain energy density in the solder joints of each model was determined and compared. Moreover, the average accumulated creep strain energy density in the solder joint was used for life prediction computation of the joint in each model.

## 5.2 Results and discussion

This section presents analysis and discussion of simulation results. The section consists of six sub-sections as follows: study on equivalent stress, study on equivalent creep strain, evaluation of hysteresis loop of solder joint in solar cell assembly, study on strain energy of solder joints evaluation of accumulation of strain energy density and effect of IMC layer on solder joint fatigue life.

### 5.2.1 Study on equivalent stress

Induced stress in solar cell solder joint is studied for all five models. The stress is analysed for both the whole solder joint inclusive of IMC layers at the two interfaces as well as solder only region exclusive of IMC layers. Presented in Fig. 5.3 are the five models showing damage distribution of equivalent stress on the whole solder joint. The Figs. 5.3(a), 5.3(b) and 5.3(e), reveal that Models 1, 2 and 5 have maximum stress at the end of the right hand side of the longitudinal section of the solder joint. However, Models 3 and 4 as shown in Figs. 5.3(c) and 5.3(d) respectively have maximum stress at the ends of the left hand side of the longitudinal section of the solder joints. Furthermore, it can be observed that the values of induced stress in the solder joints are different for all the models. Model 4 has the largest maximum stress of 10MPa while Model 1 has the smallest maximum stress of 6.62MPa. Besides, the damage distribution seems to be uniformly spread along the entire longitudinal section of the solder joints for all the five models.

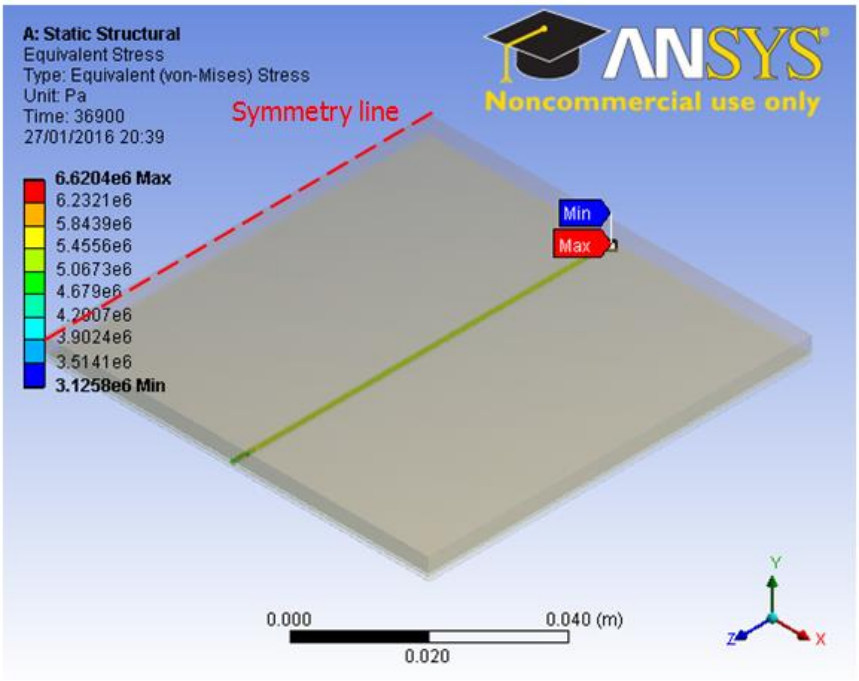


**(a) Stress on model 1 whole joint**

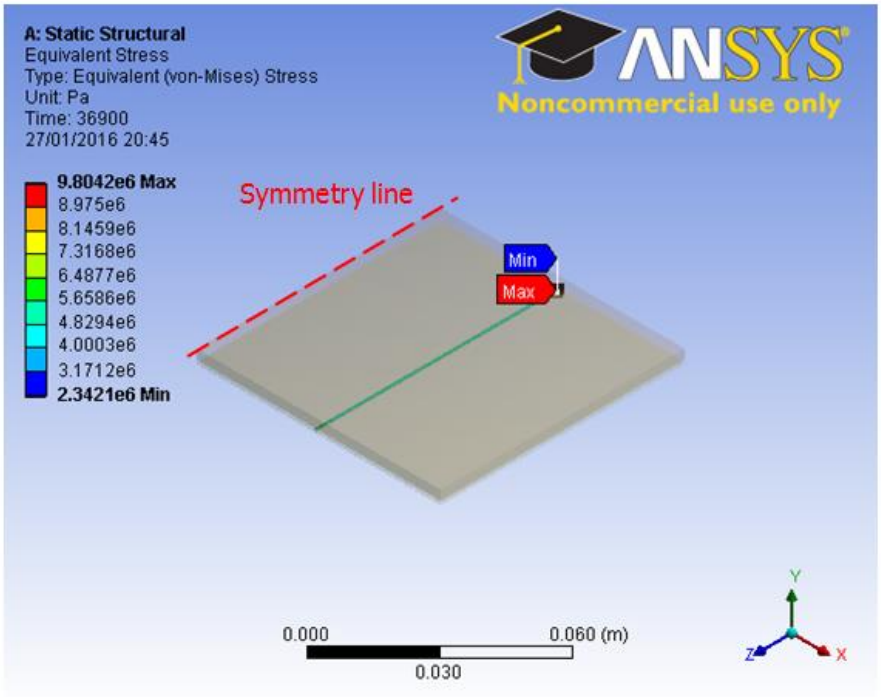


**(b) Stress on model 2 whole joint**

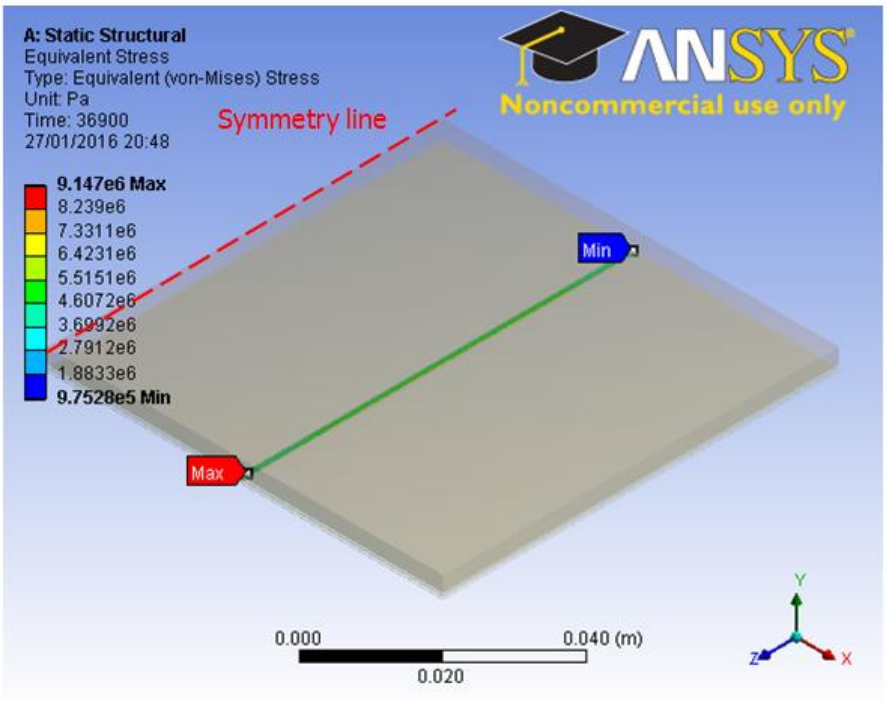


**(c) Stress on model 3 whole joint**

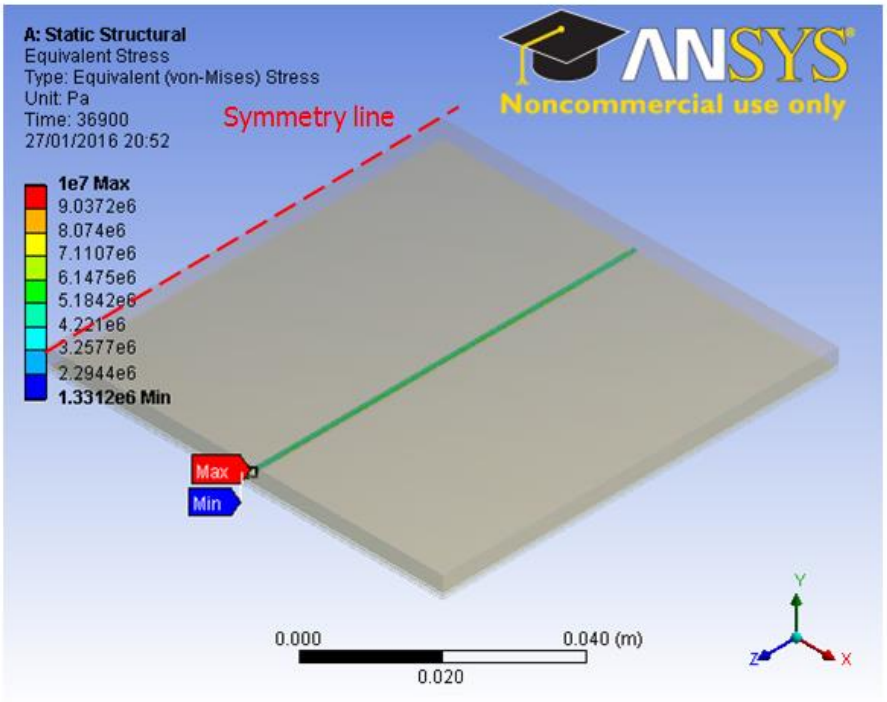


**(d) Stress on model 4 whole joint**

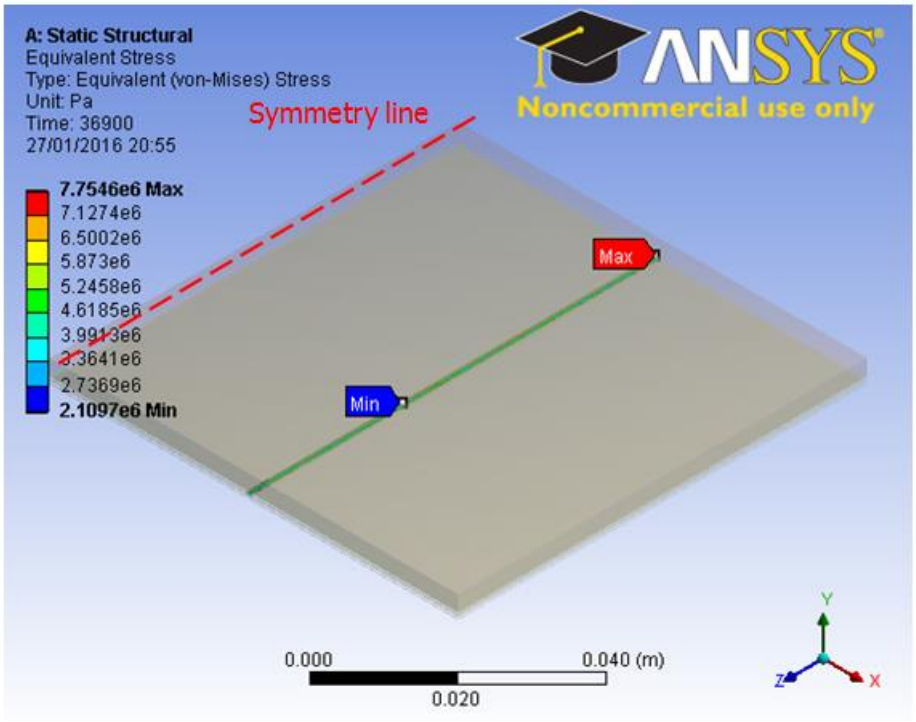


**(e) Stress on model 5 whole joint**

**Figure 5.3 Damage distributions of equivalent stress on the whole solder joint in models showing:**
**(a) Stress on model 1 whole joint**
**(b) Stress on model 2 whole joint**
**(c) Stress on model 3 whole joint**
**(d) Stress on model 4 whole joint**
**(e) Stress on model 5 whole joint**

While the damage in the whole solder joint appears to be mild as shown in the preceding models of Fig. 5.3, the actual situation in the solder only region is different. Figure 5.4 shows the damage in the solder only region in the five models subjected to stress. In all the five models, the damage in the solder only region is more pronounced than in the whole solder joint. Consequently, models with whole solder joint which include IMC may give a false impression of the damage in the solder joint. Therefore, it is crucial to separately study the solder only region which provides the critical interconnection for solar cell assembly. The maximum stress in the solder

joint of Models 1 and 5 presented in Figs. 5.4(a) and 5.4(e) is located at the end of right hand side of the solder joint and the damage spreads along the longitudinal section of the joints; whereas for Model 2 shown in Fig. 5.4(b) the damage is more pronounced at both ends of the joint with the maximum stress located at the end of the right hand side of the joint. Moreover, Models 1 and 5 show a more pronounced damage distribution over a long stretch of the mid-section of the longitudinal section of the solder joint compared to Model 2. In the case of Models 3 and 4 as presented in Figs. 5.4(c) and 5.4(d) the maximum stress is located at the end of the left hand side of the longitudinal section of the solder joint. Additionally, whereas the damage distribution in Models 1 and 5 is more pronounced over a long stretch of the longitudinal section of the solder joint, that of Models 2, 3 and 4 is more severe around the left and right hand side end of the solder joints.

Furthermore, a close observation of the IMC layers shows that the IMC layer at the Ag bus-bar/solder interface has greater damage distribution compared to the IMC layer at the Cu ribbon/solder interface. This is consistent with experimental findings by Schmitt *et al.* (2012). Accordingly, the differences observed in the two sets of models for whole solder joint and solder only regions further justifies the need to study the effect of IMC inclusion in solder joint models for accurate prediction of solder joint fatigue life.

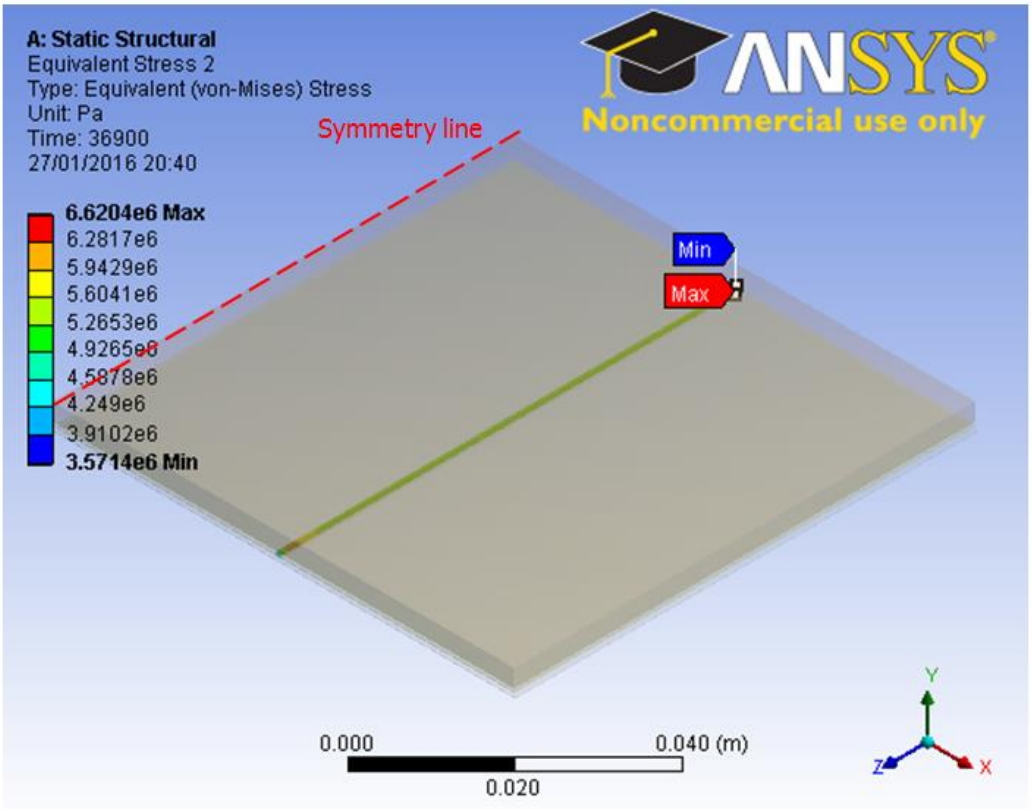


**(a) Stress on model 1 solder only region**

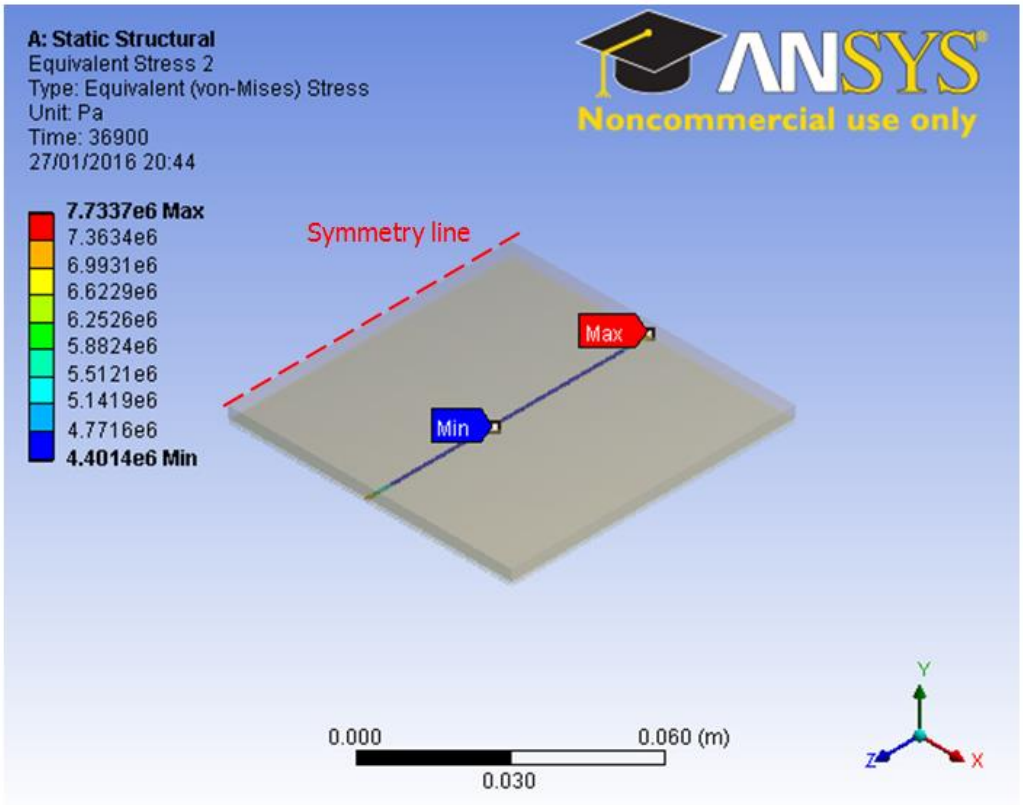


**(b) Stress on model 2 solder only region**

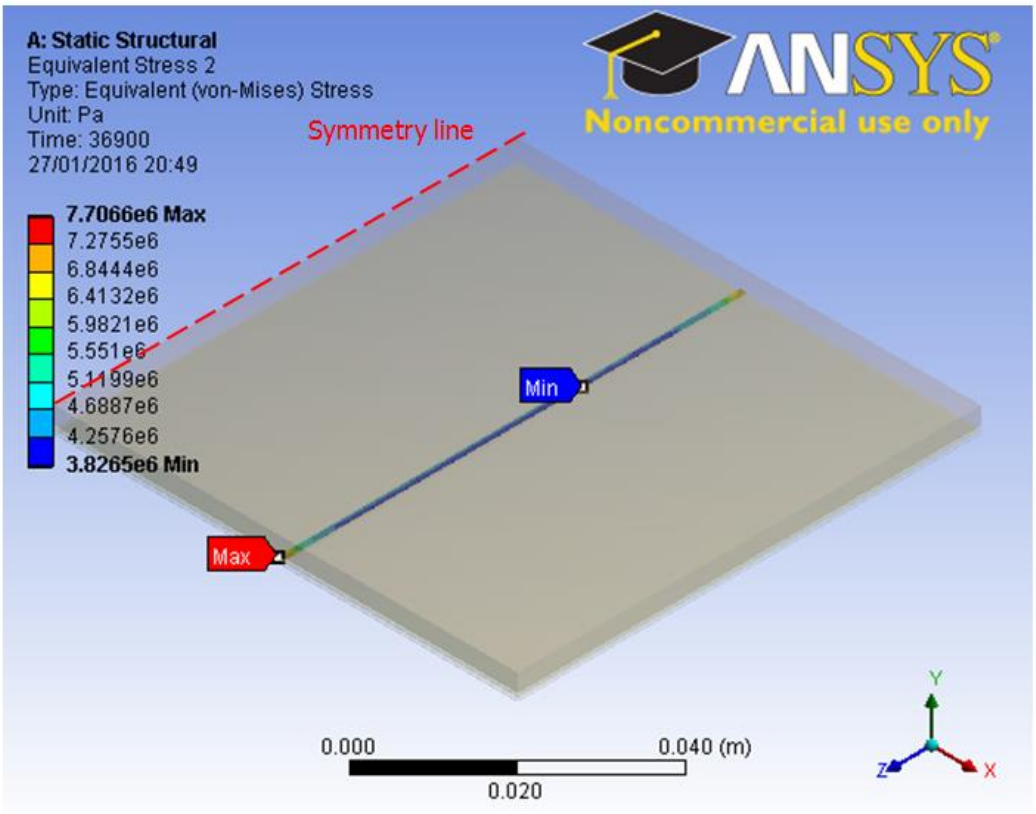


**(c) Stress on model 3 solder only region**

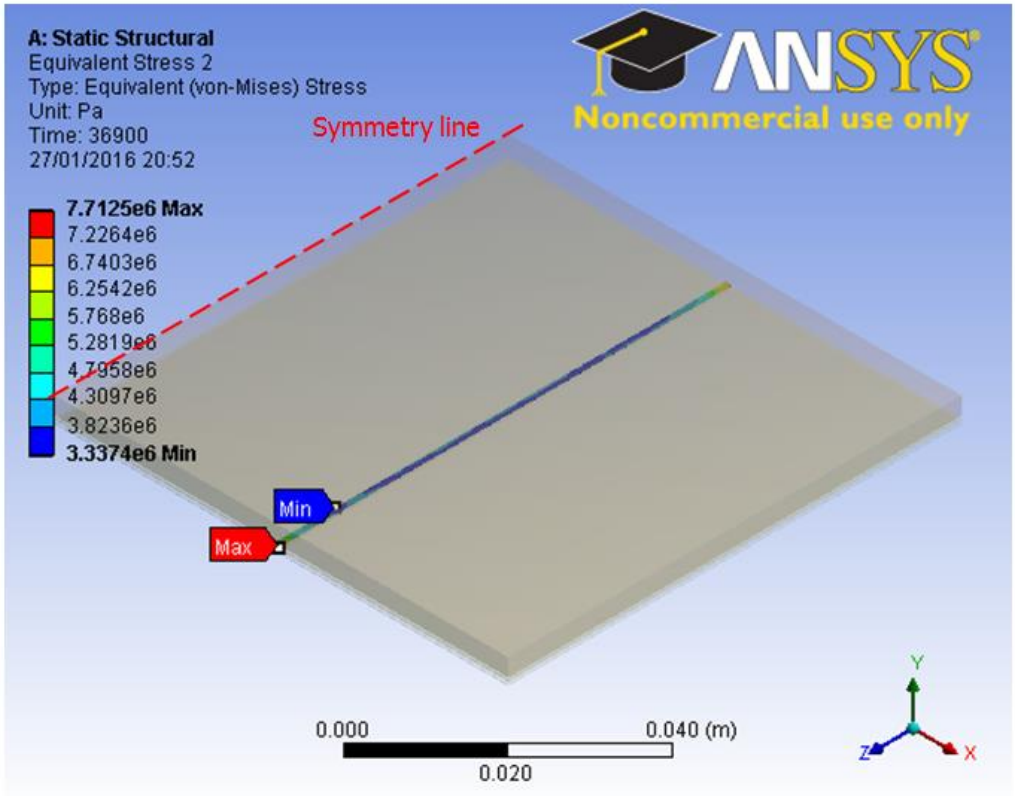


**(d) Stress on model 4 solder only region**

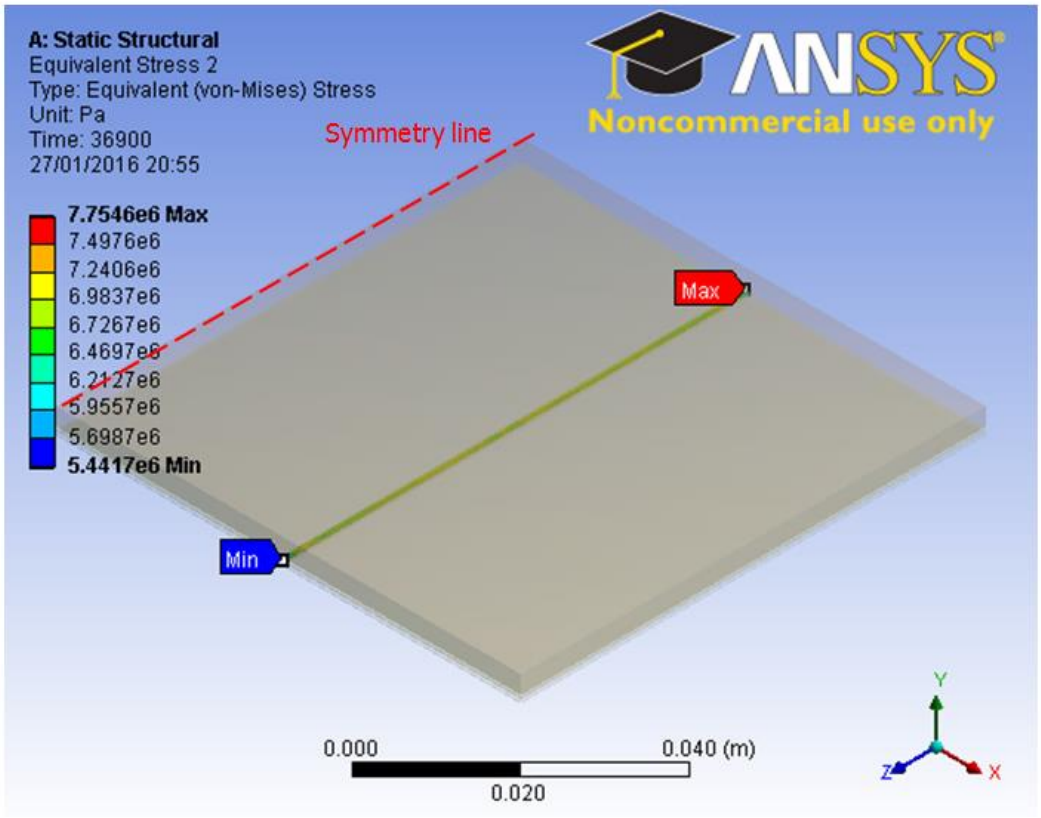


**(e) Stress on model 5 solder only region**

**Figure 5.4 Damage distribution of equivalent stress on the solder only region showing:**
**(a) Stress on model 1 solder only region**
**(b) Stress on model 2 solder only region**
**(c) Stress on model 3 solder only region**
**(d) Stress on model 4 solder only region**
**(e) Stress on model 5 solder only region**

### 5.2.2 Study on equivalent creep strain

Figure 5.5 shows five geometric models of solder joint in solar cell assembly showing damage distribution of equivalent creep strain on solder joint. Figure 5.5(a) shows the maximum creep strain in solder joint of Model 1 located a few millimetres to the right hand side of the joint and the damage spread along the longitudinal section whereas for Model 2 shown in Fig. 5.5(b) the maximum creep strain is located at about the end of the left hand

side of the solder joint with a milder damage along the longitudinal section of the joint. The maximum creep strain on solder joint of Model 3 as shown in Fig. 5.5(c) is located close to the end of the right hand side of the joint and the damage mildly spread along the longitudinal section of the joint. Model 4 in Fig. 5.5(d) has maximum creep strain located a few millimetres to the left hand side of the joint and the damage spread along a large portion of the longitudinal section of the joint. Yet, Model 5 presented in 5.5(e) has maximum creep strain located at the end of the right hand side of the joint and the damage is more obvious at the two ends of the solder joint.

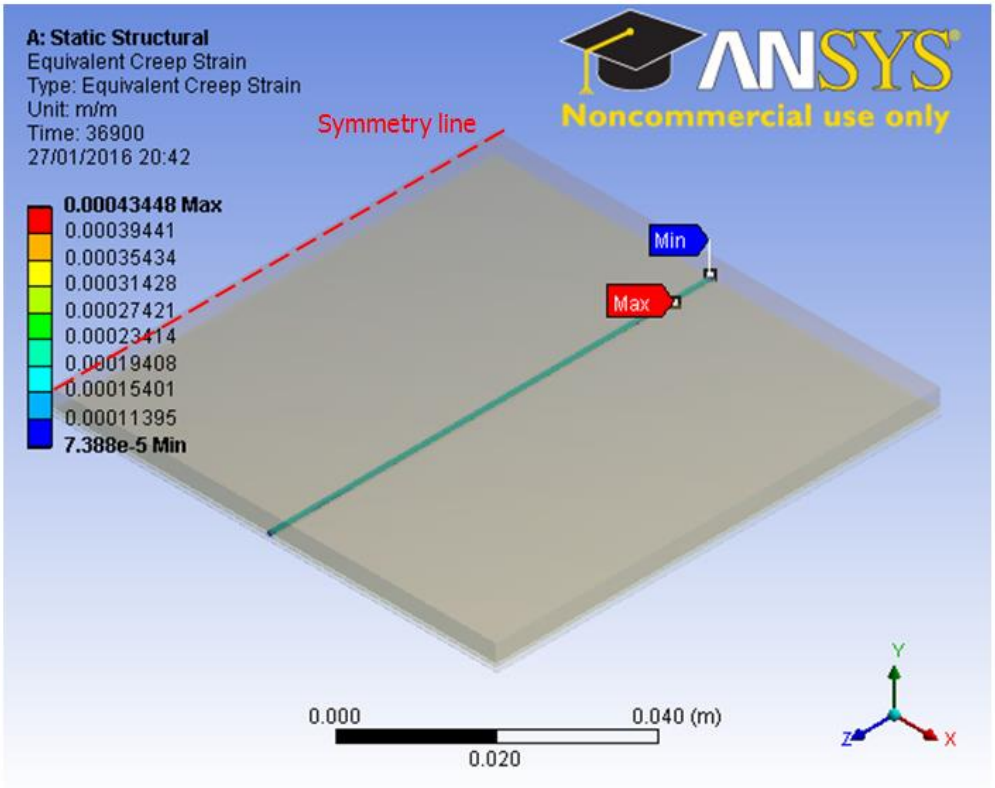


**(a) Strain on model 1 whole joint**

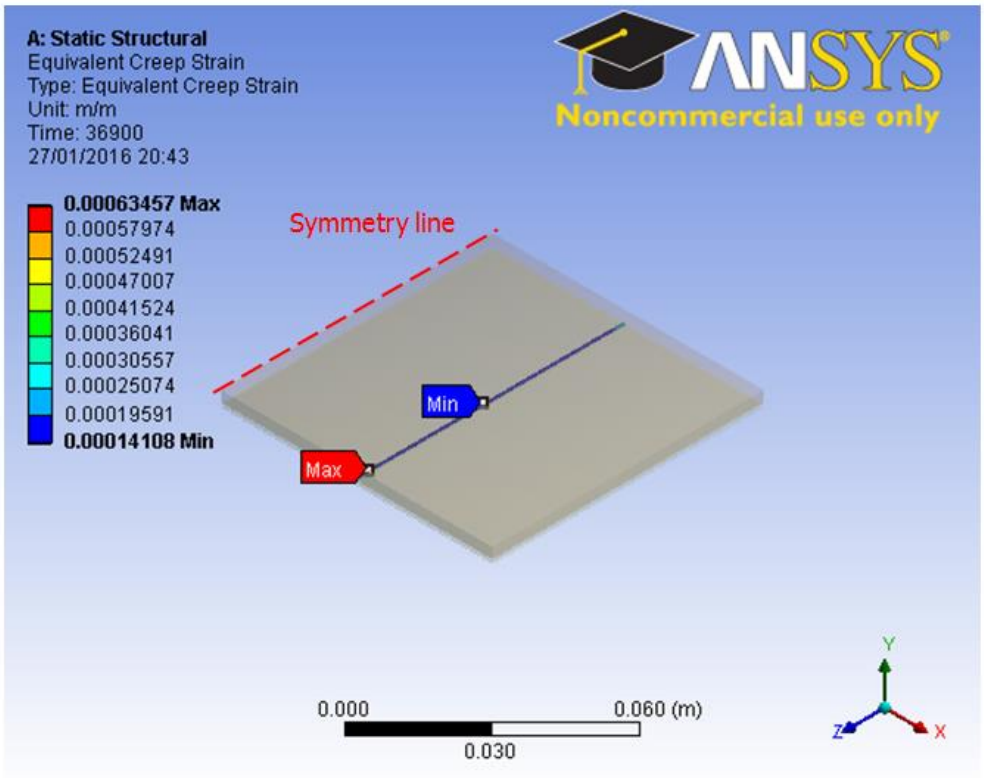


**(b) Strain on model 2 whole joint**

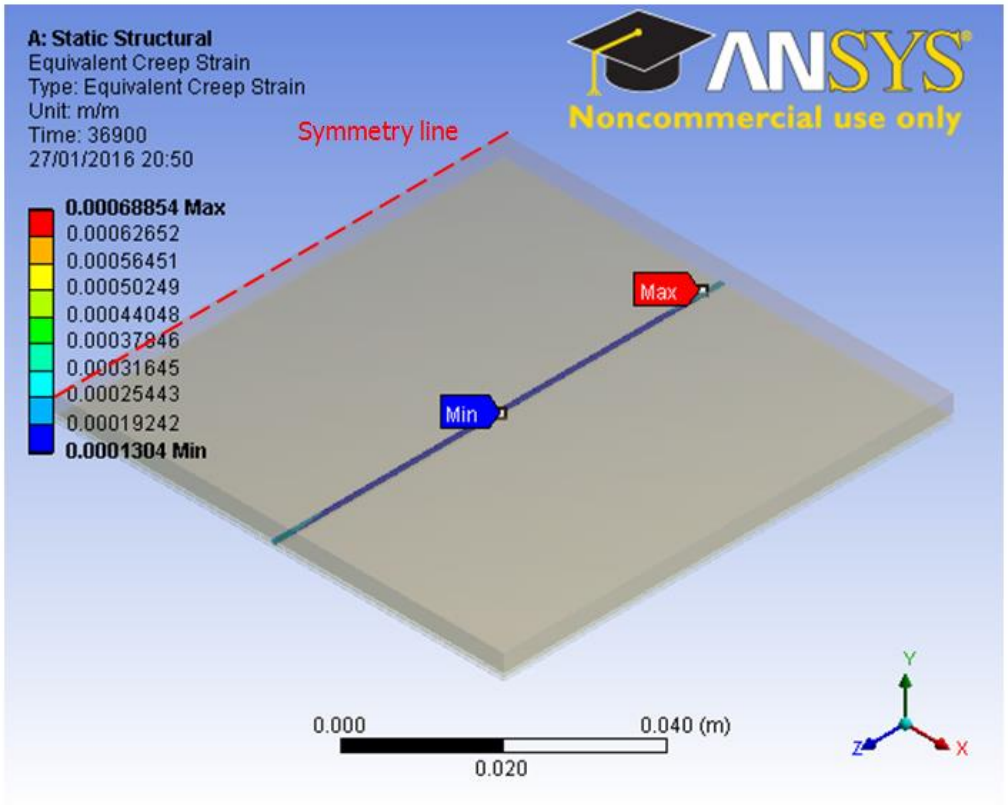


**(c) Strain on model 3 whole joint**

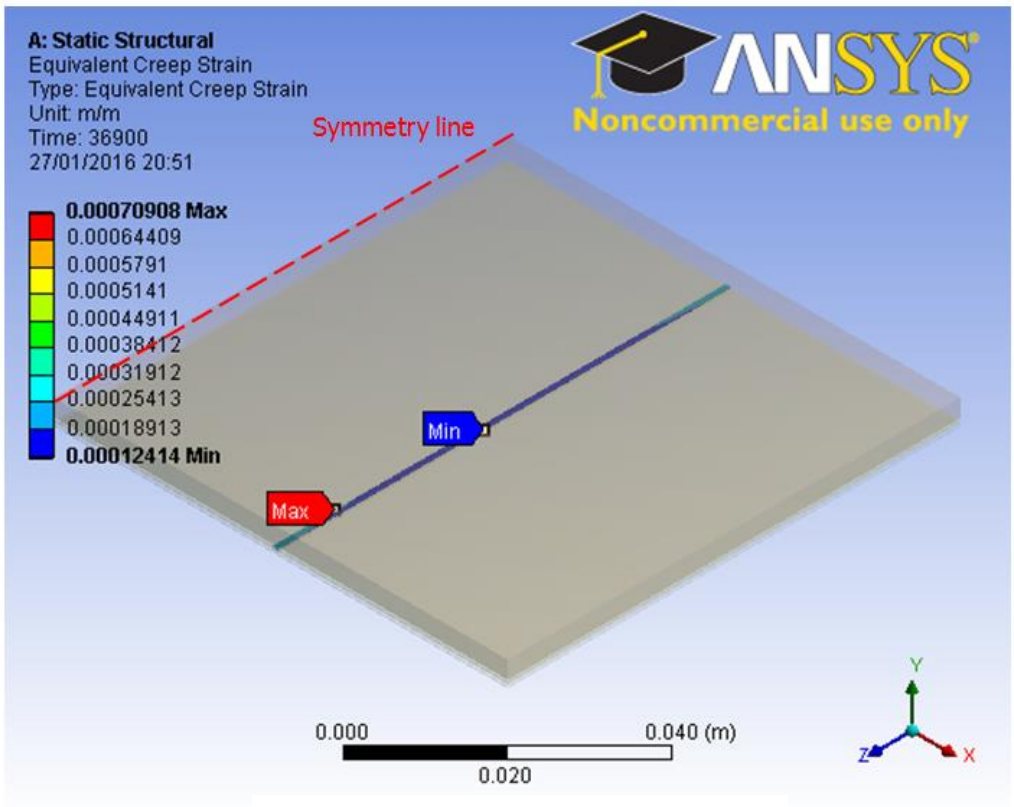


**(d) Strain on model 4 whole joint**

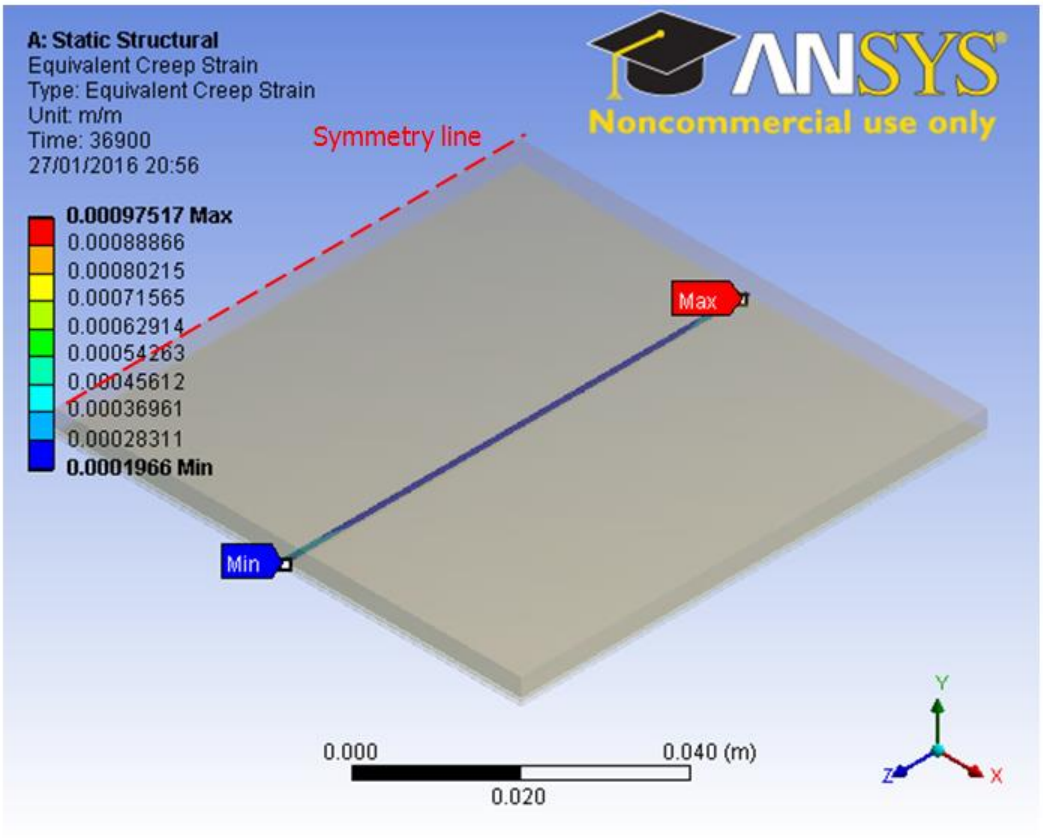


**(e) Strain on model 5 whole joint**

**Figure 5.5 Damage distribution of equivalent creep strain on the whole solder joint showing:**
**(a) Strain on model 1 whole joint**
**(b) Strain on model 2 whole joint**
**(c) Strain on model 3 whole joint**
**(d) Strain on model 4 whole joint**
**(e) Strain on model 5 whole joint**

The damage distribution of equivalent creep strain on whole solder joints of all the five models presented in Fig. 5.5 show that the largest maximum equivalent creep strain is 9.7517E-04m/m in Model 5 as shown in Fig. 5.5(e). This is not surprising because Model 5 has the largest IMC thickness of 4μm and thus, the smallest solder region volume of 0.936mm$^3$ as can be seen in Table 5.1. On the other hand, Model 1 has the least maximum equivalent creep strain of 4.3448E-04m/m as shown in Fig. 5.5(a). This is expected as

Model 1 has the smallest IMC thickness and the largest solder region volume of 1.404mm$^3$. The foregoing results further confirm that bigger IMC thickness in solder joint compels the joint to experience larger strain. Conversely, smaller IMC thickness in solder joint compels the joint to experience lesser strain. Thus IMC thickness significantly impacts solder joint in solar cell assembly.

### 5.2.3 Evaluation of hysteresis loop of solder joints in solar cell assembly

The damage distribution of stress and creep strain on solder joint of five models have been presented in Figs. 5.3, 5.4 and 5.5. Figure 5.3 shows the stress in the whole joint of the models whereas the stress in solder only region is presented in Fig. 5.4. However, the stress values in the whole joint are different from the stress values in the solder only region. For instance, the stress in the whole joint of Model 4 is 10MPa as shown in Fig. 5.3(d) which is higher than the stress in solder only region which is 7.7125MPa for the same Model 4 shown in Fig. 5.4(d). In order to highlight the differences in stress values between whole joint and solder only region, a plot of the relationship between stress and creep strains in the solder joints is made using values obtained from simulation results. Figure 5.6 shows the plot of the relationship between stress and creep strains in the solder joints of solar cell models for both the whole joint and solder only region. The figure shows five hysteresis loops each for models of whole joint and solder region which

formed as a result of thermal cycling. The area of each hysteresis loop represents the visco-plastic energy density per cycle or simply the fatigue damage accumulating per cycle in the models. As can be seen in the figure, each model has a different hysteresis loop; therefore, the fatigue damage in each model is different from the other. In addition, it can be observed that induced stress in models of whole joint is higher than in models with solder region only due to the presence of IMCs in the whole joint.

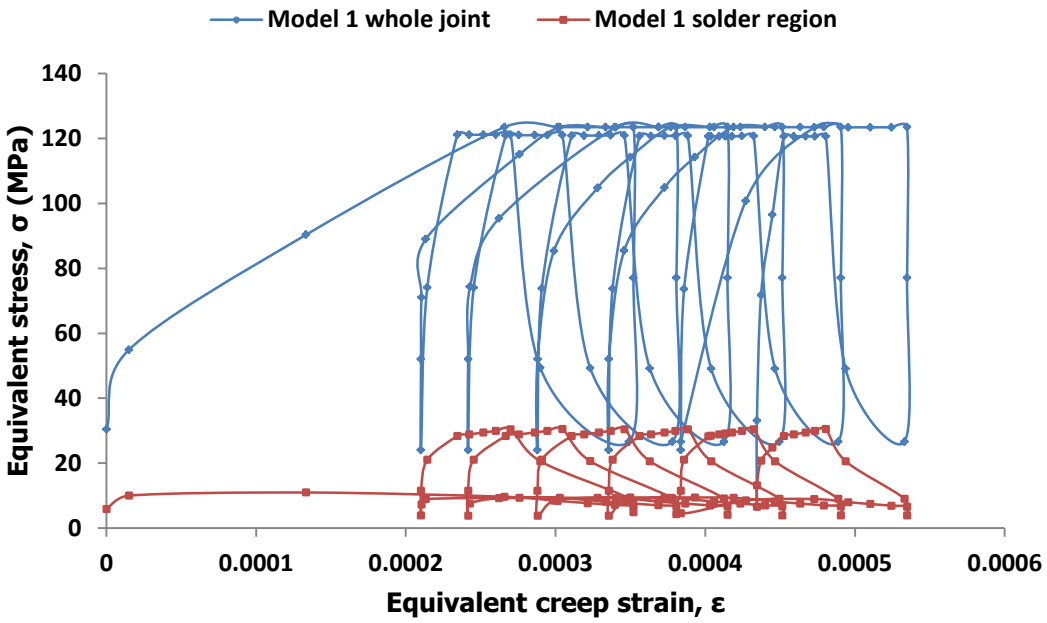


**(a) Stress and strain relationship in whole joint and solder region for model 1**

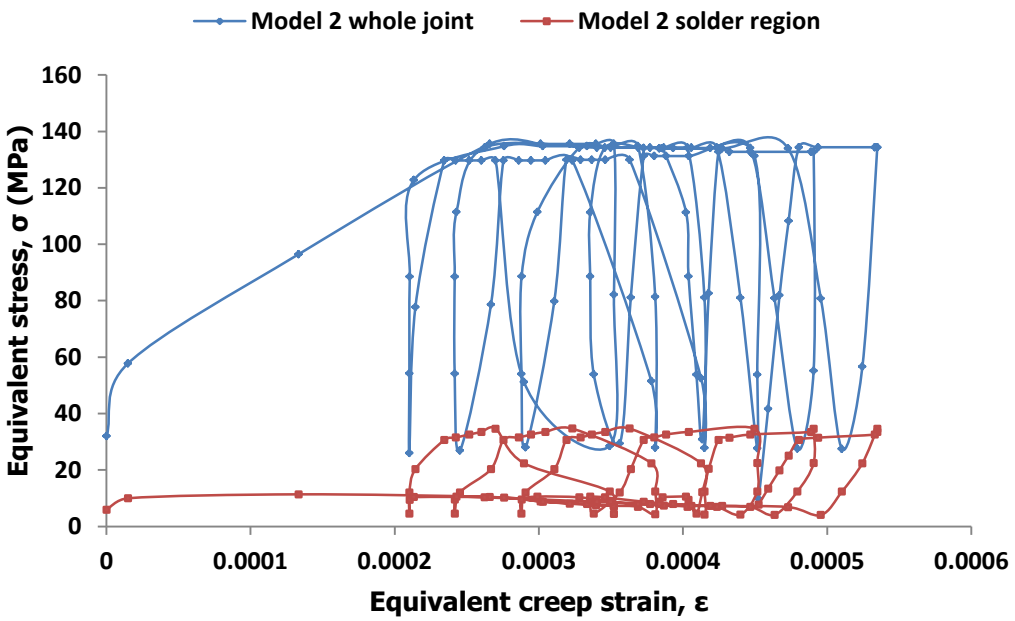


**(b) Stress and strain relationship in whole joint and solder region for model 2**

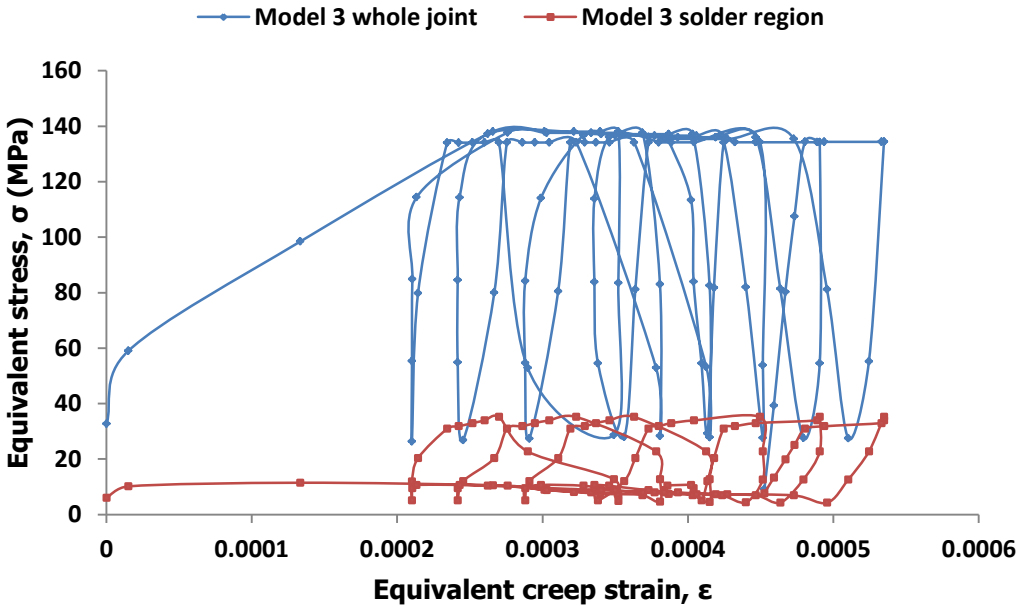


**(c) Stress and strain relationship in whole joint and solder region for model 3**

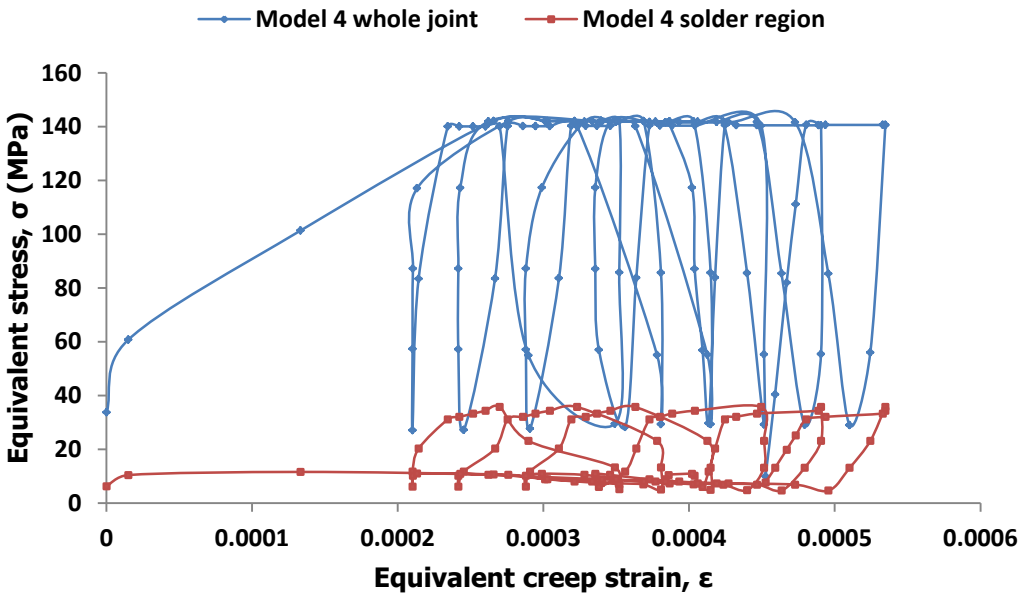


**(d) Stress and strain relationship in whole joint and solder region for model 4**

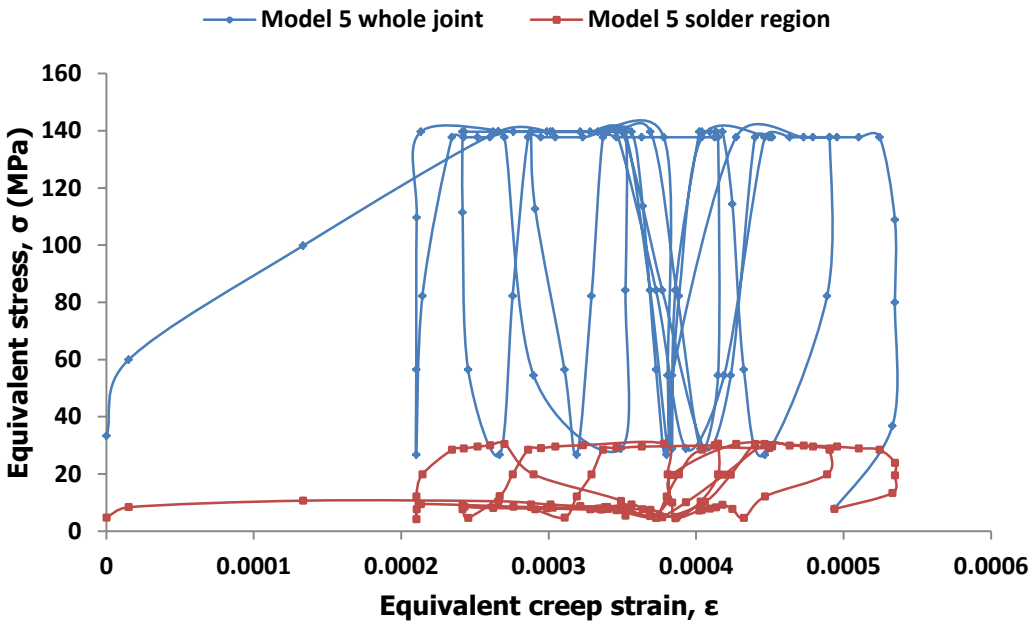


**(e) Stress and strain relationship in whole joint and solder region for model 5**

**Figure 5.6 Relationship between stress and creep strain in the solar cell models showing:**
**(a) Stress and strain relationship in Model 1**
**(b) Stress and strain relationship in Model 2**
**(c) Stress and strain relationship in Model 3**
**(d) Stress and strain relationship in Model 4**
**(e) Stress and strain relationship in Model 5**

Furthermore, it can be observed from Fig. 5.6 as well as from Figs. 5.3 and 5.4 that values of equivalent stress for models of whole joints are higher than those of solder only region. For instance, the least maximum equivalent stress in whole solder joint is about 6.6204MPa while the largest maximum equivalent stress is about 10MPa as can be observed in Fig. 5.3(a) and Fig. 5.3(d) respectively. On the other hand, the least maximum equivalent stress in solder only region is about 6.6204MPa while the largest maximum equivalent stress is about 7.7546MPa as shown in Fig. 5.4(a) and Fig. 5.4(e) respectively. Thus induced stress in whole solder joint is higher than that of solder only region. This suggests that the presence of IMC in whole solder joint results in larger induced stress in the solder joint compared with solder only region.

### 5.2.4 Evaluation of accumulation of strain energy density

Induced creep deformation is stored internally throughout the volume of the solar cell solder joint as creep strain energy during thermal cycling. The volume average method discussed in chapter 2 was used to convert the creep strain energy obtained from simulation results into accumulated strain energy density for each of the five models. In order to get accurate results, average accumulated strain energy density values are used for computations. Presented in Fig. 5.7 is a plot of accumulated strain energy density in $mJ/mm^3$ against temperature profile step. It can be observed in Fig. 5.7(a) that at the commencement of thermal cycling, Model 5 with 4μm

IMC thickness has the highest accumulated strain energy density in whole solder joint. However, as thermal cycling continues, it appears that Model 4 with 3μm has the peak accumulated strain energy density in the solder joint. However, average accumulated strain energy density values for whole joint indicate that Model 5 has the largest value of 0.040412mJ/mm$^3$ while Model 1 (1μm thickness) has the smallest value of 0.03436mJ/mm$^3$. Similarly, the situation in solder only region as shown in Fig. 5.7(b) is that Models 1 and 5 have the least and highest average values of accumulated strain energy density in the solder only regions as 0.03818mJ/mm$^3$ and 0.06735mJ/mm$^3$ respectively. Moreover, comparison of Fig. 5.7(a) and Fig. 5.7(b) indicates that accumulated strain energy density is higher in solder only regions than in whole solder joints. The average values of accumulated strain energy density in the whole joint as well as in solder only regions are presented in Table 5.2. This implies that as IMC thickness increases, accumulated strain energy density increases as well in the solder regions. This further confirms that solder joints are affected by the presence of IMCs.

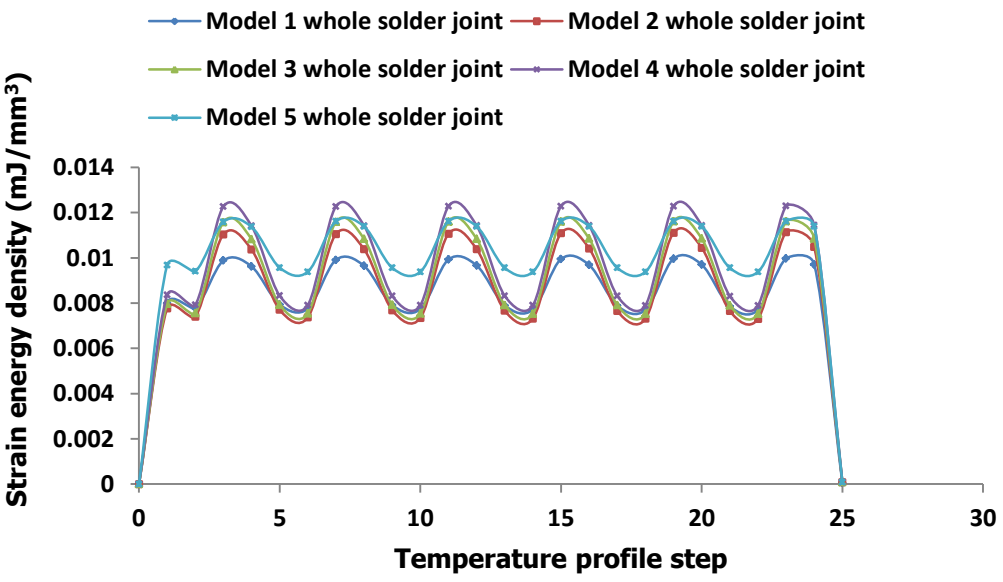


(a)

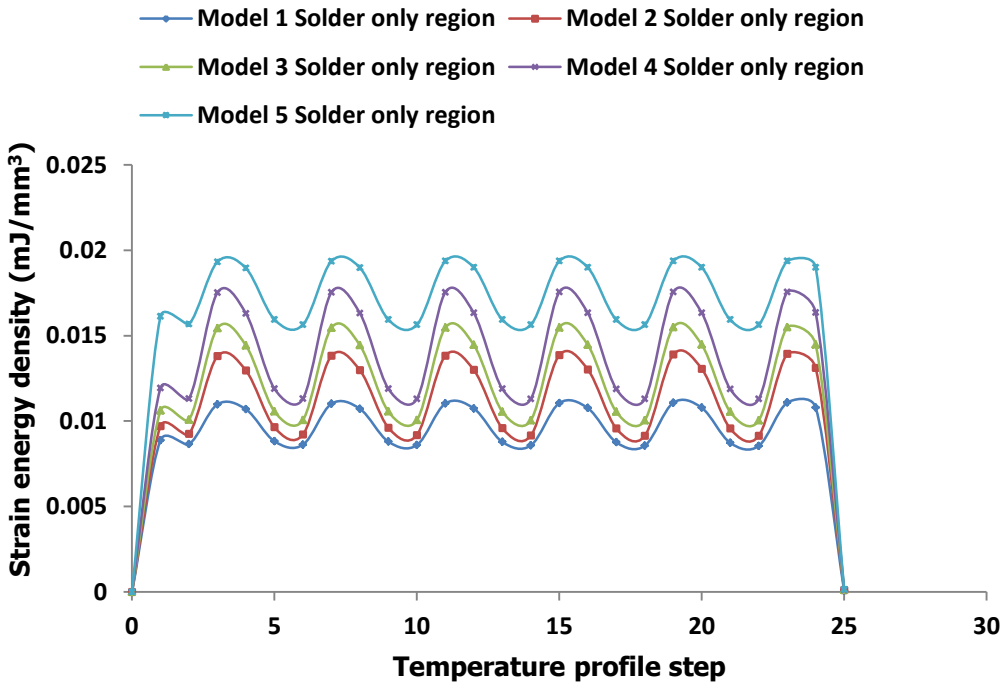


(b)

**Figure 5.7 Plot of strain energy density for models against temperature profile step showing strain energy density for:**
**(a) Whole solder joint (b) Solder only region**

### 5.2.5 Effect of IMC layer on solder joint fatigue life

The solar cell solder joint service life for the five geometric models can be predicted using fatigue models such as Syed's model presented in Eq. 2.11. The values of average change in accumulated creep strain energy density per cycle ($\Delta\omega_{acc}$) of the models are inputted into Eq. 2.11 to compute fatigue life of each model. The fatigue life is also stated as mean-time-to-failure (MTTF) or cycles to failure. The results of the fatigue life computation for the five models are presented in Table 5.2 consisting of predicted life for whole solder layers as well as predicted life for solder only regions. The results in Table 5.2 indicate that Model 1 with IMC thickness of 1μm has the highest fatigue life of 15317 cycles to failure and the corresponding fatigue life for solder region is 13785 cycles to failure. Likewise, Model 5 with IMC thickness of 4μm has the lowest fatigue life of 13023 cycles to failure and the corresponding fatigue life for solder region is 7814 cycles to failure. Moreover, these results are used to analyse the effect of IMC layer on solder fatigue life prediction.

**Table 5.2 Predicted fatigue life for models with varied IMC layer thickness**

| Model No. | IMC thickness (μm) | Whole solder $\Delta\omega_{acc}$ (mJ/mm$^3$) | Solder region $\Delta\omega_{acc}$ (mJ/mm$^3$) | Whole solder predicted life (cycles) | Solder region predicted life (cycles) |
|---|---|---|---|---|---|
| **1** | **1.0** | **0.03436** | **0.03818** | **15317** | **13785** |
| **2** | **2.0** | **0.03567** | **0.04458** | **14756** | **11806** |
| **3** | **2.5** | **0.03713** | **0.04950** | **14176** | **10632** |
| **4** | **3.0** | **0.03927** | **0.05609** | **13405** | **9383** |
| **5** | **4.0** | **0.04041** | **0.06735** | **13023** | **7814** |

Results of fatigue life in Table 5.2 are plotted in Fig. 5.8 showing whole joint life and solder region life versus IMC thickness. It can be observed from Fig. 5.8 that as IMC thickness increases, fatigue life for both the whole solder joint and solder region decreases. Moreover, fatigue life for solder region is lower than that of whole solder joint.

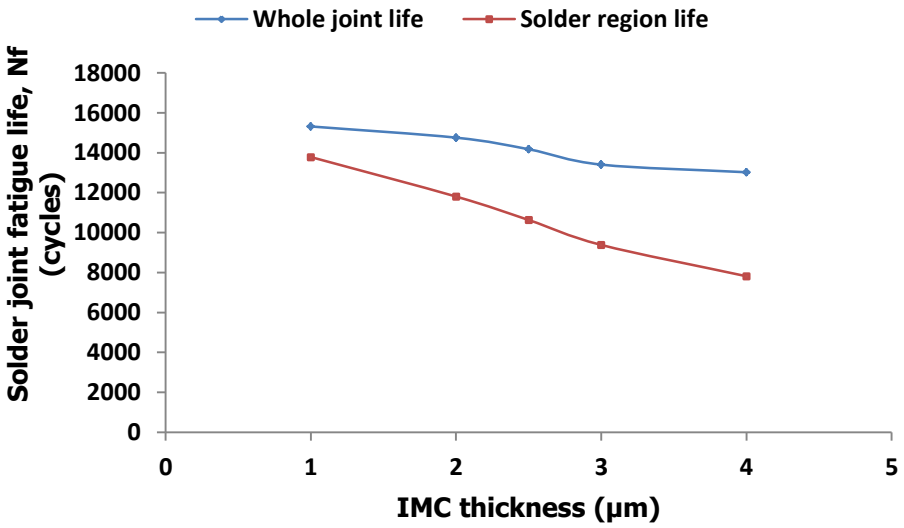


**Figure 5.8 Plot of predicted solder joint fatigue life versus IMC thickness**

It has been reported by several researchers that numerous PV modules fail during field operations or accelerated life testing. According to an IEA report on field study of PV modules in operation for 8 years, Kontges *et al*. (2014) reported that 2% of the modules were expected to fail after 11-12 years due to defective interconnections. Similarly, DeGraaff *et al.* (2011) reported that a field observation of PV modules produced by 21 different manufacturers revealed that about 4% of the modules showed signs of failure during the first 15 years. Furthermore, Kohl *et al*. (2009) in SunPower (2013) reported that in a German four-year project, a group of PV modules from 7 different

manufacturers were subjected to damp heat ageing test. The results showed significant performance degradation such that projected lifetime was less than 20 years (10950 cycles to failure). Likewise, in an experimental study, Kumar and Sarkar (2013) subjected 20 PV modules to a single constant stress accelerated life test and computed the least life to be 21 years (11497 cycles to failure). This accelerated life test result together with ageing test result is used alongside whole solder joint predicted fatigue life for the five models as well as the expected 25 years lifetime or 13688 cycles to failure (Guyenot, *et al.*, 2011) mentioned in section 4.3.5 to plot Fig. 5.9. The Fig. 5.9 is a plot of IMC layer thickness versus predicted solder joint fatigue life of the five models compared with test and expected life. The plot of the figure reveals that fatigue life of Models 1, 2 and 3 are close to the expected fatigue life of solder joint while Models 4 and 5 have shorter fatigue lives. Experimental test life is the shortest and the reason for this could be due to several factors such as solder joint design, solder composition, experimental set-up or other factors. The reason for the longer fatigue life when IMC thickness is smaller is because as IMC thickness increases, solder volume decreases thereby limiting the capacity and integrity of the solder joint to provide the desired interconnection. Consequently, the solder joint becomes greatly damaged and ultimately results in fatigue failure of the joint. Therefore, the MTTF of the assembly solder joints depends on the thickness of IMC layer. Hence, thin IMC layer is better for the solder joint than thick IMC layer. For that reason, solder joints in solar cell assembly should be designed in such a way that minimal IMC layers will develop throughout the

lifespan of the joints irrespective of the thermo-mechanical loading applied. This will ensure that the solder joint fulfil their functional life before the IMC layers become detrimentally thick.

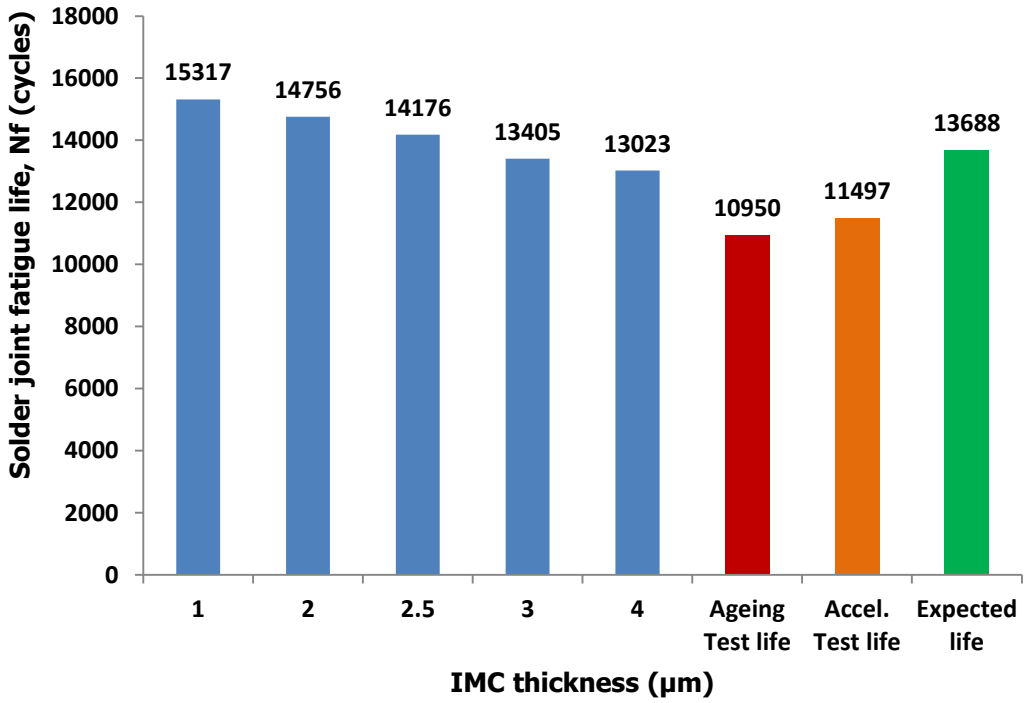


**Figure 5.9 Plot of predicted solder joint fatigue life of models versus IMC layer thickness compared with test and expected values**

## 5.3 Conclusions

In this chapter, the study of the effect of IMC thickness on thermo-mechanical reliability of solar cell solder joint was presented. The study demonstrates that hysteresis loop of the whole joint has larger area than that of solder region. It might be due to more dissipation of accumulated creep strain energy density per cycle in the whole joint which has larger volume compared to that accumulated in the solder region which has smaller

volume. Since the creep energy is a damage measurement index, the higher the energy accumulated in a joint without dissipation, the higher the damage on the joint. Furthermore, the modelling and simulation results indicate that average accumulated strain energy density values for whole joint in Model 5 is the largest with a value of 0.040412mJ/mm$^3$ while Model 1 has the smallest value of 0.03436mJ/mm$^3$. Also, Models 1 and 5 have the least and highest average value of accumulated strain energy density in the solder only region with value of as 0.03818mJ/mm$^3$ and 0.06735mJ/mm$^3$ respectively. This shows that the solder only region accumulates more damage than the whole joint due to the presence and growth of IMC in the solder joint. Therefore, it can be concluded that the presence and growth of IMC in the joint decreases its thermo-mechanical reliability. This conclusion is further strengthened and confirmed by the result of the study on fatigue life of the joints. The finding from analysis of the results demonstrates that the rate of degradation of the joints depends on the thickness of layer of IMC. It can be concluded from this result that the fatigue life of solder joints containing IMC layer decreases linearly as the IMC thickness grows arithmetically during assembly operations as well as during service lifetime of the solar cell assembly. Other critical parameters of solder joint are its thickness and width. Solder joint thickness is affected by thermo-mechanical stresses during service operations and can lead to fatigue failure of the joints. Therefore, in the following chapter, the study of the effect of solder joint thickness on thermo-mechanical fatigue of solder joint in solar cell assembly is presented.

# CHAPTER 6

# EVALUATION OF THE EFFECT OF SOLDER JOINT THICKNESS ON THERMO-MECHANICAL FATIGUE LIFE OF SOLDER JOINTS IN SOLAR CELL ASSEMBLY

# Chapter 6

# Evaluation of the Effect of Solder Joint Thickness on Thermo-mechanical Fatigue Life of Solder Joints in Solar Cell Assembly

## 6.1 Introduction

The study on the effect of IMC thickness on solder joint thermo-mechanical fatigue life was presented in the previous chapter. The impacts of IMC thickness on solder joint fatigue life necessitates a study of the geometric parameters of solder joint especially solder joint thickness and width. In addition, during PV module service operations, thermo-mechanical stresses develop in solder joint and depending on its thickness fatigue failure of the joints can occur. Therefore an evaluation of the effect of solder joint thickness is presented in this chapter. It is necessary that solder joints have a thickness that accumulates minimal creep strain energy density in order to ensure longer fatigue life. In view of the foregoing, this study evaluates the effect of solder joint thickness on thermo-mechanical reliability of solder joints as well as establishes a basis for determination of appropriate solder joint thickness for solar cell assembly.

This chapter describes the approach used for the study, presents a theoretical analysis of effect of solder joint thickness on flexural stiffness and results obtained from modelling and simulation as well as discussion. The results and discussion are presented in three sub-sections as follows: study

on stress and strain of solder joints in solar cell assembly, study on creep energy density in solder joints and effect of solder joint thickness on thermo-mechanical reliability of solder joints in solar cell assembly.

In order to study the effect of solder joint thickness on thermo-mechanical reliability of solder joints in solar cell assembly, a theoretical analysis of effect of solder joint thickness on flexural stiffness is carried out and in addition FEM discussed in section 3.2.2.1 is utilized for this investigation. This study is carried out using commercial ANSYS Academic Research Finite Element package. Due to the magnitude of computations involved, the High Performance Computation (HPC) was executed using a Bespoke Work Station computer in the School of Engineering. In order to lessen modelling time and disc space, quarter symmetry of the geometric models were simulated. Also, Garofalo-Arrhenius creep model discussed in section 3.2.2.2 is used for this study. Furthermore, the study utilizes 156 x 156 $mm^2$ multicrystalline silicon solar cell assembly. Presented in Fig. 6.1 is a cross-section of solar cell model showing solder joint thickness.

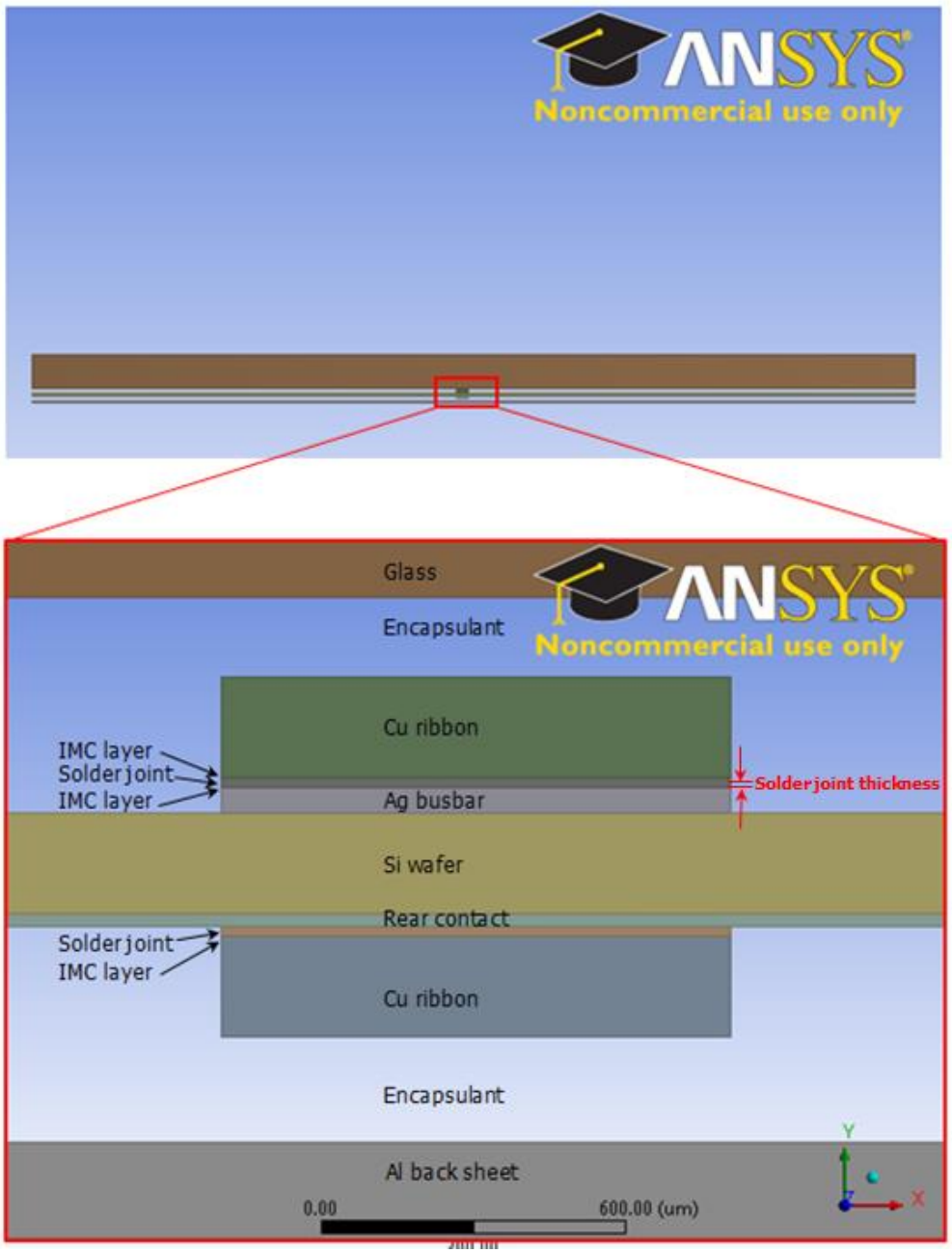


**Figure 6.1 Cross-section of solar cell model showing solder joint thickness**

Though 156 x 156 $mm^2$ size of multicrystalline silicon solar cell assembly is universally used, the dimension of solder joint thickness is not standardized. Consequently, several researchers and manufacturers use various solder joint thickness in the range of 10μm to 40μm (Wirth, 2010; Rogelj, *et al.*, 2012; Jung and Kontges, 2012; Wiese *et al.*, 2009 and Chen, *et al.*, 2008).

In this study, solder joint thickness of 20μm, 22μm, 25μm, 27μm and 30μm are used in five separate geometric models which are assigned numbers 1, 2, 3, 4 and 5 respectively. Also, each of the models has an IMC thickness of 2.5μm and a solder joint width of 1000μm. This implies that the solder joint volume in each model is varied such that as solder joint thickness ($T_{SJ}$) increases solder joint volume increases as well. The parameters of the five geometric models with varied solder joint thicknesses are presented in Table 6.1.

**Table 6.1 Parameters of models with varied solder joint thickness**

| Model number | IMC thickness (μm) | Solder joint thickness (μm) | Solder joint width (μm) | Whole joint Vol. ($mm^3$) | Solder region Vol. ($mm^3$) |
|---|---|---|---|---|---|
| **1** | **2.5** | **20** | **1000** | **1.560** | **1.170** |
| **2** | **2.5** | **22** | **1000** | **1.716** | **1.326** |
| **3** | **2.5** | **25** | **1000** | **1.950** | **1.560** |
| **4** | **2.5** | **27** | **1000** | **2.106** | **1.716** |
| **5** | **2.5** | **30** | **1000** | **2.340** | **1.950** |

Using the data in Table 6.1, Fig. 6.2 is plotted which is a plot of solder volume in whole joint against solder joint thickness for each corresponding model. The figure shows that as model number increases from Model 1 ($T_{SJ}$ 20μm) to Model 5 ($T_{SJ}$ 30μm), solder joint thickness and solder volume in whole joint increases as well.

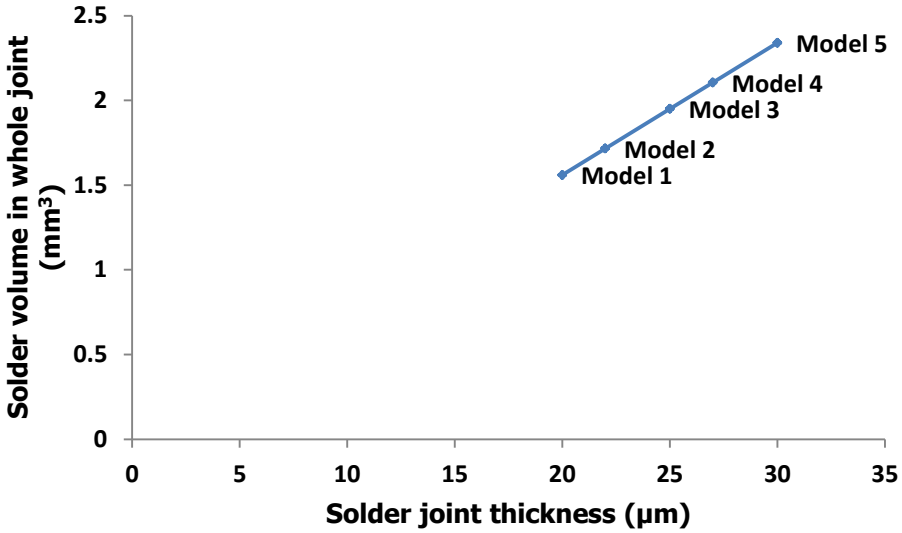


**Figure 6.2 Plot of solder volume in whole joint against solder joint thickness**

Using the approach implemented in previous chapters, the five geometric models were subjected to six accelerated thermal cycling in 25 load steps between -40$^{o}$C to 85$^{o}$C. The temperature loading started from 25$^{o}$C, ramped up at a rate of 3$^{o}$C/min to 85$^{o}$C, where it had hot dwell for 20 min. It was then ramped down to -40$^{o}$C at a rate of 6$^{o}$C/min, where it had cold dwell for 20 min. The thermal cycling profile presented in section 3.2.2.2.2 was used to simulate actual cycling profile used during thermal load test.

## 6.2 Results and discussion

This section discusses the results obtained from analysis of flexural stiffness as well as modelling and simulation carried out. The section is presented in three sub-sections as follows: study on stress and strain in solder joints of

solar cell assembly, study on creep energy density in solder joints, and effect of solder joint thickness on fatigue life.

### 6.2.1 Effect of solder joint thickness on flexural stiffness

Determination of solder joint flexural stiffness is essential to know the relationship between it and solder joint thickness in particular. This is necessary in order to avoid inducing cyclic stress in the solder joint excessively which occurs when the flexural stiffness is too high. Therefore, the relationship between flexural stiffness and solder joint thickness and its effect on the thermo-mechanical reliability of solder joint is investigated using the varied solder joint thicknesses of the geometric models shown in Table 6.1. From Table 6.1, solder joint thickness and width are obtained and inputted into Eq. 2.7 to compute the value of flexural stiffness for each of the models. Also used in Eq. 2.7 is the value of Young's modulus, $E$ which value is 43GPa as shown in Table 3.1. The results obtained are presented in Table 6.2 where $C = \frac{E}{12}$ is constant for all the five models.

**Table 6.2 Values of flexural stiffness for varied solder joint thickness**

| Model number | Solder joint thickness (μm) | Solder joint width (μm) | C (GPa) | Flexural stiffness ($N \cdot m^2 \times 10^{-6}$) |
|---|---|---|---|---|
| **1** | **20** | **1000** | **3.58** | **0.0716** |
| **2** | **22** | **1000** | **3.58** | **0.0788** |
| **3** | **25** | **1000** | **3.58** | **0.0895** |
| **4** | **27** | **1000** | **3.58** | **0.0967** |
| **5** | **30** | **1000** | **3.58** | **0.1074** |

The results presented in Table 6.2 are used to plot flexural stiffness against solder joint thickness as shown in Fig. 6.3.

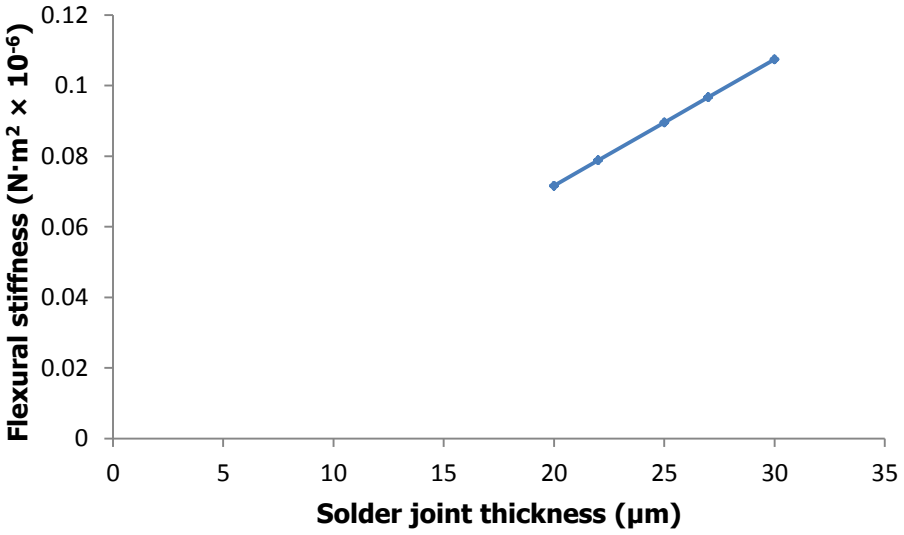


**Figure 6.3 Plot of flexural stiffness against solder joint thickness**

The plot shown in Fig. 6.3 indicates that as solder joint thickness increases, flexural stiffness increases. For instance, a solder joint thickness of 20μm corresponds to a flexural stiffness of $0.0716 \times 10^{-6}$ $N \cdot m^2$ while for a solder joint thickness of 30μm, the flexural stiffness is $0.1074 \times 10^{-6}$ $N \cdot m^2$. It can be inferred from the results that increase in solder joint thickness produces greater resistance to bending. Hence greater resistance to bending implies

increase in residual stress during thermal cycling. This result is consistent with solder joint behaviour in similar findings by other researchers. Lai *et al*. (2013) in a related study on crystalline silicon solar cells, found that at hot-air temperature, increase in solder joint thickness results in residual stress increase. Similarly, it was also found that increase in solder joint width results in residual stress increase. Likewise, Wang *et al.* (2004) in an experimental study discovered that residual stress induced during solder reflow process affects the flexing strength of solder joints such that the bending force declines and the strain becomes severe after a long time of baking.

The foregoing analysis suggests that increase in solder joint thickness affects interconnect flexibility of solder joint which can result in failure of the solder joint interconnection. The failure of solder joint interconnection implies non-delivery of generated electricity to the required point. Hence, more study is required to obtain greater understanding on the effect of stress, strain and strain energy during thermal cycling. Strain energy result is used to obtain strain energy density which is in turn used to predict the fatigue life of solder joint. Therefore, the study of solder joint equivalent stress, equivalent strain and strain energy density was carried out by modelling and simulation of the five geometric models with varied solder joint thicknesses of 20μm, 22μm, 25μm, 27μm and 30μm. The results obtained were analysed and discussed

accordingly. The results and discussion are presented in the following sections.

### 6.2.2 Study on stress and strain in solder joints of solar cell assembly

It is essential that stress and strain in solder joint are studied with regards to solder joint thickness ($T_{SJ}$) for better understanding of the fatigue failure of the joint under induced stress and strain. The five geometric models being studied were simulated and Fig. 6.4 shows damage distribution of equivalent stress on the whole solder joint of the five geometric models. It can be observed from the Figs. 6.4(a), 6.4(b) and 6.4(c) that Models 1 ($T_{SJ}$ 20μm), 2 ($T_{SJ}$ 22μm), and 3 ($T_{SJ}$ 25μm) respectively have maximum stress around the end of the longitudinal left hand side section of the whole solder joint with values of 9.147MPa, 8.883MPa and 8.8406MPa respectively. Models 4 ($T_{SJ}$ 27μm) and 5 ($T_{SJ}$ 30μm) as shown in Figs. 6.4(d) and 6.4(e) respectively have maximum stress at the end of the right hand side section of the joints with values of 7.9909MPa and 8.0538MPa respectively. This is because Models 1 to 3 have smaller $T_{SJ}$ as different from those of Models 4 and 5 which are bigger. Moreover, the damage distributions in all the five models seem to be uniformly spread along the entire length of the solder joint. This suggests that as the solder joint thickness increases, maximum stress position changes probably due to solder grain boundary dislocations resulting from thermal effects as well as expansion and contraction of solder joint and other interconnects.

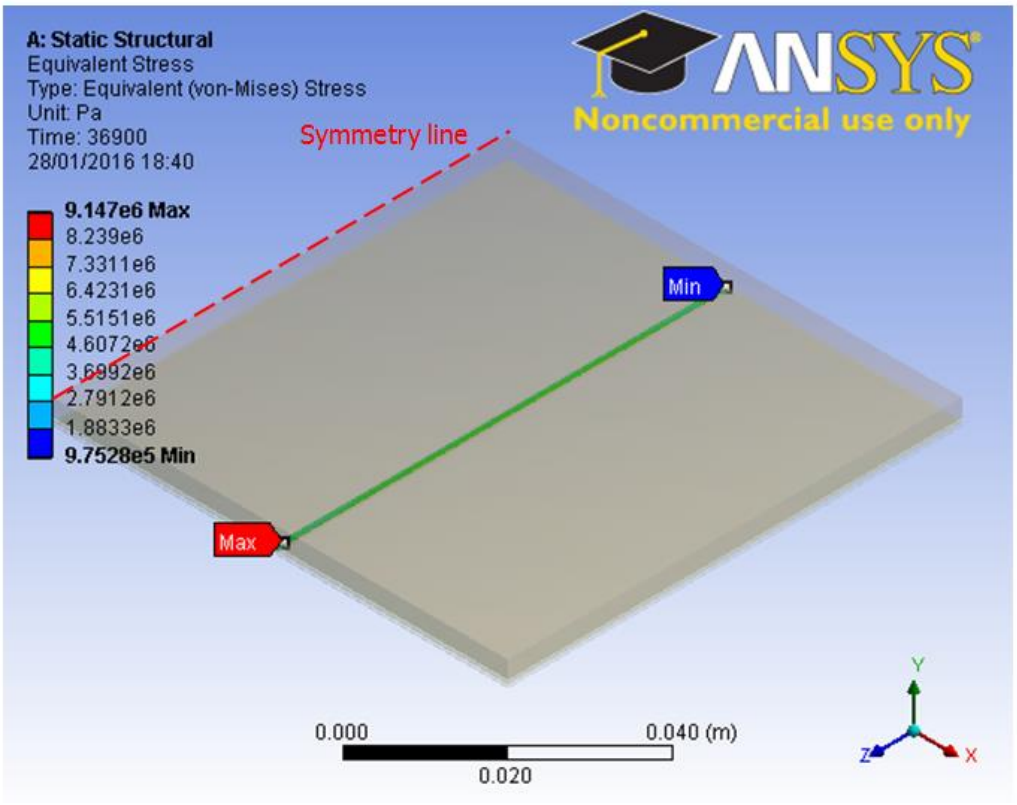


**(a) Stress on model 1 whole joint**

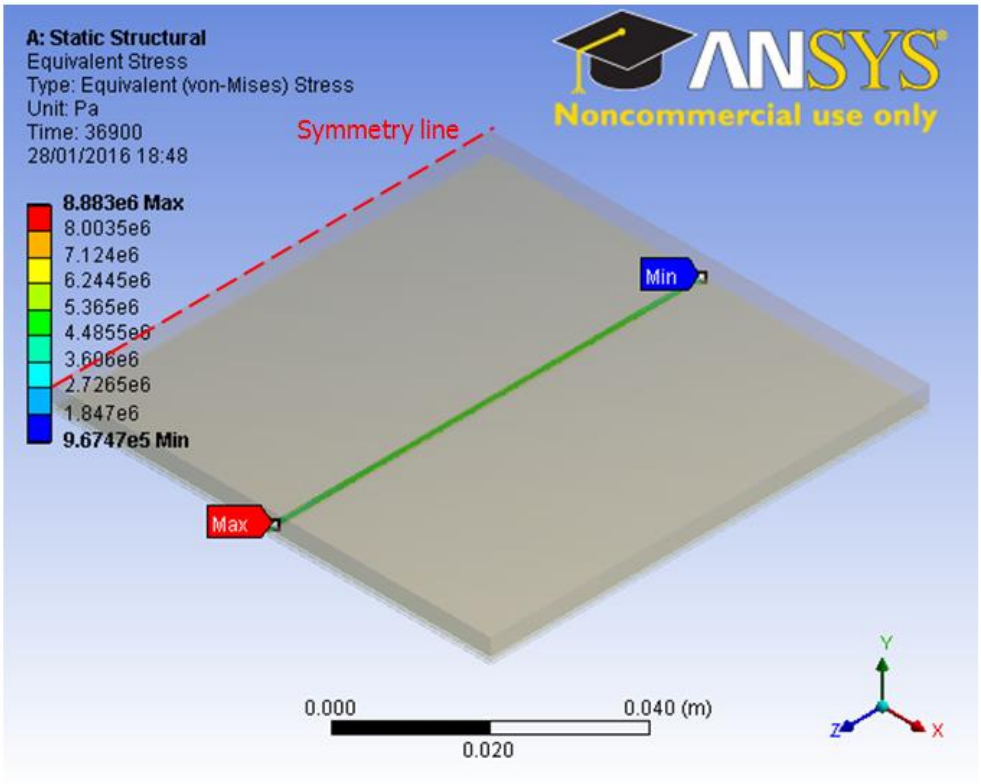


**(b) Stress on model 2 whole joint**

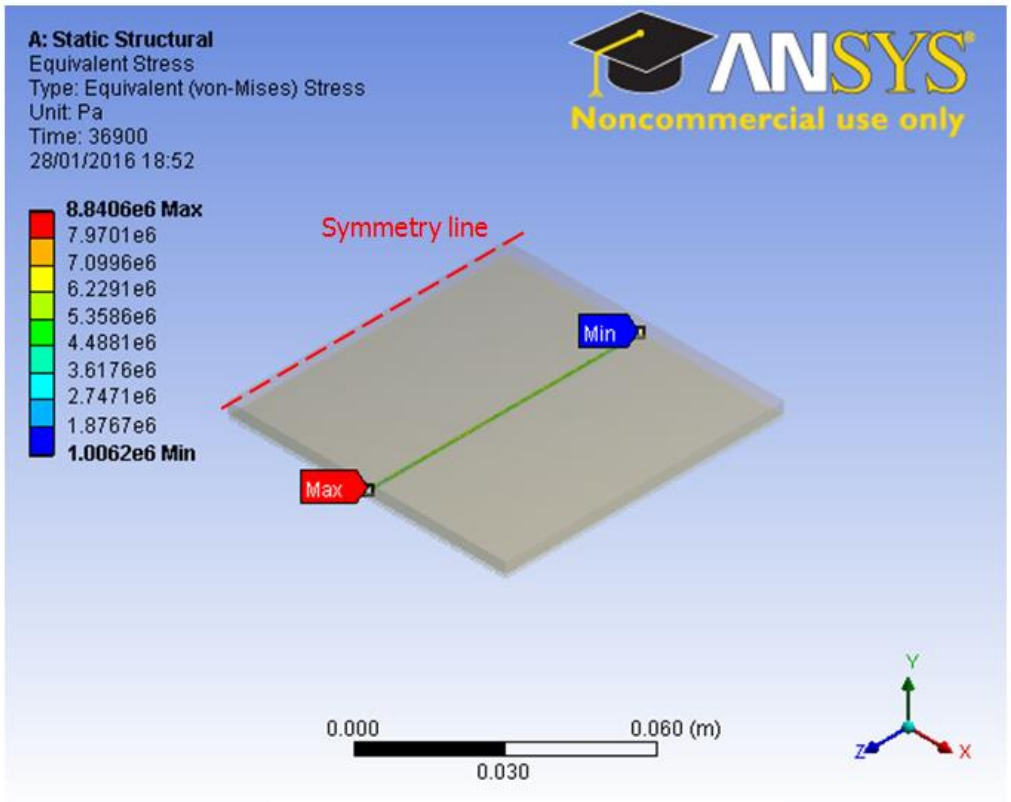


**(c) Stress on model 3 whole joint**

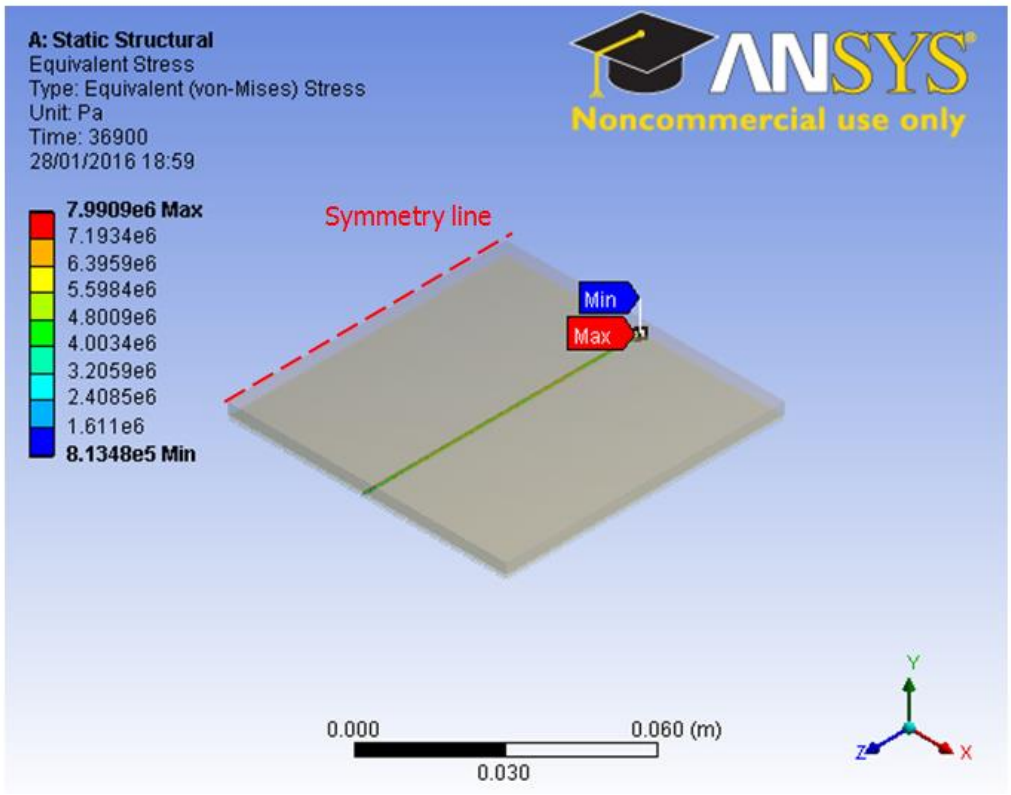


**(d) Stress on model 4 whole joint**

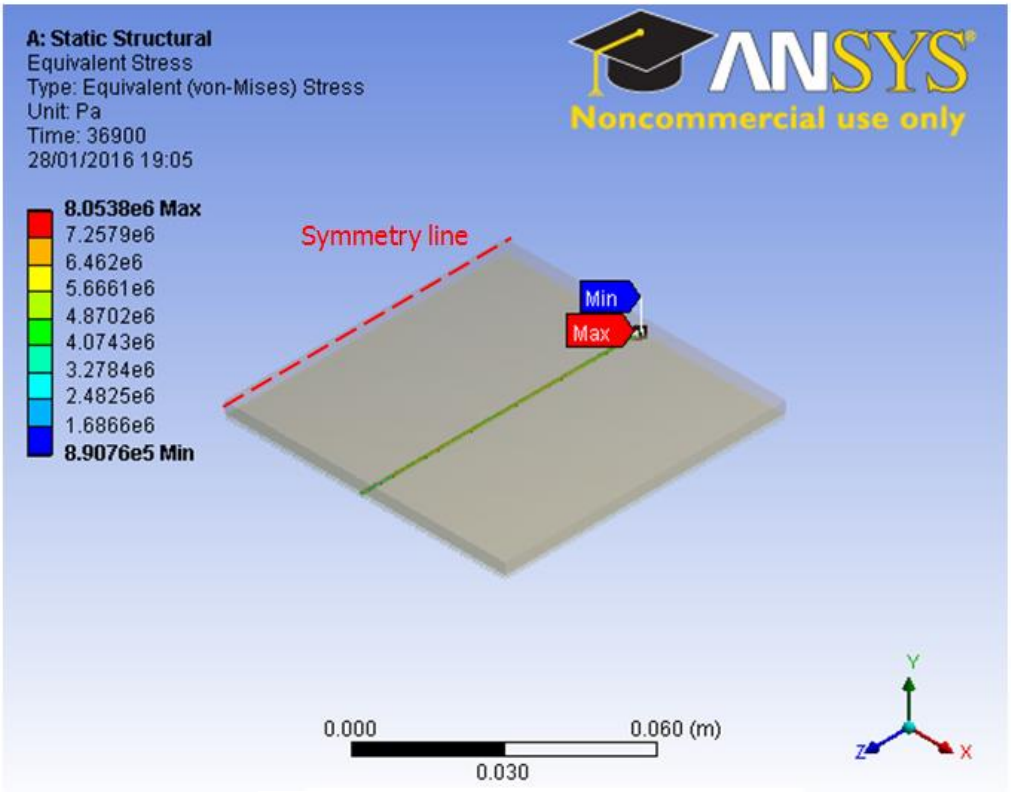


**(e) Stress on model 5 whole joint**

**Figure 6.4 Equivalent stress damage distribution on solder joint with varied thickness showing:**
**(a) Stress on model 1 whole joint**
**(b) Stress on model 2 whole joint**
**(c) Stress on model 3 whole joint**
**(d) Stress on model 4 whole joint**
**(e) Stress on model 5 whole joint**

Figure 6.5 shows the creep strain damage distribution in the whole solder joint for the five models. In all the models presented in Fig. 6.5, the maximum creep strain is located towards the end of the longitudinal right hand side (RHS) section of the whole solder joint. In Figs. 6.5(a) and 6.5(b), the creep strain damage distribution in the corresponding Models 1 and 2 seems to be mild along the longitudinal section of the solder joints with maximum values of 6.8854E-04m/m and 6.6284E-04m/m respectively. However, that of Models 3, 4 and 5 shown in Figs. 6.5(c), 6.5(d) and 6.5(e)

respectively, appears to be more severe and evenly spread along the entire longitudinal section of the solder joints with maximum creep strain values of 6.3546E-04m/m, 6.4073E-04m/m and 6.4159E-04m/m correspondingly. These foregoing results clearly show that various solder joint thicknesses impact solder joint behaviour such that as the joint thickness increases, more creep strain is induced in the joint. Consequently, a thicker solder joint in a solar cell assembly may result in an earlier fatigue failure compared with a thinner solder joint.

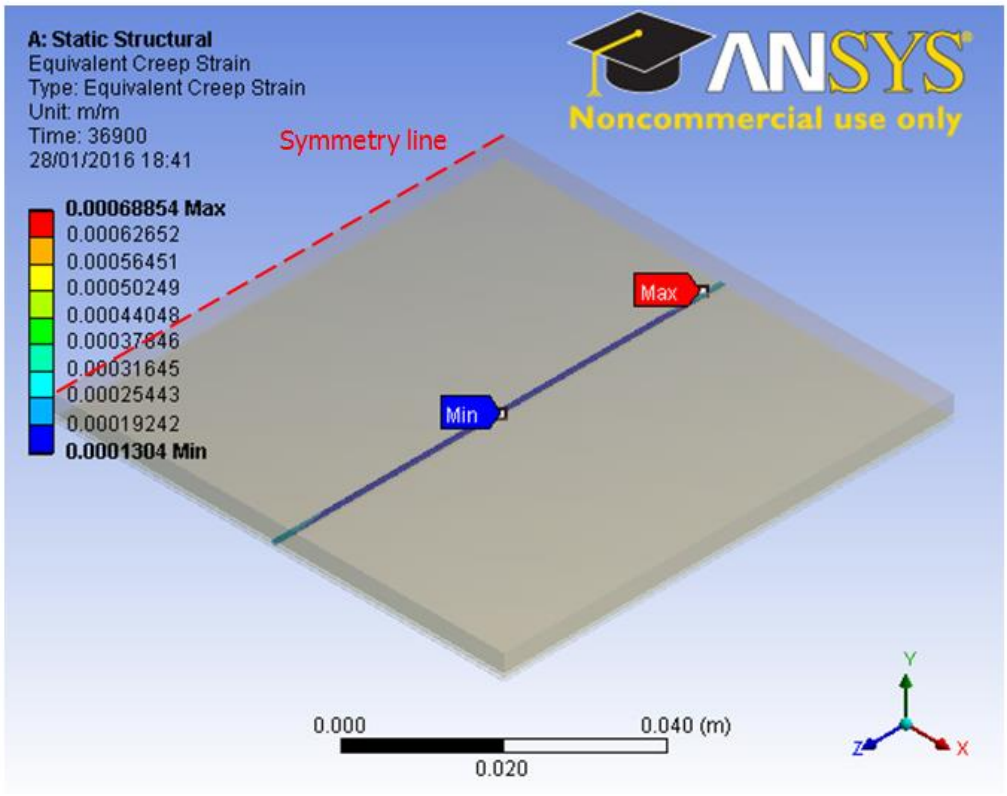


**(a) Strain on model 1 whole joint**

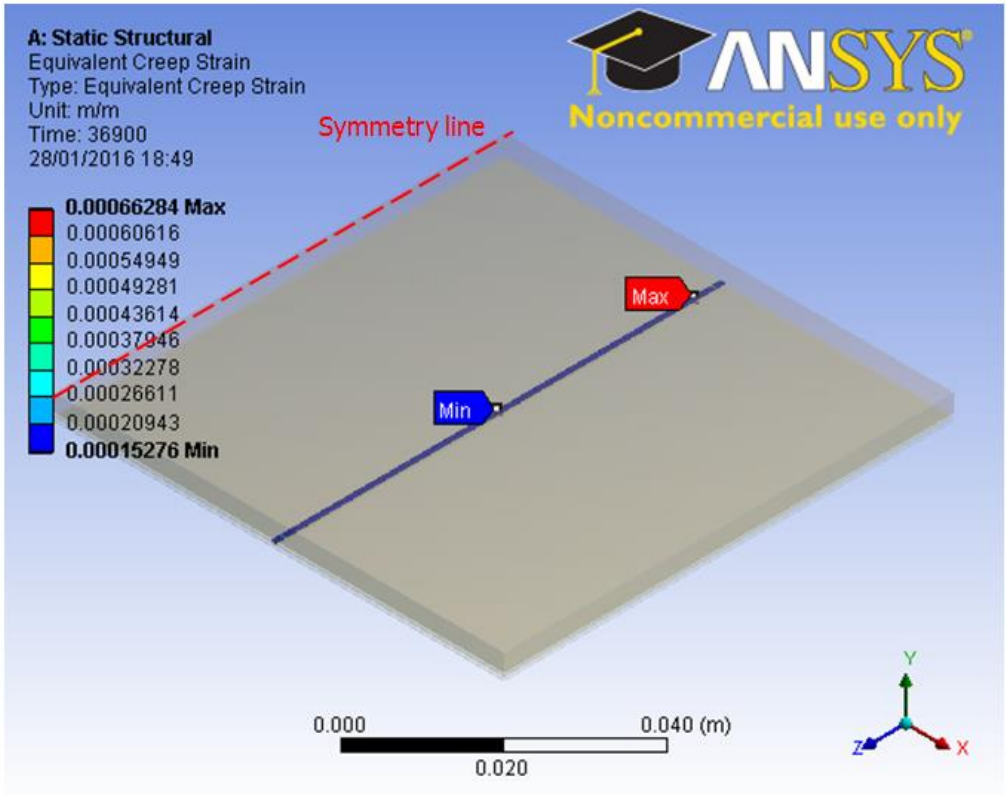


**(b) Strain on model 2 whole joint**

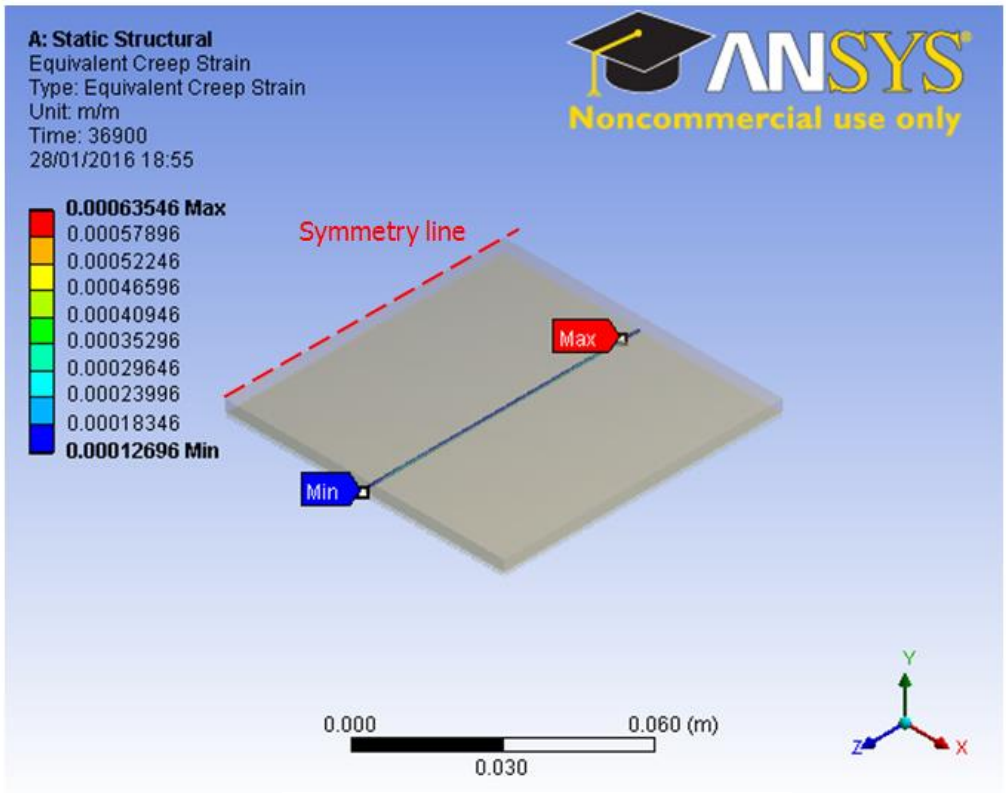


**(c) Strain on model 3 whole joint**

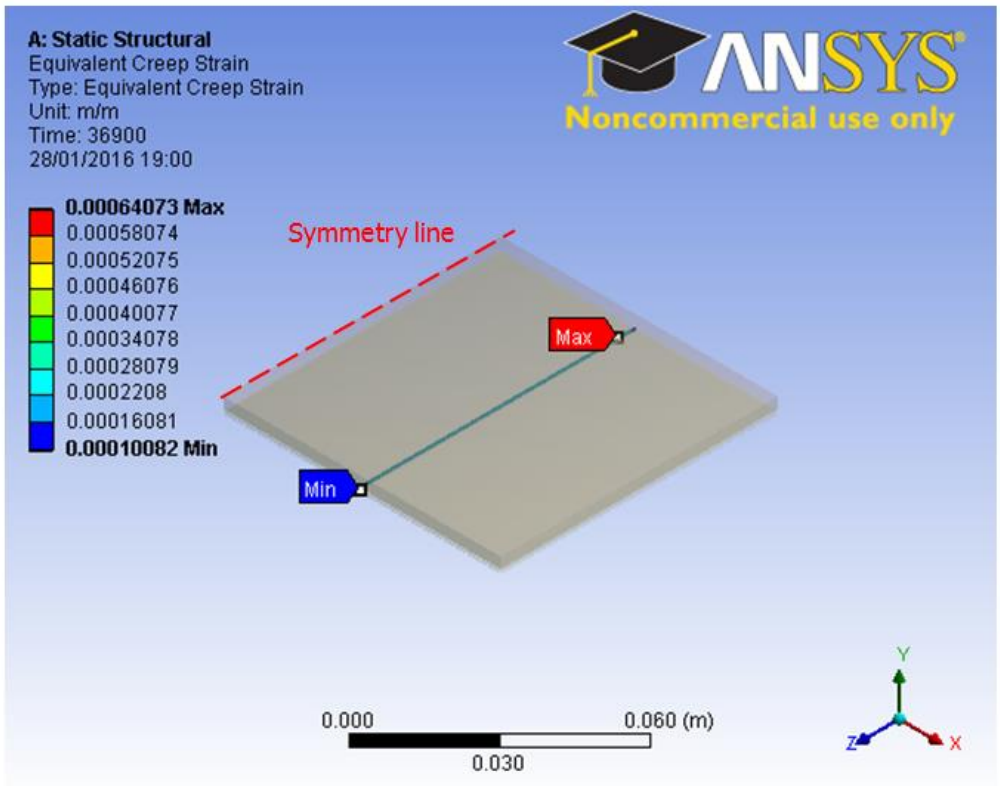


**(d) Strain on model 4 whole joint**

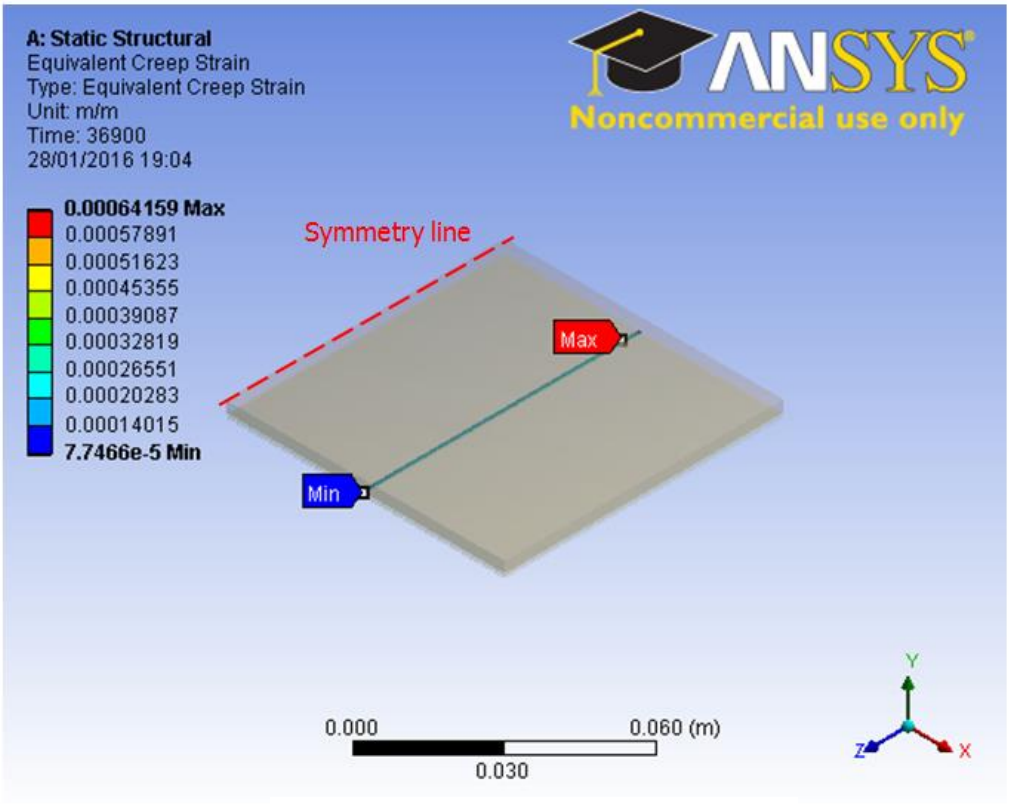


**(e) Strain on model 5 whole joint**

**Figure 6.5 Equivalent creep strain damage distribution on the solder joint showing:**
**(a) Strain on model 1 whole joint**
**(b) Strain on model 2 whole joint**
**(c) Strain on model 3 whole joint**
**(d) Strain on model 4 whole joint**
**(e) Strain on model 5 whole joint**

Figure 6.6 shows a plot of equivalent creep strain in solder joint against temperature profile step. The figure shows that at the end of 25 load steps, creep strain progressively increased in solder joint of all the five models as thermal cycling increased from a value of 0m/m to a maximum accumulated value of almost 9E-04m/m. Furthermore, a close observation of the plot in Fig. 6.6 reveals that the strain profile for Model 1 has more pronounced displacement compared with that of the other four models. Also, the

displacement of the strain profile of other models progressively decreases to the minimum in Model 5. However, the strain profiles of Model 5 have larger amplitudes than those of the other models and progressively decrease to the minimum in Model 1. This result suggests that Model 5 has the highest damage than the other models with a maximum accumulated creep strain value of almost 9E-04m/m whereas in the other models the damage decreases leading to the minimum damage in Model 1 with a maximum accumulated creep strain of about 7E-04m/m.

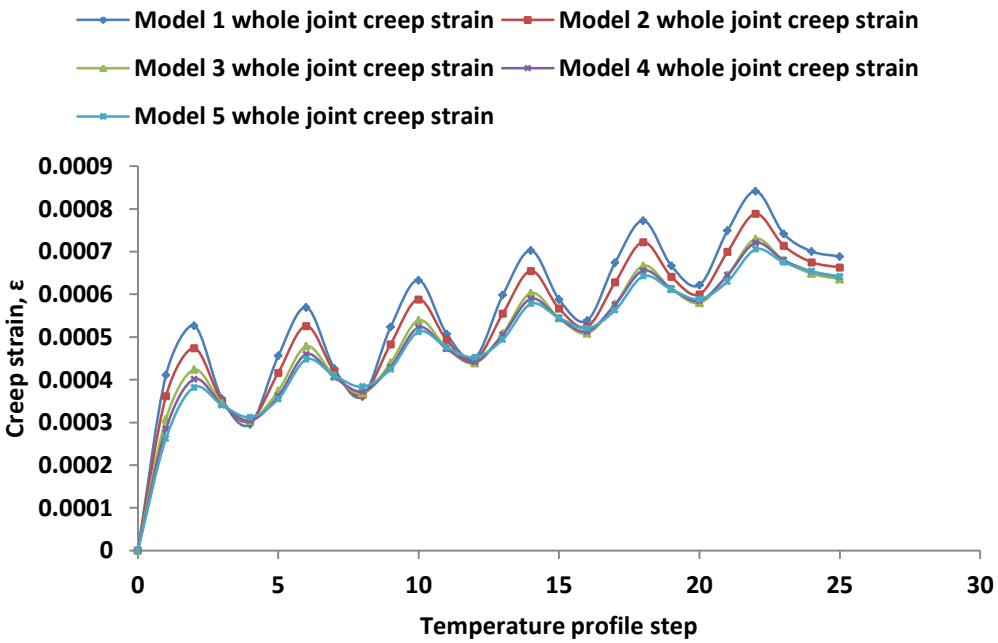


**Figure 6.6 Plot of equivalent creep strain on solder joint against temperature profile step**

The relationship between the stress and creep strain in solder joints of the five models with varied solder joint thickness is presented in Fig. 6.7 as hysteresis loop. The fatigue damage accumulating per cycle in the solder

joint of each model can be computed from the area of its hysteresis loop. Therefore, as can be seen in Fig. 6.7, each model has a unique hysteresis loop and corresponding fatigue damage. Also from the figure, it can be seen that all the five Models have maximum induced stress in the whole solder joint with values ranging from 135MPa to 140MPa. This further implies that all the various solder joint thicknesses undergo fatigue damage in the joint in a similar manner.

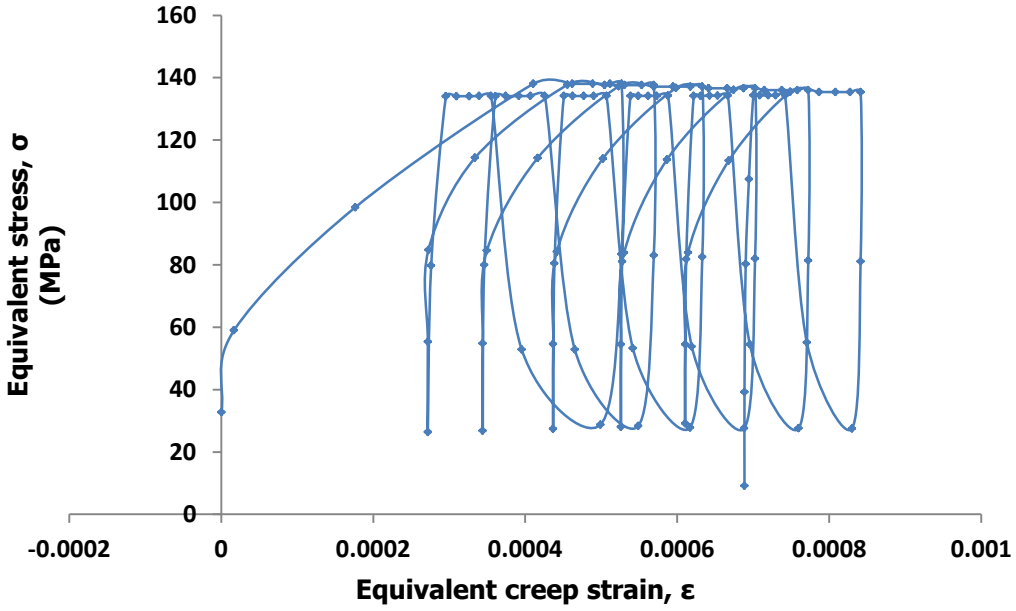


**(a) Stress and creep strain relationship in solder joint of Model 1**

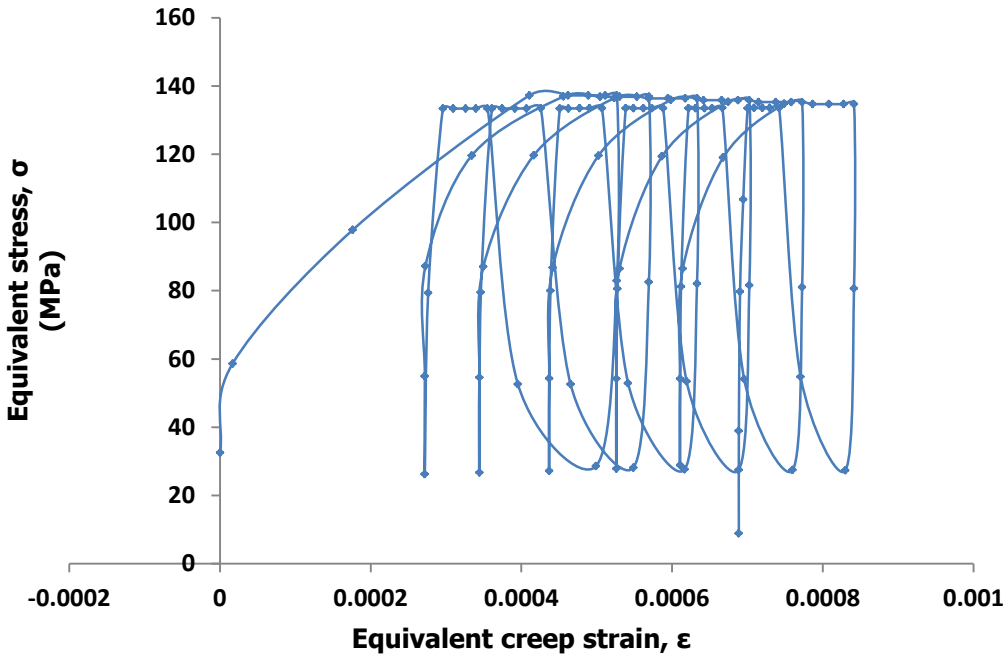


**(b) Stress and creep strain relationship in solder joint of Model 2**

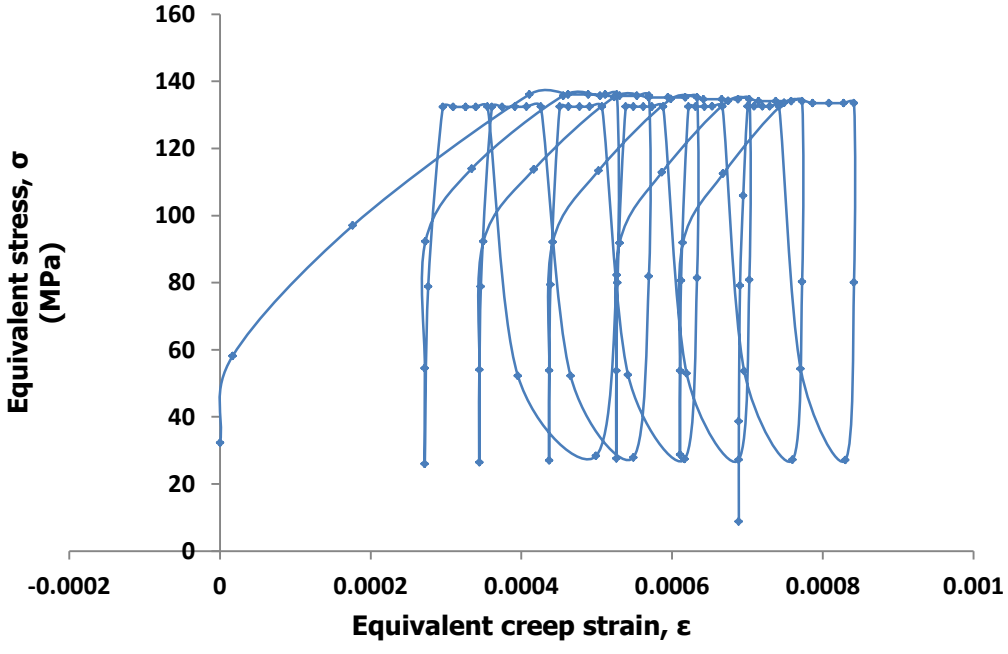


**(c) Stress and creep strain relationship in solder joint of Model 3**

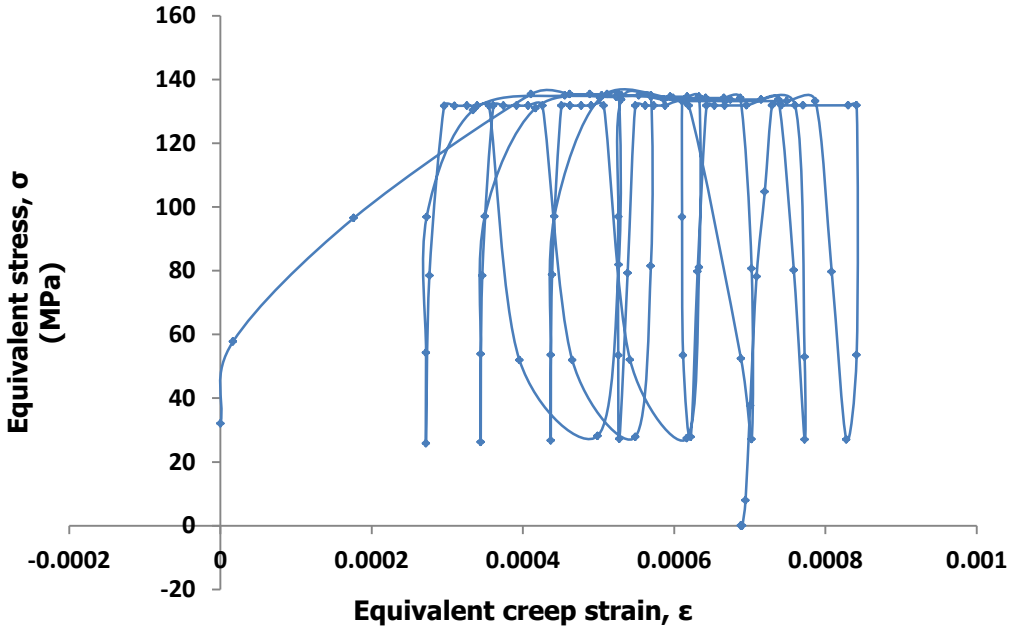


**(d) Stress and creep strain relationship in solder joint of Model 4**

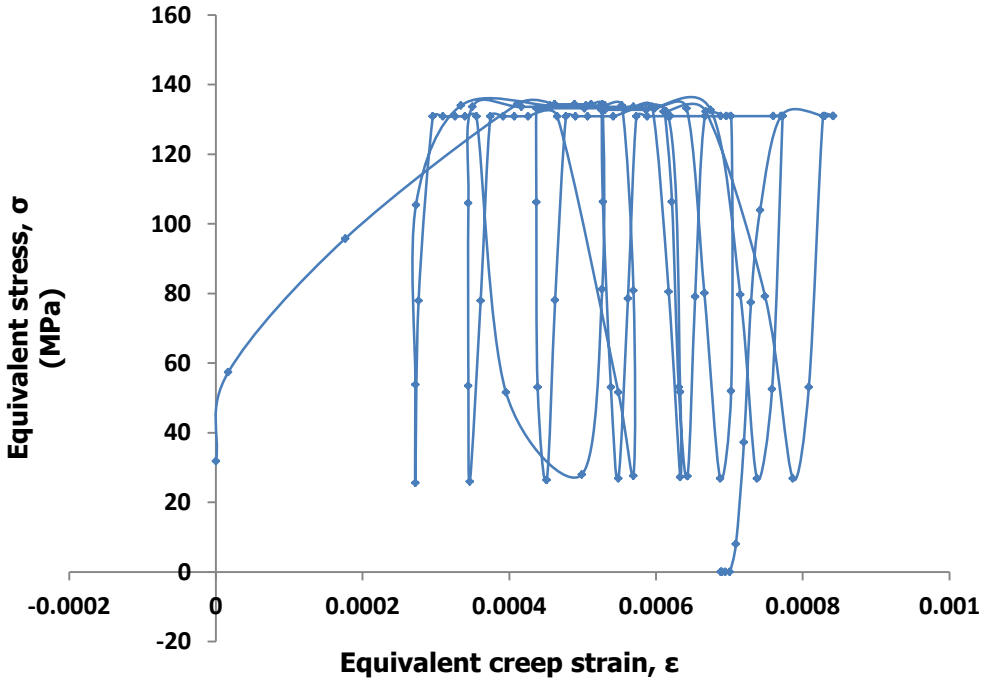


**(e) Stress and creep strain relationship in solder joint of Model 5**

**Figure 6.7 Relationship between stress and creep strain in solder joints for models with varied solder joint thickness showing:**
**(a) Stress and strain relationship in solder joint of model 1**
**(b) Stress and strain relationship in solder joint of model 2**
**(c) Stress and strain relationship in solder joint of model 3**
**(d) Stress and strain relationship in solder joint of model 4**
**(e) Stress and strain relationship in solder joint of model 5**

### 6.2.3 Study on creep energy density in solder joints

The principal damage mechanism in solar cell solder joint is the accumulation of creep–fatigue damage which over time eventually leads to crack initiation and propagation. As mentioned previously, accumulation of creep strain energy density is used to measure the damage in solder joint. Presented in Table 6.3 is average change in creep strain energy density per cycle for various solder joint thicknesses. It can be seen from Table 6.3 that Model 1 has the least average creep energy density per cycle of 0.03713mJ/mm$^3$ while Model 5 has the highest with a value of 0.04876mJ/mm$^3$. Furthermore, from Table 6.3, average creep energy density per cycle increases progressively from the least value in Model 1 followed by values of Models 2, 3, 4 and 5 which are 0.04007mJ/mm$^3$, 0.04383mJ/mm$^3$, 0.04594mJ/mm$^3$ and 0.04876mJ/mm$^3$respectively. Thus, the average creep energy density per cycle increases from the least value in Model 1 to the highest value in Model 5 as solder joint thickness increases from 20μm to 30μm. This result indicates that since Model 1 accumulates the least creep strain energy density in the solder joint, it has the least damage and is the least likely joint to fail among the five models. On the other hand, Model 5 has the highest creep strain energy density in the solder joint, which implies that it has the largest damage among the five models and is the most likely joint to fail. This result is consistent with the general expectation that as solder joint thickness increases in solar cell assembly, the joint becomes stiffer and cannot deflect easily during expansion and contraction when subjected to

thermal cycling. Hence, more cyclic stresses which cause damage are induced in a thicker solder joint than in a thinner solder joint.

**Table 6.3 Average change in creep strain energy density per cycle in varied solder joint thickness**

| Model number | Solder joint thickness (μm) | Solder volume in whole joint ($mm^3$) | Average change in creep strain energy density per cycle, $\Delta\omega_{acc}$ ($mJ/mm^3$) |
|---|---|---|---|
| **1** | **20** | **1.560** | **0.03713** |
| **2** | **22** | **1.716** | **0.04007** |
| **3** | **25** | **1.950** | **0.04383** |
| **4** | **27** | **2.106** | **0.04594** |
| **5** | **30** | **2.340** | **0.04876** |

Figure 6.8 shows a plot of strain energy density in solder joint against load step for six thermal cycles. The plot shows that Model 5 has the highest accumulated strain energy density of about 0.014mJ/$mm^3$ in the solder joint followed by Models 4, 3, 2 and 1 with values of about 0.0137mJ/$mm^3$ 0.013mJ/$mm^3$ 0.0122mJ/$mm^3$ and 0.0117mJ/$mm^3$ respectively. This result confirms the discussion in the preceding sub-section, such that the highest accumulated strain energy density in Model 5 indicates highest fatigue damage while Model 1 with the least accumulated strain energy density has the lowest fatigue damage in solder joint. Therefore Model 5 has the highest likelihood of fatigue failure due to its highest fatigue damage accumulation whereas Model 1 has the least likelihood of fatigue failure due to its lowest fatigue damage accumulation.

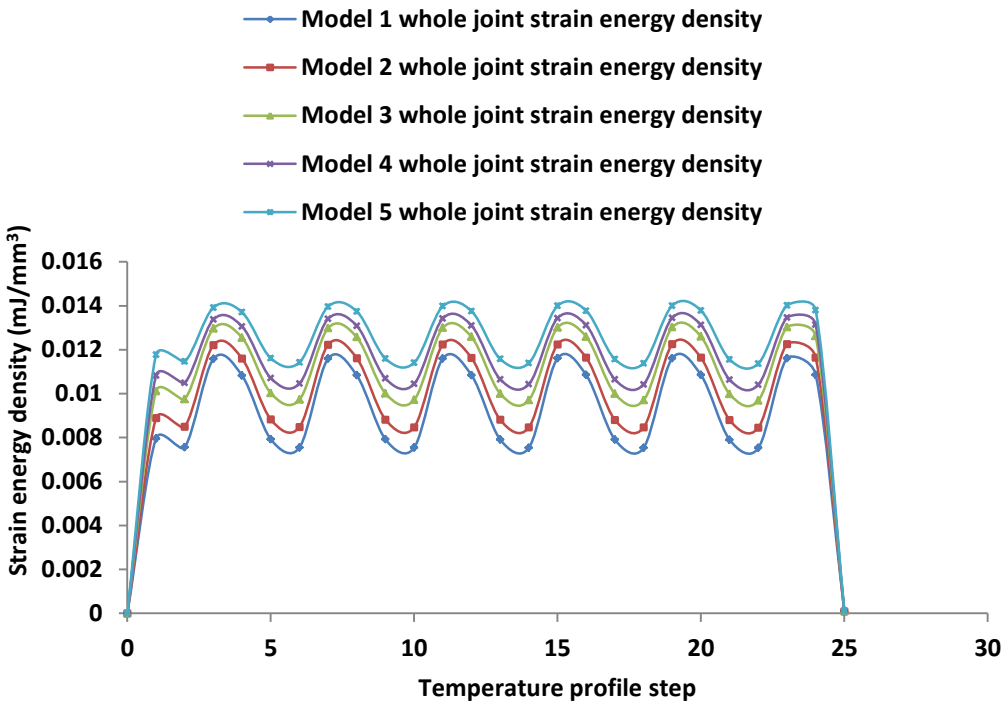


**Figure 6.8 Plot of strain energy density in solder joint against temperature profile step**

### 6.2.4 Effect of solder joint thickness on fatigue life of solder joints

The fatigue life of solar cell solder joint for each of the five joint thicknesses is predicted using fatigue models. The results of the computation are obtained and then compared to determine the effect of solder joint thickness on the fatigue life of the solder joints. The average accumulated change in creep strain energy density per cycle ($\Delta\omega_{acc}$) presented in Table 6.3 is used in Eq. 2.11 to compute the number of cycles to failure for each of the five models and the results are presented in Table 6.4. The results indicate that Model 1 with solder joint thickness of 20μm has the highest fatigue life of

14174 cycles to failure whereas Model 5 with solder joint thickness of 30μm has the lowest fatigue life of 10794 cycles to failure.

**Table 6.4 Effect of solder joint thickness on fatigue life**

| Model number | Solder joint thickness(μm) | $\Delta\omega_{acc}$ ($mJ/mm^3$) | Predicted life (cycles) |
|---|---|---|---|
| **1** | **20** | **0.03713** | **14174** |
| **2** | **22** | **0.04007** | **13134** |
| **3** | **25** | **0.04383** | **12008** |
| **4** | **27** | **0.04594** | **11456** |
| **5** | **30** | **0.04876** | **10794** |

Furthermore, Fig. 6.9 shows a plot of predicted solder joint fatigue life against solder joint thickness. The plot shows that the fatigue life of the solder joint in the models decreases as the solder joint thickness increases. This is expected due to the fundamental failure mechanism of solder joint fatigue failure. The reason is because as the solder volume increases, the solder joint becomes stiffer and provides stronger support to the interconnects. However, as the solder joint becomes stiffer and rigid, the joint accumulates more stresses during thermal cycling resulting in faster fatigue failure. Conversely, as solder volume reduces, the solder joint becomes more flexible thereby accumulating less stresses during thermal cycling and slower fatigue failure. Besides, this result is consistent with similar results obtained by other researchers such as Fan *et al*. (2010) in their study on wafer level packaging.

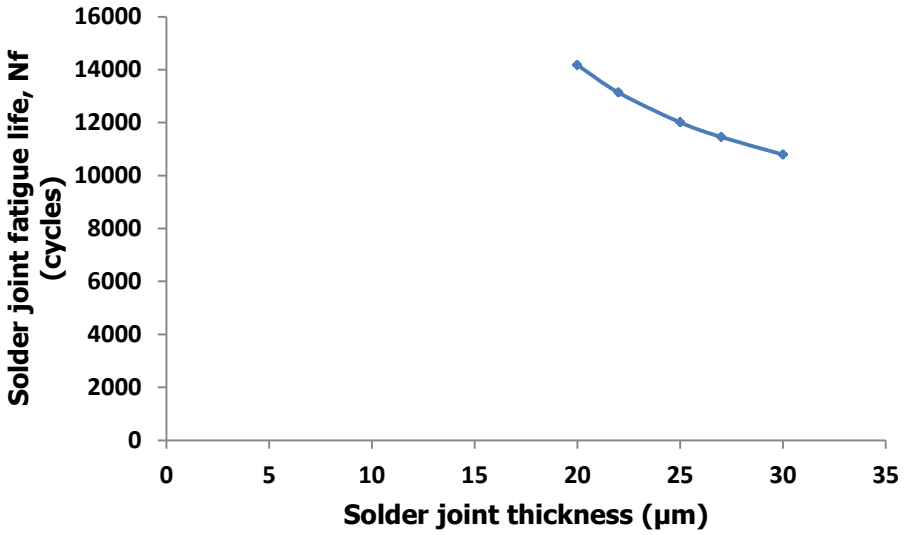


**Figure 6.9 Plot of predicted solder joint fatigue life versus model number for varied thickness**

Therefore, the result implies that solder joint thickness has significant impact on the thermo-mechanical fatigue life of solder joints in crystalline silicon solar cell assembly. Consequently, the solder joint thickness is a critical parameter of the joint and should be taken into consideration during the design of solder interconnection of solar cell assembly to ensure thermo-mechanical reliability of the joint.

## 6.3 Conclusions

An evaluation of the effect of solder joint thickness on thermomechanical reliability of solder joints in crystalline silicon solar cell assembly was presented in this chapter. The results obtained from this study show that solder joint thickness of solar cell assembly have significant effect on solder

joint thermo-mechanical reliability. This is due to increase in thermo-mechanical stresses induced in the joints during thermal loading as the solder joint thickness increases. Therefore, appropriate solder joint thickness should be used in solar cell assembly in order to reduce thermo-mechanical stresses in the joint and extend fatigue life of the joint. The other critical geometric parameter of solder joint is the width. The solder joint width provides contact interface area between the solder layer and the other interconnects in solar cell assembly. However, wider solder joint, increase shadowing losses of solar cell. Hence the study of the effect of solder joint width on thermo-mechanical fatigue life of solder joint in solar cell assembly is presented in the following chapter.

# CHAPTER 7

# EVALUATION OF THE EFFECT OF SOLDER JOINT WIDTH ON THERMO-MECHANICAL FATIGUE LIFE OF SOLDER JOINTS IN SOLAR CELL ASSEMBLY

# Chapter 7

# Evaluation of the Effect of Solder Joint Width on Thermo-mechanical Fatigue Life of Solder Joints in Solar Cell Assembly

## 7.1 Introduction

In the foregoing chapter, the effect of critical solder joint geometric parameters commenced with the study of effect of solder joint thickness on thermo-mechanical fatigue life of solder joints in solar cell assembly. Following up on that study this chapter presents the study of effect of solder joint width on thermo-mechanical fatigue life of solder joints in solar cell assembly. It is desirable that solder joint width is minimized to reduce shadowing losses because the wider the solder joint, the wider the shadow on the solar cell and the lesser the amount of current generated by the solar cell. On the other hand, it is crucial to ensure that solder joint width is adequate in order to enable minimal accumulation of creep strain energy density thereby facilitating longer fatigue life. This situation lends credence to the need for the study of the effect of solder joint width on the thermo-mechanical fatigue life of solder joints in solar cell assembly. Presented in this chapter is the methodology employed in this study. Furthermore, results obtained from modelling and simulation as well as discussion are presented in three sub-sections as follows: study on stress and strain of solder joints in solar cell assembly, study on creep energy density in solder joints and effect of solder joint width on fatigue life.

This study utilized FEM discussed in section 3.2.2.1 for this investigation. Also, Garofalo-Arrhenius creep model discussed in section 3.2.2.2 was used for this study. Presented in Fig. 7.1 is a cross-section of solar cell model showing solder joint width.

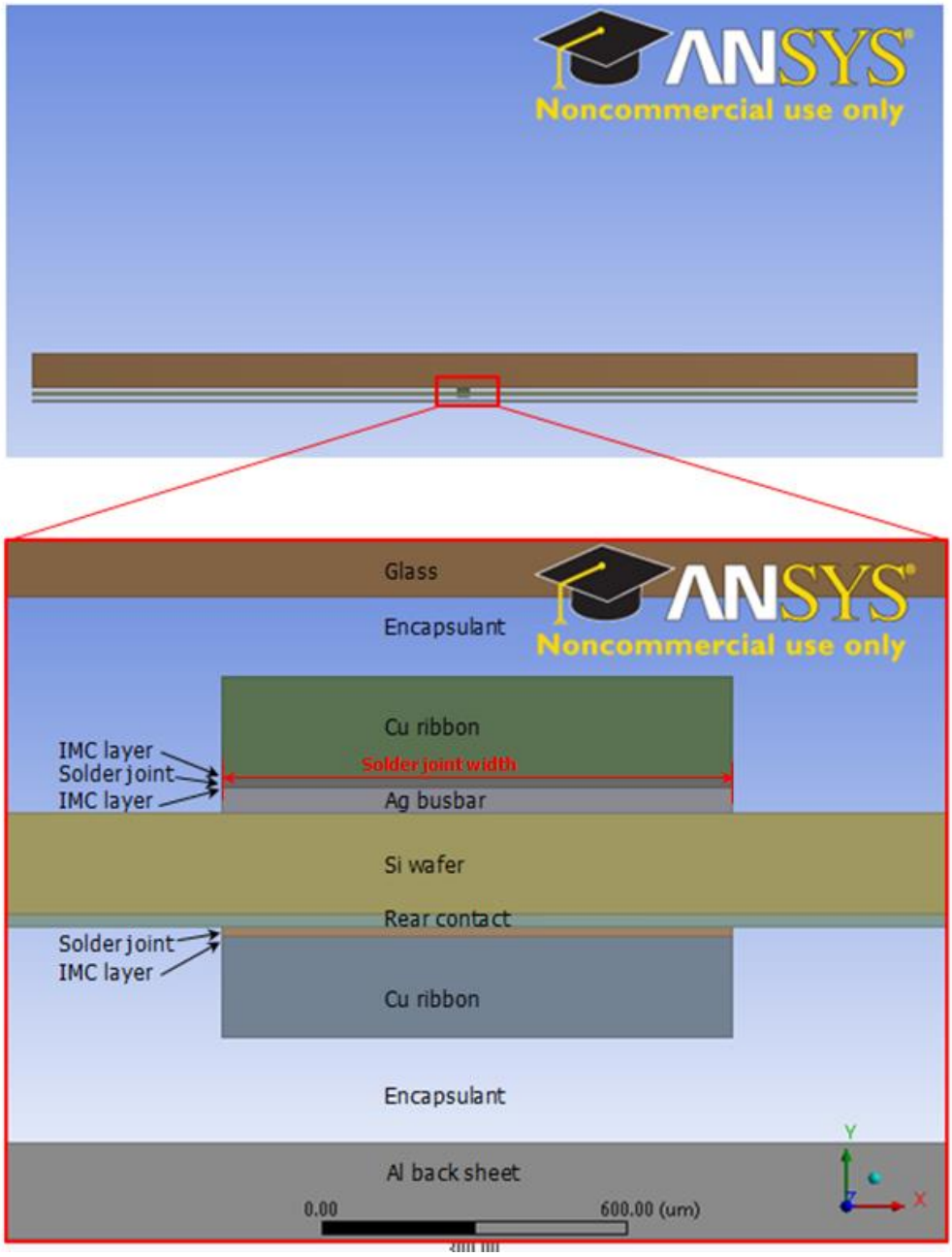


**Figure 7.1 Cross-section of solar cell model showing solder joint width**

It should be noted that numerous researchers and manufacturers use various solder joint widths ranging from 1000μm to 3000μm (Cuddalorepatta, *et al.*, 2010; Klengel, *et al.*, 2011; Gierth, *et al.*, 2012). However, it is desirable that smaller solder joint widths are used for solar cell interconnection in order to minimize shadowing losses on the solar cell. Minimized shadowing losses results in greater surface area of the solar cell, hence more quantity of electricity can be generated. In this study, solder joint width selected for five separate geometric models are 1000μm, 1100μm, 1200μm, 1300μm and 1400μm and the models are assigned numbers 1, 2, 3, 4 and 5 respectively. Correspondingly, each of the models has an IMC thickness of 2.5μm and a solder joint thickness of 20μm. Consequently, the solder joint width in each model is varied such that as solder joint width increases solder joint volume increases as well. The parameters of the five geometric models with varied solder joint width are presented in Table 7.1. The table shows that as solder joint width increases solder volume in whole joint increases as well.

**Table 7.1 Parameters of models with varied solder joint width**

| Model number | IMC thickness (μm) | Solder joint thickness (μm) | Solder joint width (μm) | Whole joint Vol. ($mm^3$) | Solder region Vol. ($mm^3$) |
|---|---|---|---|---|---|
| **1** | **2.5** | **20** | **1000** | **1.560** | **1.170** |
| **2** | **2.5** | **20** | **1100** | **1.716** | **1.287** |
| **3** | **2.5** | **20** | **1200** | **1.872** | **1.404** |
| **4** | **2.5** | **20** | **1300** | **2.028** | **1.521** |
| **5** | **2.5** | **20** | **1400** | **2.184** | **1.638** |

Figure 7.2 is a plot of solder volume in whole joint against solder joint thickness while Fig. 7.3 is a plot of solder volume in solder region against solder region volume respectively. Figure 7.2 shows that as solder joint width increases solder volume in whole joint increases as well. Similarly, Fig. 7.3 shows that solder volume in solder only region increases as solder joint width increases.

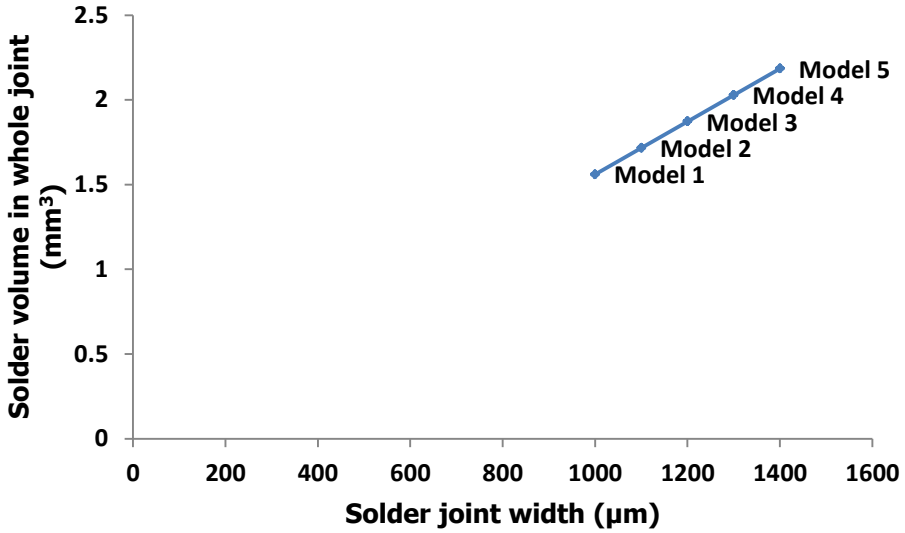


**Figure 7.2 Plot of solder volume in whole joint against solder joint width**

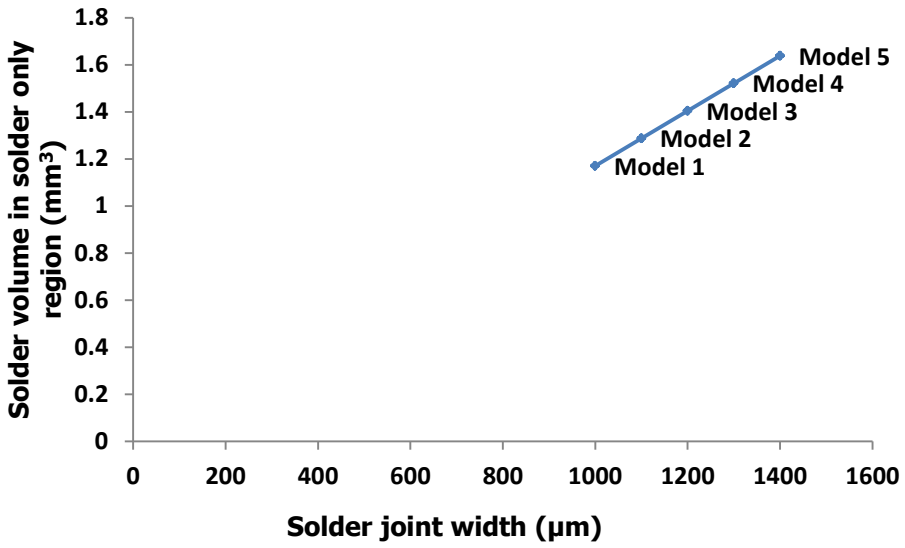


**Figure 7.3 Plot of solder volume in solder region against solder joint width**

The five geometric models of 156 x 156 $mm^2$ multi-crystalline silicon solar cell assembly were simulated by subjecting them to six accelerated thermal cycling in 25 load steps between -40$^oC$ to 85$^oC$. The temperature loading started from 25$^oC$, ramped up at a rate of 3$^oC$/min to 85$^oC$, where it had hot dwell for 20 min. It was then ramped down to -40$^oC$ at a rate of 6$^oC$/min, where it had cold dwell for 20 min. The thermal cycling profile presented in section 3.2.2.2.2 was used to simulate actual cycling profile used during thermal load test.

## 7.2 Results and discussion

This section presents results and discussion based on the modelling and simulation implemented. The section is comprised of three sub-sections which are: study on stress and strain in solder joints of solar cell assembly,

study on creep energy density in solder joints, and effect of solder joint width on fatigue life.

### 7.2.1 Study on stress and strain of solder joints in solar cell assembly

Stress and strain induced in solder joint of solar cell assembly can cause fatigue failure of the joint. The implication is that energy generated by the solar cell will not have passage access to Cu ribbon strip for onward delivery to the required point. For that reason, it is crucial that a study of stress and strain in solder joint is carried out to obtain proper understanding of the failure of solder joint with regards to solder joint width ($W_{SJ}$). Figure 7.4 presents the five models showing damage distribution of equivalent stress on the whole solder joint. Model 1 shown in Fig. 7.4(a) has the least solder joint width of 1000μm while Model 5 shown in Fig. 7.4(e) has the widest joint of 1400μm. The figure shows that all the five models have maximum stress at the left end of the longitudinal section of the whole solder joint. Furthermore, the damage distribution is evenly spread along the longitudinal section of the whole joint. However, it appears on close observation, that as the solder joint width increases, the damage distribution becomes milder. Thus the damage distribution in Model 1 ($W_{SJ}$ 1000μm) shown in Fig. 7.4(a), seems to be more severe than that of Model 2 ($W_{SJ}$ 1100μm) shown in Fig. 7.4(b) as observed in the colour variation. This trend of reduced severity continues in the remaining Models 3 ($W_{SJ}$ 1200μm), 4 ($W_{SJ}$ 1300μm) and 5

($W_{SJ}$ 1400μm) as shown in Figs. 7.4(c), 7.4(d) and 7.4(e) respectively. It can also be observed that the minimum stress is located on the right hand side (RHS) of Models 1 and 5 as shown in Figs. 7.4(c) and 7.4(d) respectively. However, the minimum stress is located on the left hand side (LHS) of Models 2, 3 and 4 as shown in Figs. 7.4(b), 7.4(c) and 7.4(d) respectively. The reason for this change in location of the stress as the solder joint width increases is not yet understood. This indicates that the stress induced in the solder joints varies with the increase in joint width in the manner that as the width increases, less stress is induced in the joint. This is due to the increase in solder volume which increases the capacity of the joint to dissipate stress in the joint as the width increases. In addition, the position of solder joint width is along the horizontal axis which makes it less affected with the expansion and contraction of the joint during thermal cycling as opposed to the situation of the joint thickness which is positioned in the vertical axis. Therefore, this result suggests that the wider the solder joint, the lower the possibility of fatigue failure.

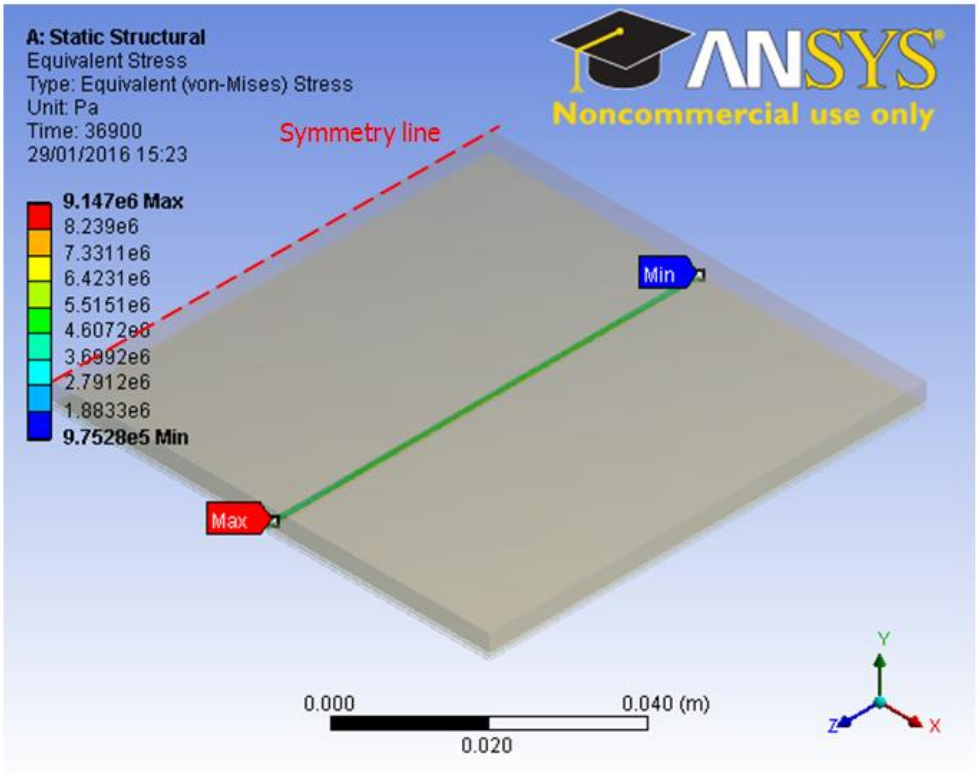


**(a) Stress on model 1 whole joint**

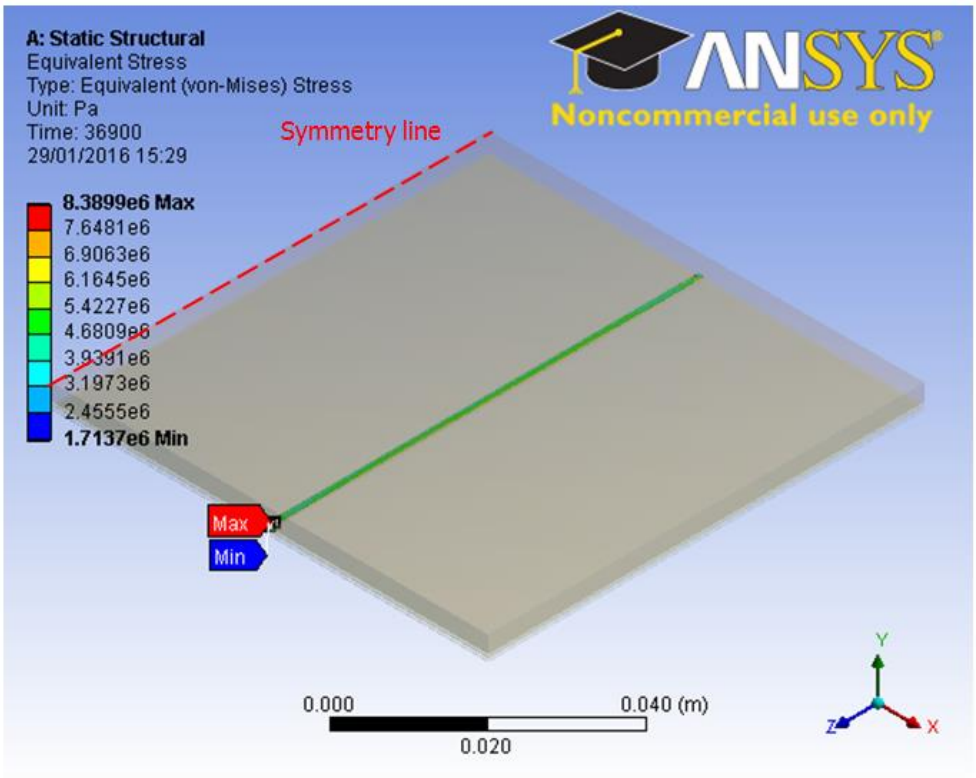


**(b) Stress on model 2 whole joint**

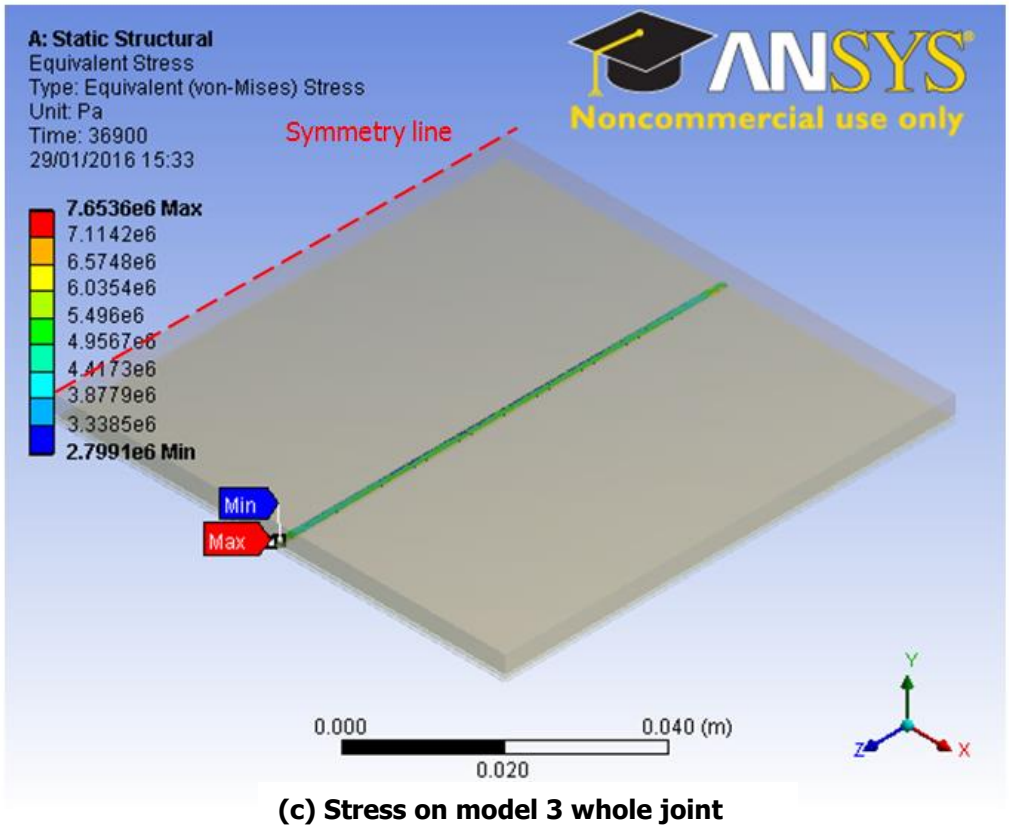


**(c) Stress on model 3 whole joint**

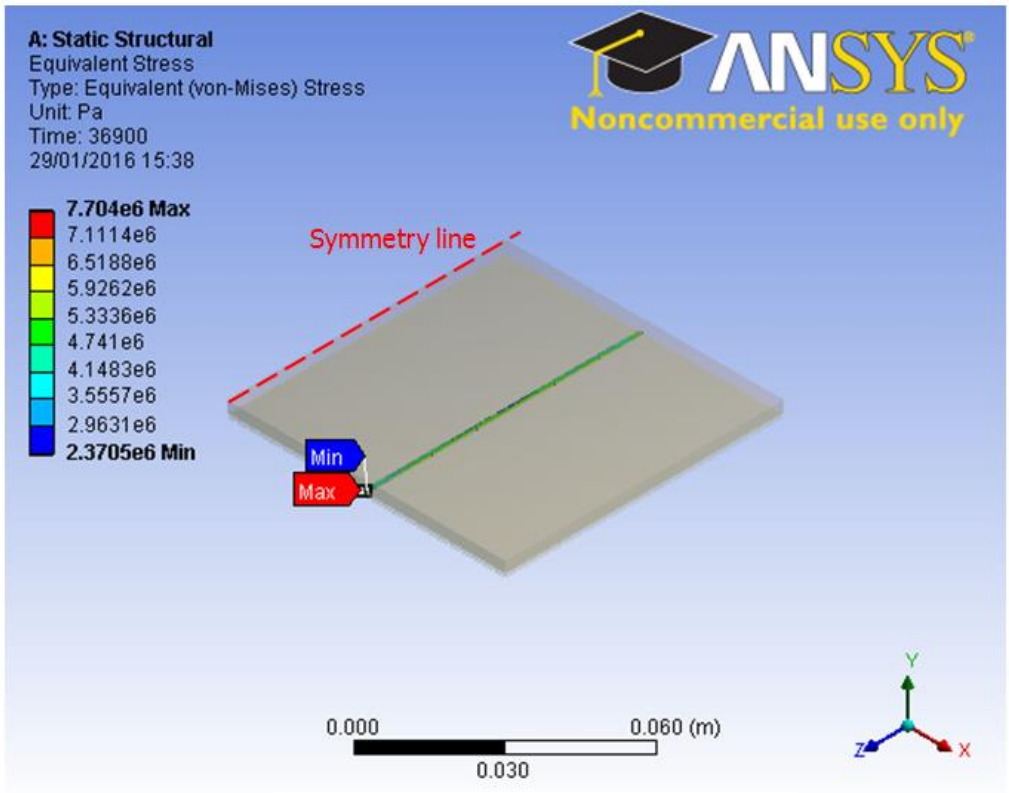


**(d) Stress on model 4 whole joint**

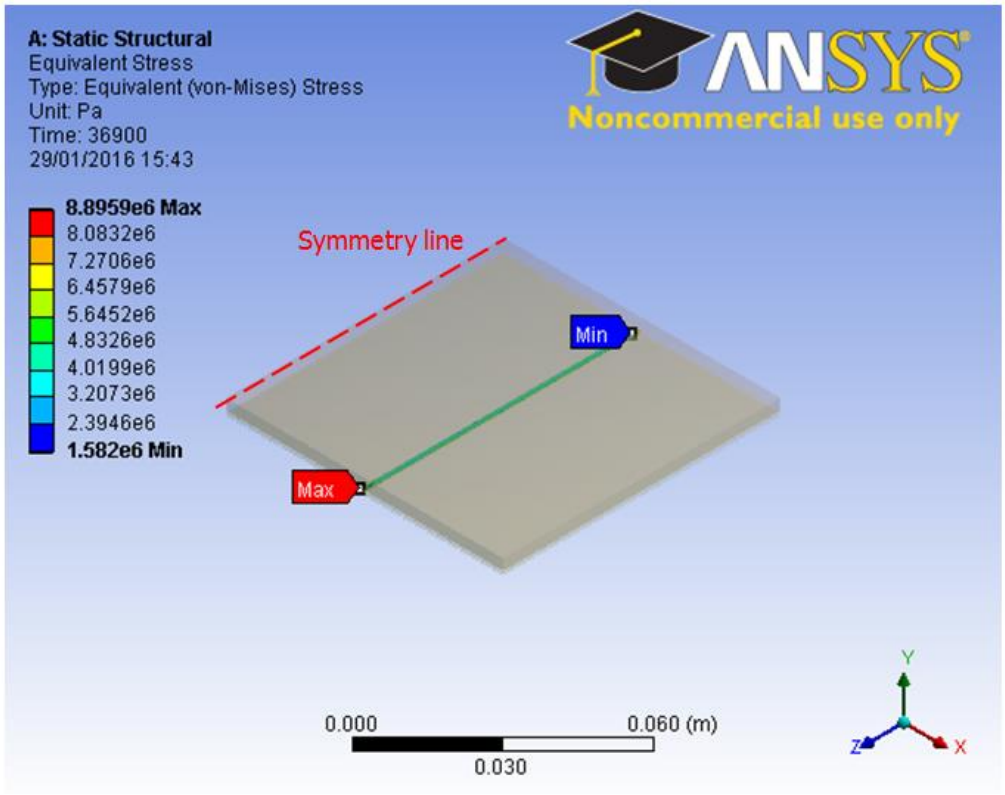


**(e) Stress on model 1 whole joint**

**Figure 7.4 Damage distribution of equivalent stress on solder joint with varied width showing:**
**(a) Stress on model 1 whole joint**
**(b) Stress on model 2 whole joint**
**(c) Stress on model 3 whole joint**
**(d) Stress on model 4 whole joint**
**(e) Stress on model 5 whole joint**

Figure 7.5 shows the creep strain damage distribution in the whole solder joint in the five models. In all the models, the damage distribution is towards the two ends of the whole joints. The maximum creep strain is towards the right side end of the joint in Models 1, 2, 3 and 4 with values of 6.8854E-04m/m, 5.9248E-04m/m, 6.0335E-04m/m and 5.583E-04m/m as shown in Figs. 7.5(a), 7.5(b), 7.5(c) and 7.5(d) respectively. Conversely, maximum creep strain is towards the left side of the joint in Model 5 with a value of 4.9321E-04m/m as shown in Fig. 7.5(e). As previously mentioned the reason for this change in location is not yet clear. However, it can be

inferred from these results that the maximum creep strain affects the whole length of the solder joint and can be located at any of the two ends of the joint depending on the solder joint width. This is consistent with what is observed practically as solder joints in solar cell assembly generally fail at the ends.

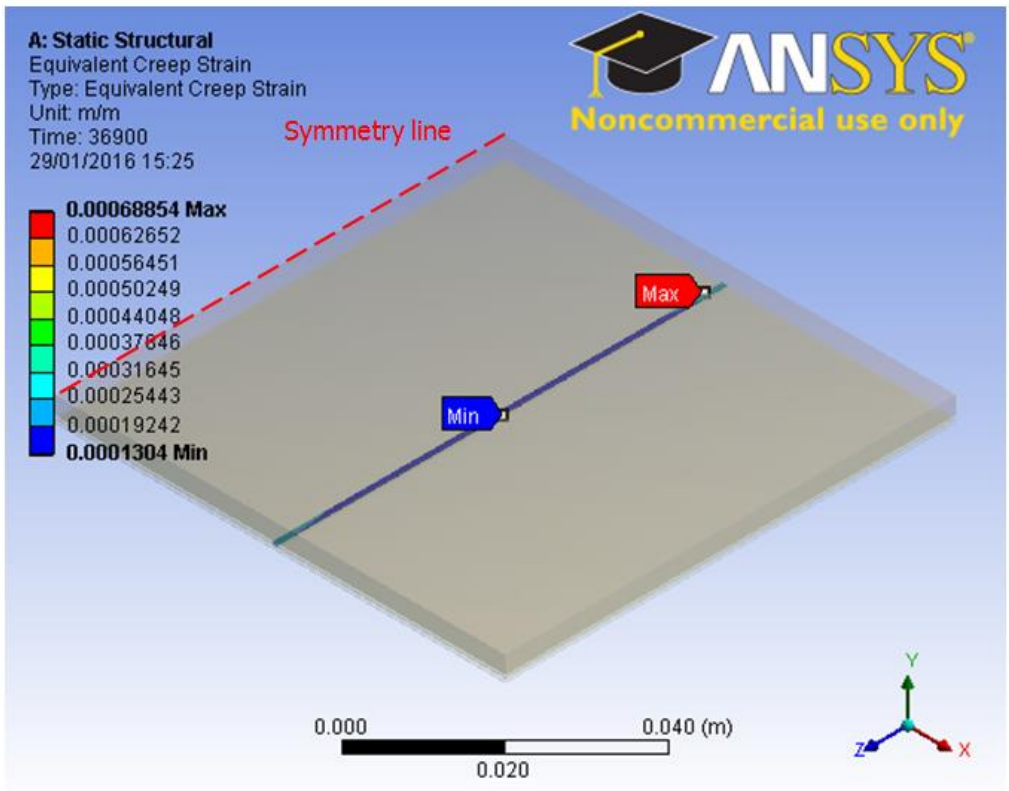


**(a) Strain on model 1 whole joint**

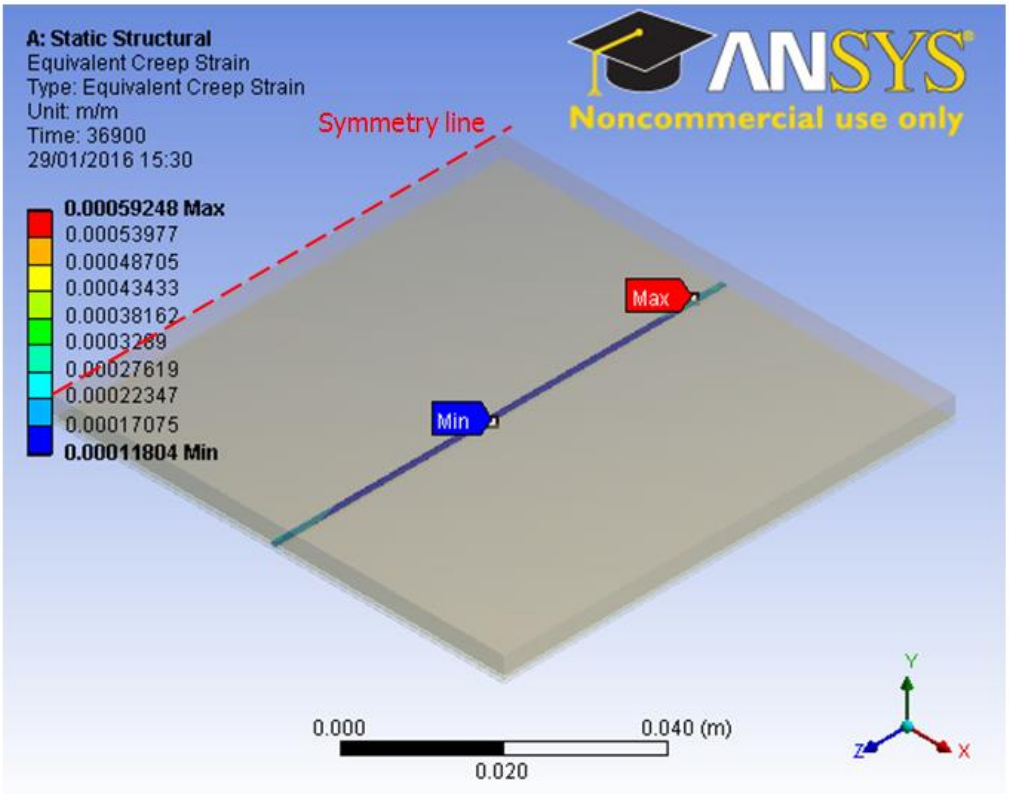


**(b) Strain on model 2 whole joint**

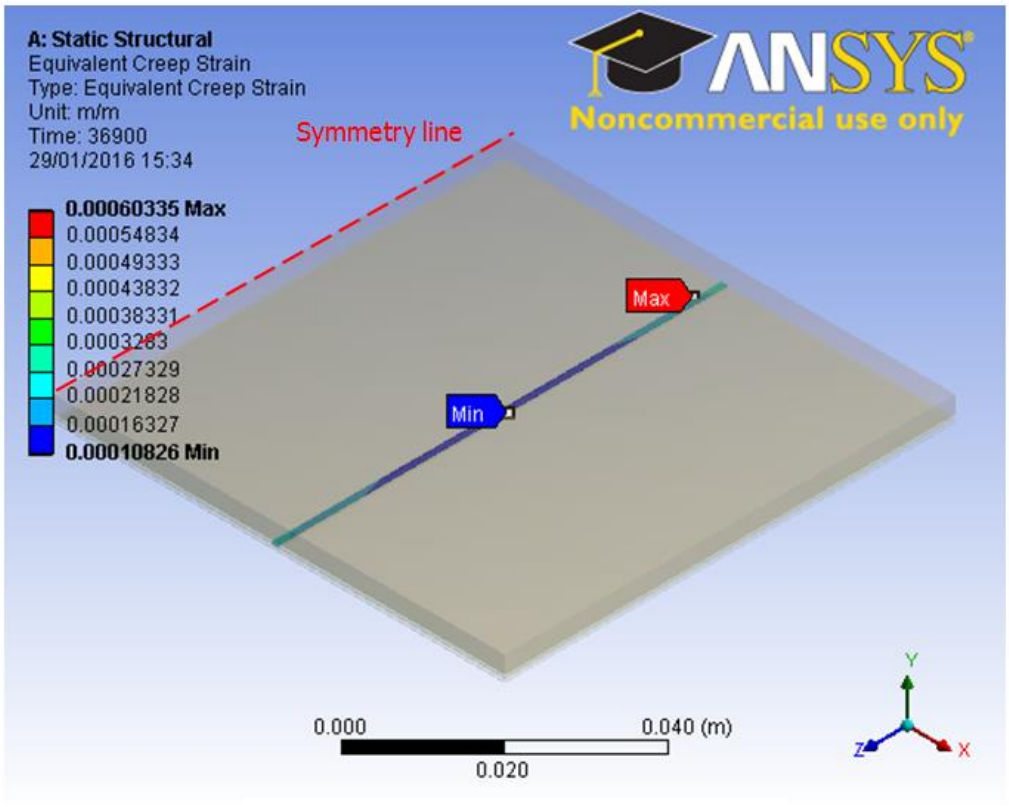


**(c) Strain on model 3 whole joint**

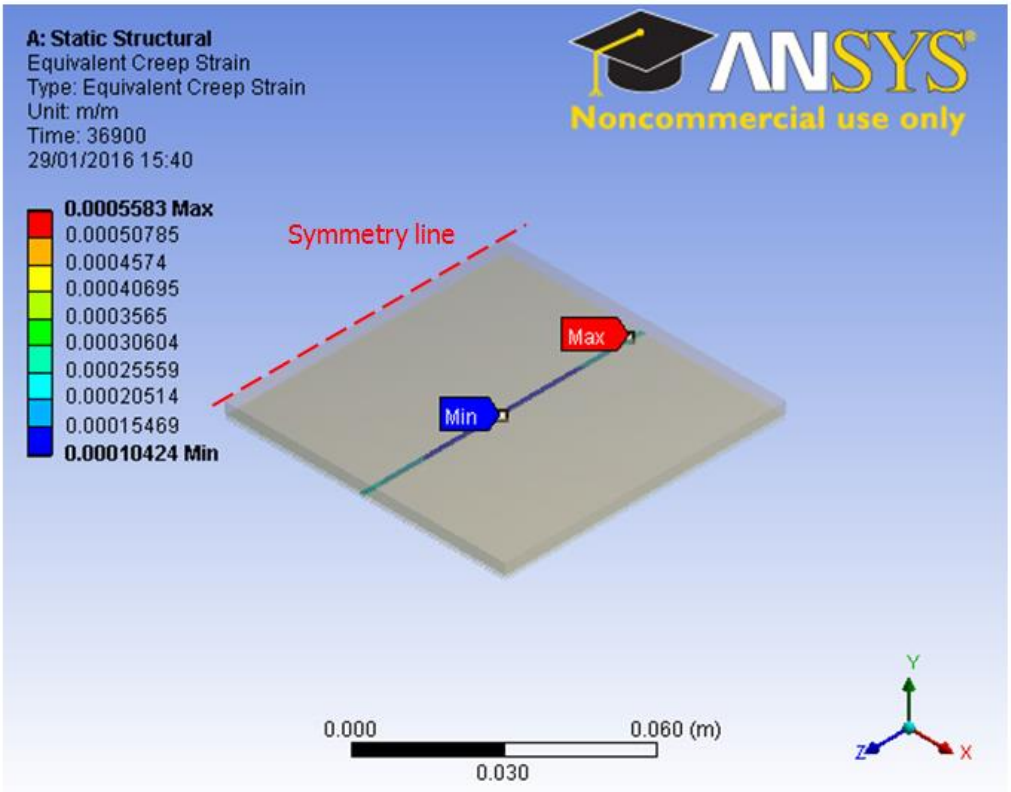


**(d) Strain on model 4 whole joint**

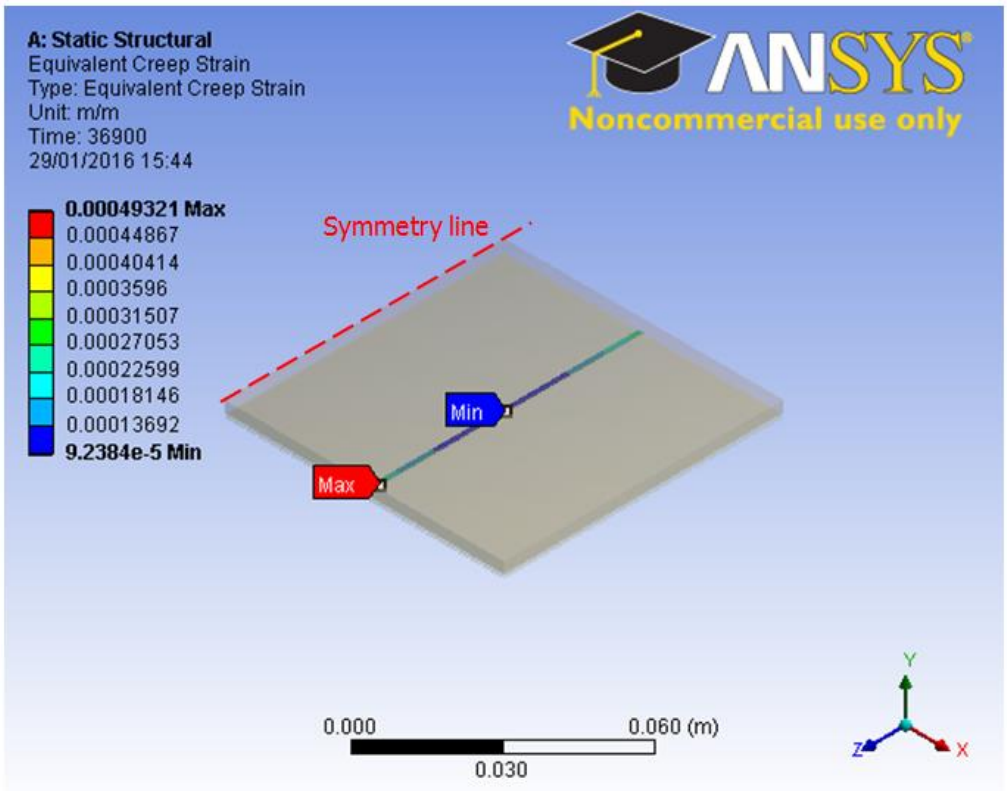


**(e) Strain on model 5 whole joint**

**Figure 7.5 Damage distribution of equivalent creep strain on solder joint with varied width showing:**
**(a) Strain on model 1 whole joint**
**(b) Strain on model 2 whole joint**
**(c) Strain on model 3 whole joint**
**(d) Strain on model 4 whole joint**
**(e) Strain on model 5 whole joint**

Figure 7.6 shows a plot of creep strain in solder joint against temperature profile step. The plot shows that as thermal loading on the solder joint progresses, creep strain increases in the joint. In addition, it can be observed from the figure that at the end of the 25 load steps, Model 1 has the highest accumulated creep strain of more than 8E-04m/m while Model 5 has the least value of about 7.5E-04m/m. Therefore, it can be inferred from these results that the smaller the solder joint width, the higher the creep strain damage. Conversely, the wider the solder joint width, the lower the

creep strain damage in the joint but the larger the shadowing losses on the solar cell surface area.

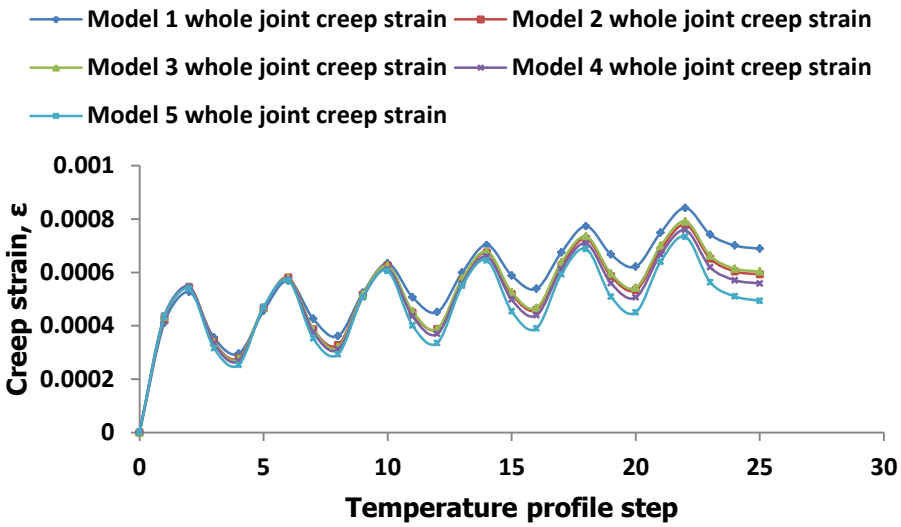


**Figure 7.6 Plot of equivalent creep strain on solder joint against temperature profile step**

The plot of stress and creep strain in solder joint of the five models is presented in Fig. 7.7. For each of the models in the figure, hysteresis loop is formed. Thus the area of the loop which represents fatigue damage accumulating per cycle in solder joint is formed for each model. It can be noted in the figure that the profile of the hysteresis loops are related to each other which implies that the difference in fatigue damage accumulated in their joints is within a range. In particular, it can be observed from Fig. 7.7 that the equivalent stress of the five models is within a range of about 135MPa to 145MPa. The study of creep strain energy density for each model is presented next in section 7.2.2 with further analysis.

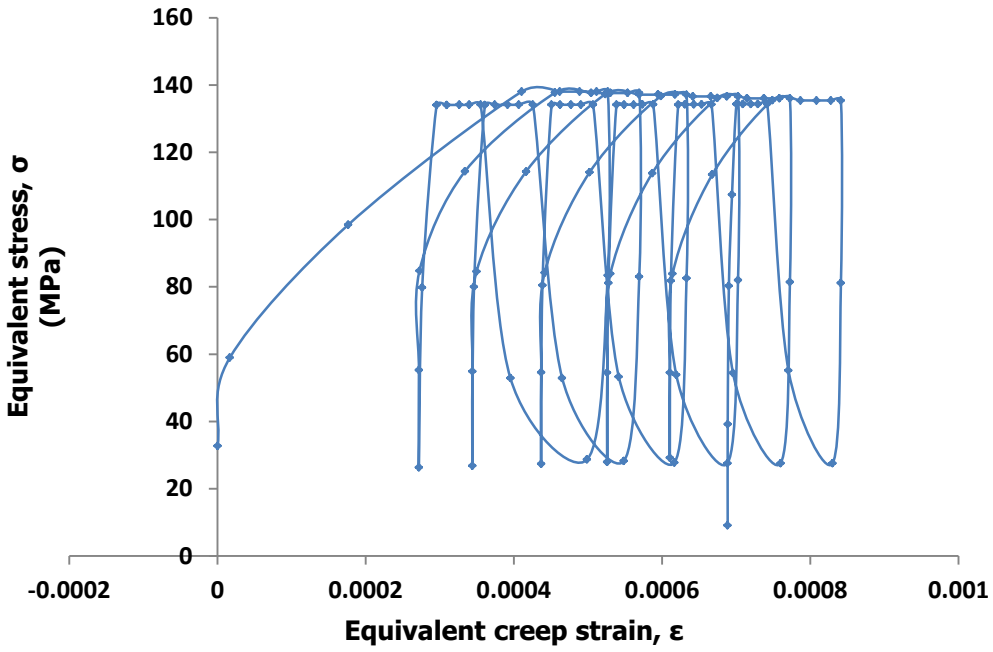


**(a) Stress and creep strain relationship in solder joint of Model 1**

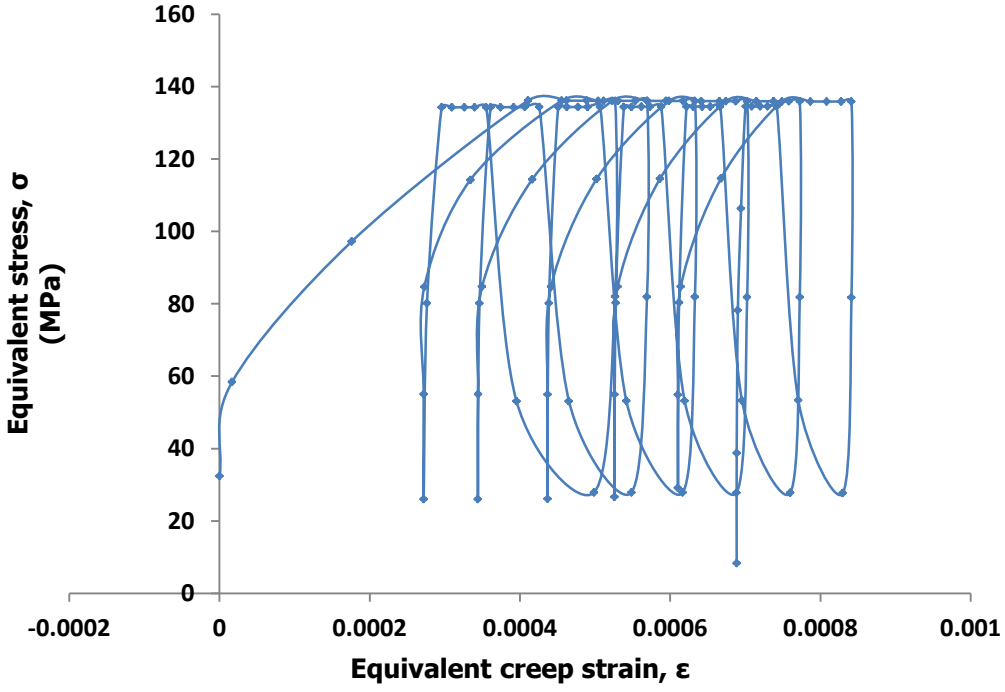


**(b) Stress and creep strain relationship in solder joint of Model 2**

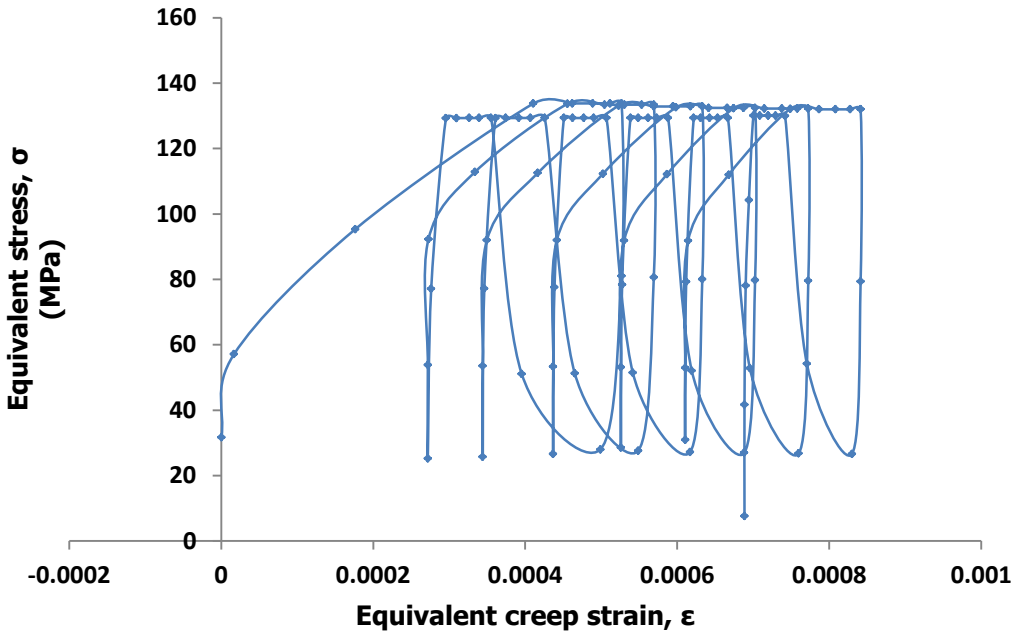


**(c) Stress and creep strain relationship in solder joint of Model 3**

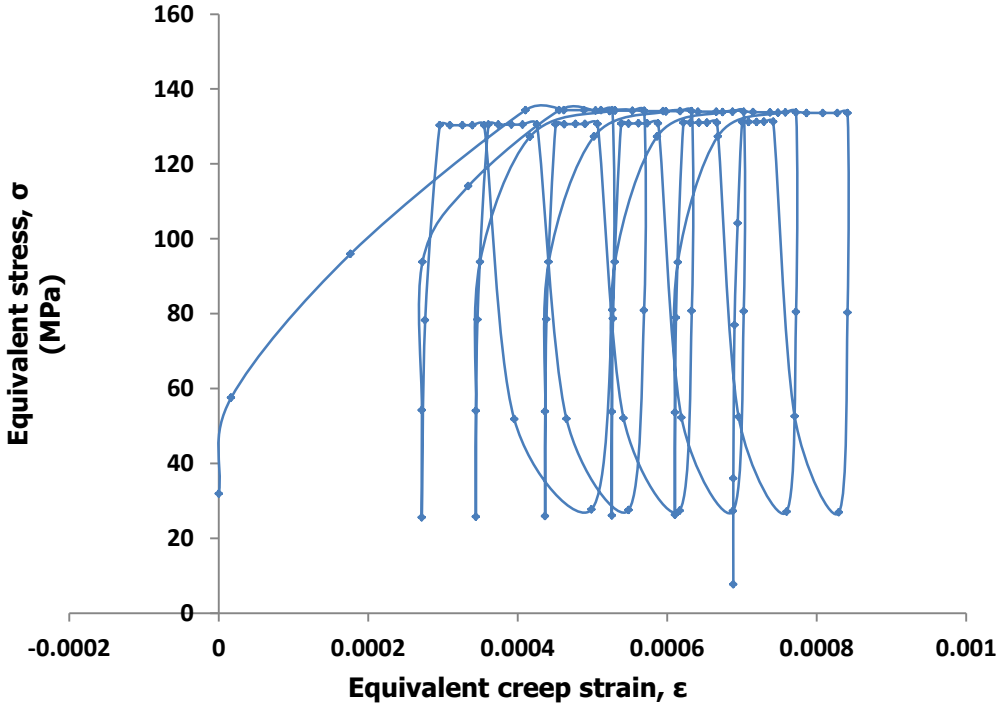


**(d) Stress and creep strain relationship in solder joint of Model 4**

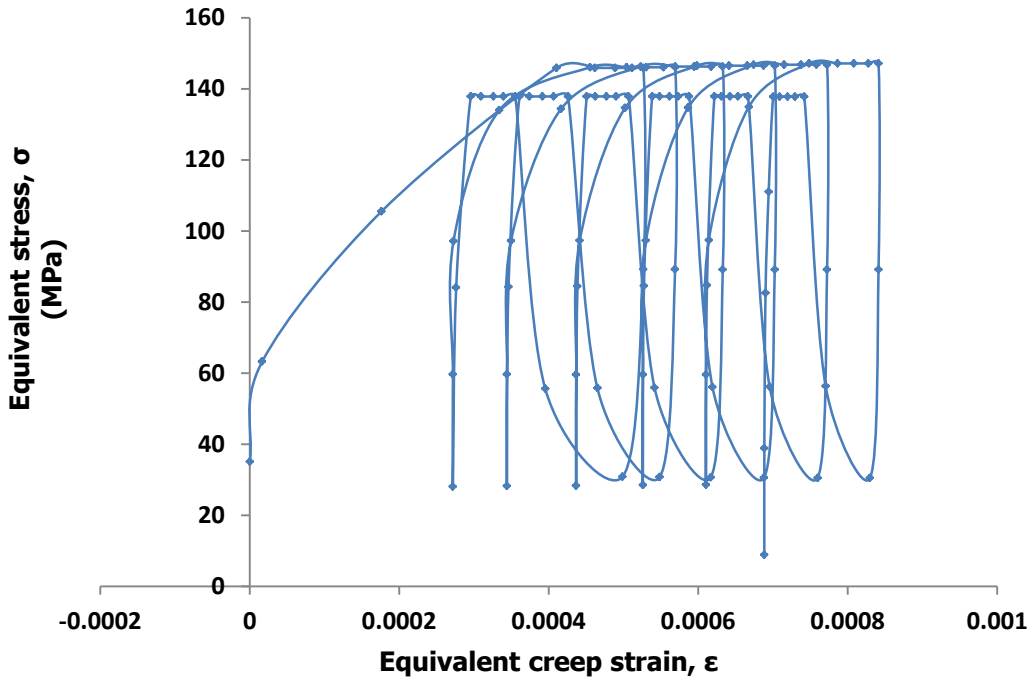


**(e) Stress and creep strain relationship in solder joint of Model 5**

**Figure 7.7 Relationship between stress and creep strain in the solder joint of solar cell models showing:**
**(a) Stress and strain relationship in solder joint of model 1**
**(b) Stress and strain relationship in solder joint of model 2**
**(c) Stress and strain relationship in solder joint of model 3**
**(d) Stress and strain relationship in solder joint of model 4**
**(e) Stress and strain relationship in solder joint of model 5**

### 7.2.2 Study on creep energy density in solder joints

In order to get a better understanding of the effect of solder joint width on thermo-mechanical reliability of solder joint, it is absolutely essential to study the creep strain energy density of the joints in the five models. Presented in Table 7.2 is accumulated average change in creep strain energy density per cycle of solder joint for various solder joint widths. A close observation of Table 7.2 reveals that Model 1 has the largest accumulated average change in creep energy density per cycle with a value of 0.03713mJ/mm$^3$ while

Model 5 has the lowest value of 0.03346mJ/mm$^3$. This implies that since Model 1 has the largest creep strain energy density in the solder joint, it is the most likely joint to fail among the five models because it incurred the largest damage. In the case of Model 5, it has the lowest creep strain energy density in the solder joint with a value of 0.03713mJ/mm$^3$ as stated earlier, which implies that it is the least likely joint to fail due to the least damage incurred among the five models.

**Table 7.2 Average change in creep strain energy density per cycle in varied solder joint width**

| Model number | Solder joint width (μm) | Solder volume in whole joint (mm$^3$) | Average change in creep strain energy density per cycle, $\Delta\omega_{acc}$ (mJ/mm$^3$) |
|---|---|---|---|
| **1** | **1000** | **1.560** | **0.03713** |
| **2** | **1100** | **1.716** | **0.03676** |
| **3** | **1200** | **1.872** | **0.03495** |
| **4** | **1300** | **2.028** | **0.03411** |
| **5** | **1400** | **2.184** | **0.03346** |

Figure 7.8 shows a plot of strain energy density in solder joint of the five models against temperature profile step. The plot shows that Models 1 and 2 have the highest and almost the same accumulated strain energy density in their solder joints with value of about 0.012mJ/mm$^3$ while Model 5 has the lowest value of about 0.0065mJ/mm$^3$. The implication of this is that higher accumulated strain energy density in Models 1 and 2 indicates higher likelihood of fatigue failure due to fatigue damage accumulated in the solder joints. Conversely, the lowest accumulated strain energy density in Model 5

implies lower likelihood of fatigue failure due to the lower fatigue damage accumulated in the solder joints. Therefore, from this result, it can be inferred that the wider the solder joints in solar cell assembly, the lower the fatigue damage in the joint.

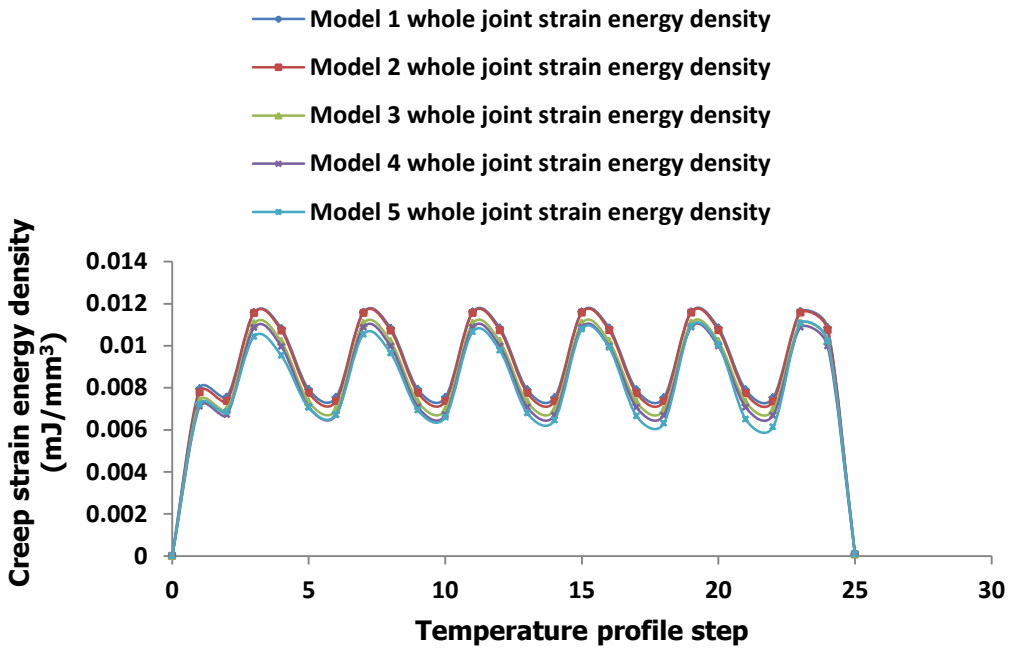


**Figure 7.8 Plot of creep strain energy density in solder joint against temperature profile step**

### 7.2.3 Effect of solder joint width on fatigue life

The solar cell solder joint fatigue life for each of the five models with varied widths is predicted using fatigue models as was done previously. The computation results obtained are then compared to determine the effect of solder joint width on the fatigue life of the solder joints. Therefore, the average change in accumulated creep strain energy density per cycle ($\Delta\omega_{acc}$) of solder joint for various solder joint widths presented in Table 7.2 are used

for fatigue life prediction. The fatigue model stated in Eq. 2.11 is used to compute the number of cycles to failure of the five models and the results are presented in Table 7.3. The computation results in Table 7.3 indicate that Model 1 with solder joint width of 1000μm has the least fatigue life of 14174 cycles to failure while Model 5 with solder joint width of 1400μm has the highest fatigue life of 15729 cycles to failure.

**Table 7.3 Effect of solder joint width on fatigue life**

| Model number | Solder joint width (μm) | $\Delta\omega_{acc}$ (mJ/mm$^3$) | Predicted life (cycles) |
|---|---|---|---|
| **1** | **1000** | **0.03713** | **14174** |
| **2** | **1100** | **0.03676** | **14317** |
| **3** | **1200** | **0.03495** | **15059** |
| **4** | **1300** | **0.03411** | **15429** |
| **5** | **1400** | **0.03346** | **15729** |

Figure 7.9 shows a plot of solder joint fatigue life versus solder joint width. The plot demonstrates that as the solder joint width increases, fatigue life increases as well. This is due to the wider interface area between the solder joint and the Si wafer. Thus, the result is consistent with the fact that the wider the solder joint, the larger the solder volume and hence the longer it takes for crack propagation along the width of the joint. Moreover, this confirms that solder joint width has significant impact on the thermo-mechanical fatigue life of solder joints in crystalline silicon solar cell assembly such that wider solder joints accumulate less fatigue damage than narrow ones. Therefore, the solder joint width is a critical parameter of solder joint

which should be taken into consideration during the design of the joint in order to ensure adequate thermo-mechanical reliability of solar cell assembly. However, in so doing, a compromise must be made between a wide solder joint and the shadowing losses arising therefrom. This is necessary to avoid significant reduction in solar cell efficiency due shadows cast by wide solder joints/Cu ribbons on the surface of the cell.

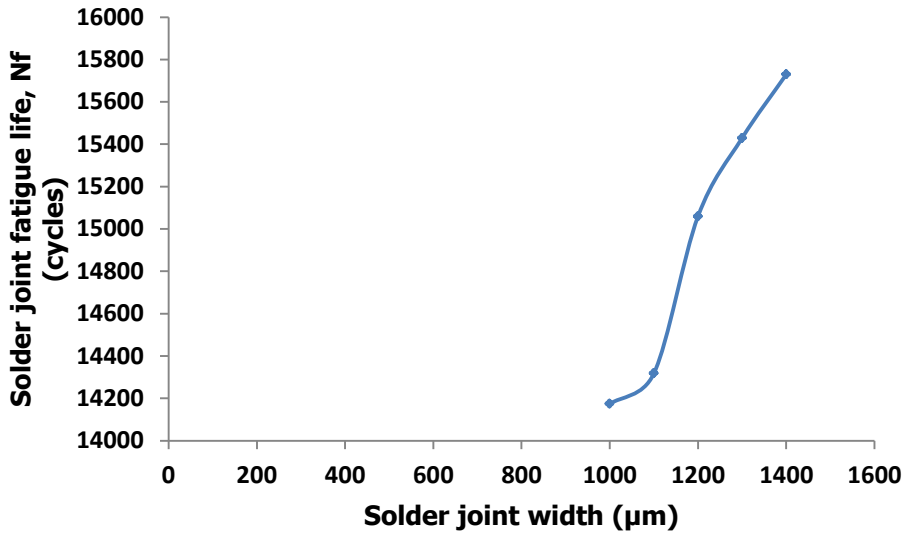


**Figure 7.9 Plot of solder joint fatigue life versus solder joint width**

## 7.3 Conclusions

The effect of solder joint width on thermo-mechanical fatigue life of solder joint in solar cell assembly was studied in this chapter. The study shows that the wider the solar cell solder joint, the longer the predicted fatigue life. The reason for this is that the wider solder joint increases the total interface area; hence it takes a longer time for solder crack propagation to go through

the contact interface. However, wider solder joints increase shadowing losses of the solar cell thereby reducing the cell efficiency. Therefore, compromise is required between increase in solder joint width and shadowing losses so that the desired thermo-mechanical fatigue life can be achieved.

In the previous two chapters, the effects of IMC thickness and solder joint thickness on thermo-mechanical fatigue life of solder joint in solar cell assembly were studied respectively. The results of the previous studies as well as the study conducted in this chapter indicate that IMC thickness, solder joint thickness and solder joint width impact the thermo-mechanical fatigue life of solder joint. It is therefore vital that these factors are studied together in order to come up with the best combination of solder joint geometric parameters that can enhance solder joint fatigue life. This is achieved through optimization aimed at improving the thermo-mechanical reliability of the joints. Accordingly, presented in the following chapter is the optimization of thermo-mechanical reliability of the solder joints in solar cell assembly.

# CHAPTER 8

# OPTIMIZATION OF THERMO-MECHANICAL RELIABILITY OF SOLDER JOINTS IN SOLAR CELL ASSEMBLY

# Chapter 8

# Optimization of Thermo-mechanical Reliability of Solder Joints in Solar Cell Assembly

## 8.1 Introduction

In the preceding three chapters, the study of the effects of IMC thickness, solder joint thickness and solder joint width on thermo-mechanical fatigue life of solder joint in solar cell assembly were presented. To ensure adequate solder joint thermo-mechanical reliability, this chapter presents optimization of these solder joint parameters in solar cell assembly to provide useful knowledge for the manufacture of crystalline PV modules. Therefore in this chapter, just as it was done in previous chapters, finite element modelling (FEM) and simulation is employed for this optimization. Furthermore, the use of the concept of design of experiment (DOE) facilitates robust design of solder joints thereby enhancing thermo-mechanical reliability of solder interconnects. As discussed in chapter 3, there are numerous DOE tools in use, yet, Taguchi method is popularly used because it is aimed at improving quality as well as allowing the effects of several factors to be determined simultaneously and efficiently (Taguchi, 1995). Application of Taguchi method for DOE in this research enables the selection of the best matching combination of geometric parameters for improving the thermo-mechanical reliability of solder joints under thermal cycling.

Based on the foregoing, FEM and Taguchi method for DOE are employed in this study to evaluate the thermo-mechanical reliability of solder joints with various sets of parameters and subjected to thermal cycling. The effects of IMC thickness ($T_{IMC}$), solder joint width ($W_{SJ}$) and solder joint thickness ($T_{SJ}$) on the thermo-mechanical reliability are also investigated for optimal parameter setting of the solder joints in crystalline silicon solar cell assembly. The solder joint formed using optimal parameter setting accumulates minimal creep strain energy density which leads to longer fatigue life due to the robustness of the joint.

### 8.3.1 Application of Taguchi method of DOE

This study utilized Taguchi method for DOE as discussed in chapter 3 to study the thermo-mechanical reliability of solder joints in solar cell assembly for optimal parameter design of the joints. The following three control factors were chosen: IMC thickness ($T_{IMC}$) with values of 1μm, 2.5μm and 4μm, solder joint width ($W_{SJ}$) with values of 1000μm, 1200μm and 1400μm as well as solder joint thickness ($T_{SJ}$) with values of 20μm, 25μm and 30μm. Also, three DOE variables or levels designated as 1, 2 and 3 which stand for low level, intermediate level and high level respectively are used in this study. These control factors and levels are presented in Table 8.1.

**Table 8.1 Control factors and levels**

| Control factor | Units | Level 1 | Level 2 | Level 3 |
|---|---|---|---|---|
| **A IMC thickness (IMCT)** | **µm** | **1** | **2.5** | **4** |
| **B Solder joint width (SJW)** | **µm** | **1000** | **1200** | **1400** |
| **C Solder joint thickness (SJT)** | **µm** | **20** | **25** | **30** |

Solder joint damage indicator is needed as a quality or response factor in Taguchi DOE for optimization. In this case creep strain energy density can be utilized as solder joint damage indicator. Creep strain energy density is a robust damage indicator of solder joint as it is based on the deformation internally stored throughout the volume of the joint during thermal loading. As a result, accumulated creep strain energy density is used in solder joint life prediction models (Syed, 2004). In this study, the change in accumulated creep strain energy density $\Delta\omega_{acc}$, of the solder joint is chosen as the quality or response factor and used in the Taguchi DOE for optimization. The objective of this optimization is to minimize the accumulated creep strain energy density $\Delta\omega_{acc}$, in the solder joint as the decrease in $\Delta\omega_{acc}$ means the enhancement of thermo-mechanical reliability. Minimization of $\Delta\omega_{acc}$ aims at making the system response as small as possible by obtaining the smaller-the-better signal-to-noise ratio. To achieve this aim, the absolute magnitude of the smaller-the-better signal-to-noise (S/N) ratio is chosen and is mathematically defined (Huan, 2010; Davies, *et al.*, 2015) and shown in Table 3.3. In this case, the value of the quality characteristic is taken to be $y \equiv \Delta\omega_{acc}$. Besides, since a numerical analysis does not create data variations, then $n = 1$. Hence, the equation of the signal-to-noise ratio transforms to:

$$S/N=-10 \log (\Delta\omega_{acc})^2 \quad (8.1)$$

The calculation of the chosen S/N ratio is through the Taguchi DOE method based on orthogonal arrays. Orthogonal array is an arrangement of numbers in columns and rows in such a way that each column represents a factor while the rows represent levels of the factors (Davies, *et al.*, 2015). The factors affect the outcome of the process under study. In this study, the $L_9$ ($3^3$) orthogonal array is applied to Taguchi DOE to investigate the effects of IMC thickness ($T_{IMC}$), solder joint width ($W_{SJ}$) and solder joint thickness ($T_{SJ}$) on the thermo-mechanical reliability of solder joints. Presented in Table 8.2 is a table of Taguchi DOE (Orthogonal array with nine designed parameters - $L_9$) showing nine models and their respective solder joint parameter level. ANSYS DesignModeller was used to build the geometric model of each designed model using their respective parameter setting.

In order to obtain the optimal parameter setting of solder joint in solar cell assembly, a main experiment must be implemented. The implementation of the main experiment commences with setting the parameter for each experimental run. Thus, each design of the solder joint is assigned its respective parameter setting as shown in Table 8.2. The geometric models of the solar cell assembly containing the solder joint are subsequently built with the appropriate parameter setting.

**Table 8.2 Table of Taguchi DOE (Orthogonal array $L_9$)**

| Model number | Factor and level | | | Parameter setting |
|---|---|---|---|---|
| | A | B | C | |
| 1 | $1_{(1)}$ | $1_{(1000)}$ | $1_{(20)}$ | A1B1C1 |
| 2 | $1_{(1)}$ | $2_{(1200)}$ | $2_{(25)}$ | A1B2C2 |
| 3 | $1_{(1)}$ | $3_{(1400)}$ | $3_{(30)}$ | A1B3C3 |
| 4 | $2_{(2.5)}$ | $1_{(1000)}$ | $2_{(25)}$ | A2B1C2 |
| 5 | $2_{(2.5)}$ | $2_{(1200)}$ | $3_{(30)}$ | A2B2C3 |
| 6 | $2_{(2.5)}$ | $3_{(1400)}$ | $1_{(20)}$ | A2B3C1 |
| 7 | $3_{(4)}$ | $1_{(1000)}$ | $3_{(30)}$ | A3B1C3 |
| 8 | $3_{(4)}$ | $2_{(1200)}$ | $1_{(20)}$ | A3B2C1 |
| 9 | $3_{(4)}$ | $3_{(1400)}$ | $2_{(25)}$ | A3B3C2 |

## 8.3 Results and discussion

This section presents results and discussion on optimization of solder joint parameter setting in three sub-sections. These are results of FEM of optimization models, evaluation of main effect and interaction and comparison of the optimal design with the worst design.

### 8.3.1 Results of FEM of optimization models

It has been stated severally that solder interconnect in the solar cell assembly is the critical constituent for consideration of thermo-mechanical reliability of the assembly. Therefore, optimizing the geometry parameters of solder joint is key to enhancing the thermo-mechanical reliability of the solder interconnects. Accordingly, the response of solder joint to thermal cycling is required to provide an insight to solder behaviour. Based on results of FEM, characterization and quantification of damage on various solder joint parameter settings is carried out. Thus simulation results showing stress,

creep strain and strain energy provide useful information on the behaviour of solder joints. In this study, nine original geometric models were built and simulated using ANSYS Academic Research Finite Element package. Presented in Fig. 8.1 are simulation results of damage distribution of solder joint in solar cell assembly for one of the models. The figure shows equivalent stress, equivalent creep strain and strain energy in the solder joint. The maximum damage distribution is at the right side edge, towards the right side edge and at the mid-section of the solder joint for stress, creep strain and strain energy respectively. This indicates that crack initiation and propagation is most likely to occur at the mid-section of the solder joint and will eventually lead to fatigue failure at that preferential failure site. A close observation of Fig. 8.1(b) reveals that the maximum creep strain damage is located at the lower side of the solder joint adjacent to silver (Ag) bus-bar which is at a similar location to a cracked solder joint in crystalline solar cell assembly shown in Fig. 8.2.

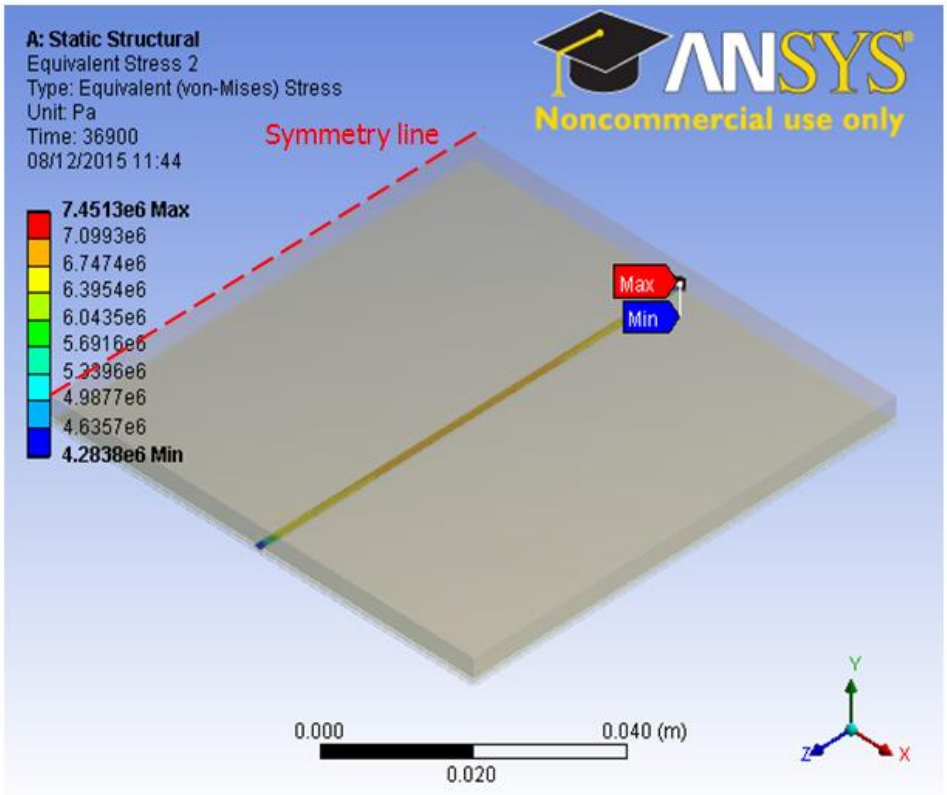


**(a) Equivalent stress of solder joint in model**

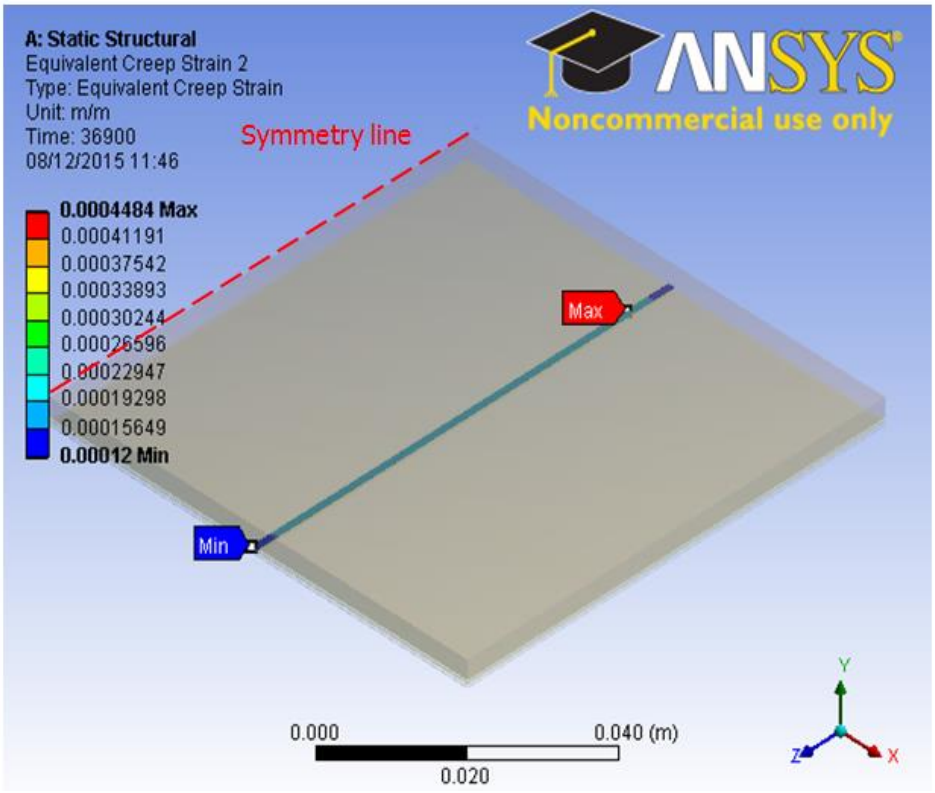


**(b) Equivalent creep strain of solder joint in model**

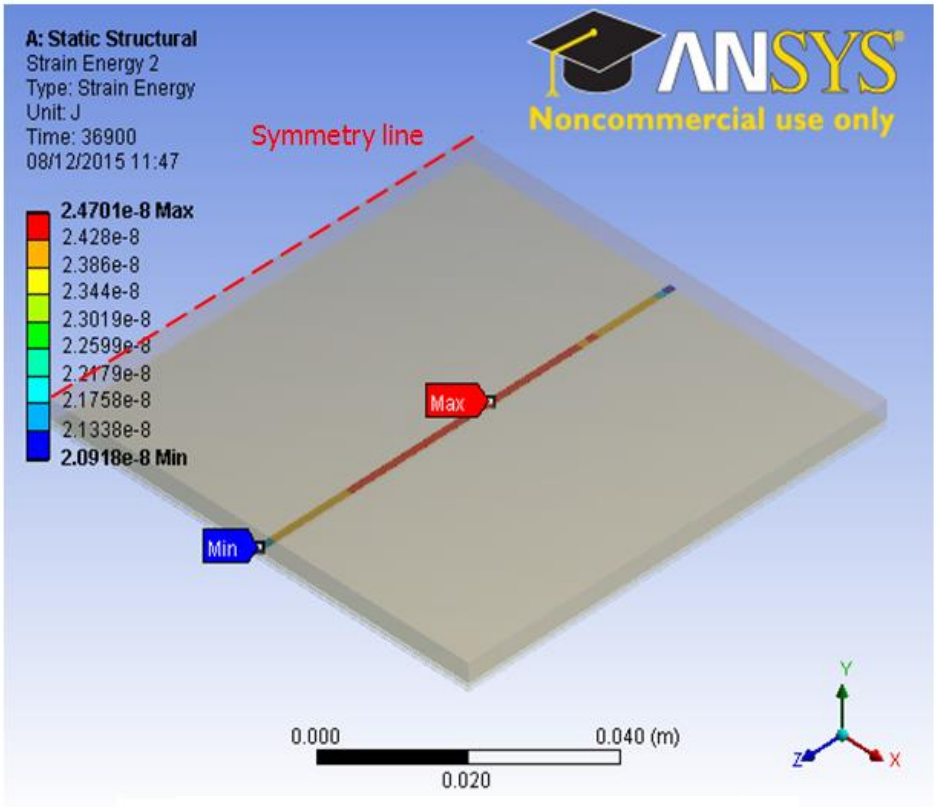


**(c) Strain energy of solder joint in model**

**Figure 8.1 Damage distribution in solder joint of solar cell assembly showing: (a) Equivalent stress (b) Equivalent creep strain (c) Strain energy**

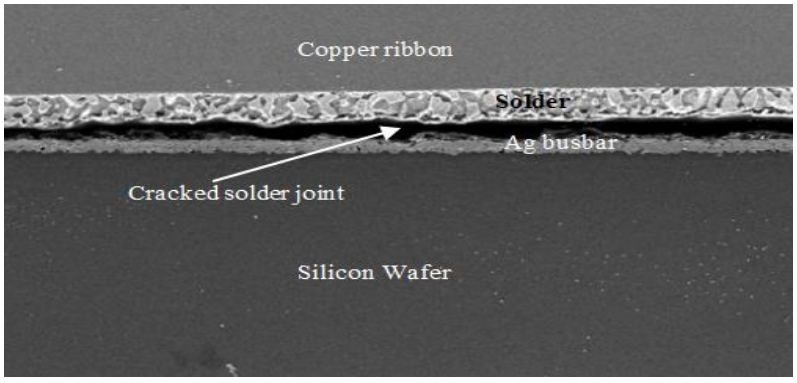


**Figure 8.2 Cracked solder joint in crystalline solar cell assembly (Jeong, *et al.*, 2012)**

The plot of change in accumulated change in creep strain energy density against designed model is presented in Fig. 8.3. It can be observed from Fig. 8.3 that model number 2 has the largest average accumulated change in creep strain energy density per cycle ($\Delta\omega_{acc}$) with a value of 0.06218mJ/mm$^3$ compared to all the other models. This implies that the solder joint in model number 2 is the most susceptible to failure compared to the others. Therefore, model number 2 has the most critical solder joint consisting of 1µm IMC thickness, 1200µm solder joint width and 25µm solder joint thickness; hence, is the worst original design compared to the other models.

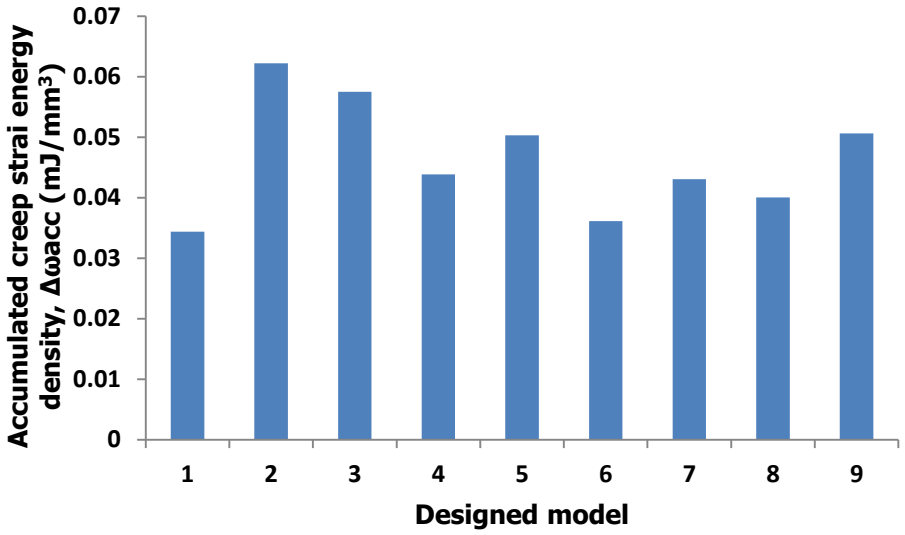


**Figure 8.3 Plot of change in accumulated creep strain energy density against designed model**

The geometric models were simulated and accumulated creep strain energy density determined from simulation results for each design. The predicted

results as well as the computed S/N ratio for each design are presented in Table 8.3.

**Table 8.3 Experimental results and S/N ratio**

| Model number | Factor and level | | | Quality/Response | S/N ratio |
|---|---|---|---|---|---|
| | A | B | C | $\Delta\omega_{acc}$ (mJ/mm$^3$) | |
| 1 | 1 | 1 | 1 | 0.03436 | 29.28 |
| 2 | 1 | 2 | 2 | 0.06218 | 24.13 |
| 3 | 1 | 3 | 3 | 0.05750 | 24.81 |
| 4 | 2 | 1 | 2 | 0.04384 | 27.16 |
| 5 | 2 | 2 | 3 | 0.05028 | 25.97 |
| 6 | 2 | 3 | 1 | 0.03613 | 28.84 |
| 7 | 3 | 1 | 3 | 0.04303 | 27.32 |
| 8 | 3 | 2 | 1 | 0.04002 | 27.95 |
| 9 | 3 | 3 | 2 | 0.05061 | 25.92 |
| Average | | | | | 26.82 |

### 8.3.2 Evaluation of main effect and interaction

The focus of this analysis is minimization of the response which is desired for average accumulated change in creep strain energy density per cycle ($\Delta\omega_{acc}$) in the solder joint. The averaged effect response for S/N ratio of each factor was investigated to determine the contributions of IMC thickness, solder joint width and solder joint thickness on the solder joint thermo-mechanical reliability. Minitab 17 statistical software was used to carry out analysis of variance (ANOVA) on the data presented in Table 8.3. The main effect plots from ANOVA are shown in Fig. 8.4 and consist of the plot for IMC thickness, solder joint width and solder joint thickness. Also, presented in Table 8.4 is the S/N response and rank for the three factors.

The means (averaged values) of S/N ratio presented in Table 8.4 and plotted in Fig. 8.4 are obtained using the data in Table 8.3 and applying Eq. 8.2 for each factor.

$$\overline{j_i} = \frac{1}{n}\sum_{j_i=1}^{n} \; j_i\Big|_{\forall j,i} \tag{8.2}$$

Where *j* may be designated as A, B or C represent factor and *i* stand for values 1, 2 or 3 represent the level. The symbols $\overline{j_i}$ and *n* are the mean of S/N ratio and the number of level in the experiment respectively. The sign $\big|_{\forall j,i}$ denotes that Eq. 8.2 is evaluated at *j* and *i* values. These means represent the factor average effects at each level. Furthermore, with reference to Table 8.4, the effect of a factor ($E_j$) is the observed range in its level. It can be represented as:

$$E_j = F_{j\max} - F_{j\min}\Big|_{\forall i} \tag{8.3}$$

Where $E_j$, is effect of factor *j* and $F_{jmax}$ and $F_{jmin}$, are maximum and minimum value of factor *j*, respectively. The sign $\big|_{\forall i}$ designates that Eq. 8.3 is evaluated across the level.

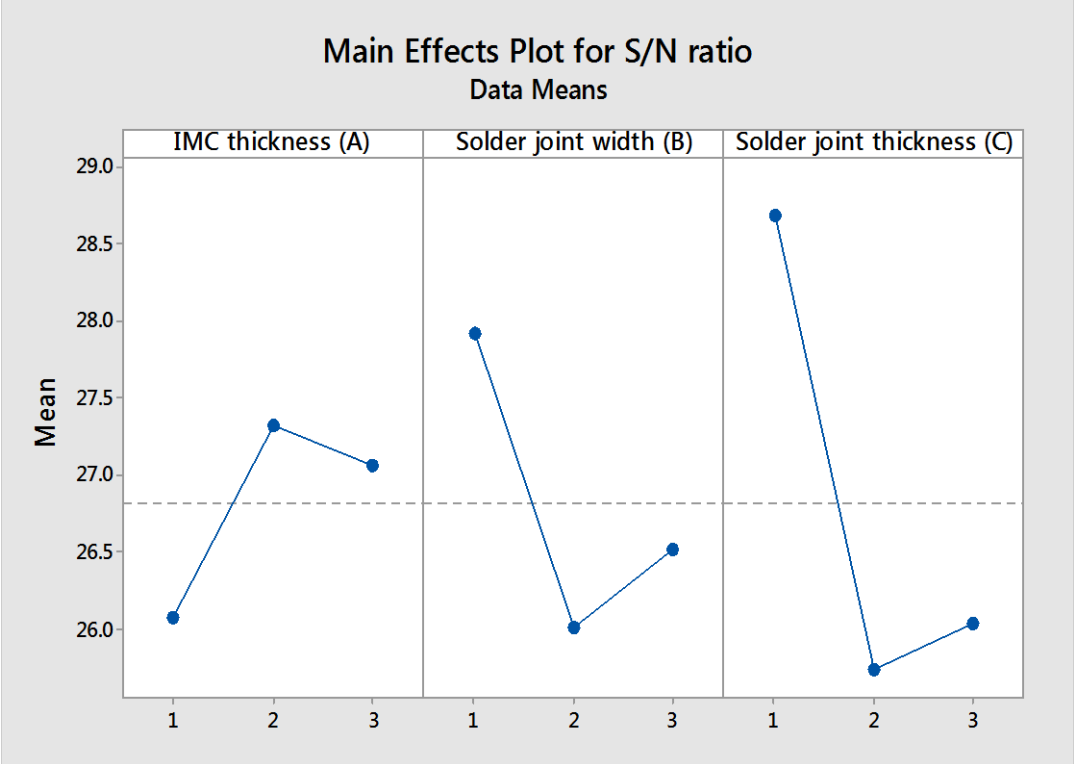


**Figure 8.4 Main effect plot of IMC thickness, solder joint width and solder joint thickness**

**Table 8.4 S/N response and rank**

| | Factor and level | | |
|---|---|---|---|
| | **A** | **B** | **C** |
| **Level 1** | **26.07** | **27.92** | **28.69** |
| **Level 2** | **27.32** | **26.02** | **25.74** |
| **Level 3** | **27.06** | **26.52** | **26.03** |
| **Effect** | **1.25** | **1.90** | **2.95** |
| **Rank** | **3** | **2** | **1** |

### 8.3.3 Comparison of the optimal design with the worst design

Results from Fig. 8.4 and Table 8.4 indicate that the most significant parameter for the thermo-mechanical reliability of solder joint is Factor C (solder joint thickness) as it has the largest effect, hence is ranked 1$^{st}$.

Factor A (IMC thickness) is the least significant as it has the least effect, hence ranked 3rd. Factor B (solder joint width) has the second largest effect as it is ranked 2nd. Furthermore, from Table 8.4, the optimal parameter setting based on maximum values is deduced to be A2B1C1 which reveal that the solder joint should have an IMC thickness of 2.5μm, width of 1000μm and thickness of 20μm.

A geometric model of solar cell assembly containing solder joint with the optimal parameters was built and simulated in order to provide results for confirmation and comparison with worst original design (Model 2). Accumulated creep strain energy density was computed from the simulation results of the optimal design and S/N ratio was computed as well. Presented in Fig. 8.5 is comparison of accumulated creep strain energy density of worst original design and optimal design. It can be observed from Fig. 8.5 that accumulated creep strain energy density in solder joint of worst original design is higher than that of optimal design. This implies that the optimal design makes the solder joint more robust than the worst original design. Comparison of the average accumulated change in creep strain energy density per cycle ($\Delta\omega_{acc}$) and the S/N ratio of the worst original design and the optimal design is presented in Table 8.5. It can be observed from Table 8.5 that the optimal design has the smallest average accumulated change in creep strain energy density per cycle ($\Delta\omega_{acc}$) compared to all the other original designs. Furthermore, the optimal design reduces the $\Delta\omega_{acc}$ by

47.96% compared to that of the worst original design thereby improving the thermo-mechanical reliability of the solder joints in crystalline silicon solar cell assembly.

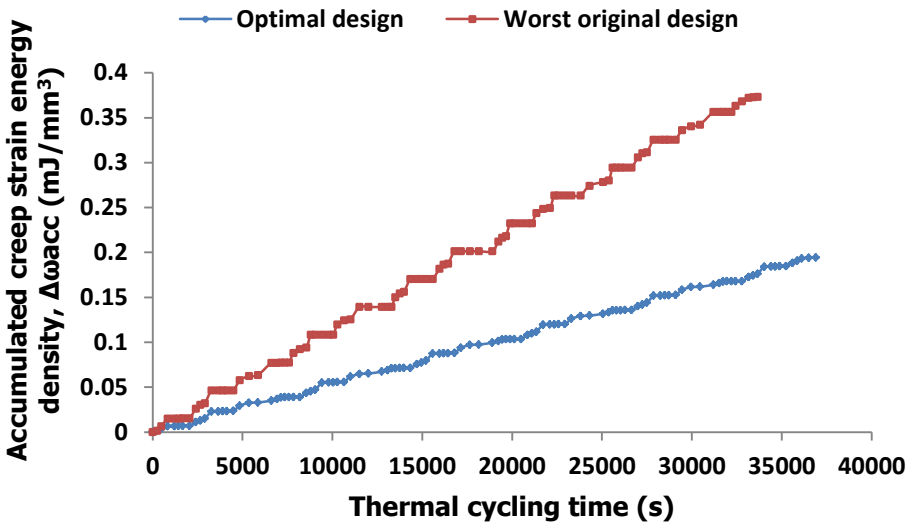


**Figure 8.5 Comparison between accumulated creep strain energy density of original design and optimal design**

**Table 8.5 Comparison of $\Delta\omega_{acc}$ in worst original and optimal designs**

| | Factors and level | | | $\Delta\omega_{acc}$ (mJ/mm$^3$) | S/N ratio |
|---|---|---|---|---|---|
| | A | B | C | | |
| **Worst original design** | 1 | 2 | 2 | 0.06218 | 24.13 |
| **Optimal design** | 2 | 1 | 1 | 0.03236 | 29.80 |
| **Reduction** | | | | 47.96% | |

Furthermore, Eq. 2.11 was used to compute fatigue life of the solder joints in worst original design as well as in optimal design. The computation results show that the optimized model is predicted to have 16264 cycles to failure

while the worst design model is predicted to have 8464 cycles to failure. These results are shown in Fig. 8.6. The predicted fatigue life of the optimized model is higher than the expected 13688 cycles to failure of a PV module designed to last for 25 years by 18.82%. In addition, the expected life of PV modules which is 13688 cycles to failure (25 years) is included in Fig. 8.6. Besides, in an experimental study, Kumar and Sarkar (2013) tested 20 PV modules for stress failure and obtained the least survival life to be 21 years (11497 cycles to failure). Similarly, in a study of field exposed PV modules, Park *et al*. (2013), predicted fatigue life of lead-based 62Sn36Pb2Ag solder joint as 4764 cycles to failure. However, it should be noted that the characteristic lifetime of lead-free solder is much longer and more reliable than that of lead-based solder at temperatures below $100^{o}$C as found by other researchers such as Meilunas *et al*. (2002) and Osterman *et al*. (2006). Therefore, it is not surprising that the fatigue life of 62Sn36Pb2Ag solder is much shorter than that of Sn3.8Ag0.7Cu solder which is used in this research. Hence, the PV module experimental test life as well as the field life of PV module with Pb-based solder is also presented in Fig. 8.6 for the sake of comparison.

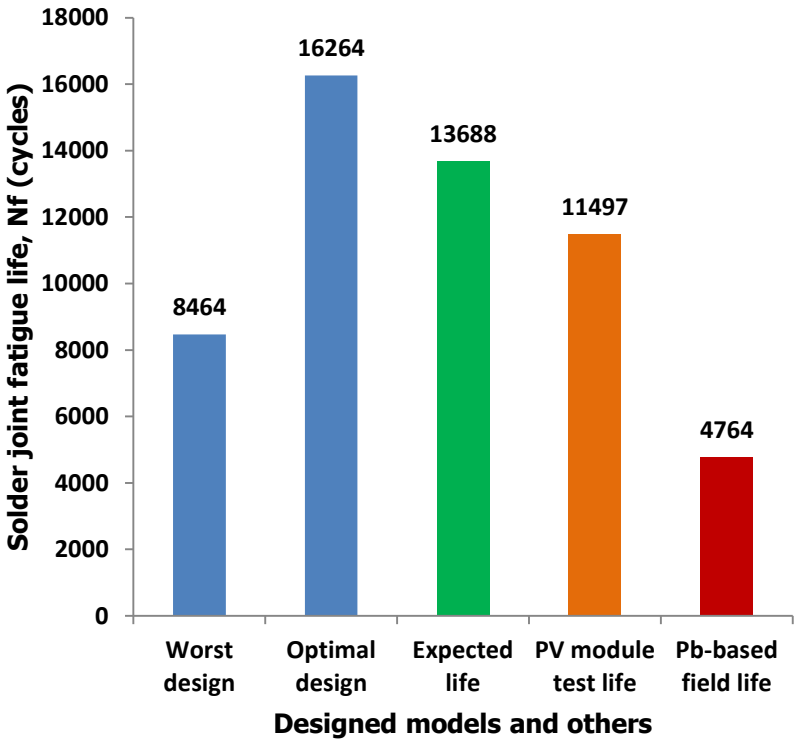


**Figure 8.6 Predicted solder joint fatigue life of design models compared with expected and test values**

It can be observed from Fig. 8.6 that the predicted solder joint fatigue life of the optimal design is almost double that of the worst original design and higher than the expected life of PV modules. This implies that the solder joint of the optimal design has uppermost thermo-mechanical reliability when compared to the others which is very desirable for the PV modules.

## 8.4 Conclusions

An investigation of the thermo-mechanical reliability of solder joints in crystalline silicon solar cell assembly using finite element modelling (FEM) and Taguchi method for DOE was presented in this chapter. The investigation aimed to study the effect of intermetallic compound (IMC)

thickness, solder joint width and solder joint thickness on the thermo-mechanical reliability of Sn3.8Ag0.7Cu solder joint with various sets of parameters and subjected to thermal cycling. The focus of this investigation was to minimize accumulated change in creep strain energy density and optimize the parameter setting of solder joint towards the enhancement of thermo-mechanical reliability of the joint.

The results of simulation carried out reveal that the maximum damage distribution is at the mid-section of the solder joint for stress, creep strain and strain energy. The maximum creep strain damage is located at the lower side of the solder joint adjacent to silver (Ag) bus-bar. This indicates that crack initiation and propagation is most likely to occur at the mid-section of the solder joint and will eventually lead to fatigue failure at that preferential failure site.

Furthermore, the outcomes of this investigation show that the magnitude of accumulated change in creep strain energy density depends on the parameter setting of solder joint. Comparison of the main effects of IMC thickness, solder joint width and solder joint thickness on the thermo-mechanical reliability of the solder joint indicates that solder joint thickness has the most significant effect.

The analysis of parameters selected towards thermo-mechanical reliability improvement of solder joint produced an optimal parameter setting which will make the joint robust. The optimal parameter setting for the solder joint

is that the solder joint thickness is 20μm, solder joint width is 1000μm and IMC thickness is 2.5μm. Also, the optimal parameter setting improves the performance of the solder joint by 47.96% compared to the worst case original parameter setting. Interestingly, the optimized model is predicted to have 16264 cycles to failure which is 18.82% higher than the expected 13688 cycles to failure of a PV module designed to last for 25 years.

In this chapter, optimization has been carried out which bring to a culmination the study of thermo-mechanical reliability of solder joints parameters in crystalline silicon solar cell assembly. The next chapter is on the conclusions drawn from the whole study and recommendations for further studies.

# CHAPTER 9

# CONCLUSIONS AND RECOMMENDATIONS

# Chapter 9

# Conclusions and Recommendations

## 9.1 Introduction

In the preceding chapter, optimization of solder joint parameters selected towards thermo-mechanical reliability improvement of solder joint was presented. This chapter outlines conclusions drawn from the whole research as well as recommendations for further work.

## 9.2 Conclusions

The study of thermo-mechanical reliability of solder joints in multi-crystalline silicon solar assembly using finite element modelling has been presented in this thesis. In the study, geometric models of solar cell assembly were built and simulated to study fatigue damage of solder joints so as to enable acquisition of scientific knowledge necessary to improve solder joint reliability of photovoltaic modules to meet their designed lifetime during field service. Based on the findings of this study, the following conclusions can be drawn:

(i) The study establishes that the presence of IMC in solder joints of solar cell assembly significantly affects solder joint fatigue life. Analysis of models of solar cell assembly shows that solder joint containing IMC has a predicted fatigue life of 15317 cycles to failure while that of

solder joint without IMC is 32493 cycles to failure. This is a 52.85% change of predicted fatigue life from solder joint without IMC. The reason for this is that IMC reduces solder volume; hence the capacity of solder joint to dissipate induced strain energy is reduced thereby shortening the fatigue life of the joint. Therefore, the result establishes that solder joint containing IMC has a considerable shorter fatigue life compared with the one without IMC. Furthermore, the results indicate that modelling solder joints in solar cell assembly without IMC layer exaggerates the joints predicted fatigue life which may lead to unexpected failures during service operations. Hence it is crucial to include IMC layer in solder joint models for the study of thermo-mechanical reliability of the joints to ensure accurate modelling and simulation results.

(ii) Another finding reveals that as IMC thickness increases in the solder joint of solar cell assembly, predicted fatigue life of the joint decreases. Results obtained indicate that when IMC thickness is 1μm, predicted fatigue life is 15317 cycles to failure, while when the thickness increases to 4μm, the predicted fatigue life decreases to 13023 cycles to failure. The decrease in solder joint predicted fatigue life is due to decrease in solder volume which reduces the capacity of the solder joint to dissipate strain energy and provide the desired long fatigue life. Thus, solder joints should be designed to have adequate capacity to withstand IMC thickness throughout the duration of the PV module lifetime.

(iii) The study also establishes that solder joint thickness impacts solder joint fatigue life such that the thicker the joint, the shorter the fatigue life. From the study results, when solder joint thickness is 20μm, predicted fatigue life is 14174 cycles to failure, while when the thickness increases to 30μm, the predicted fatigue life decreases to 10794 cycles to failure. This is due to thermo-mechanical stresses induced in the solder joints during thermal loading which accelerate fatigue damage in the joints as thickness increases. Therefore, appropriate solder joint thickness should be used in solar cell assembly in order to reduce thermo-mechanical stresses in the joint and extend fatigue life of the joint.

(iv) The study also shows that the wider the solar cell solder joint, the longer the fatigue life. The study results demonstrate that when solder joint width is 1000μm, predicted fatigue life is 14174 cycles to failure, while when the width increases to 1400μm, the predicted fatigue life increases to 15729 cycles to failure. The reason for the increase in predicted fatigue life can be attributed to decrease in accumulated strain energy density due to the increase in total interface area of the solder joint. It is for this reason that when a crack develops in the solder joint, it takes a longer time for solder crack propagation through the contact interface of a wider solder joint than a narrow one. However, wider solder joints increase shadowing losses of the solar cell thereby reducing the cell efficiency. Therefore,

compromise is required between increase in solder joint width and shadowing losses as well as desired fatigue life.

(v) Furthermore, the findings outlined above demonstrate that geometric parameters of solder joint in solar cell assembly have significant impacts on thermo-mechanical reliability of the joints. For that reason, optimization of solder joint parameter setting is essential to obtain a joint which accumulates minimal creep strain energy density and potential for longer fatigue life.

(vi) Results from optimization conducted indicate that solder joint thickness has the most significant effect on the thermo-mechanical reliability of solder joints. Analysis of results selected towards thermo-mechanical reliability improvement shows the design with optimal parameter setting to be: solder joint thickness - 20μm, solder joint width - 1000μm, and IMC thickness – 2.5μm. Furthermore, the optimized model has the least damage in the solder joint and shows a reduction of 47.96% in accumulated creep strain energy density per cycle compared to the worst case original model. Moreover, the optimized model has 16264 cycles to failure compared with the expected 13688 cycles to failure of a PV module designed to last for 25 years. This indicates that the optimized model has 18.82% longer fatigue life to design expectation.

Based on these findings, the author recommends that manufacturers of wafer-based crystalline silicon photovoltaic modules use this study to analyse

and optimize their designs in order to enhance the thermo-mechanical reliability of solder joints.

## 9.3 Recommendations for further work

In order to further improve the research carried out, some recommendations are presented in the following two sub-sections: General recommendations and specific recommendations.

### 9.3.1 General recommendations

Several sets of simulation were carried out in this research and the results obtained should be validated accordingly. Therefore, it is proper to conduct experiments based on the simulations carried out in order to validate the simulation results. Additionally, this work can further be expanded to include varying the thickness of silicon wafers. This is necessary because the current trend is towards manufacture of thinner silicon wafers. Results obtained from such studies will be beneficial to both PV module manufacturers and researchers.

### 9.3.2 Specific recommendations

In addition to the general recommendations presented in the preceding section, the following are specific recommendations for future improvement of this work:

(i) Although an optimized model was developed through DOE and virtual experiments via simulation, it is necessary to design practical

experiments to determine fatigue damage in the solder joints so as to validate simulation results. Such experimental validation of the optimized model will provide valuable insight on the deviation or otherwise of the experimental and simulation results.

(ii) The fatigue model used in this study was developed by Syed (2004) for microelectronics solder joints. However, solder joints in solar cell assembly have a much larger area than the joints in electronic devices. Therefore, it is recommended that fatigue model be developed and experimentally validated for the large area solder joints in solar cell assembly. This will improve the accuracy of results in this study.

# REFERENCES


Aberle, A.G. (2009) Thin-film Solar Cells. *Thin Solid Films*, 517, pp.4706–4710.

Alawadhi, E.M. (2010) *Finite element Simulations Using ANSYS.* 1st ed. Florida: CRC Press, Taylor & Francis Group LLC.

Amalu, E.H. and Ekere, N.N. (2012) High temperature reliability of lead-free solder joints in a flip chip assembly. *Journal of Materials Processing Technology*. 212, pp.471-483.

Arangú, A.A.V. Ponce-Alcántara, S. and Sánchez, G. (2014) Optical characterization of backsheets to improve the power of photovoltaic modules. *Proceedings of the 8th International Photovoltaic Power Generation Conference and Exhibition, SNEC*, Shanghai, China. 20-22 May.

Ardani, K. and Margolis, R. (2011) *2010 Solar Technologies Market Report*. National Renewable Energy Laboratory: Golden, Colorado, USA. p. 1-136.

Armstrong, S. Hurley, W.G. (2010) A thermal model for photovoltaic panels under varying atmospheric conditions. *Applied Thermal Engineering*, 30, pp.1488-1495.

Arndt, R. and Puto, R. (2011) Basic understanding of IEC standard testing for photovoltaic panels. *IN Compliance Magazine: 2011 Annual Guide*, Hopedale, MA: Same Page Publication, pp. 194–205.

Benham, P.P., Crawford, R.J., and Amstrong, C.G. (1996) *Mechanics of Engineering Materials*. 2nd ed. Essex: Longman.

Betts, A.K. (2004) The diurnal cycle over land. [Accessed 3 November 2014]. Available at: <http://alanbetts.com/workspace/uploads/ec-sem01_betts-1274648223.pdf>.

Bultman, J.H., Weeber, A.W., Brieko, M.W., Hoornstra, J., Burgers, A.R., Dijkstra JA, Tip, A.C. and Schuurmans, F.M. (2000) Pin up module: a design for higher efficiency, easy module manufacturing and attractive appearance. *Proceedings of the 16th EPVSC*, Glasgow 2000, pp.1210–1213. [Accessed 26 November 2012]. Available at: <http://www.ecn.nl/docs/library/report/2000/rx00010.pdf>.

Burger, B., Kiefer, K., Kost C., Nold, S., Philipps S., Preu, R., Schlegl T., Stryi-Hipp, G., Willeke, G., Wirth, H., Brucker, I., Haberle, A., Schacht, V. and Warmuth W. (2015) *Photovoltaics Report*. Fraunhofer Institute for Solar Energy Systems ISE: Freiburg, Germany. p. 1-43.

Burger, B., Kiefer, K., Kost, C., Nold, S., Phillips, S., Preu, R., Schindler, R., Schlegl., Stryl-Hipp, G., Willieke, G., Wirth, H., Brucker, I., Haberle, A., Schacht, V. and Warmuth, W. (2014) *Photovoltaic Report*. Freiburg: Fraunhofer Institute for Solar Energy Systems ISE. pp.1-42.

Cartwright, J., Stadterman, T., Jackson M. and Huang, Z. (1999) Draft Assessment of Reliability Prediction Methodologies. *CALCE Electronic Products and Systems Consortium* [online]. pp.1-24 [Acessed 25 November 2013]. Available at: <http://www.calce.umd.edu/general/projects/BenchRel.pdf>.

Chawner, J. (2012) Accuracy, Convergence and Mesh Quality [online]. [Accessed 15 May 2016]. Available at: <http://www.pointwise.com/theconnector/May-2012/Mesh-Quality.shtml>.

Che, F.X. and Pang, J.H.L. (2004) Thermal fatigue reliability analysis for PBGA with Sn-3.8Ag-0.7Cu solder joints. *Proceedings of 6th IEEE Electronics Packaging Technology Conference,* Singapore 8-10 December. IEEE, pp.787-792.

Che, F.X. and Pang, J.H.L. (2012a) Characterization of IMC layer and its effect on thermomechanical fatigue life of Sn-3.8Ag-0.7Cu solder joints. *Journal of Alloys and Compounds*, 541, pp.6-13.

Che, F.X. and Pang, J.H.L. (2012b) Fatigue Reliability Analysis of Sn-Ag-Cu Solder Joints Subject to Thermal Cycling. *IEEE Transaction on Device and Materials Reliability*, 13(1), pp.36-49.

Che, F.X., Pang, J.H.L., Xiong, B.S., Xu, L. and Low, T.H. (2005) Lead Free Solder Joint Reliability Characterization for PBGA, PQFP AND TSSOP Assemblies. *Proceedings of 55$^{th}$ ECTC*. Florida, USA. pp.916-921.

Chen, Y.M., Chiu, Y. and Wu, H. (2012) Improved testing of soldered interconnects quality on silicon solar cell. *Global Perspective on Engineering Management*, 1(2), pp.51-58.

Chen, C-H., Lin, F-M., Hu, H-T. and Yeh, F-Y. (2008) Residual stress and bow analysis for silicon solar cell induced by soldering. *International symposium on solar cell technologies*, Taipei, Taiwan, 4-6 December, pp.1-3.

Chiou, Y-C., Jen, Y-M. and Huang, S-H. (2011) Finite element based fatigue life estimation of the solder joints with effect of intermetallic compound growth. *Microelectronics Reliability*, 51, pp.2319-2329.

Chomsamutr, K. and Jongprasithporn, S. (2012) Optimization parameters of tool life model using the Taguchi approach and response surface methodology*. International Journal of Computer Science,* 9*,* pp.120–125*.*

Chuang, W-H., Luger, T., Fettig, R.K. and Ghodssi, R. (2004) Mechanical Property Characterization of LPCVD Silicon Nitride Thin Films at Cryogenic Temperatures. *Journal of Microelectromechanical Systems,* 13(5), pp.870-879.

Cuddalorepatta, G., Abhijit, D., Scott, S., Jerome, M., Todd. T. and James L. (2010) Durability of Pb-free solder between copper interconnect and silicon in photovoltaic cells. *Progress in Photovoltaics: Research and Applications*. 18(3), pp.168-182.

Cutter, A.F. (2012) *The Electrician's Green Handbook*. Clifton Park, New York: Delmar.

Davies, R., Coole, T. and Osypiw, D. (2015) A Review of Traditional and Taguchi Design of Experiments: Devising a Method Selection Criteria, *Proceedings of 25th Flexible Automation and Intelligent Manufacturing*. University of Wolverhampton, Wolverhampton. 23-26 June, Gloucester: The Choir Press, pp.308-315.

DeGraaff, D., Lacerda, R. and Campeau Z. (2011) Degradation Mechanisms in Si Module Technologies Obsereved in the Field: Their Analysis and Statistics. *Photovoltaic Module Reliability Workshop.* Golden, Colorado, USA. pp. 1-25.

Diebold, U. (2003) The Surface Science of Titanium Dioxide. *Surface Science Report*s, 8, pp.53-229.

Dirjish, M., (2012) What's The Difference Between Thin-Film And Crystalline-Silicon Solar Panels. *Electronic Design eNewsletter*, Penton Media Inc.: Newyork, USA. pp.1-6.

Dwayne, R.S. (2009) *Transient and steady-state creep in a Sn-Ag-Cu lead-free solder alloy: Experiments amd modelling* [online]. PhD. Thesis, University of Toronto. [Accessed 21 November 2014]. Available at: < https://tspace.library.utoronto.ca/bitstream/1807/26476/1/Shirley_Dwayne_R_200906_PhD_thesis.pdf>.

Eitner, U., Pander, M., Kajari-Schröder, S., Köntges, M. and Altenbach, H. (2011) Thermomechanics of PV Modules Including the Viscoelasticity of Eva. *Proceedings of 26th European Photovoltaic Solar Energy Conference and Exhibition*. Hamburg, Germany. pp.3267-3269.

Engelmaier, W. (1997) Solder joints in electronics: design for reliability. *Proceedings of TMS Annual Meeting on Design and Reliability of Solders and Solder Interconnections*, pp.9–19.

Etnier, S.A. (2001) Flexural and Torsional Stiffness in Multi-Jointed Biological Beams. *Biological Bulletin*, 200(1), pp.1–8.

Erath, D. (2010) Printing Techniques in the c-Si PV Industry – A Brief Technological Overview. *International Circular Of Graphic Education and Research*, 3, pp.8-15.

Fan, X.J., Varia, B. and Han, Q. (2010) Design and optimization of thermo-mechanical reliability in wafer level packaging. *Microelectronics Reliability*, 50(4), pp.536-546.

Gierth, P., Rebenklau, L. and Michaelis, A. (2012) Evaluation of Soldering Processes for High Efficiency Solar Cells. *35th International Spring Seminar on Electronics Technology*. Vienna, Austria. pp.133-137.

Gress, P.J., Windenborg, P.I., Varlamov, S. and Aberle, A.G. (2010) Wire bonding as a Cell Interconnection Technique for Polycrystalline Silicon Thin-film Solar Cells on Glass. *Progress in Photovoltaics: Research and Applications,* 18, pp.221-228.

Goodrich, A., Hacke, P., Wang, Q., Sopori, B., Margolis, R., James, T.L. and Woodhouse, M. (2013) A wafer-based monocrystalline silicon photovoltaics roadmap: Utilizing known technology improvement opportunities for further reductions in manufacturing costs. *Solar Energy Materials & Solar Cells*, 114, pp.110-136.

Granata JE, Boyson WE, Kratochvil JA, Quitana MA. (2009) Long-Term Performance and Reliability Assessment of 8 PV Arrays at Sandia National Laboratories. *Proceedings of 34th IEEE Photovoltaic Specialist Conference*, Philadelphia, PA, pp.1486–1491.

Grunow, P. (2010) Soldering of crystalline silicon modules: losses, reliability and improvements. *Proceedings of the 2nd Workshop on Metallization for Crystalline Silicon Solar Cells*. Constance, Germany, 14-15 April, pp.59-62.

Guyenot, M., Peter, E., Zerrer, P., Kraemer, F. and Wiese, S. (2011) Enhancing the lifetime prediction methodology for photovoltaic modules. *Proceedings of 12th Int. Conf. on Thermal, Mechanical and Multiphysics Simulation and Experiments in Microelectronics and Microsystems*. Linz, Austria, pp. 1-4.

Han, C., Park, N. and Jeong, J. (2012) Lifetime Prediction of Silicon PV Module Ribbon Wire in Three Local Weathers. *Photovoltaic Module Reliability Workshop.* Golden, Colorado, USA. [Accessed 14 Dec 2012] Available at: <http://www1.eere.energy.gov/solar/pdfs/pvmrw12_poster_si_han.pdf>.

Hopcroft, M.A., Nix, W.D. and Kenny, T.W. (2010) What is the Young's Modulus of Silicon? *Journal of Microelectromechanical Systems*. 19(2), pp.229-238.

Huan, Y., Xue, S., Zhang, L., Ji, F. and Dei, W. (2010) Reliability evaluation of CSP soldered joints based on FEM and Taguchi method. *Computational Materials Science*, 48, pp.509-512.

Hund, T. and Burchett, S.N. (1991) Solder fatigue reduction in point focus photovoltaic concentrator modules. Proceedings of *22nd IEEE Photovoltaic Specialists Conference*, Las Vegas, NV. pp.754–759.

Jeong, J., Nochang, P., Wonsik, H. and Changwoon, H. (2011) Analysis for the Degradation Mechanism of Photovoltaic Ribbon Wire under Thermal Cycling. *Proceedings of 37th Photovoltaic Specialists Conference*, Seattle, WA. USA, pp.003159-003161.

Jeong, J.S., Park, N. and Han, C. (2012) Field Failure Mechanism Study of Solder Interconnection for Crystalline Silicon Photovoltaic Module. *Microelectronics Reliability*. 52, pp.2326-2330.

JMP Release 8. (2009) *Design of Experiments*. 2nd ed. SAS Institute: Cary, NC, USA, pp.1-286.

Jong, P. (2006) High Efficiency Solar Modules: Why traditional concepts fail and how it will bring us to back-contact module assembly. Presentation to Joint Solar Panel. pp.1-27.

Jung, V. and Kontges, M. (2013) Al/Ni : V/Ag metal stacks as rear-side metallization for crystalline silicon solar cells. *Progress in photovoltaics*, 21(5), pp.876–883.

Kato, K. (2012) PV module failures observed in the field. *Proceedings of 27th European PV Solar Energy Conference and Exhibition*, FranKfurt, Germany. 26-29 September.

Kerschaver, E.V. and Beaucarne, G. (2010) Back-contact solar cells: a review. *Progress in Photovoltaics: Research and Applications*, 14(2), pp. 107-23.

Kim, Y-K., Kim, J-C. and Choi, J-H. (2010) Design Optimization of Ball Grid Array Packaging by the Taguchi Method. *Journal of the Microelectronics and Packaging Society*, 17(4), pp.67-72.

Klengel, R., Petzold, M., Schade, D. and Sykes, B. (2011) Improved Testing of Soldered Busbar Interconnects on Silicon Solar Cells. *Proceedings of 18th European Microelectronics and Packaging Conference*,. Brighton.

Klengel, R., Härtel, R., Schindler, S., Schade, D. and Sykes, B. (2011) Evaluation of the Mechanical Strength of Solar Cell Solder Joint Interconnects and Their Microstructural Properties by Developing a New Test and Inspection Equipment. *26th European Photovoltaic Solar Energy Conference and Exhibition*, Hamburg, Germany. pp.1507-1511.

Klutke, G-A., Kiessler, P.C. and Wortman, M.A. (2003) A Critical Look at the Bathtub Curve. *IEEE Transactions on Reliability*, 52(1), pp. 125–129.

Knupp, P.M. (2007) Remarks on Mesh Quality. *45th AIAA Aerospace Sciences Meeting and Exhibition*, Reno, Nevada, USA. 7-10 January. pp.1-10.

Kohl, M., Weiss K., Heck, M. and Philipp, D. (2009) PV Reliability: Results of a German four-year joint project Part I: Accelerated ageing tests and modelling of degradation. *24th European Photovoltaic Solar Energy Conference and Exhibition.* Hamburg, Germany. 21-25 September.

Kontges, M., Kurtz. S., Packard, C., Jahn U., Berger, K.A., Kato, K., Friesen, T., Liu H. and Iseghem H. (2014) Review of Failures of Photovoltaic Modules. *International Energy Agency IEA-PVPS Task 13 Report,* pp. 1-140.

Kraemer, F., Wiese, S., Peter, E.B. and Seib, J. (2013) Mechanical problems of novel back contact solar modules. *Microelectronics Reliability*, 53(8), pp. 1095–100.

Kumar, S. and Sarkar, B. (2013) Design for Reliability with Weibull Analysis for Photovoltaic Modules. *International Journal of Current Engineering and Technology*. 3(1), pp.129-134.

Ladani, L.J. (2008) Reliability estimation for large-area solder joints using explicit modeling of damage. *IEEE Trans on Device and Material Reliability*, 8 (2), pp. 375–386.

Ladani, L.J. (2010) Numerical analysis of thermo-mechanical reliability of through silicon vias (TSVs) and solder interconnects in 3-dimensional integrated circuits. *Microelectronics Engineering*, 87, pp.208-215.

Lai, C.M., Su, C.H. and Lin, K.M. (2013) Analysis of the thermal stress and warpage induced by soldering in monocrystalline silicon cells. *Applied Thermal Engineering*, 55, pp.7–16.

Lechovič, E., Erika, H., Beáta, S., Ingrid, K. and Koloman, U. (2009) Solder Joint Reliability. [Accessed 12 March 2013]. Available at: <https://www.mtf.stuba.sk/docs/internetovy_casopis/2009/1/hodulova.pdf>.

Lee, W.W., Nguyen, L.T. and Selvaduray, G.S. (2000) Solder joint fatigue models: review and applicability to chip scale packages. *Microelectronics Reliability*, 40(2), pp.231-244.

Löffler, J., Wipliez, L., Soppe, W., Keijzer, M., Bosman, J., Lamers, M., Mewe, A., Weeber, A., Bennett, I. and Jong, P. (2010) Laser processing for advanced solar cells. *Proceedings of the 11th International Symposium on Laser Precision Microfabrication*, Stuttgart, Germany, 7-11 June. [Accessed 11 February 2013] Available at: <ftp://ftp.ecn.nl/pub/www/library/report/2010/m10035.pdf>.

McCluskey, F.P. (2010) Reliability Modeling for Photovoltaic Modules. *NREL Photovoltaic Module Reliability Workshop,* Denver, Colorado. [Accessed 4 December 2012] Available at: <http://www1.eere.energy.gov/solar/pdfs/pvrw2010_mccluskey.pdf>.

Meilunas, M., Primavera, A. and Dunford, S.O. (2002) Reliability and Failure Analysis of Lead-Free Solder Joints. *Proceedings of the IPC Annual Meeting*, New Orleans, LA, pp.S08-5-1- S08-5-14.

Mette, A. (2007) *New concepts for front side metallization of industrial silicon solar cells* [online]. Ph.D. Thesis, University of Freiburg in the Breisgau, Germany. [Accessed 8 February 2013]. Available at: <https://www.freidok.uni-freiburg.de/data/3782>.

Montgomery, D.C. (2013) *Design and Analysis of Experiments*. 8th ed. Danvers: John Wiley & Sons, Inc.

Morris, J. W., Song, H.G. and Hua, F. (2003) Creep Properties of Sn-rich Solder Joints. *Proceedings of 53rd ECTC*. New Orleans, Louisiana, USA. pp.54-57.

Moyer, J., Zhang, W., Kurtz, E., Tavares, R., Buzby, D. and Kleinbach, S. (2010) The Role of Silver Contact Paste on Reliable Connectivity Systems. *Proceedings of 25th European Photovoltaic Solar Energy Conference and Exhibition.* Valencia, Spain, 6–10 September, pp. 2624–2630.

Nagel, H., Aberle, A.G. and Hezel, R. (1999) Optimised Antireflection Coatings for Planar Silicon Solar Cells using Remote PECVD Silicon Nitride and Porous Silicon Dioxide. *Progress in Photovoltaics: Research and Applications*, 7, pp.245-260.

Pang, J.H.L and Che, F.X. (2006) Isothermal Cyclic Bend Fatigue Test Method for Lead Free Solder Joints. *Proceedings of 10th Intersociety Conference on Thermal and Thermomechanical Phenomena in Electronics Systems.* San Diego, California, USA. pp.1011-1017.

Pang, J.H.L., (2012) *Lead Free Solder: Mechanics and Reliability* - Theory on Mechanics of Solder Material. Berlin: Springer.

Park, N., Jeong, J. and Han, C. (2014) Estimation of the degradation rate of multi-crystalline silicon photovoltaic module under thermal cycling stress. *Microelectronics Reliability*, 54, pp.1562-1566.

Park, N., Han, C., Jeong J. and Kim, D. (2013 ) Lifetime prediction model of thermal fatigue stress on crystalline silicon photovoltaic module. *39th IEEE Photovoltaic Specialists Conference.* Tampa, FL. 16-21 June. pp.1575-1578.

Pei, M. and J. Qu. (2005) Constitutive Modeling of Lead-Free Solders. *Proceedings of 10th International Symposium on Advanced Packaging Materials: Processes, Properties and Interfaces*. University of California, Irvine 16-18 March, IEEE, pp.45-49.

Pregelj, A., Begovic, M., Rohatgi, A. and Ristow, A. (2001) Estimation of PV system reliability parameters. *Proceedings of 17th European Photovoltaic Solar Energy Conference and Exhibition.* Munich, Germany, 22–26 October, pp. 558–561.

Rogelj, I., Ziger, P. and Eiselt, P. (2012) PV Ribbon: Overview of Product Specifications and Comparison of Production Processes. *China PV Technology International Conference*. 21-22 March. Shanghai, China.

Saga, T., (2010) Advances in crystalline silicon solar cell technology for industrial mass production. *NPG Asia Materials*, 2(3), pp.96-102.

Sakamoto, S., T. Kobayashi, and S. Nonomura, (2012) Epidemiological Analysis of Degradation in Silicon Photovoltaic Modules. *Japanese Journal of Applied Physics*, 51, pp.1-4.

Schmitt, P., Kaiser, P., Savio, C., Tranitz, M. and Eitner, U. (2012) Intermetallic Phase Growth and Reliability of Sn-Ag-Soldered Solar Cells. *Energy Procedia*. 27, pp.664-669.

Schubert, A., Dudek, R., Auerswald, E., Gollhardt, A., Michel, B. and Reicbl, H. (2003) Fatigue Life Models of SnAgCu and SnPb Solder Joints Evaluated by Experiements and Simulations. *Proceedings of 53rd ECTC*. New Orleans, Louisiana, USA. pp.603-610.

Shah, A.V., Schade, H., Vanecek, M., Meier, J., Vallat-Sauvain, E., Wyrsch, N., Kroll, U., Droz, C. and Bailat, J. (2004) Thin-film silicon solar cell technology. *Progress in Photovoltaics: Research and Applications*, 12(2-3), pp.113-142.

Shengwei, M. (2011) Top 5 misunderstandings on good mesh [online]. [Accessed 19 December 2015]. Available at: <http://caewatch.com/top-5-misunderstandings-on-good-mesh/>.

Shu, M.H., Hsu, B.M. and Hu, M.C. (2012) Optimal combination of soldering conditions of BGA for halogen free and lead free SMT green processes. *Microelectronics Reliability,* 52(11), pp.2690-2700.

Sigmund, O. and Petersson, J. (1998) Numerical instabilities in topology optimization: Asurvey on procedures dealing with checkerboards, mesh-dependencies and local minima. *Structural Optimization*, 16, pp.68-75.

Sitaraman, S.K. and Kacker, K. (2005) Thermo-Mechanical Reliability Prediction for Lead-Free Solder Interconnects: Lead-Free Solder Interconnect Reliability. *Electronic Device Failure Analysis Society/ASM International*, pp.181-198.

Skoczek, A., Sample, T. and Dunlop, E.D. (2009) The results of performance measurements of field-aged crystalline silicon photovoltaic modules. *Progress in Photovoltaics: Research and Applications*, 17(4), pp.227-40.

Sopori, B., Butterfield, B. and Amieva, J. (2004) Detailed Characterization of AR Coatings on Si Solar Cells: A New Application of GT-FabScan 6000. *14th Workshop on Crystalline Silicon Solar Cells and Modules*. Winter Park, Colorado. 8–11 August.

SunPower (2013) SunPower Module 40-year Useful Life. *SunPower Corporation, USA.* pp. 1-14.

Sunshot Initiative, (2013a) *Amorphous Silicon*. Energy Efficiency & Renewable Energy, 1-2. [Acessed 30 October 2013]. Available at: <http://energy.gov/eere/sunshot/photovoltaics-research-and-development>.

Sunshot Initiative, (2013b) *Cadmium Telluride*. Energy Efficiency & Renewable Energy, 1-2. [Acessed 30 October 2013]. Available at: <http://energy.gov/eere/sunshot/photovoltaics-research-and-development>.

Sunshot Initiative, (2013c) *Copper Indium Gallium Diselenide*. Energy Efficiency & Renewable Energy, 1-2. [Acessed 30 October 2013]. Available at: <http://energy.gov/eere/sunshot/photovoltaics-research-and-development>.

Syed, A. (2004) Accumulated Creep Strain and Energy Density Based Fatigue Life Prediction Models for SnAgCu Solder Joints. *Proceedings of 54th ECTC*. Las Vegas, USA. pp.737-746.

Taguchi, G. (1995) Quality Engineering (Taguchi Methods) for the Development of Electronic Circuit Technology. *IEEE Transactions on Reliability*, 44, pp.225-229.

Teimouri, M. and Gupta, A.K. (2013) On the Three-parameter Weibull Distribution Shape Parameter Estimation. *Journal of Data Science,* 11, pp.403-414.

Thakur, S., Kaisare, A. and Tonapi, S. (2012) Thermo-mechanical analysis of a typical solar module: A parametric study. *13th IEEE Intersociety Conference on Thermal and Thermomechanical Phenomena in Electronic Systems (ITherm),* San Diego, CA, USA, 30 May -1 June 1 2012, pp.1255 – 1263.

Thornburg, H.J. (2012) Overview of the PETTT Workshop on Mesh Quality/ Resolution, Practice, Current Research and Future Directions. *American Institute of Aeronautics and Astronautics* paper no. 2012-0606.

Wang, J., He, P. and Xiao, F. (2004) The effect of residual stress on the flexing strength of PCB assembly," in *High Density Microsystem Design and Packaging and Component Failure Analysis, HDP'04, Proceeding of the Sixth IEEE CPMT Conference,* pp.146-150.

Webb, J.E. and Hamilton, J.P. (2011) Physical Properties of Glass and the Requirements for Photovoltaic Modules. *Proceedings of Photovoltaic Module Reliability Workshop*, Golden, Colorado, USA. pp.1-18.

Wiese, S., Kraemer, F., Betzl, N. and Wald, D. (2010) Interconnection Technologies for Photovoltaic Modules – Analysis of technological and mechanical Problems. *Proceedings of EuroSimE 2010*, Bordeaux, France, April 26-28, pp.345-350.

Wiese, S., Kraemer, F., Peter, E. and Seib, J. (2012) Mechanical Problems of novel Back Contact Solar Modules. *Proceedings of 13th International Conference on Thermal, Mechanical and Multi-Physics Simulation and Experiments in Microelectronics and Microsystems, EuroSimE.* Cascais, near Lisbon, Portugal.

Wiese, S., Meier, R., Kraemer, F. and Bagdahn, J. (2009) Constitutive behaviour of copper ribbons used in solar cell assembly processes. *10th International Conference on Thermal, Mechanical and Multi-Physics simulation and Experiments in Microelectronics and Microsystems, EuroSimE 2009.* IEEE. 11-14 August 2015, pp.197-200.

Wiese, S., Meusel, E. and Wolter, K-J. (2003) Microstructural Dependence of Constitutive Properties of Eutectic SnAg and SnAgCu Solders. *Proceedings of 53rd ECTC*. New Orleans, Louisiana, USA. pp.197-206.

Willeke, G.P. and Weber, E.R. (2013) *Semiconductors and Semimetals: Advances in Photovoltaics*. 1st ed., 89(2). San Diego: Academic Press

Wirth, H. (2010) Lasers in wafer-based PV module production. *Laser Technik Journal*, 7(4), pp.36-38.

Wohlgemuth. J., Cunningham, D.W., Nguyen, A., Kelly, G. and Amin, D. (2010) Failure Modes of Crystalline Si Modules. *PV Module Reliaibility Workshop*. Denver, Colorado, USA. pp.1-33.

Wohlgemuth, J.H. (2008) Reliability of PV Systems. *Proceedings of SPIE conference*. Reliability of Photovoltaic Cells, Modules, Components, and Systems. San Diego 10 September. 7048, pp.704802-1 – 704802-13.

Xakalashe, B.S. and Tangstad M. (2011) Silicon processing: from quartz to crystalline silicon solar cells. *Proceedings of Southern African Institute of Mining and Metallurgy in Southern African Pyrometallurgy*. Johannesburg, 6-9 March. pp.83-99.

Yang, P. and Tan, G. (2011) Taguchi-numerical approach on thermomechanical reliability for PBGA. *International Journal of Numerical Modelling: Electronic Networks, Devices Field*, 24(5), pp.437–447.

Yang, T.L., Huang K.Y., Yang, S., Hsieh, H.H. and Kao, C.R. (2014) Growth kinetics of $Ag_3Sn$ in silicon solar cells with a sintered Ag metallization layer. *Solar Energy Materials & Solar Cells,* 123, pp.139–143.

Ye, H., Xue, S., Zhang, L., Ji, F. and Dai, W. (2010) Reliability evaluation of CSP soldered joints based on FEM and Taguchi method. *Computational Materials Science*, 48(3), pp.509-512.

Zeman, M. (2009) *Heterojunction silicon based solar cells* [online]. [Accessed 12 December 2012]. Available at: <http://www.jointsolarpanel.nl/fileadmin/jointsolarpanel/user/documents/seminar2009/4_Miro_Zeman_Delft_University_of_Technology.pdf >.

Zemen, Y.,Teusch, H-S., Kropke, G., Pingel, S. and Held, S. (2012) The Impact of Busbar Surface Topology and Solar Cells Soldering Process. *Proceedings of 27th European Photovoltaic Solar Energy Conference and Exhibition.* Frankfurt, Germany, 24–28 September, pp.2030–2034.

Zhang, L., Sun, L., Zhong, S-J. Ma, J. and Bao, L. (2015) Reliability of Pb-free solder joints in FCBGA using finite element simulation and Taguchi method. *Proceedings of 16th International Conference on Electronic Packaging Technology (ICEPT),* IEEE, pp.197-200.

Zhang, Q., Dasgupta, A. and Haswell, P. (2003) Viscoplastic Constitutive Properties and Energy-Partioning Model of Lead-Free Sn3.9Ag0.6Cu Solder Alloy. *Proceedings of 53rd ECTC*. New Orleans, Louisiana, USA. pp.1862-1868.

# Appendix A: Minitab 17 Analysis of Variance (ANOVA) for Optimization of Solder Joints

Method

Factor coding (-1, 0, +1)

Factor Information

| Factor | Type | Levels | Values |
|---|---|---|---|
| IMC thickness (A) | Fixed | 3 | 1, 2, 3 |
| Solder joint width (B) | Fixed | 3 | 1, 2, 3 |
| Solder joint thickness (C) | Fixed | 3 | 1, 2, 3 |

Analysis of Variance

| Source | DF | Adj SS | Adj MS | F-Value | P-Value |
|---|---|---|---|---|---|
| IMC thickness (A) | 2 | 2.6102 | 1.3051 | 9.50 | 0.095 |
| Solder joint width (B) | 2 | 5.8301 | 2.9150 | 21.21 | 0.045 |
| Solder joint thickness (C) | 2 | 15.8681 | 7.9340 | 57.73 | 0.017 |
| Error | 2 | 0.2749 | 0.1374 | | |
| Total | 8 | 24.5832 | | | |

Model Summary

| S | R-sq | R-sq(adj) | R-sq(pred) |
|---|---|---|---|
| 0.370720 | 98.88% | 95.53% | 77.36% |

Coefficients

| Term | Coef | SE Coef | T-Value | P-Value | VIF |
|---|---|---|---|---|---|
| Constant | 26.820 | 0.124 | 217.04 | 0.000 | |
| IMC thickness (A) | | | | | |
| 1 | -0.747 | 0.175 | -4.27 | 0.051 | 1.33 |
| 2 | 0.503 | 0.175 | 2.88 | 0.102 | 1.33 |
| Solder joint width (B) | | | | | |
| 1 | 1.100 | 0.175 | 6.29 | 0.024 | 1.33 |
| 2 | -0.803 | 0.175 | -4.60 | 0.044 | 1.33 |
| Solder joint thickness (C) | | | | | |
| 1 | 1.870 | 0.175 | 10.70 | 0.009 | 1.33 |
| 2 | -1.083 | 0.175 | -6.20 | 0.025 | 1.33 |

Regression Equation

S/N ratio = 26.820 - 0.747 IMC thickness (A)_1 + 0.503 IMC thickness (A)_2
+ 0.243 IMC thickness (A)_3 + 1.100 Solder joint width (B)_1
- 0.803 Solder joint width (B)_2 -
0.297 Solder joint width (B)_3
+ 1.870 Solder joint thickness (C)_1 -
1.083 Solder joint thickness (C)_2
- 0.787 Solder joint thickness (C)_3

## Appendix B: Published Journal Papers

1. M.T. **Zarmai**, N.N. Ekere, C. F. Oduoza, E.H. Amalu. A review of interconnection technologies for improved crystalline silicon solar cell photovoltaic module assembly. Applied Energy (Elsevier), 154 (2015), 173-182.

2. M.T. **Zarmai**, N.N. Ekere, C. F. Oduoza, E.H. Amalu. Effect of intermetallic compounds on thermo-mechanical reliability of lead-free solder joints in solar cell assembly. International Journal of Mechanical Engineering (IJME), Vol. 4. Issue 6, 2015, 29-38.

3. M.T. **Zarmai**, N.N. Ekere, C. F. Oduoza, E.H. Amalu. Optimization of thermo-mechanical reliability of solder joints in crystalline silicon solar cell assembly. Microelectronics Reliability (Elsevier) – (Article in press - http://dx.doi.org/10.1016/j.microrel.2015.12.031).

## Appendix C: Conference Papers Presented

1. M.T. **Zarmai**, N.N. Ekere, C. F. Oduoza, E.H. Amalu. Effect of IMC thickness on thermo-mechanical reliability of lead-free solder joints in solar cell assembly. Proceedings of TechConnect Conference, Washington DC, USA, 2015, Vol. 4, pp. 286-289.

2. M.T. **Zarmai**, N.N. Ekere, C. F. Oduoza, E.H. Amalu. Thermo-mechanical reliability of lead-free solder joints in solar cell assembly. Proceedings of the 25th International Conference on Flexible Automation and Intelligent Manufacturing (FAIM), Wolverhampton, UK, 2015, Vol. 1, pp. 640-647.

3. M.T. **Zarmai**, N.N. Ekere, C. F. Oduoza, E.H. Amalu. Effect of intermetallic compounds on thermo-mechanical reliability of lead-free solder joints in solar cell assembly. Proceedings of Asia-Pacific Conference on Engineering & Applied Sciences (APCEAS), Osaka, Japan, 2015, Part 1, pp. 328-336.